

STOCHASTIC AND SEISMIC DESIGN RESPONSE OF LINEAR AND NONLINEAR STRUCTURES

By

Gustavo Omar Maldonado

Dissertation submitted to the Faculty of the
Virginia Polytechnic Institute and State University
in partial fulfillment of the requirements for the degree of
DOCTOR OF PHILOSOPHY


in

Engineering Mechanics

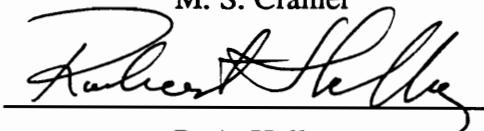
APPROVED:



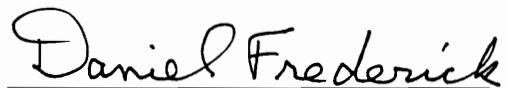
M. P. Singh, Chairman



M. S. Cramer



R. A. Heller



D. Frederick.



T. Kuppusamy

August, 1992
Blacksburg, Virginia

**Stochastic and Seismic Design Response
of Linear and Nonlinear Structures**

by

Gustavo O. Maldonado

Dr. M. P. Singh, Chairman

Department of Engineering Science and Mechanics

(ABSTRACT)

New methods for calculating the stochastic and seismic design response of linear and nonlinear structures are presented.

For linear structures, two approaches are developed: (1) the modified mode displacement approach for classically as well as non-classically damped structures, and (2) the generalized force derivative approach for classically damped structures. Both techniques improve the calculation of the pseudostatic contribution of the truncated modes without including them in the analysis. In particular, the modified mode displacement approach is a useful tool for the calculation of seismic design responses affected by the contributions of higher modes. It properly considers the modal correlations as well as the correlation between retained and truncated modes. It is as fast as the mode acceleration method of structural dynamics and it only requires the commonly used ground response spectra employed by the classical mode displacement approach. On the other hand, the generalized force derivative approach requires the input to be defined in terms of its power spectral density function, but it improves even further the estimation of the missing mass effect due to the truncation of modes.

For nonlinear structures, the stochastic equivalent linearization technique is employed to develop response spectrum approaches for hysteretic shear buildings and for two dimensional frames with plastic hinges. For this purpose, a generalized modal analysis technique is successfully employed. The proposed response spectrum approaches require the input be defined in terms of the response spectrum of first order oscillators as well as in terms of the commonly used ground response spectra. For shear buildings, the work is extended to include the calculation of floor response spectra. A simulation study is performed to compare the results obtained by the proposed approach.

ACKNOWLEDGEMENTS

The author is greatly indebted to his major professor, Dr. Mahendra P. Singh, for his invaluable guidance, advice and support. Also the special assistance of Dr. Robert A. Heller during the most critical moments is deeply appreciated.

The author extends his most sincere appreciation to Dr. M. S. Cramer, Dr. D. Frederick, Dr. T. Kuppusamy and Dr. S. Thangjitham who served on his graduate committee and provided useful suggestions and comments.

The initial guidance and recommendations of Dr. Fabio Casciati and Dr. Lucia Faravelli, as well as the fruitful discussions with Dr. Luis E. Suarez deserve special thanks.

This research work would not have been completed without the unconditional love and spiritual encouragement provided to the author by his wife Marcela, his daughter Maria Virginia and his family from overseas.

Finally, the author wishes to express his gratitude to all his friends who made Blacksburg a wonderful place to live, especially Lucinda Willis, Raúl Andruet, Sanjeev Malushte, Dean Mook, Mohammad Rohanimanesh and Robert Simonds.

Contents

1	Introduction	1
2	Modified Mode Displacement Response Spectrum Method for Classically Damped Structures	5
2.1	Introduction	5
2.2	Modified Mode Displacement Approach	9
2.3	Mean Square Value Response	15
2.4	Response Spectrum Method by the MMD approach	23
2.5	Numerical Results	27
2.6	Conclusions	39
3	Modified Mode Displacement Response Spectrum Method for Non-classically Damped Structures	41
3.1	Introduction	41
3.2	Response by Modified Mode Displacement	43
3.3	Mean Square Value of the Response Quantity $R(t)$	49
3.4	Response Spectrum Method by the MMD approach	57
3.5	Numerical Results	59
3.6	Conclusions	70

4	Random Response of Structures by a Force Derivative Approach	71
4.1	Introduction	71
4.2	Modal Analysis and Truncated MD Approach	73
4.3	First Order Force Derivative Approach	75
4.4	Second Order Force Derivative Approach	76
4.5	N^{th} Order Force Derivative Approach	78
4.6	Random Response: Auto-Correlation Function of $R(t)$	82
4.7	Random Response: Stationary Mean Square Value of $R(t)$	84
4.7.1	Contribution of the Retained Modes	85
4.7.2	Contribution Due to the Correlation Between Retained and Truncated Modes	86
4.7.3	Contribution of the Truncated Modes	87
4.7.4	Final Expression for $E[R^2(t)]$	90
4.8	Numerical Results	91
4.9	Conclusions	103
5	Response Spectrum Method for Hysteretic Shear Buildings	105
5.1	Introduction	105
5.2	The Shear Building Model	107
5.3	Governing Equations	108
5.4	Solution of the Linearized Governing Equations	114
5.5	Response Covariance Matrix of the Linearized System	116
5.5.1	Terms associated with only real eigenproperties: $\Sigma_{lm}^R(\omega)$	119
5.5.2	Terms associated with real and complex eigenproperties: $\Sigma_{lm}^{RC}(\omega)$	120

5.5.3	Terms associated with only complex eigenproperties: $\Sigma_{lm}^C(\omega)$. .	122
5.5.4	Final Expression for each Component of the Covariance Matrix	124
5.6	Response Spectrum Method	125
5.7	Summary of the Iterative Scheme	127
5.8	Interstory Shear Responses	130
5.9	Absolute Acceleration Response of a Floor	132
5.10	Floor Response Spectra	138
5.11	Numerical Results	143
5.12	Conclusions	183
6	Response Spectrum Method for 2D Frames with Plastic Hinges	188
6.1	Introduction	188
6.2	Equations of Motion	189
6.3	Plane Frame Element with Plastic Hinges	191
6.3.1	2D Elastic Frame Element	192
6.3.2	Inelastic Nodal Forces	199
6.3.3	Constitutive Equations	203
6.3.4	Parameters of the Constitutive Model	208
6.4	Response of the Linearized Governing Equations	212
6.5	Response Covariance Matrix and Response Spectrum Method	215
6.6	Response Statistics Required by the Linearization Coefficients	217
6.7	Numerical Results	219
6.8	Conclusions	224

7 Summary and Recommendations for Future Work	229
APPENDIXES	232
A Common Partial Fractions	232
A.1 Case I	232
A.2 Case II	234
A.3 Case III	236
A.4 Case IV	238
B Integration by Parts of the Duhamel Integral	241
C Recursive Formula for Pseudo-Flexibility Matrices	245
C.1 Pseudo-Flexibility Matrices for all Modes	245
C.2 Pseudo-Flexibility Matrices for Lower and Higher Modes	247
D Calculation of a Classical Damping Matrix from a Truncated Modal Analysis	250
E Bouc-Wen Constitutive Model	255
F Linearization Coefficients	260
G Frequency Integrals	264
References	269
Vita	274

List of Figures

2.1	Schematic of the beam analyzed.	28
2.2	Percent error in the root mean square value of a bending moment obtained for Kanai-Tajimi spectral density function by different approaches with increasing number of modes for: (A) stiff beam, and (B) flexible beam.	31
2.3	Percent contribution of various terms in the equation for the the total mean square response obtained with different number of modes for: (A) stiff beam, and (B) flexible beam.	32
2.4	Percent error in the bending moment design response obtained for response spectrum input by different approaches with increasing number of modes for: (A) stiff beam, and (B) flexible beam.	34
2.5	Schematic of the structure analyzed in the example problem.	35
2.6	Percent error in the root mean square value of a bending moment obtained for a Kanai-Tajimi spectral density function by different approaches with increasing number of modes for: (A) stiff frame, and (B) flexible frame.	37
2.7	Percent error in a bending moment design response obtained for response spectrum input by different approaches with increasing number of modes for: (A) stiff frame, and (B) flexible frame.	38
3.1	Schematic of the structure analyzed.	60
3.2	Percent error in the root mean square value of a bending moment obtained for Kanai-Tajimi input by different approaches with increasing number of modes — Low frequency structure.	64

3.3	Percent error in the root mean square value of a bending moment obtained for Kanai-Tajimi input by different approaches with increasing number of modes — Medium frequency structure.	65
3.4	Percent error in the root mean square value of a bending moment obtained for Kanai-Tajimi input by different approaches with increasing number of modes — High frequency structure.	66
3.5	Percent error in the design value of a bending moment obtained for response spectrum input by different approaches with increasing number of modes — Low frequency structure.	67
3.6	Percent error in the design value of a bending moment obtained for response spectrum input by different approaches with increasing number of modes — Medium frequency structure.	68
3.7	Percent error in the design value of a bending moment obtained for response spectrum input by different approaches with increasing number of modes — High frequency structure.	69
4.1	(A) Schematic of the multi-span beam and (B) Band-limited white noise spectral density input considered in the analysis.	92
4.2	Convergence of the normalized mean square value of a bending moment with increasing number of integrations by parts: No modes within the input frequency range.	98
4.3	Convergence of the normalized mean square value of a bending moment with increasing number of integrations by parts: No modes within the input frequency range and higher values of the frequency ratio r_c	99
4.4	Convergence of the normalized mean square value of a bending moment with increasing number of integrations by parts: The first mode is within the input frequency range.	101
4.5	Convergence of the normalized mean square value of a bending moment with increasing number of integrations by parts: The first five modes are within the input frequency range.	102
5.1	Schematic of the 4-story shear building.	144
5.2	Ground response spectra for the second order oscillator: (A) Pseudo-acceleration spectra, (B) Relative velocity spectra.	145

5.3	Spectra for the first order oscillator: (A) Ground response spectra for relative displacement, (B) Peak factors for relative displacements. . .	146
5.4	Peak factor spectra for the second order oscillator: (A) Peak factors for pseudo-acceleration, (B) Peak factors for relative velocity.	148
5.5	Maximum shear force vs. maximum ground acceleration in various stories of the structure.	150
5.6	Maximum ductilities vs. maximum ground acceleration in various stories of the structure.	151
5.7	Coefficient of linearization a_i vs. maximum ground acceleration in various stories of the structure.	152
5.8	Coefficient of linearization b_i vs. maximum ground acceleration in various stories of the structure.	154
5.9	Maximum shear forces vs. yield level of interstory drifts for various stories of the structure.	155
5.10	Maximum shear forces vs. yield level of interstory drifts for different values of the exponent parameter.	156
5.11	Maximum ductility ratios in various stories of the structure vs. maximum ground acceleration. (Yield level = 0.4 in; $\alpha = 0.05$; $\eta = 9$). . .	158
5.12	Maximum absolute accelerations for various floors of the structure vs. (A) maximum ground acceleration and (B) yield level ($\alpha = 0.05$; $\eta = 9$).160	
5.13	Floor response spectra of absolute acceleration in floor 1 for different yield levels. (Max. ground accel. = 0.4 g; $\alpha = 0.05$; $\eta = 9$; equip. damp. ratio = 0.005).	161
5.14	Floor response spectra of absolute acceleration in floor 4 for different yield levels. (Max. ground accel. = 0.4 g; $\alpha = 0.05$; $\eta = 9$; equip. damp. ratio = 0.005).	162
5.15	Floor response spectra ratios of absolute acceleration in (A) floor 1 and (B) floor 4 for different yield levels Y. (Max. ground accel. = 0.4 g; $\alpha = 0.05$; $\eta = 9$; equip. damp. ratio = 0.005).	163
5.16	Floor response spectra for the root mean square value of absolute acceleration in floor 2 for different yield levels Y. (Max. ground accel. = 0.4 g; $\alpha = 0.05$; $\eta = 3$; equip. damp. ratio = 0.005).	165

5.17	Ground response spectra for the second order oscillator: (A) Pseudo-acceleration spectra, (B) Relative velocity spectra.	167
5.18	Spectra for the first order oscillator: (A) Ground response spectra for relative displacement, (B) Peak factors for relative displacements. . .	168
5.19	Peak factor spectra for the second order oscillator: (A) Peak factors for pseudo-acceleration, (B) Peak factors for relative velocity.	169
5.20	Normalized damping ratios (with respect to the elastic case) vs. yield level of interstory drifts for various modes of the structure.	170
5.21	Normalized frequencies (with respect to the elastic case) vs. yield level of interstory drifts for various modes of the structure.	171
5.22	Floor response spectra of absolute acceleration for floor 1 (equip. damp. ratio = 5%). (A) Stochastic equivalent linearization, (B) Time history analysis.	176
5.23	Floor response spectra of absolute acceleration for floor 3 (equip. damp. ratio = 5%). (A) Stochastic equivalent linearization, (B) Time history analysis.	177
5.24	Floor response spectra of absolute acceleration for floor 5 (equip. damp. ratio = 5%). (A) Stochastic equivalent linearization, (B) Time history analysis.	178
5.25	Floor response spectra ratio of absolute acceleration for floor 1 (equip. damp. ratio = 5%). (A) Stochastic equivalent linearization, (B) Time history analysis.	180
5.26	Floor response spectra ratio of absolute acceleration for floor 3 (equip. damp. ratio = 5%). (A) Stochastic equivalent linearization, (B) Time history analysis.	181
5.27	Floor response spectra ratio of absolute acceleration for floor 5 (equip. damp. ratio = 5%). (A) Stochastic equivalent linearization, (B) Time history analysis.	182
5.28	Joint probability density functions for the normalized auxiliary variable and the normalized interstory drift velocity for floor 1 and ductility 2.	184
5.29	Joint probability density functions for the normalized auxiliary variable and the normalized interstory drift velocity for floor 1 and ductility 4.	185

6.1	Two dimensional elastic frame element: (A) Nodal displacements, (B) Nodal forces, (C) Undeformed and deformed states.	195
6.2	Deformed elastic element: (A) due to nodal forces, and (C) due to equivalent nodal efforts.	199
6.3	Constitutive law of the plastic hinges: (A) Moment at the hinge vs. hinge rotation, (B) Auxiliary variable vs. hinge rotation.	210
6.4	Schematic of the structures considered in the numerical results: (A) Single-story frame, (B) Two-story frame.	220
6.5	Normalized equivalent damping ratios of the single-story frame for different levels of yielding moment at the plastic hinges.	222
6.6	Normalized maximum shear forces of the single-story frame for different levels of yielding moment at the plastic hinges.	223
6.7	Normalized standard deviation of the horizontal drift of the single-story frame for different levels of yielding moment at the plastic hinges. The input is defined by a Kanai-Tajimi spectral density function. . .	225
6.8	Coefficient of linearization, a_i , of the two-story frame for different levels of yielding moment at the plastic hinges.	226
6.9	Normalized maximum shears forces at the base of the three columns of the two-story structure for different levels of yielding moment at the plastic hinges.	227
E.1	Bouc-Wen hysteretic model: (A) Force vs. displacement, and (B) Auxiliary variable vs. displacement	257

List of Tables

2.1	Natural frequencies of the flexible and stiff beams.	28
2.2	Natural frequencies of the flexible and stiff building.	33
3.1	First ten natural frequencies and damping ratios for the three structures.	61
4.1	First seven values of Δ_k	89
5.1	Structural characteristics of the 4-DOF structure.	144
5.2	Hysteretic parameters of the 4-DOF structure.	144
5.3	Hysteretic parameters of the nearly elasto-plastic 4-DOF structure. .	157
5.4	Structural characteristics of the 5-DOF structure.	164
5.5	Hysteretic parameters of the 5-DOF structure.	164
5.6	Equivalent frequencies and damping ratios of the stochastically equiv- alent linear structures.	173
5.7	Comparison of interstory shears obtained by the proposed response spectrum approach and by time history simulation.	174
5.8	Percent error in the floor spectra at the vicinity of the first and second peaks.	183
C.1	Dimensions of the matrices associates to the lower and higher modes	249

Chapter 1

Introduction

The seismic design of important civil engineering structures are usually performed by employing a time history analysis or a response spectrum analysis. In the first, the seismic motions are defined by ground acceleration time histories and it requires a laborious step-by-step calculation scheme. This method can be used to determine the response of linear as well as nonlinear structures. The response spectrum method, on the other hand, is used to calculate design response for input prescribed by design ground response spectra. However, it is restricted to linear structures. It uses modal analysis to uncouple the equations of motion and calculates the design response by an appropriate combination of the maximum responses for each mode. The maximum modal response values are directly defined in terms of ground response spectra.

For the combination of the maximum modal responses, several modal combination rules have been developed. The earliest of these combination rules is commonly referred to as the square root of the sum of the squares (SRSS). This is based on the assumption that the maximum modal responses do not occur at the same time and

are statistically uncorrelated. This assumption is obviously not true. It is especially not true when the structural modes are close to each other. It is also not true for the well separated modes, if at least one of the two modes is beyond the frequency range of the input. These especial cases required modifications to the SRSS approach. Several methods have been developed which account for the correlation between the modes. The first very popular method was developed by Rosenblueth and Elorduy. This was based on the assumption that the input was a white noise. The restriction of the white noise was removed by Singh and Chu [45], where an improved modal combination rule was proposed. Since then there have been other combination rules, but usually are some minor modifications of the Rosenblueth and Elorduy's rule. The background details of these various methods are presented in chapter 2 and 3 where we now propose a new rule which, of course, considers the correlation between the closely spaced modes as well as the correlation between the higher and low frequency modes. However, the proposed method does not require explicit calculation of these high frequency modes. Therefore, it is especially effective when mode truncation is performed in the response calculation. This new approach is called as the modified mode displacement (MMD) response spectrum approach. The development of this approach for the classically damped structures is presented in chapter 2 and for the non-classically damped structures is presented in chapter 3.

The calculation of the higher modes of a system is usually associated with larger numerical errors than the error for the lower modes. Fortunately, however, in most dynamic analyses, especially in seismic analyses, the contribution of higher modes to a response quantity is usually quite insignificant. Thus it is a common practice to ignore the higher modes in a modal analysis procedure. Which higher modes can be ignored in the calculation, depends upon the range of frequencies present in the

input motion. The modes which are much higher than the highest frequency of the input, can be comfortably ignored. However, ignoring the modes with frequencies close to the highest frequency of the input, can cause error. How can one reduce this error of mode truncation is the subject of the study presented in chapter 4. A procedure called force derivative method is presented to minimize this error. The higher the order of the force derivative approach used, the smaller will be the error in the calculated response. In this chapter, a recursive, easy to implement, scheme is developed to obtain the higher order terms in the proposed approach. This method has practical implication inasmuch as it can be used with advantage to improve the accuracy of modal synthesis methods, see Suarez and Singh [51].

A common modal analysis approach or the spectrum approaches developed above are not, of course, applicable to nonlinearly behaving structures. Thus they can not be used for buildings or structures which yield during a strong ground shaking. However, in the current design practice, buildings are expected to yield and behave nonlinearly during a design level ground shaking. In this work, a generalized response spectrum method, based on the concept of equivalent linearization, is developed to analyze nonlinear hysteretic structures and calculate their design response in terms of site ground response spectra. A more complete background and the details of the proposed approaches are described in two chapters. chapter 5 considers shear buildings with nonlinear shear stiffnesses distributed along the interstory elements, and chapter 6 considers two-dimensional structural frames with concentrated plastic hinges.

The nonlinear hysteretic characteristics of the materials are modeled by the versatile constitutive differential equations provided by Bouc-Wen [9, 56, 57]. A

stochastic linearization procedure determines a linear system which is statistically equivalent to the nonlinear governing equations. The coefficients of the linear system are selected such that they minimize the mean square error introduced by the linearization process. The linearization coefficients are functions of the response statistics of the actual nonlinear system which are not known a priori. An iterative scheme, such as the fixed point iterations or the faster Newton method, are employed to overcome this difficulty. The linearization is based on the assumption that the response statistics of the nonlinear system are equal to the gaussian response statistics of the linear system. Since the linearized system is not self adjoint, the right and left complex eigenproperties are required in the analysis. Complete details of the proposed method are given in chapters 5 and 6.

The final concluding remarks, and recommendations for future studies are given in chapter 7.

Chapter 2

Modified Mode Displacement Response Spectrum Method for Classically Damped Structures

2.1 Introduction

The aseismic design of important civil engineering structures requires the application of methods and procedures of structural dynamics and random vibrations. This chapter presents a new response spectrum approach based on a suitable combination of the mode displacement (MD) and mode acceleration (MA) methods of structural dynamics. The proposed method includes the effect of the higher modes even though they may be truncated and not explicitly considered in the analysis.

The analysis to calculate the design response of elastic multi-degree-of-freedom structures, when subjected to ground excitation, can be performed deterministically or stochastically. The deterministic approach is characterized by the use of one or several ground acceleration time histories. For this purpose, any good direct

integration technique can be applied to solve the coupled equations of motion. A major drawback of the time history analysis is that it requires a large amount of computer time as such analyses are to be performed for a large set of ground motions to obtain the design response. Often a large set of design ground motions may also not be available for a site. For design purposes, the site motion characteristics are often defined in terms of ground response spectra. In fact, in the current seismic design practice, the ground response spectra are considered to be best workable tool to prescribe the design ground motion. The methods which use such inputs directly, in the calculation of design response are called as the response spectrum methods.

The response spectrum methods are developed on the basis of random vibration analysis of structures. They all use the well known modal analysis technique. Since the higher modes usually do not contribute significantly to the seismic response, and also since their calculation involves larger error, it is common to use only a first few lower modes and completely ignore higher modes in response spectrum analyses. This omission of higher modes is known as the truncation of modes.

The error in the response caused by the truncation of higher modes is usually acceptable. But in some cases, this error can also be too large to be ignored completely. This can happen in the calculation of the response of stiff structural systems. Also, some response quantities which have a significant contribution from the high frequency modes may also be sensitive to this mode truncation error. These errors are present in the time history analyses as well as in the response spectrum method of analyses. The error caused by the truncation of modes has also been called as *the missing mass effect* [39].

The most commonly used formulation in modal analysis is the mode displacement formulation. However, to reduce this error in the time history and response spectrum analyses for seismic motions, the mode acceleration formulation [60] of structural dynamics can be effectively utilized. Successful application of this formulation for time history analysis was demonstrated by Singh and Ghafory-Ashtiany [46]. For design response calculations also, mode acceleration-based response spectrum approaches have been proposed by Singh [44] and Singh and Mehta [50] for classically damped structures. These response spectrum approaches required that the seismic design inputs be defined in terms of the relative acceleration and relative velocity response spectra. The design inputs in terms of the relative acceleration spectra (similar to the design inputs in terms of the pseudo-acceleration spectra) could also be developed, but this is rarely done. Since the current practice of seismic structural analysis is oriented towards the use of the pseudo-acceleration spectra, it would be desirable to have a spectrum approach which could employ pseudo-acceleration spectra rather than relative acceleration spectra and which would also be able to account for the missing mass effect caused by the truncation of modes. Gupta and Cordero [19] and Gupta and Chen [18] have proposed a response spectrum approach, which, they claim, provides acceptable results through the use of some empirical factors.

Besides the problem of missing mass effect, a response spectrum approach must also be able to account for the correlation between modes. In the earliest versions of the response spectrum methods, this correlation was ignored and the method of the square root of the sum of the squares (SRSS) was commonly used to obtain the design response from the maximum modal responses. Rosenblueth and Elorduy [41] were probably the first to provide a rational approach to account for this correlation.

Their approach is still the most popular. The calculation of the modal correlation term in this approach is based on the assumption of the base input being a white noise. CQC [59] is another approach which is based on the assumption of a white noise as the base input. These two approaches provide similar results. For structures whose dominant modes fall within the dominant excitation frequency range, these approaches can include modal correlation properly and thus provide accurate response results. However, because of the assumption of a white noise input, there could be errors in the response calculated by these approaches for stiff structural systems whose dominant modes are outside the range of the input motion frequencies. A comparative study of the method proposed in references [50], [41] and [59] has also been made by Villaverde [55].

Singh and Chu [45] had proposed a response spectrum approach where the modal correlation between the low and high frequency modes was properly included without making the assumption of the base input being a white noise. However, the missing mass effect caused by the truncation of modes cannot be corrected in this approach if only a limited number of modes are used.

In this chapter, the mode acceleration and the mode displacement approaches are combined to develop an approach which is called the modified mode displacement approach for classically damped structures. A similar approach is also developed for non-classically damped structures in the next chapter. An initial and a reduced versions of this method is published in references [47, 48]. This approach can effectively reduce the missing mass effect error, without explicitly including the high frequency modes in the analysis. Also, the correlation between the lower modes themselves as well as their correlation with the truncated higher modes is included. Numerical

examples are presented to demonstrate the effectiveness of the proposed approach as well as to compare its efficiency with other commonly used approaches.

2.2 Modified Mode Displacement Approach

The equations of motion for a linear elastic structure with n degrees of freedom and subjected to ground excitation in one direction, can be written in general form as:

$$[M] \{\ddot{X}(t)\} + [C] \{\dot{X}(t)\} + [K] \{X(t)\} = -[M] \{\mathcal{I}\} \ddot{x}_g(t) \quad (2.1)$$

where $[M]$, $[C]$, and $[K]$ are matrices of dimension $(n \times n)$, and they indicate, respectively, the mass, damping and stiffness matrices of the system; $\{X(t)\}$ is the vector of relative displacements with respect to the ground, and a dot over a variable indicates its time derivative; the vector $\{\mathcal{I}\}$ contains the ground motion influence coefficients; and $\ddot{x}_g(t)$ is the ground acceleration.

For linear systems, equation (2.1) can be decoupled by employing the modal analysis, which uses the following change of coordinates:

$$\{X(t)\} = [\Phi] \{Z(t)\}, \quad (2.2)$$

where the columns of the modal matrix $[\Phi]$ are the n eigenvectors $\{\phi\}_j$ corresponding to the undamped and homogeneous version of equation (2.1). The vector $\{Z(t)\}$ contains the so called principal coordinates of the system. The eigenanalysis also provides the n eigenvalues $\lambda_j = -\omega_j^2$, where ω_j is the natural frequency of the j^{th} mode. The matrix $[\Phi]$ is orthogonal to the mass and stiffness matrices and can be normalized with respect to the mass matrix to get

$$[\Phi]^T [M] [\Phi] = [I], \quad (2.3)$$

where $[I]$ is the $(n \times n)$ identity matrix. Also,

$$[\Phi]^T [K] [\Phi] = [\Lambda] , \quad (2.4)$$

where $[\Lambda]$ is the diagonal modal stiffness matrix, entries of which contain the eigenvalues $\lambda_j = \omega_j^2$. For classically damped systems, the modal matrix $[\Phi]$ is also orthogonal to the damping matrix $[C]$, that is

$$[\Phi]^T [C] [\Phi] = [D] , \quad (2.5)$$

where $[D]$ is the diagonal modal damping matrix whose n entries are $(2\beta_j \omega_j)$ $j = 1, \dots, n$. The uncoupling of equation (2.1) is achieved by the substitution of equation (2.2) into (2.1), premultiplying it by $[\Phi]^T$, and considering the orthogonality properties given in equations (2.3-2.5). This leads to the following system of uncoupled equations:

$$\{\ddot{Z}(t)\} + [D] \{\dot{Z}(t)\} + [\Lambda] \{Z(t)\} = -[\Phi]^T [M] \{\mathcal{I}\} \ddot{x}_g(t) \quad (2.6)$$

Or in a single equation format as:

$$\ddot{z}_j(t) + 2\beta_j \omega_j \dot{z}_j(t) + \omega_j^2 z_j(t) = -\gamma_j \ddot{x}_g(t) \quad , \quad j = 1, \dots, n , \quad (2.7)$$

where γ_j is the j^{th} participation factor defined as

$$\gamma_j = \{\phi\}_j^T [M] \{\mathcal{I}\} . \quad (2.8)$$

The solution of equation (2.7) for quiescent initial conditions is

$$z_j(t) = -\gamma_j \int_0^t h_j(t - \tau) \ddot{x}_g(\tau) d\tau \quad , \quad j = 1, \dots, n , \quad (2.9)$$

where $h_j(t)$ is the unit impulse response function:

$$h_j(t) = \frac{e^{-\beta_j \omega_j t}}{\omega_{dj}} \sin(\omega_{dj} t) , \quad (2.10)$$

and ω_{dj} is the j^{th} damped frequency:

$$\omega_{dj} = \omega_j \sqrt{1 - \beta_j^2} . \quad (2.11)$$

By invoking equation (2.2), we can write for the original vector $\{X(t)\}$ as

$$\{X(t)\} = [\phi] \{Z(t)\} = \sum_{j=1}^n \{\Phi\}_j z_j(t) . \quad (2.12)$$

Any response quantity $R(t)$, obtained as a linear combination of the components of vector $\{X(t)\}$, can also be expressed as

$$R(t) = \{\mathcal{R}\}^T \{X(t)\} = \sum_{j=1}^n \rho_j z_j(t) , \quad (2.13)$$

where $\{\mathcal{R}\}$ is the vector containing the coefficients of the linear transformation, and ρ_j is the j^{th} modal response quantity defined by

$$\rho_j = \{\mathcal{R}\}^T \{\phi\}_j . \quad (2.14)$$

Equation (2.12) or (2.13) constitute the basis of the mode displacement (MD) approach of structural dynamics [15]. It is assumed that the modes and their respective frequencies are ordered by increasing frequencies. It should be noticed that these equations consider the contribution of all n modes. However, for a large number of cases the contribution of the high frequency modes is negligible, and the summation can be truncated to consider just the first r lower modes, ($r < n$). That is,

$$R(t) \approx \sum_{j=1}^r \rho_j z_j(t) , \quad (2.15)$$

which is just an approximation to the actual value of $R(t)$. It has been shown earlier Singh and Chu [45] that a response spectrum approach based on this MD method requires the base input to be defined in terms of the relative displacement (or the more commonly used pseudo-acceleration) and relative velocity ground spectra.

For some response quantities, the error due to the truncation of modes can become significant. It depends upon the contribution of the forcing function to the response quantity at the truncated frequencies of the structure. The mode acceleration (MA) approach of structural dynamics [15] was first proposed to approximate the contribution of the truncated higher modes and reduce the error. In this approach equation (ref1.13) is modified, with substitution of $z_j(t)$ in terms of $\ddot{z}(t)_j$ and $\dot{z}_j(t)$ from equation (2.7), as follows:

$$R(t) = \sum_{j=1}^n \rho_j \left(\frac{-\gamma_j \ddot{x}_g(t) - \ddot{z}_j(t) - 2\beta_j \omega_j \dot{z}_j(t)}{\omega_j^2} \right), \quad (2.16)$$

which can be rearranged to provide:

$$R(t) = -\ddot{x}_g(t) \sum_{j=1}^n \left(\frac{\rho_j \gamma_j}{\omega_j^2} \right) - \sum_{j=1}^n \frac{\rho_j}{\omega_j^2} (\ddot{z}_j(t) + 2\beta_j \omega_j \dot{z}_j(t)). \quad (2.17)$$

The first summation term of this equation has been shown [50] to be the static response caused by the inertial forces corresponding to a ground acceleration of unit magnitude. For completeness, this is shown here also in a slightly different form. By considering the vectors

$$\{\rho\} = \{\mathcal{R}\}^T [\Phi] \quad , \quad \{\gamma\} = [\Phi]^T [M] \{\mathcal{I}\}, \quad (2.18)$$

which, respectively, contain the modal response quantities and the modal participation factors, it is possible to write for this summation term as follows:

$$\sum_{j=1}^n \left(\frac{\rho_j \gamma_j}{\omega_j^2} \right) = \{\rho\}^T [\Lambda]^{-1} \{\gamma\} = \{\mathcal{R}\}^T [\Phi] [\Lambda]^{-1} [\Phi]^T [M] \{\mathcal{I}\}. \quad (2.19)$$

The diagonal matrix $[\Lambda]^{-1}$ can be deduced from equation (2.4) as

$$[\Lambda]^{-1} = [\Phi]^{-1} [K]^{-1} [\Phi]^{-T}. \quad (2.20)$$

Substitution of this equation into equation (2.19) provides us:

$$\sum_{j=1}^n \left(\frac{\rho_j \gamma_j}{\omega_j^2} \right) = \{\mathcal{R}\}^T [K]^{-1} [M] \{\mathcal{I}\} = \{\mathcal{R}\}^T \{X_s\} = R_s, \quad (2.21)$$

where $\{X_s\}$ is the solution of the following static system

$$[K] \{X_s\} = [M] \{\mathcal{I}\} , \quad (2.22)$$

and R_s is the corresponding static solution of the response quantity of interest. Equation (2.21) can be substituted into equation (2.17) to get

$$R(t) = -\ddot{x}_g(t) R_s - \sum_{j=1}^n \frac{\rho_j}{\omega_j^2} (\ddot{z}_j(t) + 2\beta_j \omega_j \dot{z}_j(t)) . \quad (2.23)$$

If the truncation of modes is effected, this expression becomes

$$R(t) \approx -\ddot{x}_g(t) R_s - \sum_{j=1}^r \frac{\rho_j}{\omega_j^2} (\ddot{z}_j(t) + 2\beta_j \omega_j \dot{z}_j(t)) , \quad (2.24)$$

which is the basis of the MA approach. The term $-\ddot{x}_g(t)R_s$ is known as the pseudo-static contribution of all modes, whereas the summation terms provides the different modal increments, from the pseudo-static response, to reach the actual dynamic response.

The MA method represents an improvement with respect to the truncated MD approach since the MA procedure considers the pseudo-static contributions of the truncated modes, which contribute to the total dynamic response in a static fashion when the higher frequencies of the forcing function are much lower than the frequencies of the upper modes. A mode acceleration-based response spectrum approach was developed by Singh [44] and Singh and Mehta [50]. However, such approach required that the base input motion be defined in terms of relative velocity and acceleration response spectra. The relative acceleration spectra similar to the commonly used pseudo-acceleration spectra can also be developed for design purposes [32], but they are rarely used. This seems to limit the utility of the previously proposed [50] mode acceleration-based response spectrum approach.

To circumvent this practical limitation of the mode acceleration formulation, equation (2.24) is modified with the help of equation (2.7) as follows. The term in the parenthesis of equation (2.24) is substituted again to get

$$R(t) \approx -\ddot{x}_g(t) R_s - \sum_{j=1}^r \frac{\rho_j}{\omega_j^2} \left(-\gamma_j \ddot{x}_g(t) - \omega_j^2 z_j(t) \right) , \quad (2.25)$$

which can be rewritten as

$$R(t) \approx -\ddot{x}_g(t) C_s + \sum_{j=1}^r \rho_j z_j(t) , \quad (2.26)$$

where the coefficient C_s is given by

$$C_s = R_s - \sum_{j=1}^r \frac{\rho_j \gamma_j}{\omega_j^2} . \quad (2.27)$$

Equation (2.26) constitutes the modified mode acceleration (MMA) approach. In a slightly different form, equation (2.26) has been used earlier [18], [27]. Recently its use in modal analysis has also been advocated by Leger and Wilson [26]. The summation term in equation (2.26) is the classical mode displacement expression with a reduced number of modes. The first term represents the pseudostatic response correction to account for the missing contribution of only the truncated higher modes.

All quantities in equation (2.26) are still expressed in terms of the characteristics of the first r modes. Also, the dynamic response term is now expressed in terms of the modal displacement z_j , unlike equation (2.24) where the dynamic term was expressed in terms of modal velocity, \dot{z}_j and acceleration \ddot{z}_j . As it is shown in the next two sections, this will be of direct help in the development of a response spectrum approach which will not require the relative acceleration spectrum of the base input.

2.3 Mean Square Value Response

For calculating the design value of a general response quantity $R(t)$ in the stochastic approach it is common to obtain its root mean square value and amplify it by a suitable peak factor. This approach also directly leads to the response spectrum approach.

In general, seismic motions can be considered as zero mean random processes. Consequently, the responses of linear systems to this type of excitations are also zero mean processes. For responses with zero mean values, their standard deviations coincide with the square root of the mean square values. That is,

$$\sigma_R = \sqrt{E[R^2(t)]}, \quad (2.28)$$

where $E[.]$ denotes the expected value of $[.]$, and σ_R is the standard deviation of $R(t)$.

To obtain the mean square value, we first obtain the response autocorrelation function. By considering equation (2.26), autocorrelation function can be expressed as

$$E[R(t_1) R(t_2)] = E \left[\left(-\tilde{x}_g(t_1) C_s + \sum_{j=1}^r \rho_j z_j(t_1) \right) \left(-\tilde{x}_g(t_2) C_s + \sum_{k=1}^r \rho_k z_k(t_2) \right) \right]. \quad (2.29)$$

It can be expanded, and the expected values distributed to provide

$$\begin{aligned} E[R(t_1) R(t_2)] &= C_s^2 E[\tilde{x}_g(t_1) \tilde{x}_g(t_2)] \\ &- C_s \sum_{j=1}^r \rho_j (E[z_j(t_1) \tilde{x}_g(t_2)] + E[\tilde{x}_g(t_1) z_j(t_2)]) \\ &+ \sum_{j=1}^r \sum_{k=1}^r \rho_j \rho_k E[z_j(t_1) z_k(t_2)]. \end{aligned} \quad (2.30)$$

This equation provides the mean square value of the response $R(t)$, by setting $t_1 = t_2 = t$ as:

$$\begin{aligned}
E[R^2(t)] &= C_s^2 E[\tilde{x}_g^2(t)] - C_s \sum_{j=1}^r \rho_j (E[z_j(t) \tilde{x}_g(t)] + E[\tilde{x}_g(t) z_j(t)]) \\
&+ \sum_{j=1}^r \sum_{k=1}^r \rho_j \rho_k E[z_j(t) z_k(t)] .
\end{aligned} \tag{2.31}$$

It is assumed that the input motions are samples of a stationary random process, although earthquake motions are not stationary process in a strict sense. In most seismic accelerograms, three different stages can be recognized. That is, (1) a initial stage, where the acceleration magnitudes are small and begin to increase, (2) a strong motion stage, characterized by large magnitudes and containing the maximum accelerations and maximum structural responses, and (3) a final stage, where the accelerations decrease till the motion subsides. A conservative assumption is to consider the earthquakes as being composed of the strong motion phase with infinite duration and stationarity characteristics. This assumption has been found to be acceptable in several earlier studies.

For stationary ground motion, the autocorrelation function for the ground acceleration can be written in terms of its spectral density function $\Phi_g(\omega)$ as:

$$E[\tilde{x}_g(t_1) \tilde{x}_g(t_2)] = \int_{-\infty}^{\infty} \Phi_g(\omega) e^{i\omega(t_1-t_2)} d\omega . \tag{2.32}$$

From which we can obtain the mean square value of the ground acceleration as:

$$E[\tilde{x}_g^2(t)] = \int_{-\infty}^{\infty} \Phi_g(\omega) d\omega = \sigma_g^2 , \tag{2.33}$$

where σ_g is the standard deviation of the ground acceleration $\tilde{x}_g(t)$.

By considering the expression of $z_j(t)$ given by equation (2.9), the crosscorrelation $E[z_j(t_1) \tilde{x}_g(t_2)]$ can be expressed as follows:

$$E[z_j(t_1) \tilde{x}_g(t_2)] = -\gamma_j \int_0^{t_1} h_j(t_1 - \tau_1) E[\tilde{x}_g(\tau_1) \tilde{x}_g(t_2)] d\tau_1 , \quad (2.34)$$

Utilizing equation (2.32) with the appropriate arguments, one obtains

$$E[z_j(t_1) \tilde{x}_g(t_2)] = -\gamma_j \int_{-\infty}^{\infty} \int_0^{t_1} \Phi_g(\omega) h_j(t_1 - \tau_1) e^{i\omega(\tau_1 - t_2)} d\tau_1 d\omega . \quad (2.35)$$

A change of variable ($u = t_1 - \tau_1$) and rearrangement of integrals yields

$$E[z_j(t_1) \tilde{x}_g(t_2)] = -\gamma_j \int_{-\infty}^{\infty} \Phi_g(\omega) e^{i\omega(t_1 - t_2)} \mathcal{H}_j^c(\omega, t_1) d\omega , \quad (2.36)$$

where

$$\mathcal{H}_j^c(\omega, t_1) = \int_0^{t_1} h_j(u) e^{-i\omega u} du \quad (2.37)$$

is the complex transient frequency response function of a damped single-degree-of-freedom oscillator. A superscript c indicates a complex quantity and the superscripts cc denote its complex conjugate. In the limit as $t_1 \rightarrow \infty$, $\mathcal{H}_j^c(\omega, t_1)$ becomes the stationary transfer function $H_j^c(\omega)$:

$$\lim_{t_1 \rightarrow \infty} \mathcal{H}_j^c(\omega, t_1) = H_j^c(\omega) = [\omega_j^2 - \omega^2 + i 2\beta_j \omega_j \omega]^{-1} , \quad (2.38)$$

which satisfies the following equations:

$$\ddot{z}_j(t) + 2\beta_j \omega_j \dot{z}_j(t) + \omega_j^2 z_j(t) = e^{i\omega t} , \quad z_j(t) = H_j^c(\omega) e^{i\omega t} . \quad (2.39)$$

Thus, as t_1 and t_2 tend to infinity, that is, when the system has been acted upon for a long time relative to its period, and the response has attained stationarity at the limit, as $t_1 \rightarrow t_2 \rightarrow t \rightarrow \infty$, equation (2.37) becomes

$$E[z_j(t_1) \tilde{x}_g(t_2)] = -\gamma_j \int_{-\infty}^{\infty} \Phi_g(\omega) H_j^c(\omega) e^{i\omega(t_1 - t_2)} d\omega . \quad (2.40)$$

Similarly, one can show that as $t_1 \rightarrow \infty$ and $t_2 \rightarrow \infty$

$$\lim_{t_1, t_2 \rightarrow \infty} E[\tilde{x}_g(t_1) z_j(t_2)] = -\gamma_j \int_{-\infty}^{\infty} \Phi_g(\omega) H_j^c(\omega) e^{i\omega(t_1-t_2)} d\omega, \quad (2.41)$$

One can also express the crosscorrelation $E[z_j(t_1) z_k(t_2)]$ in terms of the spectral density and frequency response function. With the help of equation (2.9), this crosscorrelation can be rewritten as

$$E[z_j(t_1) z_k(t_2)] = \gamma_j \gamma_k \int_0^{t_1} \int_0^{t_2} h_j(t_1-\tau_1) h_k(t_2-\tau_2) E[\tilde{x}_g(\tau_1) \tilde{x}_g(\tau_2)] d\tau_1 d\tau_2, \quad (2.42)$$

Substituting equation (2.32), with the appropriate arguments, one obtains:

$$E[z_j(t_1) z_k(t_2)] = \gamma_j \gamma_k \int_{-\infty}^{\infty} \int_0^{t_1} \int_0^{t_2} \Phi_g(\omega) h_j(t_1-\tau_1) h_k(t_2-\tau_2) e^{i\omega(\tau_1-\tau_2)} d\tau_1 d\tau_2 d\omega. \quad (2.43)$$

Again with a change of variables as $u = t_1 - \tau_1$, $v = t_2 - \tau_2$, and a rearrangement of integrals yields

$$E[z_j(t_1) z_k(t_2)] = \gamma_j \gamma_k \int_{-\infty}^{\infty} \Phi_g(\omega) e^{i\omega(t_1-t_2)} \int_0^{t_1} h_j(u) e^{-i\omega u} du \int_0^{t_2} h_k(v) e^{i\omega v} dv d\omega, \quad (2.44)$$

where equation (2.37) and its complex conjugate can be invoked to write

$$E[z_j(t_1) z_k(t_2)] = \gamma_j \gamma_k \int_{-\infty}^{\infty} \Phi_g(\omega) e^{i\omega(t_1-t_2)} \mathcal{H}_j^c(\omega, t_1) \mathcal{H}_k^{cc}(\omega, t_2) d\omega. \quad (2.45)$$

Again for large time values of t_1 and t_2 , the crosscorrelation attains a stationary value as

$$E[z_j(t_1) z_k(t_2)] = \gamma_j \gamma_k \int_{-\infty}^{\infty} \Phi_g(\omega) H_j^c(\omega) H_k^{cc}(\omega) e^{i\omega(t_1-t_2)} d\omega. \quad (2.46)$$

Equations (2.33), (2.40), (2.41), and (2.46) with $t_1 = t_2 = t$, can now be substituted into equation (2.32) to get the stationary mean square value of the response

$R(t)$ as,

$$\begin{aligned} E[R^2(t)] &= C_s^2 \sigma_g^2 + C_s \sum_{j=1}^r \rho_j \gamma_j \int_{-\infty}^{\infty} \Phi(\omega) [H_j^c(\omega) + H_j^{cc}(\omega)] d\omega \\ &+ \sum_{j=1}^r \sum_{k=1}^r \rho_j \rho_k \gamma_j \gamma_k \int_{-\infty}^{\infty} \Phi_g(\omega) H_j^c(\omega) H_k^{cc}(\omega) d\omega . \end{aligned} \quad (2.47)$$

The double summation terms can be decomposed into two terms. Terms with $j = k$ (also called as the diagonal terms), and terms with $j \neq k$ (off-diagonal terms). The, equation (2.47) is rewritten as follows:

$$\begin{aligned} E[R^2(t)] &= C_s^2 \sigma_g^2 + C_s \sum_{j=1}^r \rho_j \gamma_j \int_{-\infty}^{\infty} \Phi(\omega) [H_j^c(\omega) + H_j^{cc}(\omega)] d\omega \\ &+ \sum_{j=1}^r \rho_j^2 \gamma_j^2 \int_{-\infty}^{\infty} \Phi_g(\omega) |H_j^c(\omega)|^2 d\omega \\ &+ \sum_{j=1}^r \sum_{\substack{k=1 \\ k \neq j}}^r \rho_j \rho_k \gamma_j \gamma_k \int_{-\infty}^{\infty} \Phi_g(\omega) H_j^c(\omega) H_k^{cc}(\omega) d\omega . \end{aligned} \quad (2.48)$$

This equation possesses four general terms. The first term represents the pseudostatic contribution of the truncated higher modes. The second term is the correlation between the pseudostatic response due to the truncated modes, and the dynamic response due to the retained modes. The last two terms are the same as those in the truncated mode displacement-based approach. The single summation part of the third term represent the squared contributions of individual modes, it is the base of the classical square root of the sum of the squares (SRSS) approach. The double summation part of the third term, on the other hand, represents the contributions due to the modal correlations between the retained modes.

To be able to obtain a response spectrum approach, it is necessary to simplify equation (2.48) further. We first examine the second term, where the sum $H_j^c(\omega) + H_j^{cc}(\omega)$ can be written as

$$[H_j^c(\omega) + H_j^{cc}(\omega)] = 2 \operatorname{Re}[H_j^c(\omega)] = 2(\omega_j^2 - \omega^2) |H_j^c(\omega)|^2 , \quad (2.49)$$

where

$$|H_j^c(\omega)|^2 = H_j^c(\omega) H_j^{cc}(\omega) = [\omega_j^4 + (4\beta_j^2 - 2)\omega_j^2 \omega^2 + \omega^4]^{-1} . \quad (2.50)$$

By utilizing equation (2.49), the integral in the second term of equation (2.48) can be written as

$$\int_{-\infty}^{\infty} \Phi(\omega) [H_j^c(\omega) + H_j^{cc}(\omega)] d\omega = 2(\omega_j^2 I_j^d - I_j^v) . \quad (2.51)$$

where the quantities I_j^d and I_j^v denote the following frequency integrals

$$I_j^d = \int_{-\infty}^{\infty} \Phi_g(\omega) |H_j^c(\omega)|^2 d\omega \quad , \quad I_j^v = \int_{-\infty}^{\infty} \Phi_g(\omega) \omega^2 |H_j^c(\omega)|^2 d\omega . \quad (2.52)$$

These integrals are, respectively, the mean square values of the relative displacement and relative velocity responses associated with the j^{th} single-degree-of-freedom oscillator, with frequency ω_j and damping ratio β_j , subjected to the base acceleration $\ddot{x}_g(t)$. For zero mean processes, these mean square values coincide with their respective variances. That is,

$$I_j^d = \sigma_{d_j}^2 \quad , \quad I_j^v = \sigma_{v_j}^2 \quad , \quad (2.53)$$

where σ_{d_j} and σ_{v_j} are the standard deviations of the relative displacement and relative velocity responses of the j^{th} oscillator. Appendix G provides closed form expressions for I_j^d and I_j^v when the spectral density function of the input is defined by a white noise or by a Kanai-Tajimi type of function.

It is noted that the frequency integral in the third term of equation (2.48) is just I_j^d . We will now express the integral in the fourth term, denoted as ζ_{jk} , in terms of the frequency integrals in equation (2.52).

$$\zeta_{jk} = \int_{-\infty}^{\infty} \Phi_g(\omega) H_j^c(\omega) H_k^{cc}(\omega) d\omega . \quad (2.54)$$

In this expression, the product $H_j^c(\omega) H_k^c(\omega)$ can be written in terms of the squared modulus of the transfer functions, that is,

$$\begin{aligned} H_j^c(\omega) H_k^c(\omega) &= [H_j^{cc}(\omega) H_k^c(\omega)] |H_j^c(\omega)|^2 |H_k^c(\omega)|^2 \\ &= [\mathcal{E}(\omega) + i \mathcal{O}(\omega)]^{-1} |H_j^c(\omega)|^2 |H_k^c(\omega)|^2, \end{aligned} \quad (2.55)$$

where $\mathcal{E}(\omega)$ and $\mathcal{O}(\omega)$ are, respectively, even and odd polynomials in ω :

$$\mathcal{E}(\omega) = \omega^4 + (4\beta_j \beta_k \omega_j \omega_k - \omega_j^2 - \omega_k^2) \omega^2 + \omega_j^2 \omega_k^2, \quad (2.56)$$

$$\mathcal{O}(\omega) = 2 [(\beta_j \omega_j - \beta_k \omega_k) \omega^3 + (\beta_k \omega_j - \beta_j \omega_k) \omega_j \omega_k \omega]. \quad (2.57)$$

Substitution of equation (2.55) into equation (2.54) renders

$$\zeta_{jk} = \int_{-\infty}^{\infty} \Phi_g(\omega) [\mathcal{E}(\omega) + i \mathcal{O}(\omega)] |H_j^c(\omega)|^2 |H_k^c(\omega)|^2 d\omega. \quad (2.58)$$

It can be noticed that the only odd function of ω , in this expression, is $\mathcal{O}(\omega)$. As a consequence, the imaginary term containing $\mathcal{O}(\omega)$ vanishes when integrated from $-\infty$ to ∞ . Therefore, the expression for ζ_{jk} is reduced to

$$\zeta_{jk} = \zeta_{kj} = \int_{-\infty}^{\infty} \Phi_g(\omega) \mathcal{E}(\omega) |H_j^c(\omega)|^2 |H_k^c(\omega)|^2 d\omega. \quad (2.59)$$

The symmetry of ζ_{jk} with respect to the indexes j and k is due to the symmetry of the polynomial \mathcal{E}_{jk} . The factors $\mathcal{E}(\omega) |H_j^c(\omega)|^2 |H_k^c(\omega)|^2$ can be expanded into the following partial fractions, by using the procedure given in Case IV of appendix A:

$$\mathcal{E}(\omega) |H_j^c(\omega)|^2 |H_k^c(\omega)|^2 = (T_{jk}^I + \omega^2 T_{jk}^{II}) |H_j^c(\omega)|^2 + (T_{jk}^{III} - \omega^2 T_{jk}^{II}) |H_j^c(\omega)|^2, \quad (2.60)$$

where the partial fraction coefficients are:

$$T_{jk}^I = [\Omega_{jk}^2 + 4\beta_j \beta_k \Omega_{jk}^3 - (1 - 4\beta_j^2) \Omega_{jk}^4] d_{jk}^{-1}, \quad (2.61)$$

$$T_{jk}^{II} = [\Omega_{jk}^2 - 1] \omega_k^{-2} d_{jk}^{-1} , \quad (2.62)$$

$$T_{jk}^{III} = [-1 + 4\beta_j^2 + 4\beta_j \beta_k \Omega_{jk} + \Omega_{jk}^2] d_{jk}^{-1} , \quad (2.63)$$

with $\Omega_{jk} = \omega_j/\omega_k$ and

$$d_{jk} = 1 + 4\beta_j \beta_k \Omega_{jk} + (4\beta_j^2 + 4\beta_k^2 - 2) \Omega_{jk}^2 + 4\beta_j \beta_k \Omega_{jk}^3 + \Omega_{jk}^4 . \quad (2.64)$$

After substitution of equation (2.60) into (2.61), the modal correlation coefficients become

$$\zeta_{jk} = \int_{-\infty}^{\infty} \Phi_g(\omega) \left[(T_{jk}^I + \omega^2 T_{jk}^{II}) |H_j^c(\omega)|^2 + (T_{jk}^{III} - \omega^2 T_{jk}^{II}) |H_k^c(\omega)|^2 \right] d\omega , \quad (2.65)$$

which can be written in terms of the frequency integrals of equation (2.52) as:

$$\zeta_{jk} = T_{jk}^I I_j^d + T_{jk}^{II} (I_j^v - I_k^v) + T_{jk}^{III} I_k^d . \quad (2.66)$$

The above mentioned symmetry $\zeta_{jk} = \zeta_{kj}$ demands that

$$T_{jk}^I = T_{kj}^{III} , \quad T_{jk}^{II} = -T_{kj}^{II} , \quad (2.67)$$

which can be easily shown to be true.

By substitution of equations (2.51), (2.52), and (2.66) into equation (2.48), we obtain the following expression for the mean square value of the response $R(t)$:

$$\begin{aligned} E[R^2(t)] &= C_s^2 \sigma_g^2 + 2 C_s \sum_{j=1}^r \rho_j \gamma_j (\omega_j^2 I_j^d - I_j^v) + \sum_{j=1}^r \rho_j^2 \gamma_j^2 I_j^d \\ &+ \sum_{j=1}^r \sum_{\substack{k=1 \\ k \neq j}}^r \rho_j \rho_k \gamma_j \gamma_k [T_{jk}^I I_j^d + T_{jk}^{II} (I_j^v - I_k^v) + T_{jk}^{III} I_k^d] , \end{aligned} \quad (2.68)$$

and, due to the symmetry of the double summation terms with respect to jk , the number of calculations can be substantially reduced by just duplicating the contri-

butions of only the upper off-diagonal terms. Thus,

$$\begin{aligned}
E[R^2(t)] &= \sigma_R^2 = C_s^2 \sigma_g^2 + 2 C_s \sum_{j=1}^r \rho_j \gamma_j \left(\omega_j^2 I_j^d - I_j^v \right) \\
&+ \sum_{j=1}^r \rho_j^2 \gamma_j^2 I_j^d + 2 \sum_{j=1}^{r-1} \sum_{k=j+1}^r \rho_j \rho_k \gamma_j \gamma_k \left[T_{jk}^I I_j^d + T_{jk}^{II} \left(I_j^v - I_k^v \right) + T_{jk}^{III} I_k^d \right].
\end{aligned} \tag{2.69}$$

This expression presents the advantages of both, the MD and the MA approaches. That is, except for the calculation of C_s by a simple static analysis, no extra information than that required by the classical MD method is needed and it also considers the contribution of the truncated modes. Equation (2.69) is used in the following section to develop a response spectrum approach.

2.4 Response Spectrum Method by the MMD approach

In the previous section, we obtained the expression for the mean square response defined in terms of the frequency integrals, which were in turn defined in terms of the ground motion spectral density functions. We will now use this expressions to obtain the design response, expressed in terms of the ground response spectra.

The design response values can be chosen to be a suitable amplified root mean square response value σ_R as:

$$\mathcal{M}_R = \mathcal{P}_R \sigma_R, \tag{2.70}$$

The amplification factor \mathcal{P}_R is often called as the peak factor for the response $R(t)$. The root mean square value σ_R is defined by equation (2.69). Equation (2.70) thus defines the design response in terms of the mean square value of the ground accelera-

tion, as well as the mean square values of the relative displacement and relative velocity responses of the single-degree-of-freedom oscillators expressed in equation (2.52). These mean square values, however, can also be defined in terms of their maximum values through their respective peak factors. For example, the mean square value of the ground acceleration can be written as:

$$\sigma_g^2 = \frac{\mathcal{M}_g^2}{\mathcal{P}_g^2} . \quad (2.71)$$

Where \mathcal{M}_g is the maximum ground acceleration and \mathcal{P}_g is the peak factor for the ground acceleration.

Similarly, the variances represented by the frequency integrals I_j^d and I_j^v , can also be expressed in terms of their maximum values and associated peak factors as:

$$I_j^d = \sigma_{d_j}^2 = \frac{\mathcal{M}_{d_j}^2}{\mathcal{P}_{d_j}^2} , \quad I_j^v = \sigma_{v_j}^2 = \frac{\mathcal{M}_{v_j}^2}{\mathcal{P}_{v_j}^2} , \quad (2.72)$$

where \mathcal{M}_{d_j} is the maximum relative displacement of the j^{th} single degree of freedom oscillator when subjected to the seismic ground acceleration $\ddot{x}_g(t)$, and \mathcal{M}_{v_j} is the maximum relative velocity of the same oscillator. The peak factors \mathcal{P}_{d_j} and \mathcal{P}_{v_j} are associated to the relative displacement and relative velocity respectively.

The maximum value \mathcal{M}_{d_j} is known as the relative displacement response spectra. It can be obtained from the commonly used pseudo-acceleration spectra \mathcal{M}_{pa_j} as:

$$\mathcal{M}_{d_j} = \omega_j^{-2} \mathcal{M}_{pa_j} . \quad (2.73)$$

\mathcal{M}_{v_j} is the relative velocity spectra. If such spectra are not available, they can be approximated by the pseudo-velocity spectra \mathcal{M}_{pv_j} as:

$$\mathcal{M}_{v_j} \approx \mathcal{M}_{pv_j} = \omega_j^{-1} \mathcal{M}_{pa_j} . \quad (2.74)$$

This approximation, however, can introduce some error in the calculation of the design response. Utilizing equations (2.69), (2.71) and (2.72) into equation (2.70) we obtain for the design response as:

$$\begin{aligned} \mathcal{M}_R^2 = & \mathcal{P}_R^2 \left\{ C_s^2 \frac{\mathcal{M}_g^2}{\mathcal{P}_g^2} + 2 C_s \sum_{j=1}^r \rho_j \gamma_j \left(\omega_j^2 \frac{\mathcal{M}_{d_j}^2}{\mathcal{P}_{d_j}^2} - \frac{\mathcal{M}_{v_j}^2}{\mathcal{P}_{v_j}^2} \right) + \sum_{j=1}^r \rho_j^2 \gamma_j^2 \frac{\mathcal{M}_{d_j}^2}{\mathcal{P}_{d_j}^2} \right. \\ & \left. + 2 \sum_{j=1}^{r-1} \sum_{k=j+1}^r \rho_j \rho_k \gamma_j \gamma_k \left[T_{jk}^I \frac{\mathcal{M}_{d_j}^2}{\mathcal{P}_{d_j}^2} + T_{jk}^{II} \left(\frac{\mathcal{M}_{v_j}^2}{\mathcal{P}_{v_j}^2} - \frac{\mathcal{M}_{v_k}^2}{\mathcal{P}_{v_k}^2} \right) + T_{jk}^{III} \frac{\mathcal{M}_{d_k}^2}{\mathcal{P}_{d_k}^2} \right] \right\}. \end{aligned} \quad (2.75)$$

The peak factors appearing in equation (2.75) can be defined in terms of a predecided probability of exceedance level. Usually they all will be slightly different from each other. However, if only a few dominant modes primarily contribute to the response quantity, then the peak factor associated with these modes will be nearly equal to the peak factor of the response. This usually is the case in seismic response analysis. It is therefore fairly accurate to assume all the peak factors to be equal. That is,

$$\left(\frac{\mathcal{P}_R}{\mathcal{P}_g} \right)^2 \approx \left(\frac{\mathcal{P}_R}{\mathcal{P}_{d_j}} \right)^2 \approx \left(\frac{\mathcal{P}_R}{\mathcal{P}_{v_j}} \right)^2 \approx 1. \quad (2.76)$$

With this assumption one obtains \mathcal{M}_R^2 to get

$$\begin{aligned} \mathcal{M}_R^2 \approx & C_s^2 \mathcal{M}_g^2 + 2 C_s \sum_{j=1}^r \rho_j \gamma_j \left(\omega_j^2 \mathcal{M}_{d_j}^2 - \mathcal{M}_{v_j}^2 \right) + \sum_{j=1}^r \rho_j^2 \gamma_j^2 \mathcal{M}_{d_j}^2 \\ & + 2 \sum_{j=1}^{r-1} \sum_{k=j+1}^r \rho_j \rho_k \gamma_j \gamma_k \left[T_{jk}^I \mathcal{M}_{d_j}^2 + T_{jk}^{II} \left(\mathcal{M}_{v_j}^2 - \mathcal{M}_{v_k}^2 \right) + T_{jk}^{III} \mathcal{M}_{d_k}^2 \right], \end{aligned} \quad (2.77)$$

If the pseudo acceleration spectra are used to define the relative displacement spectra, equation (2.76) can be written as

$$\begin{aligned} \mathcal{M}_R^2 \approx & C_s^2 \mathcal{M}_g^2 + 2 C_s \sum_{j=1}^r \rho_j \gamma_j \left(\frac{\mathcal{M}_{pa_j}^2}{\omega_j^2} - \mathcal{M}_{v_j}^2 \right) + \sum_{j=1}^r \rho_j^2 \gamma_j^2 \frac{\mathcal{M}_{pa_j}^2}{\omega_j^4} \\ & + 2 \sum_{j=1}^{r-1} \sum_{k=j+1}^r \rho_j \rho_k \gamma_j \gamma_k \left[T_{jk}^I \frac{\mathcal{M}_{pa_j}^2}{\omega_j^4} + T_{jk}^{II} \left(\mathcal{M}_{v_j}^2 - \mathcal{M}_{v_k}^2 \right) + T_{jk}^{III} \frac{\mathcal{M}_{pa_k}^2}{\omega_k^4} \right]. \end{aligned} \quad (2.78)$$

Equation (2.78) is the statement of the proposed response spectrum approach for calculating the design response from prescribed ground response spectra. Again,

as mentioned in the previous section, the last two terms in equation (2.78) are the same as those in the mode displacement-based response spectrum approach, implemented with the first r modes. The single summation part of these two terms is the classical SRSS approach. The first term of equation (2.78) is the pseudostatic response contribution of the truncated higher modes to the squared response. The second term represents the correlation between the pseudostatic response due to the truncated modes and the dynamic response due to the retained modes. The relative contributions of these terms with respect to the total response are reported in the following section for various numerical examples considered herein.

By considering the expression of C_s , equation (2.27), it can be noticed that this coefficient depends on the number of retained modes. It becomes zero when all n modes are included in the dynamic analysis, and consequently, the MMD approach of equation (2.78) reduces to the MD approach without truncation of upper modes.

Both equations (2.77) and (2.78) use the relative velocity spectra $\mathcal{M}_{v,j}$, but such spectra are not always available. The earthquake engineering community have commonly used the pseudo-velocity spectra $\mathcal{M}_{pv,j}$ as a replacement. $\mathcal{M}_{pv,j}$ can be obtained from the pseudo-acceleration spectra $\mathcal{M}_{pa,j}$ as

$$\mathcal{M}_{pv,j} = \mathcal{M}_{pa,j}/\omega_j . \quad (2.79)$$

However, substitution of equation (2.79) into equations (2.77) or (2.78) shows that the second term in these equations vanishes. This implies that the contribution due to the correlation between truncated and retained modes becomes zero with this assumption. It introduces error in the double summation terms as well. The use of the pseudo-velocity as a replacement of the relative velocity is also analyzed in the numerical examples presented in the next section.

2.5 Numerical Results

To demonstrate the effectiveness of the proposed approach with regard to its capability to reduce the missing mass effect error, herein some numerical results are presented. The results are obtained for structures with well separated as well as closely spaced frequencies. The structure with separated frequencies considered here is a five-span continuous beam excited at its support. The model of the beam is shown in figure 2.1. The beam is discretized into 26 finite elements with 48 degrees of freedom. The mass of the beam is included through the consistent mass matrix in the analysis. In addition, each node also supports a lumped mass. The results are presented for (i) a rather stiff beam and (ii) a flexible beam. The first few frequencies of the two beams are shown in table 2.1 and it is seen that they are well separated. The numerical results are obtained for the bending moment in the beam at node 11. For this structure, the product $(\rho_j \gamma_j)$ is relatively high, even for high frequency modes, thus showing the importance of these modes in the calculation of response. A Kanai-Tajimi spectral density function with the cut-off frequency of 16 Hz and a set of pseudo-acceleration and relative velocity response spectra are considered as seismic inputs applied to this structure. For the stochastic input, the root mean square value of the response has been obtained, whereas for the response spectrum input, the response value of design interest has been obtained.

For the sake of comparison, the response values have been obtained by the following approaches: (i) the modified mode displacement (MMD) approach developed herein; (ii) the mode acceleration (MA) approach proposed in Reference [50]; (iii) the mode displacement (MD) approach of Reference [45] with truncated number of

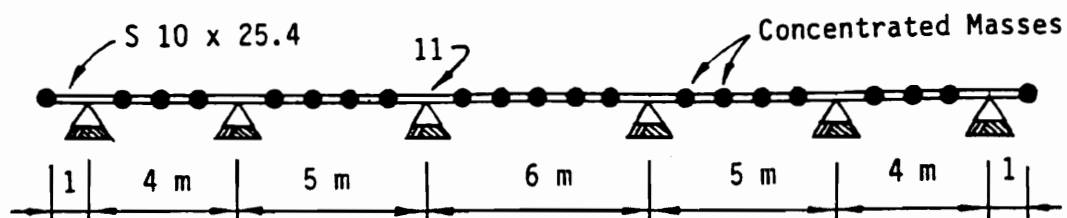


Figure 2.1: Schematic of the beam analyzed.

Table 2.1: Natural frequencies of the flexible and stiff beams.

Mode	Frequencies (Hz)	
	Flexible beam	Stiff beam
1	5.006	19.969
2	7.038	28.556
3	7.880	32.378
4	9.905	41.406
5	10.689	44.166
6	17.714	73.031
7	18.656	81.050
8	19.763	83.454
9	26.937	108.375
10	28.860	115.999
⋮	⋮	⋮
48	4230.627	4238.074

modes; (iv) the CQC approach of Reference [59] and the Rosenblueth and Elorduy approach of Reference [41] (they give almost identical results); (v) the classical square root of the sum of the squares (SRSS) approach; and (vi) the absolute sum (ABS) approach. The response value obtained by the mode displacement approach with the complete set of modes used in the analysis (that is, the values obtained from equation (2.69) with $r = n$ and $C_s = 0$, for the stochastic response, and the corresponding response spectrum expression presented in Reference [45] and in equation (2.78) with $r = n$ and $C_s = 0$, for the design response) are the benchmark values against which the values obtained by the above approaches have been compared. The differences between the benchmark response and the response values obtained by the various approaches are presented as per cent errors. All response values are obtained for a modal damping ratio of 0.03.

Figure 2.2 shows the error in the root mean square response of a bending moment in the stiff and flexible beams obtained by various approaches for increasing number of modes. The stiff beam results are shown in the top-half portion and the flexible beam results in the bottom-half portion of the figure. It is observed that for both beams the proposed approach and the mode acceleration approach both provide results with the least error for a given number of modes. The errors in the results obtained by the SRSS and CQC approaches are high even when a large number of modes are considered in the analysis; when all modes of the beam have been included this error is about 45 per cent for the stiff beam and about 20 per cent for the flexible beam. In the CQC approach, this large error is due to an improper consideration of modal correlation of the high frequency modes. For stiff structures the absolute-sum approach will usually provide better results than the SRSS and CQC approaches; this is because even the well separated modes in such structures, especially the ones with

frequencies outside the frequency range of the input, will be strongly correlated. For flexible structures, on the other hand, the absolute-sum approach provides absurd results.

In figure 2.3 we compare the contributions of various terms of equation (2.69) towards the total mean square response. The curve identified by PS shows the contribution of the pseudostatic term with increasing number of modes. When only the first few modes are considered, this contribution is quite large, especially in the stiff beam. Of course, this contribution decreases as more and more modes are considered. The symbol MD identifies the curve showing the contribution of the mode displacement term. As expected, this contribution approaches the total response as more and more modes are considered. This figure also shows the contribution of the term associated with the correlation of the pseudostatic and dynamic parts of the response. It is seen that this correlation is not insignificant, especially when only a few lower modes are considered. This is contrary to what was assumed by Gupta and Chen [18]. It is seen from equation (2.69) that this term will be zero only when the mean square values of the relative and pseudo-velocities are equal. This happens only when the input is a true white noise.

The results shown in figure 2.4 are obtained for the support input defined by response spectra. The pseudo-acceleration spectra resembled the spectra defined in reference [38] which are prescribed for the design of nuclear power plants by the Nuclear Regulatory Commission. Here, the benchmark response value is obtained from the response spectrum approach developed in Reference [45] without truncation of any modes. The validity of this approach has been verified by a numerical simulation study reported in Reference [17]. As mentioned before, the differences between the

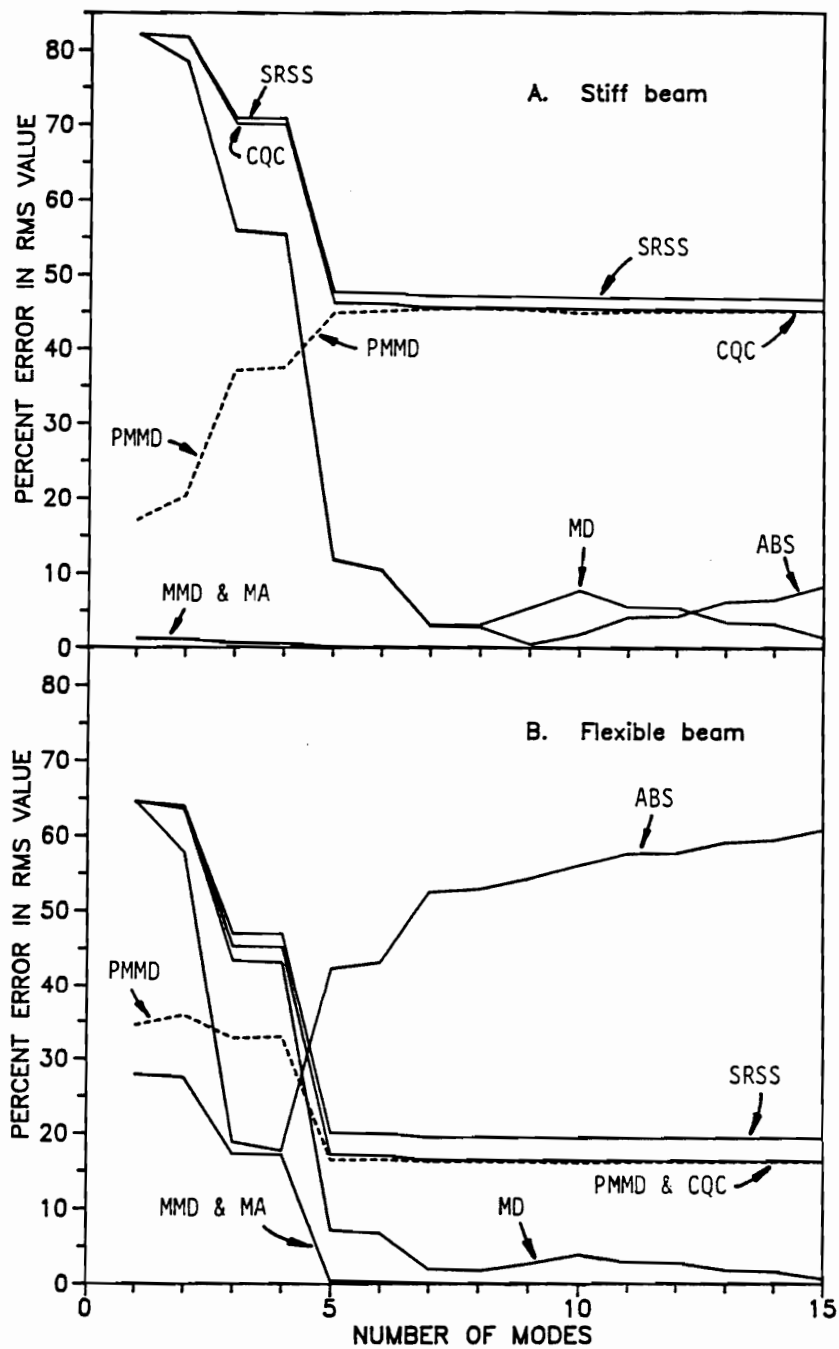


Figure 2.2: Percent error in the root mean square value of a bending moment obtained for Kanai-Tajimi spectral density function by different approaches with increasing number of modes for: (A) stiff beam, and (B) flexible beam.

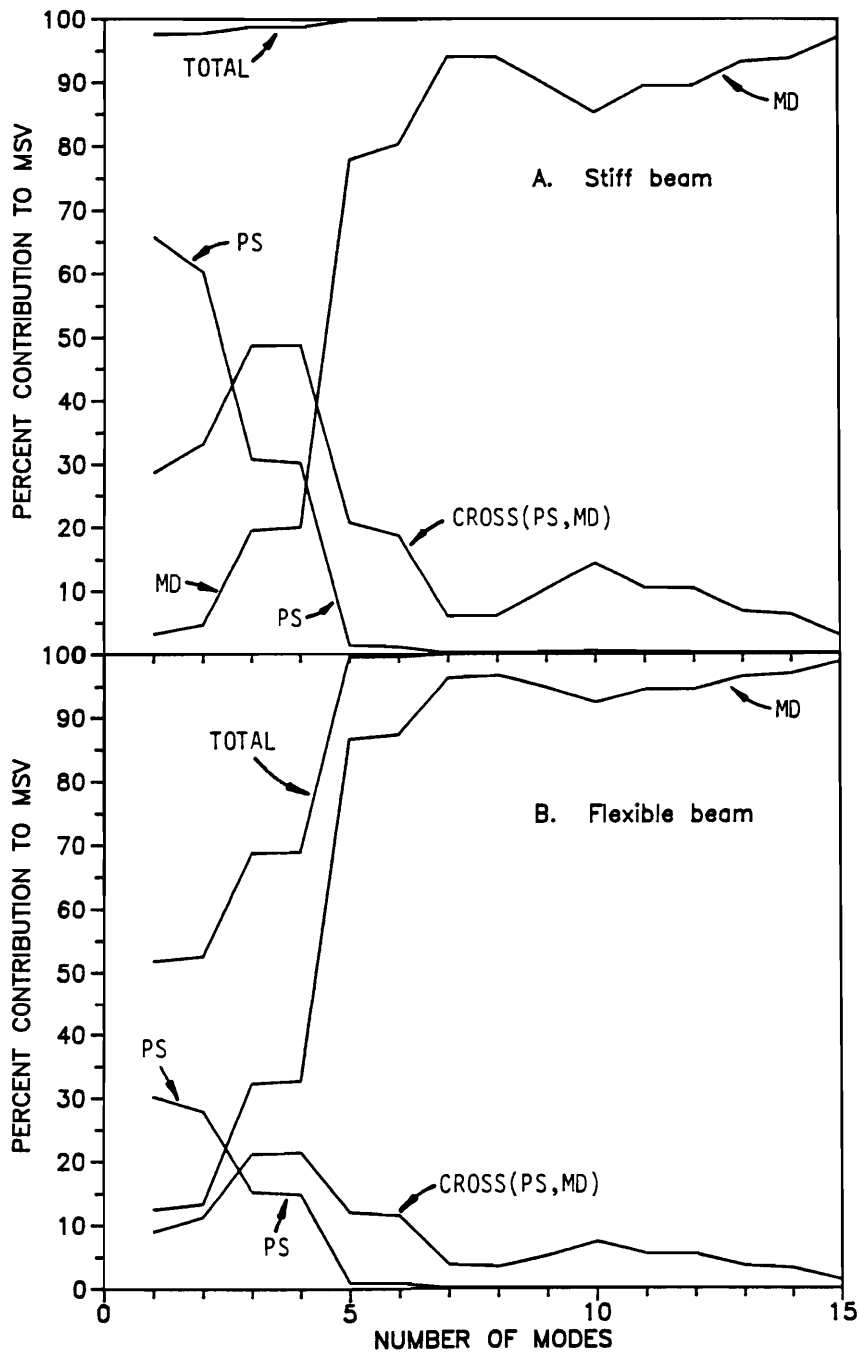


Figure 2.3: Percent contribution of various terms in the equation for the the total mean square response obtained with different number of modes for: (A) stiff beam, and (B) flexible beam.

benchmark result and the results obtained by the proposed approach are superior to those obtained by all other approaches. This superiority is especially impressive for the stiff beam. Again, the errors in the CQC and SRSS approaches are quite high, and especially so for the stiff beam.

Next some similar numerical results obtained for a 18-degrees-of-freedom building (6 stories) are shown in figure 2.5. The stiffness properties of the structure were chosen such that the frequencies are closely spaced, causing a strong correlation between the modes. Again, a relatively stiff and a relatively flexible structure were considered. The first few frequencies of the structures are shown in table 2.2. This structure was also analyzed for two inputs: (i) a Kanai-Tajimi spectral density function with a cut-off frequency of 16 Hz and (ii) the response spectra used to obtain the results in figure 2.4.

Table 2.2: Natural frequencies of the flexible and stiff building

<i>Frequencies (Hz)</i>		
<i>Mode</i>	<i>Flexible</i>	<i>Stiff</i>
1	4.997	19.987
2	5.002	20.006
3	9.081	36.322
4	11.118	44.471
5	11.123	44.491
6	15.735	62.941
7	16.393	65.571
8	16.551	66.204
9	20.885	83.541
10	20.934	83.736
⋮	⋮	⋮
18	75.508	302.032

Figure 2.6 depicts the percent error in the root mean square response for the stiff

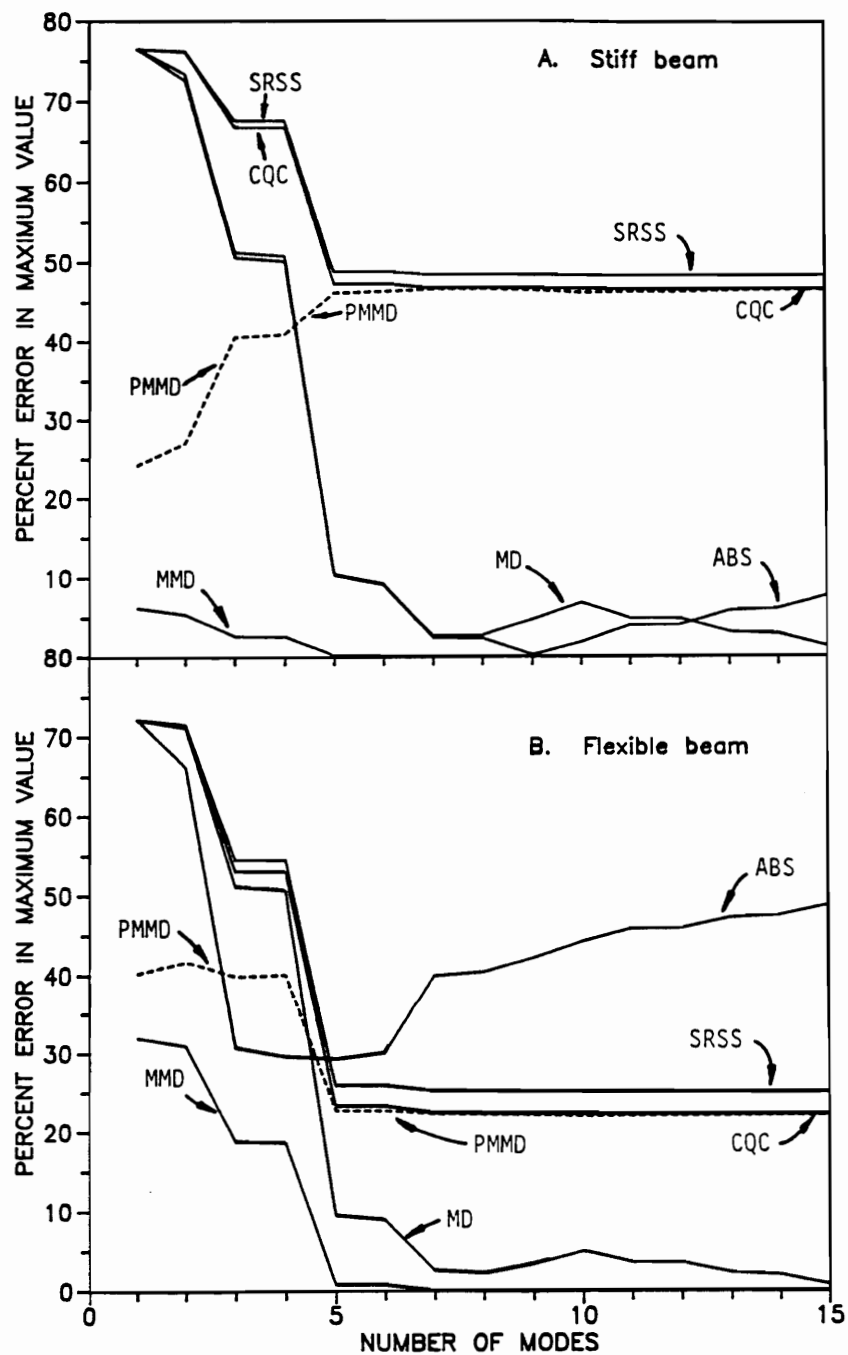


Figure 2.4: Percent error in the bending moment design response obtained for response spectrum input by different approaches with increasing number of modes for: (A) stiff beam, and (B) flexible beam.

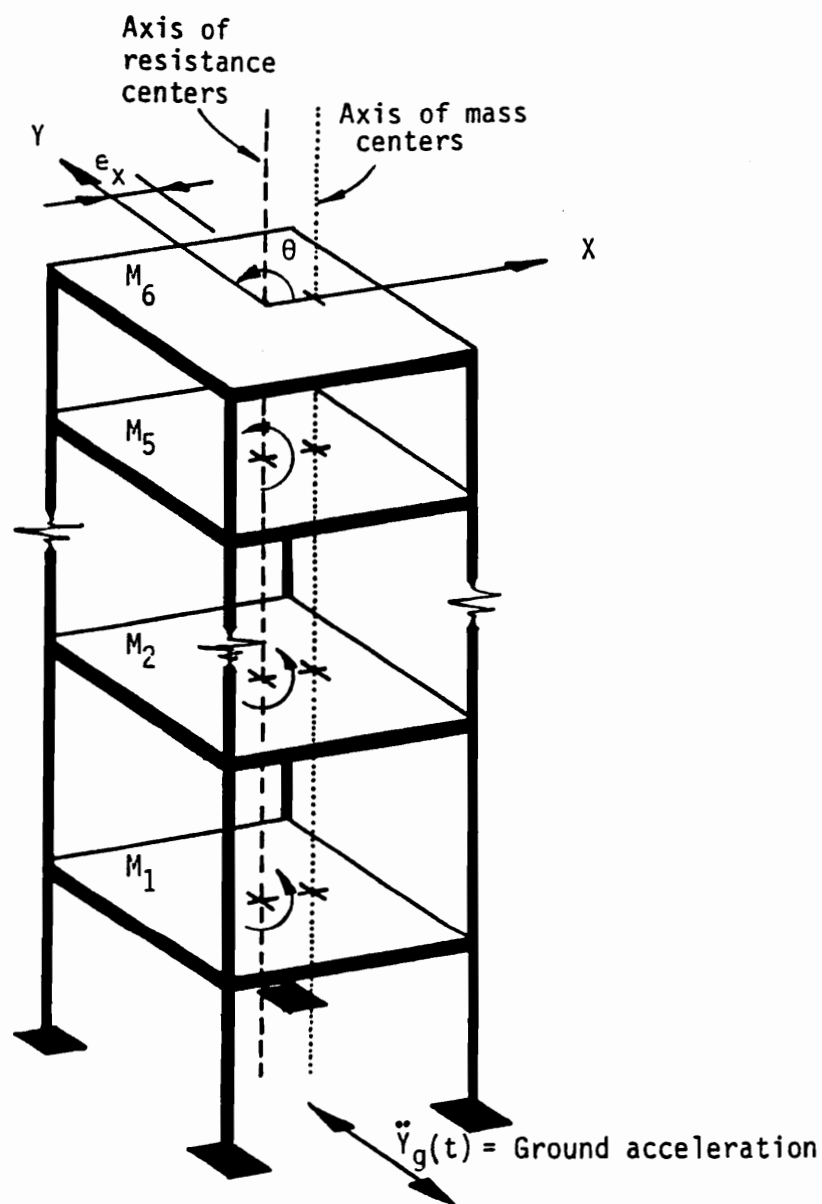


Figure 2.5: Schematic of the structure analyzed in the example problem.

and flexible structures obtained by various approaches for the stochastic input. It is clear from the figure that the proposed approach performs the best again, giving least error in the response for a given number of modes. For the stiff structure, the performance of the proposed approach is especially remarkable, as with just 2 modes considered in the analysis the mode truncation error is practically eliminated. The SRSS approach performs worst, even with the flexible structure, because of ignoring modal correlation completely. For the reasons cited earlier, the absolute sum approach again gives very good results for the stiff structure; also for the flexible structure the error increases again. The CQC does very well for the flexible structure, but for the stiff structure the error, even with the complete set of modes considered in the analysis is rather high, at about 20 per cent. The errors for this structure are, in general, smaller than the error for the beam, discussed earlier. It is primarily due to the fact that, even in the stiff structure, the product $(\rho_j \gamma_j)$ was significant only for the first three modes whereas in the beam this product was relatively large, even for several higher modes. Thus, ignoring higher modes did not make as much difference in this structure as it did in the case of the beam.

Figure 2.7 shows results similar to those in figure 2.6, but for the response spectrum input. Here again, the proposed approach performs the best and errors in the results by other methods are similar to those in figure 2.6.

Many of the proposed spectrum approaches implicitly assume that the relative and pseudo-velocity responses of an oscillator excited by ground motion are equal. This assumption avoids the need of specifying the relative velocity response spectra for the base input motion, as this can now be obtained from the commonly prescribed pseudo-acceleration response spectra. However, this assumption introduces

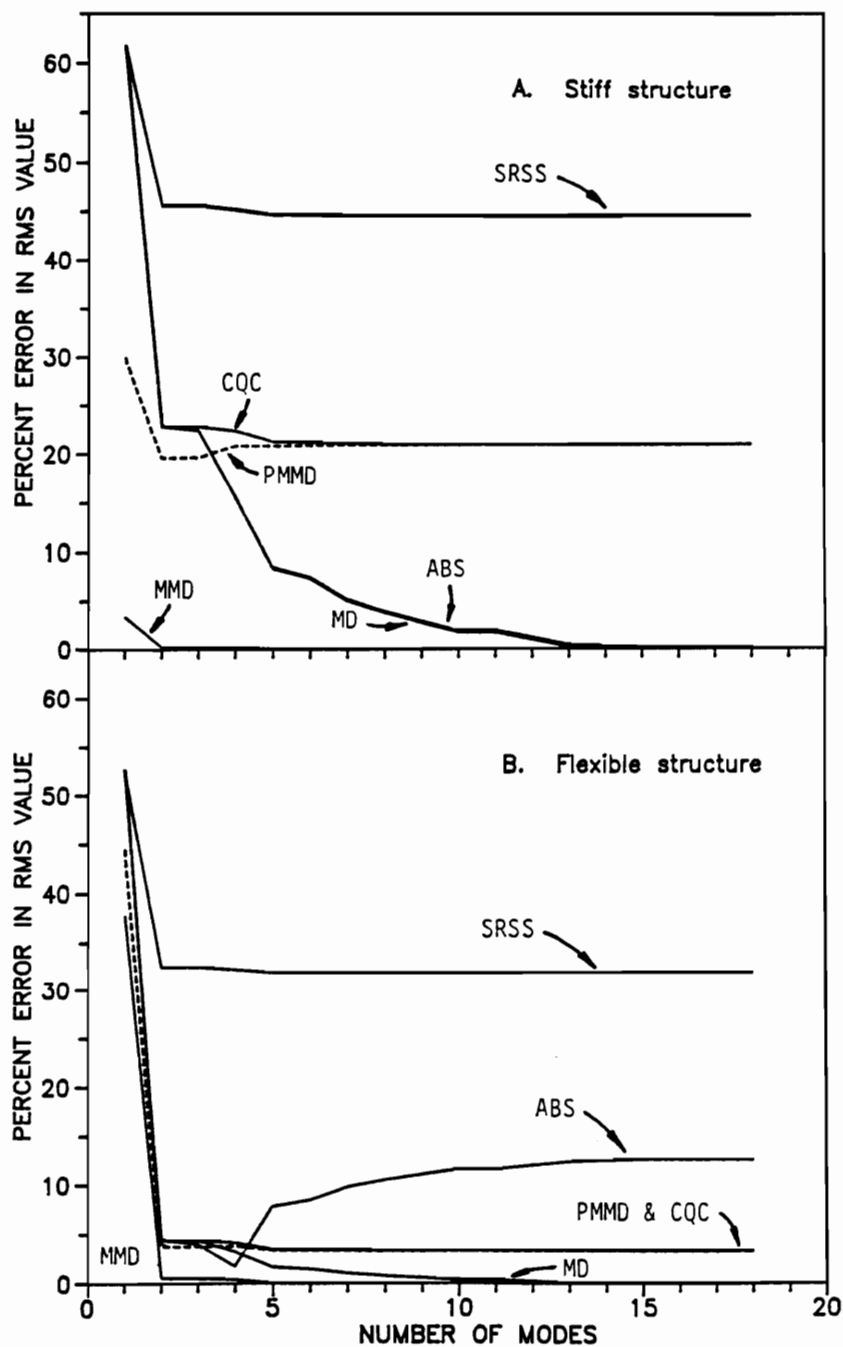


Figure 2.6: Percent error in the root mean square value of a bending moment obtained for a Kanai-Tajimi spectral density function by different approaches with increasing number of modes for: (A) stiff frame, and (B) flexible frame.

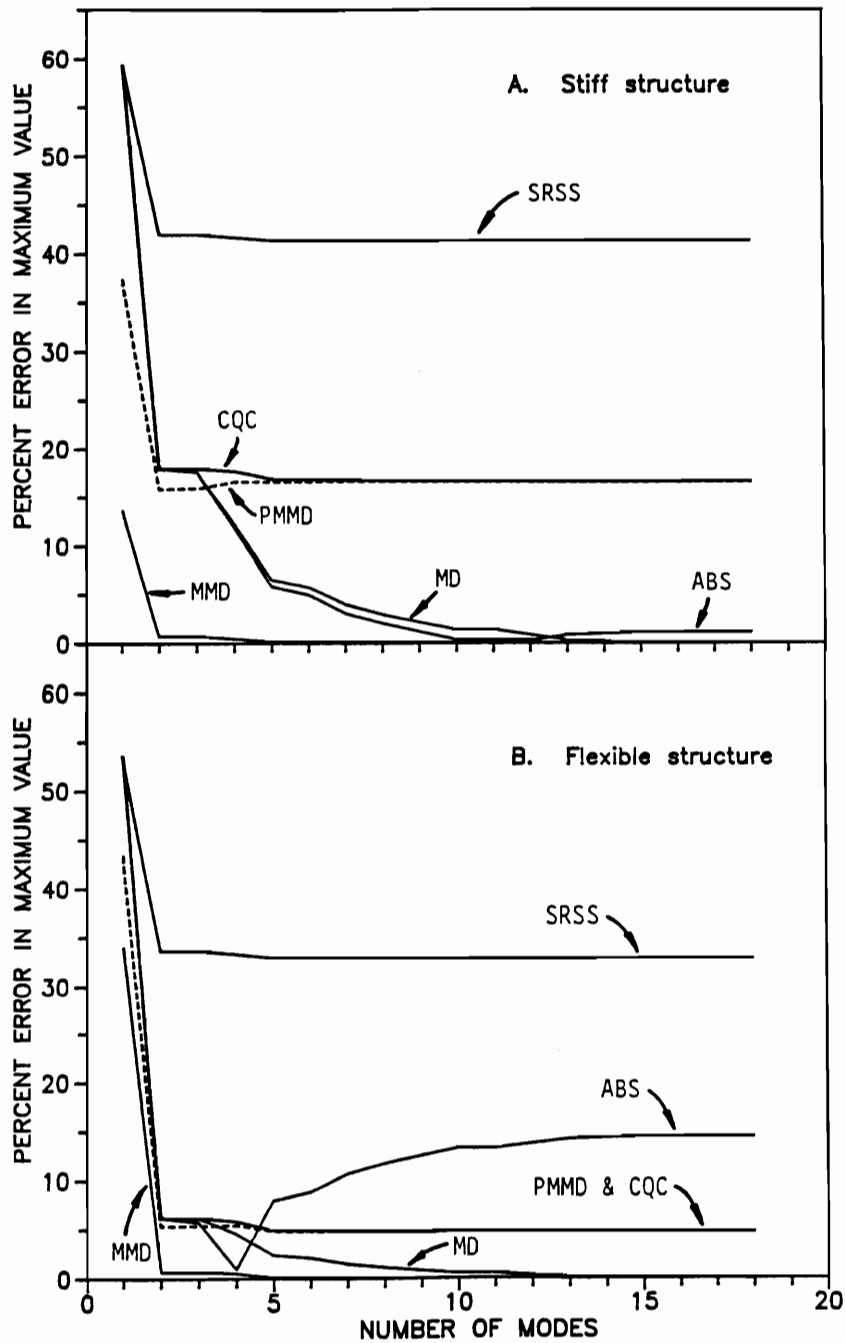


Figure 2.7: Percent error in a bending moment design response obtained for response spectrum input by different approaches with increasing number of modes for: (A) stiff frame, and (B) flexible frame.

inaccuracy in the calculated response, as is shown by the dashed curves (identified by PMMD) in figures 2.2 and 2.6 obtained for the Kanai-Tajimi spectral density function input and in figures 2.4 and 2.7 obtained for the response spectra as the input. These curves show the error in the response calculated by the proposed approach but with the incorrect assumption of the relative velocity response being equal to the pseudo-velocity response. It is seen that the effect of this assumption in the proposed approach is to increase the error in a stiff structure. This shows that it is important to define design input in terms of the relative velocity spectra in addition to the pseudo-acceleration spectra, if one wants to calculate the response accurately. Also as one would expect, the results obtained with this approximation approach the results of methods in references [41] and [59] as we increase the number of modes.

2.6 Conclusions

A response spectrum method is presented for an accurate calculation of the design response. The method combines the advantages of the mode acceleration and mode displacement formulations. It reduces the error caused by the truncation of modes, and it uses the same input required by the mode displacement-based response spectrum approach. The relative acceleration spectra, which were required as input in the mode acceleration-based response spectrum approach, are not required in this approach. It is shown through numerical examples that, for a given number of modes used in the analysis, this approach gives much less error in the response than some other currently used response spectrum approaches. The approach is effective in providing accurate seismic response of stiff as well as flexible structures equally. However, the improvements in the accuracy of the response of stiff structural systems

are more impressive. To capture the contribution of all significant modes, one should consider at least the modes which are within the cut-off frequency of the input plus a few more following modes. The higher modes need not be calculated; their effect is included through a pseudostatic response term.

Chapter 3

Modified Mode Displacement Response Spectrum Method for Non-classically Damped Structures

3.1 Introduction

In many situations, it may not be justified to assume the energy dissipation characteristics of a structural system to be classically damped. This precludes the use of the undamped modes in their dynamic analysis. However, by utilizing the damped eigenproperties one can still analyze non-classically damped systems by a mode superposition approach [33]. This approach has been used by several investigators [43, 46, 21, 20, 53, 54] for time history and response spectrum analyses of non-classically damped systems.

As is commonly done in the analysis of classically damped structures, one can also truncate high frequency modes in the dynamic analysis of non-classically damped systems as well. In most cases, this truncation does not cause any accuracy problems in the calculated response. Yet in some situations involving stiff structural systems and the response quantities affected by the high frequency modes, this truncation can cause such problems. The previous chapter presented a response spectrum method to reduce the error due to truncation of modes in classically damped systems. This chapter presents now a similar method to reduce the mode truncation error in non-classically damped structures.

In the past, two formulations have been used to develop the response spectrum methods for non-classically damped structures: (1) mode displacement formulation and (2) mode acceleration formulation. The methods developed by Singh [43], Igusa, Der Kiureghian and Sackman [21] and Villaverde [54] are based on the mode displacement formulation whereas the method developed by Singh and McCown [49] is based on the mode acceleration formulation. The mode acceleration approach has been shown [49] to be very effective in reducing the error due to the truncation of modes. But as it was the case with classically damped structures, this approach requires that the base input be described in terms of the relative acceleration and relative velocity response spectra. Since these spectra are not commonly used in the earthquake engineering community, the mode acceleration-based response spectrum approach has lacked practical appeal. The mode displacement approaches, on the other hand, do not have this problem, but they are not as efficient and accurate as the mode acceleration approach in reducing the mode truncation error. That is, for a given number of modes used in an analysis the mode displacement approach do not provide as accurate response as the mode acceleration approach.

Basically, this chapter extends the idea presented in the previous chapter to develop a response spectrum method for non-classically damped structures. In this formulation, the advantages of both approaches, the mode acceleration-based approach and the mode displacement-based approach, are combined to obtain a response spectrum method which (1) utilizes the commonly prescribed form of base response spectra like a mode displacement approach does and (2) reduces the mode truncation error as effectively as a mode acceleration approach would without using the high frequency modes explicitly. The main idea behind the formulation presented here is the same as the one used in the previous chapter, but the details are quite different.

3.2 Response by Modified Mode Displacement

The equations of motion for an elastic structure with n degrees of freedom, and subjected to ground acceleration $\ddot{x}_g(t)$ at its base, can be expressed as:

$$[M] \{\ddot{X}(t)\} + [C] \{\dot{X}(t)\} + [K] \{X(t)\} = -[M] \{I\} \ddot{x}_g(t), \quad (3.1)$$

where $[M]$, $[C]$ and $[K]$ are the $(n \times n)$ symmetric structural matrices for the mass, damping and stiffness respectively; $\{X(t)\}$ is the vector of structural displacements with respect to the ground; $\{I\}$ is the vector of ground motion influence coefficients and a dot over a variable represents its time derivative.

For the general case in which the damping matrix $[C]$ is non-proportional or non-classical, equation (3.1) can be written as the following system of first order equations:

$$[A] \{\dot{Y}(t)\} + [B] \{Y(t)\} = -[D] \left\{ \begin{matrix} \{0\} \\ \{I\} \end{matrix} \right\} \ddot{x}_g(t), \quad (3.2)$$

where $\{Y(t)\}$ is the $(2n \times 1)$ state vector. Its first n elements are the elements of the relative velocity vector $\{\dot{X}(t)\}$, and the remaining n elements belong to the relative displacement vector $\{X(t)\}$. The matrices $[A]$, $[B]$ and $[D]$ of dimension $(2n \times 2n)$ are defined as:

$$[A] = \begin{bmatrix} [0] & [M] \\ [M] & [C] \end{bmatrix} \quad , \quad [B] = \begin{bmatrix} -[M] & [0] \\ [0] & [K] \end{bmatrix} \quad , \quad [D] = \begin{bmatrix} [0] & [0] \\ [0] & [M] \end{bmatrix} . \quad (3.3)$$

Equation (3.2) can be decoupled by utilizing the eigenproperties of the following associated eigenvalue problem:

$$\lambda_j [A] \{\phi\}_j = [B] \{\phi\}_j \quad ; \quad j = 1, \dots, 2n \quad (3.4)$$

The solution of equation (3.4) provides $2n$ eigenvalues λ_j and their corresponding $2n$ eigenvectors $\{\phi\}_j$. However, due to the characteristics of the system, these eigenproperties are given in n pairs of complex and conjugate quantities. That is, the eigenanalysis provides n pairs of complex and conjugate eigenvalues (λ_j^c , λ_j^{cc} , $j = 1, \dots, n$) and their corresponding n pairs of complex and conjugate eigenvectors ($\{\phi^c\}_j$, $\{\phi^{cc}\}_j$, $j=1, \dots, n$). The eigenvalues are considered to be ordered with increasing magnitude with the ones with positive imaginary part preceding those with negative imaginary part. That is, the eigenvalue with the smallest magnitude and positive imaginary part is denoted as $\lambda_1 = \lambda_1^c$, its complex conjugate as $\lambda_2 = \lambda_1^{cc}$, the one with largest magnitude and positive imaginary part is $\lambda_{2n-1} = \lambda_n^c$, and its complex conjugate is $\lambda_{2n} = \lambda_n^{cc}$. Similarly, the order of the eigenvectors is determined by the order of their associated eigenvalues.

The modal matrix $[\Phi]$ contains the eigenvectors, and after normalization with

respect to matrix $[A]$, presents the following orthonormal properties:

$$[\Phi]^T [A] [\Phi] = [I] \quad , \quad [\Phi]^T [B] [\Phi] = [\Lambda] \quad , \quad (3.5)$$

where $[I]$ is the $(2n \times 2n)$ identity matrix and $[\Lambda]$ is a diagonal matrix containing the eigenvalues.

As indicated by Singh [43], the system frequencies ω_j , and the modal damping ratios β_j , can be related to the real and imaginary parts of the eigenvalues as:

$$\lambda_j^c = \beta_j \omega_j + i \omega_j \sqrt{1 - \beta_j^2} \quad , \quad \omega_j = |\lambda_j^c| \quad , \quad \beta_j = \frac{Re(\lambda_j)}{\omega_j} \quad , \quad j = 1, \dots, n. \quad (3.6)$$

Equation (3.2) can be decoupled by premultiplying it by $[\Phi]^T$, by using the following standard transformation of coordinates

$$\{Y(t)\} = [\Phi] \{Z(t)\} \quad , \quad (3.7)$$

and by considering the orthogonality properties indicated in equation (3.6). The resulting $2n$ decoupled equations for the principal coordinates $z_j(t)$ are

$$\dot{z}_j(t) + \lambda_j z_j(t) = -\gamma_j \ddot{x}_g(t) \quad , \quad j = 1, \dots, 2n \quad , \quad (3.8)$$

where γ_j is the j^{th} participation factor defined as

$$\gamma_j = \{\phi\}_j^T [D] \begin{Bmatrix} \{0\} \\ \{I\} \end{Bmatrix} = \{\bar{\phi}\}_j^T [M] \{I\} \quad ; \quad j = 1, \dots, 2n \quad . \quad (3.9)$$

In this equation, the quantity indicated as $\{\bar{\phi}\}_j$ is the lower half of the j^{th} eigenvector $\{\phi\}_j$.

For a given ground motion $\ddot{x}_g(t)$ and quiescent initial conditions, equation (3.8) can be solved for all $z_j(t)$ to get

$$z_j(t) = -\gamma_j \int_0^t \ddot{x}_g(\tau) e^{-\lambda_j(t-\tau)} d\tau \quad , \quad j = 1, \dots, 2n \quad . \quad (3.10)$$

Such solution, can then be used to calculate the relative displacement vector as follows:

$$\{X(t)\} = \{\bar{Y}(t)\} = [\bar{\Phi}] \{Z(t)\} = \sum_{j=1}^{2n} \{\bar{\phi}\}_j z_j(t), \quad (3.11)$$

where a bar over a quantity indicates its lower half. Also, any response quantity $R(t)$, which is linearly related to the relative displacement vector, can be written in terms of the solutions $z_j(t)$ as follows:

$$R(t) = \left\{ \begin{matrix} \{0\} \\ \{\mathcal{R}\} \end{matrix} \right\}^T \{Y(t)\} = \{\mathcal{R}\}^T \{X(t)\} = \sum_{j=1}^{2n} \rho_j z_j(t). \quad (3.12)$$

Where $\{\mathcal{R}\}$ is the vector containing the n constant coefficients to linearly combine the n elements of the relative displacement vector $\{x(t)\}$, and ρ_j is the j^{th} modal response $R(t)$. It is obtained by a simple linear transformation of $\{\bar{\phi}\}_j$ as:

$$\rho_j = \{\mathcal{R}\}^T \{\bar{\phi}\}_j ; \quad j = 1, \dots, 2n. \quad (3.13)$$

Equation (3.12) is a statement of the mode displacement formulation for calculating the response of non-classically damped systems. To avoid calculation of all eigenproperties, one can use only a first few eigenproperties in the summation of equation (3.12). This is equivalent to the procedure of mode truncation, commonly used with classically damped systems. The implementation of the truncation requires the above mentioned rearrangement of the modal frequencies in increasing order to identify the lower modes. These lower modes and their complex conjugate are, then, used in the summation in equation (3.12) and the remaining higher modes are discarded. As was the case with classically damped structures, this omission or truncation of higher modes from the analysis does not cause any significant error in the calculated response in most structures. But in some stiff structures and some response quantities affected by high frequency modes, this truncation of modes can also cause significant error in the calculated response.

For non-classically damped structures also this truncation error can be controlled, and in fact practically eliminated, by adopting the mode acceleration formulation as shown by Singh and McCown [49]. The method proposed herein is an improvement of the approach proposed by Singh and McCown.

In the mode acceleration formulation, one rewrites equation (3.12) by substituting the principal coordinates $z_j(t)$ by the expression $-[\gamma_j \ddot{x}_g + \dot{z}_j]/\lambda_j$, obtained from equation (3.8), to get

$$R(t) = -\ddot{x}_g(t) \sum_{j=1}^{2n} \frac{\rho_j \gamma_j}{\lambda_j} - \sum_{j=1}^{2n} \frac{\rho_j \dot{z}_j(t)}{\lambda_j} \quad (3.14)$$

As it was the case in the previous chapter, for classically damped structures, the summation factor in the first term of equation (3.14), though expressed in terms of the eigenproperties, can also be calculated by a simple static analysis as it is shown below. For this purpose, such term is denoted by R_s and it can be expressed as

$$R_s = \sum_{j=1}^{2n} \frac{\rho_j \gamma_j}{\lambda_j} = \{\mathcal{R}\}^T [\Lambda]^{-1} \{\gamma\}, \quad (3.15)$$

where the vectors $\{\rho\}^T$ and $\{\gamma\}$ contain the modal response quantities and the participation factors respectively. Their expressions are

$$\{\rho\}^T = \left\{ \begin{matrix} \{0\} \\ \{\mathcal{R}\} \end{matrix} \right\}^T [\Phi] \quad , \quad \{\gamma\} = [\Phi]^T [D] \left\{ \begin{matrix} \{0\} \\ \{\mathcal{I}\} \end{matrix} \right\}. \quad (3.16)$$

Equation (3.6) can be used to obtain matrix $[\Lambda]^{-1}$ as

$$[\Lambda]^{-1} = [\Phi]^{-1} [B]^{-1} [\Phi]^{-T}. \quad (3.17)$$

Substitution of equations (3.16) and (3.17) into equation (3.15) provides

$$R_s = \left\{ \begin{matrix} \{0\} \\ \{\mathcal{R}\} \end{matrix} \right\}^T [B]^{-1} [D] \left\{ \begin{matrix} \{0\} \\ \{\mathcal{I}\} \end{matrix} \right\} = \{\mathcal{R}\}^T [K]^{-1} [M] \{\mathcal{I}\} = \{\mathcal{R}\}^T \{X_s\}, \quad (3.18)$$

where $\{X_s\}$ is the static solution of the following system

$$[K] \{X_s\} = [M] \{\mathcal{I}\} . \quad (3.19)$$

The above analysis demonstrated that R_s is the static response associated to the response quantity $R(t)$ when the system is subjected to the load $[M] \{\mathcal{I}\}$. In terms of R_s , equation (3.14) can be rewritten as

$$R(t) = -\ddot{x}_g(t) R_s - \sum_{j=1}^{2r} \frac{\rho_j \dot{z}_j(t)}{\lambda_j} , \quad (3.20)$$

where now the summation is carried over the first r modes or eigenproperties. Equation (3.20) is known as the mode acceleration approach, and it formed the basis of the response spectrum method proposed by Singh and McCown [49]. As in the case of classically damped structures (previous chapter), this formulation required that the ground input be defined in terms of the relative acceleration and relative velocity spectra. As mentioned earlier, this particular form of input requirement is the main practical drawback of this approach. To eliminate this limitation, it is possible to reuse equation (3.8) to substitute for \dot{z}_j in terms of $\ddot{x}_g(t)$ and $z_j(t)$ in equation (3.20), and obtain

$$R(t) = -R_s \ddot{x}_g(t) + \sum_{j=1}^{2r} \frac{\rho_j}{\lambda_j} [\gamma_j \ddot{x}_g(t) + \lambda_j z_j(t)] , \quad (3.21)$$

or in a more compact notation

$$R(t) = -C_s \ddot{x}_g(t) + \sum_{j=1}^{2r} \rho_j z_j(t) , \quad (3.22)$$

where C_s is defined as

$$C_s = R_s - \sum_{j=1}^{2r} \frac{\rho_j \gamma_j}{\lambda_j} , \quad (3.23)$$

and it represents the response (per unit ground acceleration) of only the truncated modes. It should be noticed that this quantity depends on the number r of truncated

modes. In particular, for $r = n$, C_s is zero and equation (3.22) reduces to the classical mode displacement approach with the total number of modes.

Equation (3.22) is as effective in eliminating the error due to mode truncation as equation (3.20), but it is expressed in terms of $z_j(t)$ in lieu of $\dot{z}_j(t)$. It will now be used to develop a response spectrum approach for calculating the design response. Since the design response can be expressed as an amplified value of the root mean square response, the next sections presents the formulation leading to the autocorrelation function of $R(t)$. equation (3.22) as follows:

3.3 Mean Square Value of the Response Quantity $R(t)$

The mean square value of the response quantity $R(t)$ can be obtained as a limiting value of its autocorrelation following a similar procedure as the one used in the previous chapter. As it was assumed in chapter 2, here also it will be considered that the input motion is a zero mean stationary process, and since the structures are linear, it implies that their responses are also stationary with zero means, and their mean square values coincide with their respective variances which can be written in terms of the autocorrelation function as

$$\lim_{t_1=t_2=t} E[R(t_1) R(t_2)] = E[R^2(t)] = \sigma_R^2 . \quad (3.24)$$

where σ_R is the standard deviation of $R(t)$.

To implement the proposed approach, the autocorrelation of $R(t)$ is written

with the help of equation (3.22) as follows

$$E[R(t_1) R(t_2)] = E \left[\left(-C_s \tilde{x}_g(t_1) + \sum_{j=1}^{2r} \rho_j z_j(t_1) \right) \left(-C_s \tilde{x}_g(t_2) + \sum_{k=1}^{2r} \rho_k z_k(t_2) \right) \right] . \quad (3.25)$$

After expanding the above equation and distributing the expected values, it becomes

$$\begin{aligned} E[R(t_1) R(t_2)] &= C_s^2 E[\tilde{x}_g(t_1) \tilde{x}_g(t_2)] \\ &\quad - C_s \sum_{j=1}^{2r} \rho_j (E[z_j(t_1) \tilde{x}_g(t_2)] + E[\tilde{x}_g(t_1) z_j(t_2)]) \\ &\quad + \sum_{j=1}^{2r} \sum_{k=1}^{2r} \rho_j \rho_k E[z_j(t_1) z_k(t_2)] . \end{aligned} \quad (3.26)$$

By setting $t_1 = t_2 = t$, this equation provides

$$\begin{aligned} E[R^2(t)] &= C_s^2 E[\tilde{x}_g^2(t)] - C_s \sum_{j=1}^{2r} \rho_j (E[z_j(t) \tilde{x}_g(t)] + E[\tilde{x}_g(t) z_j(t)]) \\ &\quad + \sum_{j=1}^{2r} \sum_{k=1}^{2r} \rho_j \rho_k E[z_j(t) z_k(t)] . \end{aligned} \quad (3.27)$$

The first expected value to be considered is the autocorrelation of the ground acceleration, which is the fourier transform of its stationary PSD function denoted as $\Phi_g(\omega)$. In chapter 2, equations (2.32) and (2.33) express such autocorrelation. The mean square value of ground acceleration in equation (4.27) can be expressed as

$$E[\tilde{x}_g(t_1) \tilde{x}_g(t_2)] = E[\tilde{x}_g^2(t)] = \int_{-\infty}^{\infty} \Phi_g(\omega) d\omega = \sigma_g^2 , \quad (3.28)$$

where σ_g is the standard deviation of the ground acceleration.

The crosscorrelations $E[z_j(t_1) \tilde{x}_g(t_2)]$ and $E[\tilde{x}_g(t_1) z_j(t_2)]$ are analyzed next.

With the help of equation (3.10), the first crosscorrelation can be written as

$$E[z_j(t_1) \tilde{x}_g(t_2)] = -\gamma_j \int_0^{t_1} e^{-\lambda_j(t_1-\tau_1)} E[\tilde{x}_g(\tau_1) \tilde{x}_g(t_2)] d\tau_1 , \quad (3.29)$$

where the indicated autocorrelation of $\tilde{x}_g(t)$ is given by

$$E[\tilde{x}_g(\tau_1) \tilde{x}_g(t_2)] = \int_{-\infty}^{\infty} \Phi_g(\omega) e^{i\omega(\tau_1-t_2)} d\omega . \quad (3.30)$$

Substitution of the above equation into equation (3.29) provides

$$E[z_j(t_1) \tilde{x}_g(t_2)] = -\gamma_j \int_{-\infty}^{\infty} \Phi_g(\omega) e^{-i\omega t_2} e^{-i\lambda_j t_1} d\omega \int_0^{t_1} e^{(\lambda_j+i\omega)\tau_1} d\tau_1 . \quad (3.31)$$

After integrating the time integral and some rearranging, equation (3.31) becomes

$$E[z_j(t_1) \tilde{x}_g(t_2)] = -\gamma_j \int_{-\infty}^{\infty} \Phi_g(\omega) e^{-i\omega t_2} \left(\frac{e^{i\omega t_1} - e^{-\lambda_j t_1}}{\lambda_j + i\omega} \right) d\omega . \quad (3.32)$$

At the limit, as $t_1 \rightarrow \infty$, $e^{-\lambda_j t_1}$ becomes zero because of the positive real part of λ_j , and equation (3.32) can be written as

$$E[z_j(t_1) \tilde{x}_g(t_2)] = -\gamma_j \int_{-\infty}^{\infty} \Phi_g(\omega) e^{i\omega(t_1-t_2)} \left(\frac{1}{\lambda_j + i\omega} \right) d\omega , \quad (3.33)$$

This equation provides the stationary value of the cross correlation terms. At $t_1 = t_2$ it renders

$$E[z_j(t) \tilde{x}_g(t)] = -\gamma_j \int_{-\infty}^{\infty} \Phi_g(\omega) \left(\frac{1}{\lambda_j + i\omega} \right) d\omega , \quad (3.34)$$

Similarly, the limit of the other crosscorrelation $E[\tilde{x}_g(t_1) z_j(t_2)]$, as $t_1 = t_2 = t \rightarrow \infty$, is given by

$$E[\tilde{x}_g(t) z_j(t)] = -\gamma_j \int_{-\infty}^{\infty} \Phi_g(\omega) \left(\frac{1}{\lambda_j - i\omega} \right) d\omega . \quad (3.35)$$

The limit of the remaining crosscorrelation $E[z_j(t_1) z_k(t_2)]$, is considered next.

For this, equation (3.10) is used to write

$$E[z_j(t_1) z_k(t_2)] = \gamma_j \gamma_k \int_0^{t_1} \int_0^{t_2} e^{-\lambda_j(t_1-\tau_1)} e^{-\lambda_k(t_2-\tau_2)} E[\tilde{x}_g(\tau_1) \tilde{x}_g(\tau_2)] d\tau_1 d\tau_2 , \quad (3.36)$$

where substitution of the autocorrelation of the ground acceleration by its fourier transform, and some rearrangement produce

$$E[z_j(t_1) z_k(t_2)] = \gamma_j \gamma_k \int_{-\infty}^{\infty} \Phi_g(\omega) \left(e^{-\lambda_j t_1} \int_0^{t_1} e^{\tau_1(\lambda_j + i\omega)} d\tau_1 \right) \times \left(e^{-\lambda_k t_2} \int_0^{t_2} e^{\tau_2(\lambda_k - i\omega)} d\tau_2 \right) d\omega . \quad (3.37)$$

After integrating the time integrals, equation (3.37) becomes

$$E[z_j(t_1) z_k(t_2)] = \gamma_j \gamma_k \int_{-\infty}^{\infty} \Phi_g(\omega) \left(\frac{e^{i\omega t_1} - e^{-\lambda_j t_1}}{\lambda_j + i\omega} \right) \left(\frac{e^{-i\omega t_2} - e^{-\lambda_k t_2}}{\lambda_k - i\omega} \right) d\omega . \quad (3.38)$$

At the limit, as $t_1 \rightarrow \infty$ and $t_2 \rightarrow \infty$, with $\Delta t = t_1 - t_2$ as a finite value, the limits of $e^{-\lambda_j t_1}$ and $e^{-\lambda_k t_2}$ become zero, and equation (3.38) renders

$$E[z_j(t_1) z_k(t_2)] = \gamma_j \gamma_k \int_{-\infty}^{\infty} \Phi_g(\omega) e^{i\omega(t_1 - t_2)} \left(\frac{1}{\lambda_j + i\omega} \right) \left(\frac{1}{\lambda_k - i\omega} \right) d\omega , \quad (3.39)$$

Substituting $t_1 = t_2$ it provides the covariance terms appearing in the last term of equation (4.27) as:

$$E[z_j(t) z_k(t)] = \gamma_j \gamma_k \int_{-\infty}^{\infty} \Phi_g(\omega) \left(\frac{1}{\lambda_j + i\omega} \right) \left(\frac{1}{\lambda_k - i\omega} \right) d\omega . \quad (3.40)$$

Equations (3.28), (3.34), (3.35) and (3.40) can now be substituted into equation (3.27) to express the mean square value of $R(t)$ as

$$E[R^2(t)] = \int_{-\infty}^{\infty} \Phi_g(\omega) \left[C_s^2 + C_s \sum_{j=1}^{2r} \left(\frac{q_j}{\lambda_j + i\omega} + \frac{q_j}{\lambda_j - i\omega} \right) + \sum_{j=1}^{2r} \sum_{k=1}^{2r} \left(\frac{q_j}{\lambda_j + i\omega} \right) \left(\frac{q_k}{\lambda_k - i\omega} \right) \right] d\omega , \quad (3.41)$$

where q_j is a complex quantity defined as

$$q_j = \rho_j \gamma_j = \delta_j + i\epsilon_j , \quad (3.42)$$

with δ_j and ε_j being its real and imaginary parts.

Equation (3.41) expresses $E[R^2(t)]$, which is a real quantity, in terms of complex quantities. To express it in terms of real quantities only, it is necessary to manipulate it even further. First consider a typical summation of $2r$ terms, on the right hand side of equation (3.41), as a summation of r complex and conjugate terms

$$\sum_{j=1}^{2r} \frac{q_j}{\lambda_j + i\omega} = \sum_{j=1}^r \left(\frac{q_j^c}{\lambda_j^c + i\omega} + \frac{q_j^{cc}}{\lambda_j^{cc} + i\omega} \right), \quad (3.43)$$

where the superscripts c and cc indicate a complex number and its conjugate, respectively. These summation terms can be written in the following form, after some simplification:

$$\sum_{j=1}^{2r} \frac{q_j}{\lambda_j + i\omega} = 2 \sum_{j=1}^r p_j^c(\omega) H_j^c(\omega), \quad (3.44)$$

where $H_j(\omega)$ is the transient transfer function of a second order single-degree-of-freedom oscillator with frequency ω_j and damping ratio β_j [see equation (2.38)], and $p_j^c(\omega)$ is the following complex quantity

$$p_j^c(\omega) = \zeta_j + i \delta_j \omega \quad , \quad \zeta_j = \frac{\text{Re}(q_j^c \lambda_j^{cc})}{2} = \omega_j (\beta_j \delta_j + \varepsilon_j \sqrt{1 - \beta_j^2}) . \quad (3.45)$$

Equation (3.44) is developed in detail by equations (5.38–5.43). Similarly, the remaining summation term in equation (3.41) can be written as

$$\sum_{k=1}^{2r} \frac{q_k}{\lambda_k - i\omega} = 2 \sum_{k=1}^r p_k^{cc}(\omega) H_k^{cc}(\omega) . \quad (3.46)$$

Substitution of equations (3.45) and (3.46) into equation (3.41) provides

$$E[R^2(t)] = \mathfrak{S}_1 + \mathfrak{S}_2 + \mathfrak{S}_3 , \quad (3.47)$$

where the three terms \mathfrak{S}_1 , \mathfrak{S}_2 and \mathfrak{S}_3 contain frequency integrals and they are defined as follows

$$\mathfrak{S}_1 = C_s^2 \int_{-\infty}^{\infty} \Phi_g(\omega) d\omega = C_s^2 \sigma_g^2 , \quad (3.48)$$

$$\mathfrak{S}_2 = 4 C_s \int_{-\infty}^{\infty} \Phi_g(\omega) \sum_{j=1}^r \text{Re} [p_j^c(\omega) H_j^c(\omega)] d\omega , \quad (3.49)$$

$$\mathfrak{S}_3 = 4 \int_{-\infty}^{\infty} \Phi_g(\omega) \sum_{j=1}^r \sum_{k=1}^r p_j^c(\omega) p_k^{cc}(\omega) H_j^c(\omega) H_k^{cc}(\omega) d\omega . \quad (3.50)$$

The term \mathfrak{S}_1 provides the pseudostatic contribution of the truncated modes, \mathfrak{S}_2 considers the correlation between the pseudostatic response of the truncated modes and the dynamic response of the retained modes, and the term \mathfrak{S}_3 is the same as provided by the classical mode displacement approach. It represents the dynamic contributions of the retained modes. The expressions for \mathfrak{S}_2 and \mathfrak{S}_3 still need to be simplified further in order to be expressed in terms of real quantities only.

Substitution of $p_j^c(\omega)$ and $H_j^c(\omega)$ by their real and imaginary components, allows \mathfrak{S}_2 to be written as

$$\mathfrak{S}_2 = 4 C_s \int_{-\infty}^{\infty} \Phi_g(\omega) \sum_{j=1}^r [\zeta_j \omega_j^2 + (\delta_j \beta_j \omega_j - \zeta_j) \omega^2] |H_j^c(\omega)|^2 d\omega , \quad (3.51)$$

or in a more compact notation

$$\mathfrak{S}_2 = 4 C_s \sum_{j=1}^r [\zeta_j \omega_j^2 I_j^d + (\delta_j \beta_j \omega_j - \zeta_j) I_j^v] , \quad (3.52)$$

where the frequency integrals I_j^d and I_j^v , have been defined in chapter 2 by equations (2.52) and (2.53). As mentioned there, they respectively represent the mean square values of the relative displacement and relative velocity responses of an oscillator excited by the ground acceleration $\ddot{x}_g(t)$. Closed form expressions for I_j^d and I_j^v are given in appendix G for commonly used power spectral density functions.

To analyze the term \mathfrak{S}_3 , it is convenient to separate it into two parts: \mathfrak{S}_{31} containing the diagonal terms with $j = k$, and \mathfrak{S}_{32} containing the off-diagonal terms with $j \neq k$. \mathfrak{S}_{31} represents the dynamic contribution of each retained mode and \mathfrak{S}_{32}

represents contributions due to the modal correlations between the retained modes. Thus,

$$\mathfrak{S}_3 = \mathfrak{S}_{31} + \mathfrak{S}_{32} \quad (3.53)$$

with

$$\mathfrak{S}_{31} = 4 \int_{-\infty}^{\infty} \Phi_g(\omega) \sum_{j=1}^r |p_j^c(\omega)|^2 |H_j^c(\omega)|^2 d\omega, \quad (3.54)$$

and

$$\mathfrak{S}_{32} = 4 \int_{-\infty}^{\infty} \Phi_g(\omega) \sum_{j=1}^r \sum_{\substack{k=1 \\ k \neq j}}^r p_j^c(\omega) p_k^{cc}(\omega) H_j^c(\omega) H_k^{cc}(\omega) d\omega. \quad (3.55)$$

Substituting for $p_j^c(\omega)$ from equation (3.45), we obtain for equation \mathfrak{S}_{31} as:

$$\mathfrak{S}_{31} = 4 \int_{-\infty}^{\infty} \Phi_g(\omega) \sum_{j=1}^r (\zeta_j^2 \delta_j^2) |H_j^c(\omega)|^2 d\omega, \quad (3.56)$$

Equation (4.55) is simplified further (see section 5.5) to express it in terms of real quantities only. This simplification leads to the following:

$$\begin{aligned} \mathfrak{S}_{32} = 8 \int_{-\infty}^{\infty} \Phi_g(\omega) \sum_{j=1}^{r-1} \sum_{k=j+1}^r & \left[(\tilde{T}_{jk}^I + \omega^2 \tilde{T}_{jk}^{II}) |H_j^c(\omega)|^2 \right. \\ & \left. + (\tilde{T}_{jk}^{III} + \omega^2 \tilde{T}_{jk}^{IV}) |H_k^c(\omega)|^2 \right] d\omega, \end{aligned} \quad (3.57)$$

where the quantities \tilde{T}_{jk}^I , \tilde{T}_{jk}^{II} , \tilde{T}_{jk}^{III} and \tilde{T}_{jk}^{IV} are the partial fraction coefficients defined as

$$\tilde{T}_{jk}^I = \left\{ 2 \eta_{jk} \left[1 - \Omega_{jk}^2 + 2(\beta_j^2 \Omega_{jk}^2 - \beta_k^2) \right] - \mu_{jk} (\Omega_{jk}^2 - \Omega_{jk}^{-2}) \right\} \Delta_{jk}^{-1}, \quad (3.58)$$

$$\tilde{T}_{jk}^{II} = \left\{ \eta_{jk} (\Omega_{jk}^2 - \Omega_{jk}^{-2}) - 2 \Omega_{jk}^{-2} \mu_{jk} \left[1 - \Omega_{jk}^2 + 2(\beta_k^2 \Omega_{jk}^2 - \beta_j^2) \right] \right\} \omega_j^{-2} \Delta_{jk}^{-1}, \quad (3.59)$$

$$\tilde{T}_{jk}^{III} = \zeta_j \zeta_k \Omega_{jk}^{-2} - \tilde{T}_{jk}^I \Omega_{jk}^{-4}, \quad (3.60)$$

$$\tilde{T}_{jk}^{IV} = \delta_j \delta_k - \tilde{T}_{jk}^{II}, \quad (3.61)$$

where

$$\Omega_{jk} = \omega_j / \omega_k, \quad (3.62)$$

$$\begin{aligned}\mu_{jk} &= \zeta_j \zeta_k (\Omega_{jk}^2 - 1) + \omega_j^2 \delta_j \delta_k \left[(1 - 4\beta_j^2) \Omega_{jk}^2 + 4\beta_j \beta_k \Omega_{jk} - 1 \right] \\ &+ 2\omega_j \Omega_{jk} (\delta_j \zeta_k - \delta_k \zeta_j) (\beta_k - \beta_j \Omega_{jk}),\end{aligned}\quad (3.63)$$

$$\begin{aligned}\eta_{jk} &= \zeta_j \zeta_k \left[1 - 4\beta_j^2 + 4\beta_j \beta_k \Omega_{jk} - \Omega_{jk}^2 \right] + \omega_j^2 \delta_j \delta_k (1 - \Omega_{jk}^2) \\ &+ 2\omega_j (\delta_j \zeta_k - \delta_k \zeta_j) (\beta_j - \beta_k \Omega_{jk}),\end{aligned}\quad (3.64)$$

$$\begin{aligned}\Delta_{jk} &= 16(\beta_j^2 + \beta_k^2 - \beta_j^4 - \beta_k^4) - \Omega_{jk}^4 - \Omega_{jk}^{-4} - 6 \\ &+ 4(\Omega_{jk}^2 + \Omega_{jk}^{-2}) \left[1 - 2(\beta_j^2 + \beta_k^2 - 2\beta_j^2 \beta_k^2) \right].\end{aligned}\quad (3.65)$$

After invoking the frequency integrals I_j^d and I_j^v , the terms \mathfrak{S}_{31} and \mathfrak{S}_{31} become

$$\mathfrak{S}_{31} = 4 \sum_{j=1}^r \left(\zeta_j^2 I_j^d + \delta_j^2 I_j^v \right). \quad (3.66)$$

$$\mathfrak{S}_{32} = 8 \sum_{j=1}^{r-1} \sum_{k=j+1}^r \left[\tilde{T}_{jk}^I I_j^d + \tilde{T}_{jk}^{II} I_j^v + \tilde{T}_{jk}^{III} I_k^d + \tilde{T}_{jk}^{IV} I_k^v \right]. \quad (3.67)$$

To avoid the calculation of \tilde{T}_{jk}^{III} and \tilde{T}_{jk}^{IV} , equations (3.60) and (3.61) can be substituted into equation (3.67) as follows

$$\mathfrak{S}_{32} = 8 \sum_{j=1}^{r-1} \sum_{k=j+1}^r \left[\tilde{T}_{jk}^I \left(I_j^d - I_k^d \Omega_{jk}^{-4} \right) + \tilde{T}_{jk}^{II} \left(I_j^v - I_k^v \right) + \zeta_j \zeta_k \Omega_{jk}^{-2} I_k^d + \delta_j \delta_k I_k^v \right]. \quad (3.68)$$

Finally, substitution of equations (3.48), (3.52), (3.66) and (3.68) into equation (3.47) provides the mean square value of the response $R(t)$ as

$$\begin{aligned}E[R^2(t)] &= C_s^2 \sigma_g^2 + 4C_s \sum_{j=1}^r \left[\zeta_j \omega_j^2 I_j^d + (\delta_j \beta_j \omega_j - \zeta_j) I_j^v \right] + 4 \sum_{j=1}^r \left(\zeta_j^2 I_j^d + \delta_j^2 I_j^v \right) \\ &+ 8 \sum_{j=1}^{r-1} \sum_{k=j+1}^r \left[\tilde{T}_{jk}^I \left(I_j^d - I_k^d \Omega_{jk}^{-4} \right) + \tilde{T}_{jk}^{II} \left(I_j^v - I_k^v \right) + \zeta_j \zeta_k \Omega_{jk}^{-2} I_k^d + \delta_j \delta_k I_k^v \right]\end{aligned}\quad (3.69)$$

This expression is used in the next section to develop a response spectrum method based on the modified mode displacement approach.

3.4 Response Spectrum Method by the MMD approach

The proposed response spectrum method provides an approximation to the maximum value of the response quantity $R(t)$, which is also known as the design value of the response $R(t)$. Here the design response value is \mathcal{M}_R .

\mathcal{M}_R is approximated by amplifying the root mean square value of $R(t)$ by a peak factor \mathcal{P}_R . For linear systems excited by zero mean processes the root mean square values of the responses coincide with their respective standard deviations. Thus,

$$\mathcal{M}_R = \mathcal{P}_R \sqrt{E[R^2(t)]} = \mathcal{P}_R \sigma_R, \quad (3.70)$$

where σ_R is the standard deviation of $R(t)$. To facilitate the notation, the following formulation provides the square of the maximum value, that is

$$\mathcal{M}_R^2 = \mathcal{P}_R^2 E[R^2(t)] = \mathcal{P}_R^2 \sigma_R^2. \quad (3.71)$$

The same rationale presented in the previous chapter to obtain the square of the design response, from the mean square response, is used here to express the design response in terms of the pseudo-acceleration spectrum value, \mathcal{M}_{pa_j} , and the relative velocity response spectrum value, \mathcal{M}_{v_j} , as follows:

$$\begin{aligned} \mathcal{M}_R^2 = & C_s^2 \mathcal{M}_g^2 + 4 C_s \sum_{j=1}^r \left[\frac{\zeta_j \mathcal{M}_{pa_j}^2}{\omega_j^2} + (\delta_j \beta_j \omega_j - \zeta_j) \mathcal{M}_{v_j}^2 \right] \\ & + 4 \sum_{j=1}^r \left(\frac{\zeta_j^2 \mathcal{M}_{pa_j}^2}{\omega_j^4} + \delta_j^2 \mathcal{M}_{v_j}^2 \right) + 8 \sum_{j=1}^{r-1} \sum_{k=j+1}^r \left[\frac{\tilde{T}_{jk}^I}{\omega_j^4} (\mathcal{M}_{pa_j}^2 - \mathcal{M}_{pa_k}^2) \right. \\ & \left. + \frac{\tilde{T}_{jk}^{II}}{\omega_j^4} (\mathcal{M}_{v_j}^2 - \mathcal{M}_{v_k}^2) + \frac{\zeta_j \zeta_k}{\omega_j^4} \mathcal{M}_{pa_k}^2 + \delta_j \delta_k \mathcal{M}_{v_k}^2 \right], \quad (3.72) \end{aligned}$$

where \mathcal{M}_g is the maximum ground acceleration.

Expression (3.72) has been obtained by assuming that all peak factors (for the ground motion and the modal responses) are approximately equal. The main advantage, of making such an assumption is that the peak factors are eliminated from the expression of \mathcal{M}_R^2 accuracy is lost.

Equation (3.72) represents a response spectrum approach for non-classically damped systems. It is seen that the last two summation terms in this equation represent the response which would be obtained if the mode displacement formulation with a reduced number of modes is used. Among these two terms, the second summation term accounts for the correlation between various modes; this term gains importance when two modal frequencies are closely spaced.

The first term in equation (3.72) accounts for the contribution of the higher modes which have been truncated. This contribution appears as a pseudostatic term as these modes are relatively rigid compared to the input frequency. In rigid structures where many modes have frequencies outside the range of the input frequencies, this term will contribute significantly. The correlation between the pseudostatic response of the higher modes and the dynamic response of the retained lower modes is considered through the second term in equation (3.72). The relative contribution of this term and other terms, of course, depends upon the frequency characteristics of the input as well as the number of modes considered in the analysis.

To obtain the design response from equation (3.72), one needs to have the modal properties, the results from a simple static analysis, as well as the input defined in terms of the pseudo-acceleration and relative velocity response spectra. Often,

however, the latter spectrum is not available in practice. In such case, it is usually assumed to be equal to the pseudo-velocity spectrum. This, of course, introduces error in the calculated response. As done in the case of classically damped systems in the previous chapter, the effect of such an assumption on the accuracy of the calculated response is also evaluated in this chapter.

3.5 Numerical Results

To illustrate the effectiveness of the proposed response spectrum approach for non-classically damped systems, here numerical results obtained for a structure with three different stiffness characteristics are presented. Figure 3.1 shows the schematic of this structure which consists of rigid slab diaphragms supported on columns and shear walls. The mass centers of the diaphragms are eccentrically placed with respect to the stiffness centers. Thus, each slab has three degrees of freedom —two translations in the x - and y -directions in the horizontal plane and a rotation about vertical z axis— with a total of 18 degrees of freedom in each structure. The stiffness and mass characteristic of the structure in various stories are chosen to give closely spaced frequencies. The first ten modal frequencies and damping ratios obtained from the complex eigenvalues in the three different stiffness cases are shown in table 3.1. The structures with these frequency characteristics are designated as flexible, medium stiff and stiff structures.

To demonstrate the effectiveness of the proposed approach in reducing the error due to truncation of modes, the numerical response results obtained by the proposed approach utilizing a smaller number of modes are compared with the bench-mark

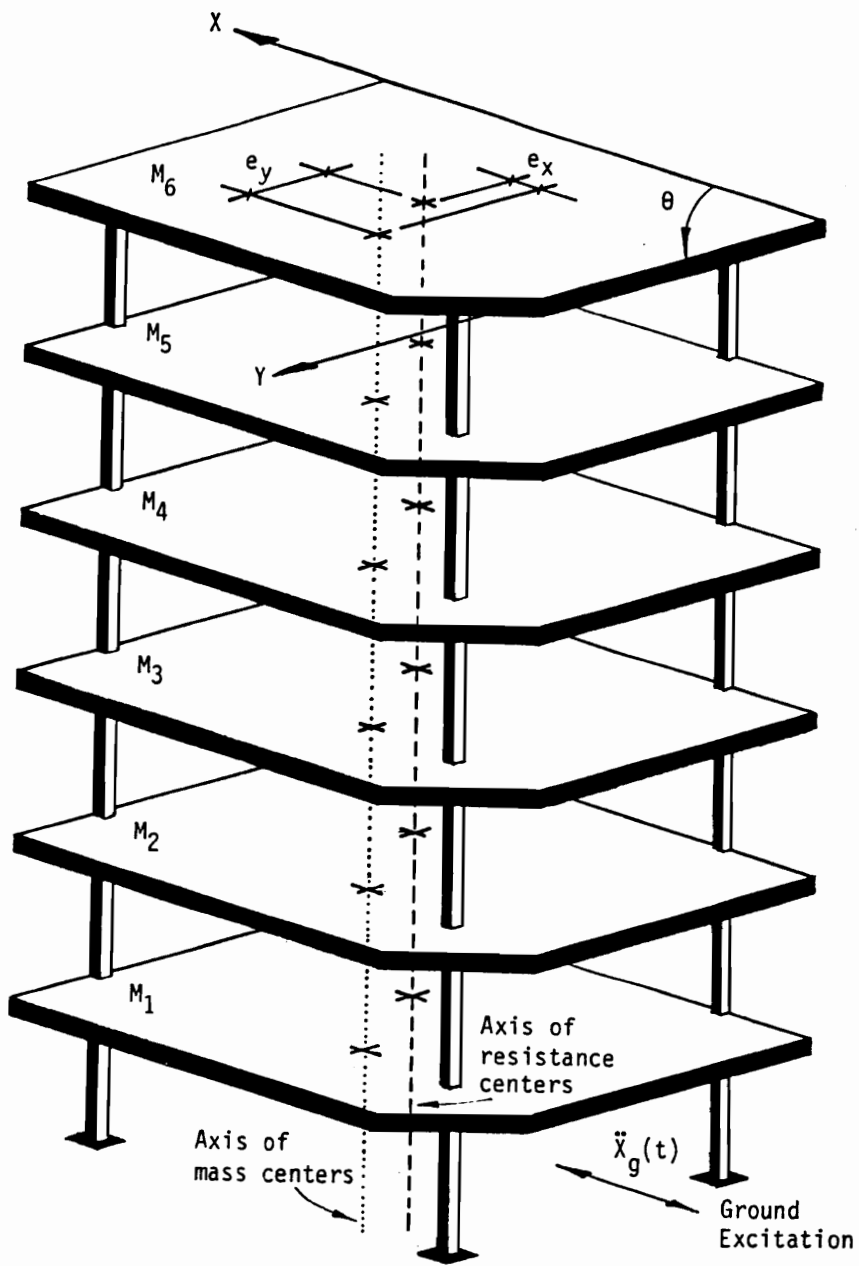


Figure 3.1: Schematic of the structure analyzed .

Table 3.1: First ten natural frequencies and damping ratios for the three structures

<i>Mode</i>	<i>Structure</i>					
	<i>Flexible</i>		<i>Medium Stiff</i>		<i>Stiff</i>	
	ω_j (Hz)	β_j (%)	ω_j (Hz)	β_j (%)	ω_j (Hz)	β_j (%)
1	5.0075	0.91	19.9872	1.37	29.9610	2.01
2	5.0078	2.24	19.9883	3.65	29.9628	5.52
3	5.3644	1.69	21.4069	2.69	32.0750	4.04
4	13.0025	2.17	51.9146	3.42	77.8514	5.07
5	13.0034	5.99	51.9212	9.62	77.8766	14.47
6	13.9180	4.38	55.5021	6.99	83.0796	10.48
7	21.0909	3.47	84.2308	5.47	126.3230	8.10
8	21.0937	9.77	84.2636	15.67	126.4331	23.61
9	22.5476	7.10	89.8509	11.34	134.4355	16.96
10	26.3587	4.31	105.2759	6.79	157.8753	10.07

results of the mode displacement approach utilizing the complete set of modes. The difference in the two results is plotted as percent error for increasing number of modes considered in the analysis in figures 3.2–3.7. All these results pertain to the bending moment response in a column in the first story. A small error indicates that the method is effective in reducing the error due to truncation of modes.

The results obtained by the proposed approach are identified by the acronym MMD (Modified Mode Displacement). Also shown in these figures are the truncation errors in the results of the (1) mode displacement approach of Reference [43], identified by letters MD and (2) mode acceleration approach of Reference [49], identified by letters MA.

Figures 3.2, 3.3 and 4.4 are for the base input defined by Kanai-Tajimi spectral density function with a cut-off frequency of 16 cps. The plotted error is in the root mean square response. Figure 3.2, 3.3 and 3.4, respectively, are for the flexible,

medium stiff and stiff structures, the dynamic properties of which are shown in table 3.1. It is seen that for any number of modes utilized in the analysis the errors in the results of the proposed approach (MMD) and mode acceleration (MA) are always the lowest. (These two approaches also provide almost identical results). Also the rate of convergence to the correct response is fastest with these two approaches. For the low frequency structure, Figure 3.2, the mode displacement approach also provides acceptable results with just a few modes considered in the analysis, as dominant modes are within the frequency range of the input. The error in the mode displacement approach, however, increases as the structure becomes more rigid, with several dominant frequencies outside the input frequency range. As seen in Figure 3.4, the error becomes insignificant in the proposed approach with only three modes considered in the analysis, whereas it remains fairly high even when a large number of modes are considered in the classical mode displacement formulation. The advantage of using the proposed modified mode displacement formulation, with rigid as well as flexible structures, is thus obvious.

The effect of the assumption that the relative velocity is the same as the pseudo-velocity on the error in the root mean square response is also shown in Figures 3.2, 3.3 and 3.4. The curve identified as PMD shows the results obtained by the mode displacement approach but with the assumption of the equality of the two velocities. Similarly, the PMMD curve shows the results obtained by the proposed modified mode displacement approach with the same assumption (The prefix P signifies that the pseudo-velocity has been used in place of the relative velocity in the calculation of these results). Comparison, of these curves with the curves obtained without any assumption about relative velocity response indicates that, when a first few modes are considered, the error in the response could be more or less without any specific

pattern. Also, when a large number of modes have been included, the error is always larger because of this assumption. Thus, in general, the assumption that relative velocity is equal to the pseudo-velocity is not acceptable.

Figures 3.5, 3.6 and 3.7 are similar to the preceding three figures except that they are for the base input defined by response spectra. These spectra are similar to the spectra commonly used for the design of nuclear power plants [38]. The results shown are thus for the design bending moment in a lower story column. The percent difference in the response values obtained by the proposed method and the benchmark value obtained by the untruncated mode displacement-based response spectrum approach are presented as percent errors in these figures. Validity of the mode displacement approach as well as the mode acceleration approach were established by numerical simulation studies using ensemble of seismic motion, as reported in References [17] and [49]. The results in these figures are similar to those in figures 3.2, 3.3 and 3.4. That is, for the low frequency structure, the mode displacement method as well as the proposed method provide accurate results. However, in the medium and high frequency structures the error in the mode displacement results remains high even when a large number of modes are used. In general the proposed method always provides the results with least error, whether the structure is stiff or not. The figures 3.5, 3.6 and 3.7 also show the results obtained with the assumption that the pseudo-velocity spectrum is the same as the relative velocity spectrum. The effect of this assumption on the error in the response is similar to the one discussed above for the root mean square response in figures 3.2, 3.3 and 3.4.

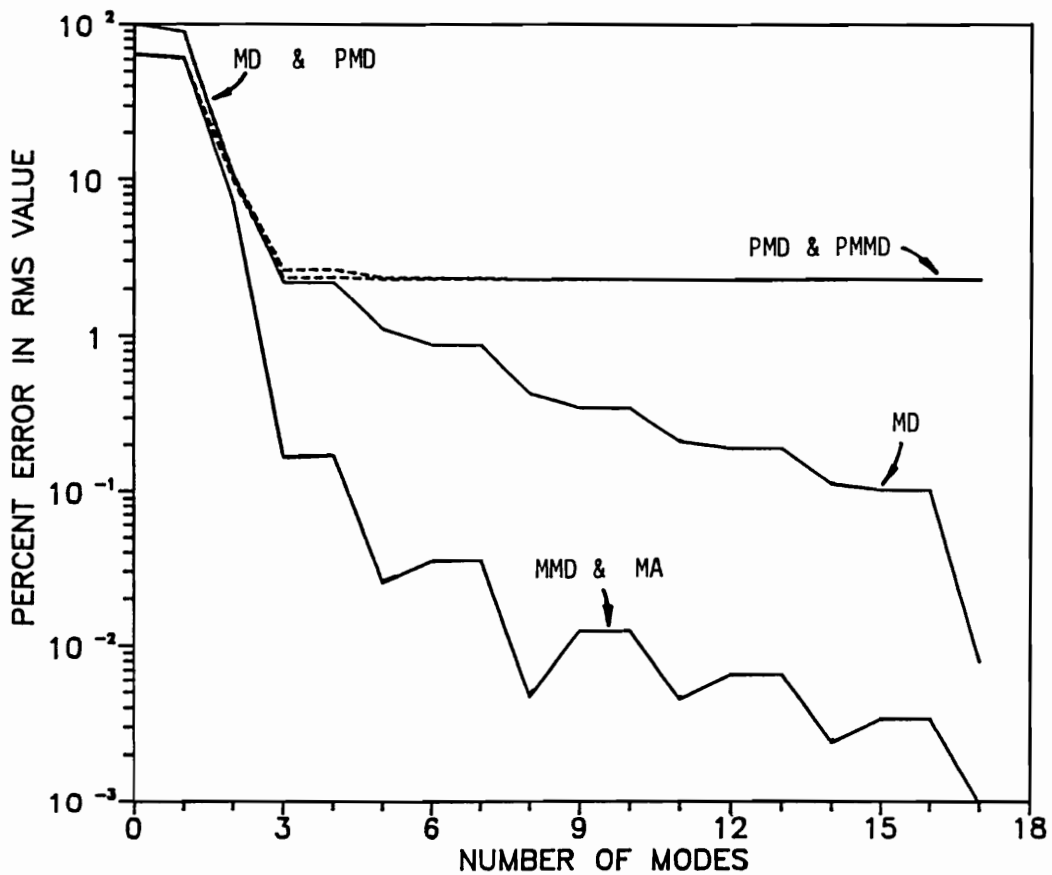


Figure 3.2: Percent error in the root mean square value of a bending moment obtained for Kanai-Tajimi input by different approaches with increasing number of modes — Low frequency structure.

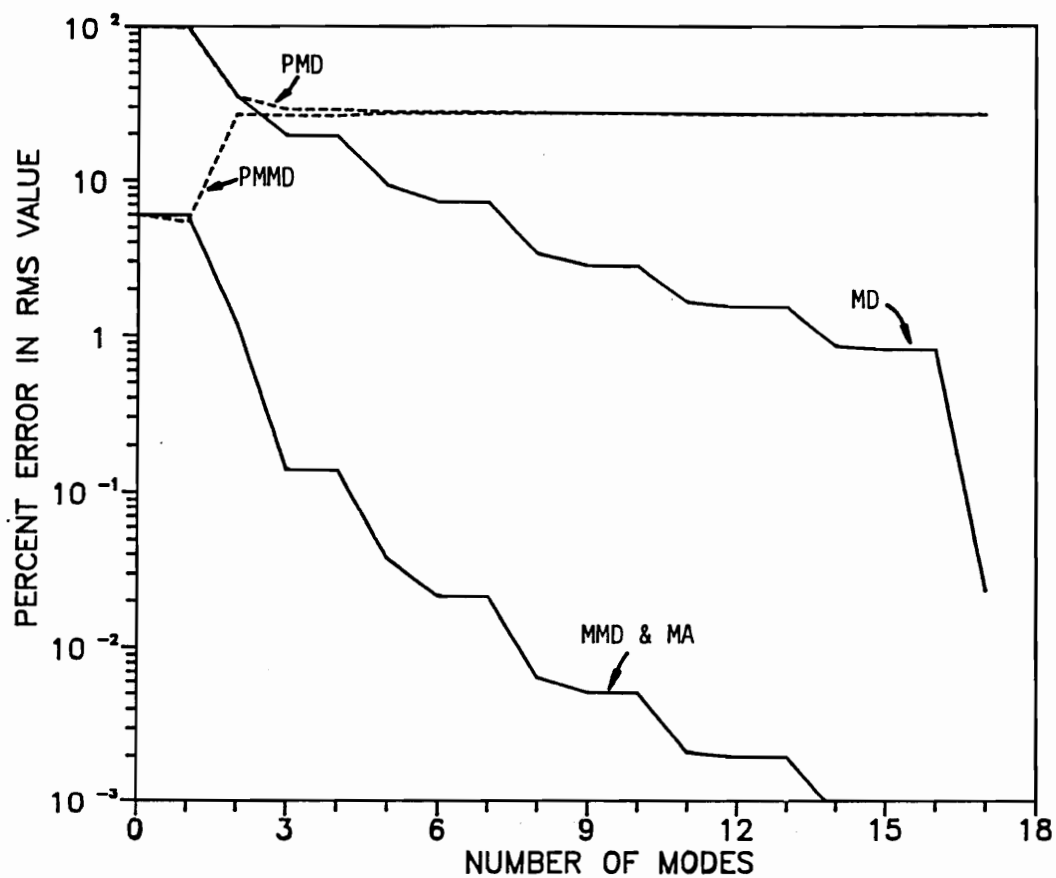


Figure 3.3: Percent error in the root mean square value of a bending moment obtained for Kanai-Tajimi input by different approaches with increasing number of modes — Medium frequency structure .

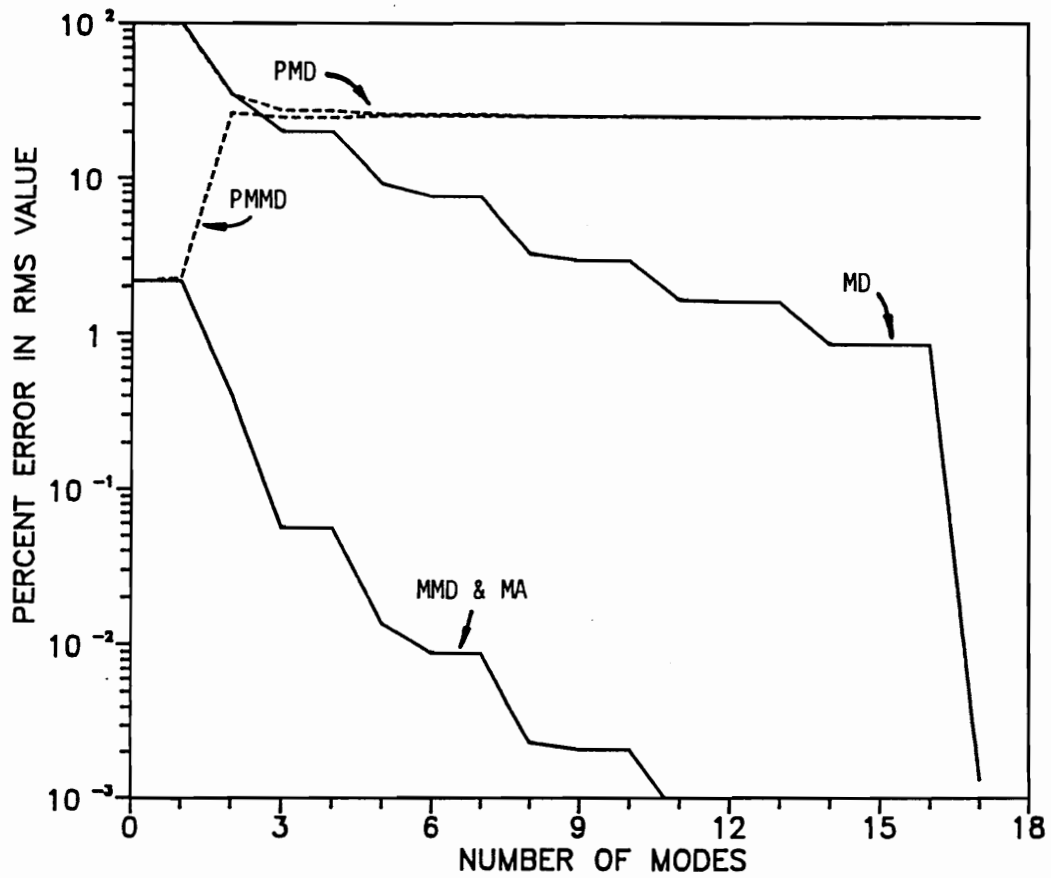


Figure 3.4: Percent error in the root mean square value of a bending moment obtained for Kanai-Tajimi input by different approaches with increasing number of modes — High frequency structure.

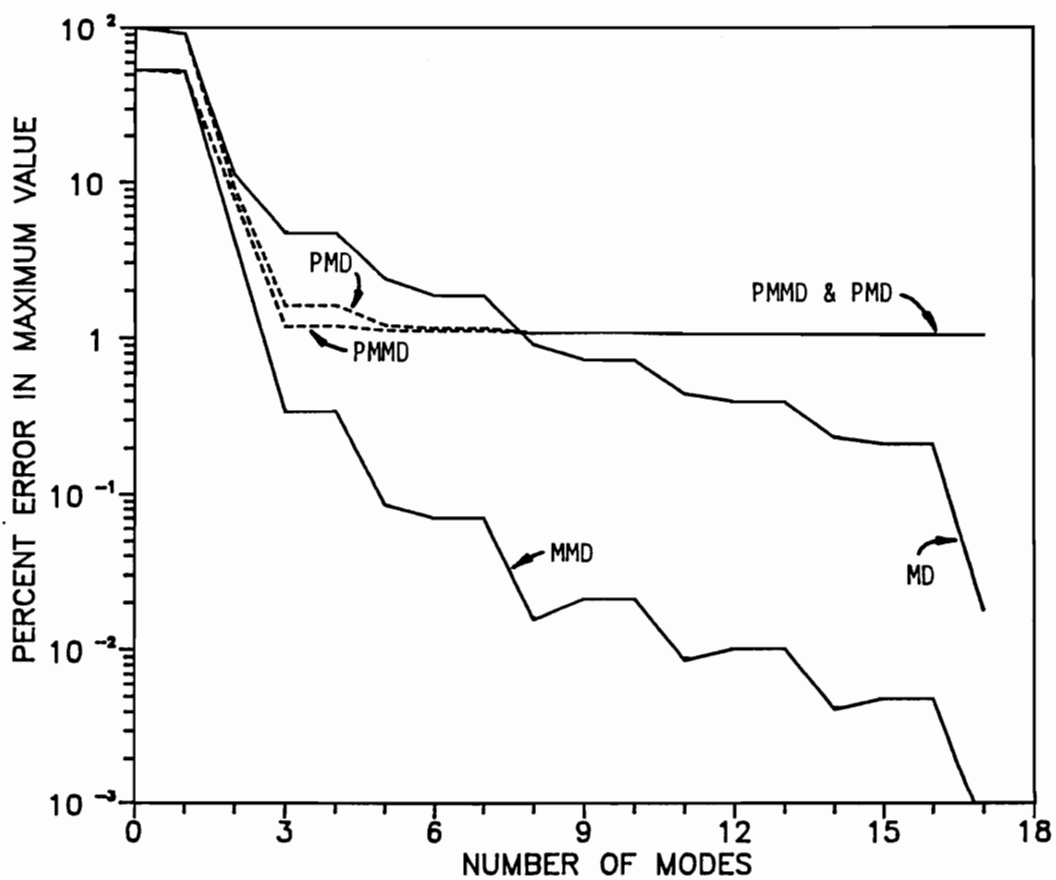


Figure 3.5: Percent error in the design value of a bending moment obtained for response spectrum input by different approaches with increasing number of modes — Low frequency structure

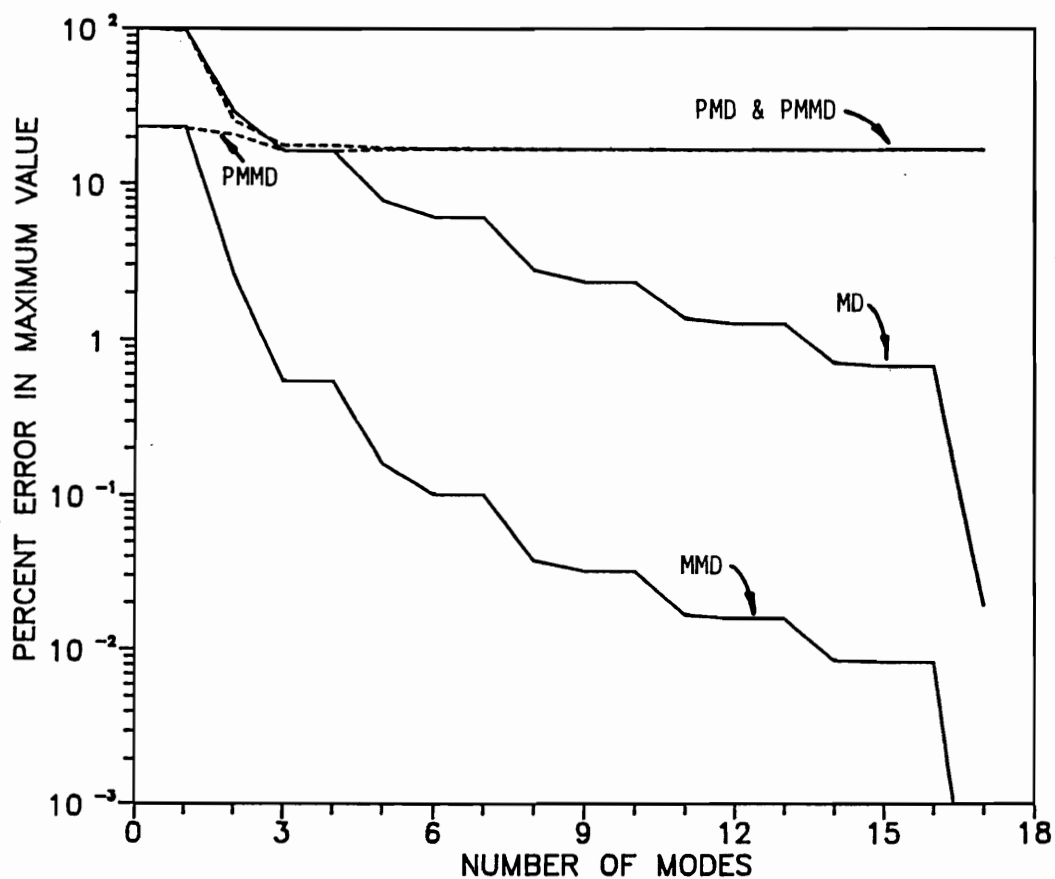


Figure 3.6: Percent error in the design value of a bending moment obtained for response spectrum input by different approaches with increasing number of modes — Medium frequency structure .

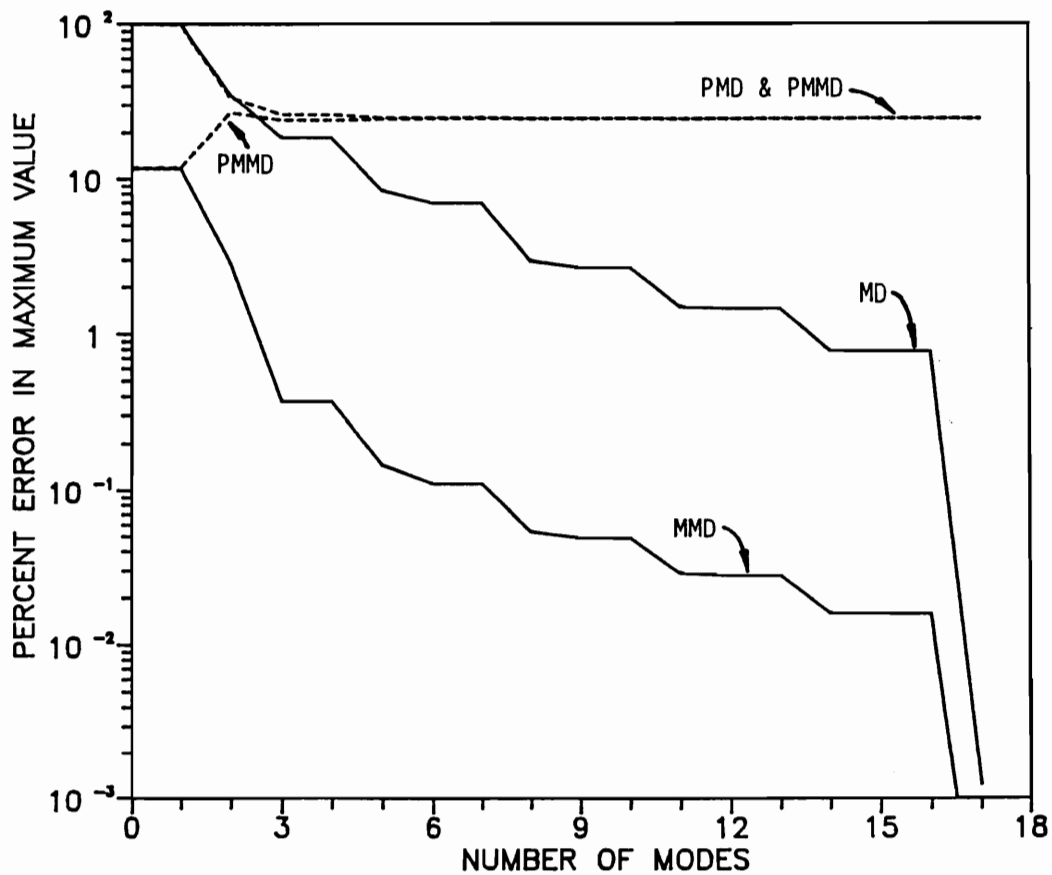


Figure 3.7: Percent error in the design value of a bending moment obtained for response spectrum input by different approaches with increasing number of modes — High frequency structure.

3.6 Conclusions

As done in the normal mode approach for classically damped structures, the truncation of modes can also be effected in the analysis of non-classically damped structures. This truncation can cause error in the calculated response. One way to eliminate this error in the seismic analysis of structures is to adopt the mode acceleration method of structural dynamics. The use of this method with response spectrum approach, however, requires that the seismic input be defined in terms of, rather, uncommon relative acceleration and relative velocity spectra. Herein, an approach combining the good features of both the mode acceleration and mode displacement methods is developed. The proposed approach does not require the input in the form of the relative acceleration spectrum; the conventionally used pseudo-acceleration spectrum can be used, yet the effect of mode truncation is virtually eliminated. The effect of the higher modes which are truncated is included in the formulation through a pseudostatic response term. The proposed methods includes the correlation between the retained modes as well as the correlation between the pseudostatic response of the truncated modes and the dynamic response of the retained modes. The numerical results show that the approach provides more accurate results than the mode displacement based approach both for the stiff as well as flexible structures. However, the improvement in the accuracy of the results of a stiff structure due to utilization of the proposed approach is quite dramatic.

Chapter 4

Random Response of Structures by a Force Derivative Approach

4.1 Introduction

To reduce the error in the response caused by a straight forward truncation of higher modes in a modal analysis procedure, the use of mode acceleration and modified mode displacement procedures was mentioned in the preceding two chapters. In these two methods, the effect of truncated higher modes is included through a pseudostatic response term. This assumes that the dynamic inertial effects of the higher modes are negligible. The validity of the assumption that a high frequency mode does not contribute dynamically to the response depends on how high the modal frequency is relative to the highest frequency in the input force. For modes with frequencies much higher than the forcing function frequencies, this assumption is quite justified as these modes virtually ride with the load without any significant dynamic distortions. However, if the highest frequency in the input is not very much smaller than the lowest frequency of the truncated modes, then the contribution of

the truncated modes can no longer be calculated by a simple static analysis as it is usually done in the mode acceleration method.

To increase the accuracy of the response in such cases, Leung [28] proposed an improvement of the mode acceleration approach for undamped structures by performing successive integration-by-parts of the convolution integral of undamped structures. As in the case of undamped systems, the accuracy of the calculated response can also be improved for damped systems by increasing the number of successive integration-by-parts. This extension of Leung's approach to damped systems has been proposed by Camarda et al [10]. They have called this approach as the *Force Derivative* approach since it involves the terms related to time derivative of the forcing function. Each integration-by-parts increases the order of the derivative of the force by one. Thus, the resulting response expressions for the damped case become quite complicated as the number of integration-by-parts is increased. To obtain numerical results for different time varying forcing functions, Camarda et al used four integration-by-parts terms involving the force derivatives of order four.

In this chapter, the force derivative approach it is further examined with the final aim of utilizing it to calculate the random response. First, the approach is generalized to include the N^{th} order force derivative terms expressed in their simplest and easy-to-calculate forms. This is achieved through a recursive definition of the terms which appear in the process of successive integration-by-parts. The N^{th} order expression is used to obtain the second order statistics of the response for stochastically defined loads. In the approaches presented in references [28] and [10] the convolution integrals involved the force derivative terms. This is, however, not the case in the formulation presented herein. This is of help in a random vibration analysis of the response. An

effective use of the force derivative approach in the development of an improved mode synthesis procedure has recently been made by Suarez and Singh [51]. Numerical results demonstrating the applicability of the proposed response calculating scheme, and the effectiveness of the approach in improving the accuracy of mode truncation analysis are presented.

4.2 Modal Analysis and Truncated MD Approach

For a classically damped linear structure with n degrees of freedom, the equations of motion can be written as:

$$[M] \{\ddot{x}(t)\} + [C] \{\dot{x}(t)\} + [K] \{X(t)\} = \{Q(t)\} \quad (4.1)$$

Where $[M]$ is the mass matrix, $[C]$ is the classical damping matrix, $[K]$ is the stiffness matrix, $\{X(t)\}$ is the response vector and $\{Q(t)\}$ is the loading vector. Also, a dot over a variable denotes its time derivative. It is assumed that the force vector is differentiable up to order N . We will also assume the following initial conditions, although they are not required to be satisfied by the following formulation.

$$\{x(0)\} = \{\dot{x}(0)\} = \{0\} . \quad (4.2)$$

The modal analysis provides the following uncoupled equations of motion:

$$\ddot{z}_j(t) + 2\beta_j \omega_j \dot{z}_j(t) + \omega_j^2 z_j(t) = p_j(t) , \quad j = 1, \dots, n , \quad (4.3)$$

Where ω_j and β_j are the frequency and damping ratio for j^{th} mode, $p_j(t)$ is the generalized modal load defined as:

$$p_j(t) = \{\phi\}_j^T \{Q(t)\} \quad (4.4)$$

The vector $\{z(t)\}$ contains the principal coordinates related to $\{X(t)\}$ as:

$$\{X(t)\} = [\Phi] \{z(t)\} = \sum_{j=1}^n \{\phi\}_j z_j(t) \quad (4.5)$$

The columns of matrix $[\Phi]$ contain the normalized modal vectors $\{\phi\}_1, \{\phi\}_2, \dots, \{\phi\}_n$, which are ordered in accordance to their associated increasing frequencies: $\omega_1 < \omega_2 < \dots < \omega_n$. This matrix, after being normalized with respect to the mass matrix, satisfies the following identities:

$$[\Phi]^T [M] [\Phi] = [I] \quad , \quad [\Phi]^T [C] [\Phi] = [D] \quad , \quad [\Phi]^T [K] [\Phi] = [\Lambda] \quad , \quad (4.6)$$

where $[I]$ is the $(n \times n)$ identity matrix, $[D]$ is the diagonal modal damping matrix with its j^{th} element defined as $(2\beta_j \omega_j)$, and $[\Lambda]$ is the diagonal modal stiffness matrix which entries contain the eigenvalues $(\lambda_j = \omega_j^2)$. Equation (4.3) is solved for $z_j(t)$ and substituted in equation (4.5) to define the response vector $\{X(t)\}$ as

$$\{X(t)\} = \sum_{j=1}^n \{\phi\}_j \int_0^t h_j(t - \tau) p_j(\tau) d\tau \quad , \quad (4.7)$$

where $h_j(t)$ is the unit impulse response function of equation (4.3)

$$h_j(t) = \frac{e^{-\beta_j \omega_j t}}{\omega_{d_j}} \sin(\omega_{d_j} t) \quad , \quad \omega_{d_j} = \omega_j \sqrt{1 - \beta_j^2} \quad , \quad (4.8)$$

If all n modes of the system are used in equation (4.7), one obtains the exact response. However, in practice only a first few modes are used. Thus, if only the first r modes are considered, one obtains an approximate value of the response as:

$$\{X(t)\}_0 = \sum_{j=1}^r \{\phi\}_j \int_0^t h_j(t - \tau) p_j(\tau) d\tau \quad . \quad (4.9)$$

Equation (4.9) is the classical truncated mode displacement approach. Here it is desired to improve this estimate of the response without including any further modes in the expression. That is, it is desired to include the effect of the higher or truncated modes without explicitly calculating them.

4.3 First Order Force Derivative Approach

The first order FD approach is based on the first integration by parts of equation (4.7). The details concerning any number of integrations by parts of the Duhamel integral are provided in appendix B. Therefore, following appendix B, the integration of equation (7) once by parts can be written as:

$$\begin{aligned} \{X(t)\} &= \sum_{j=1}^n \{\phi\}_j \frac{1}{\omega_j^2} \ddot{p}_j(t) - \sum_{j=1}^n \{\phi\}_j \left[\left(\frac{2\beta_j}{\omega_j} \right) \dot{h}_j(t) + \frac{1}{\omega_j^2} \ddot{h}_j(t) \right] p_j(0) \\ &\quad - \sum_{j=1}^n \{\phi\}_j \left[\left(\frac{2\beta_j}{\omega_j} \right) \int_0^t h_j(t-\tau) \dot{p}_j(\tau) d\tau + \left(\frac{1}{\omega_j^2} \right) \int_0^t \dot{h}_j(t-\tau) \ddot{p}_j(\tau) d\tau \right]. \end{aligned} \quad (4.10)$$

It is easy to show, [15, 50], that the first summation term of equation (4.10) can be obtained as the static solution of the following expression:

$$\sum_{j=1}^n \{\phi\}_j \frac{1}{\omega_j^2} \ddot{p}_j(t) = [\Phi] [\Lambda]^{-1} [\Phi]^T \{Q(t)\} = [K]^{-1} \{Q(t)\} \quad (4.11)$$

Substituting equation (4.11) in (4.10) and truncating the second and third summations up to r modes, one obtains, what here is called, the first order approximation of the true response as follows:

$$\begin{aligned} \{X(t)\}_1 &= [K]^{-1} \{Q(t)\} - \sum_{j=1}^r \{\phi\}_j \left[\left(\frac{2\beta_j}{\omega_j} \right) \dot{h}_j(t) + \frac{1}{\omega_j^2} \ddot{h}_j(t) \right] p_j(0) \\ &\quad - \sum_{j=1}^r \{\phi\}_j \left[\left(\frac{2\beta_j}{\omega_j} \right) \int_0^t h_j(t-\tau) \dot{p}_j(\tau) d\tau + \left(\frac{1}{\omega_j^2} \right) \int_0^t \dot{h}_j(t-\tau) \ddot{p}_j(\tau) d\tau \right]. \end{aligned} \quad (4.12)$$

Also, if the truncation of modes is effected in equation (4.10), one obtains the zero order approximation $\{X(t)\}_0$. That is,

$$\begin{aligned} \{X(t)\}_0 &= \sum_{j=1}^r \{\phi\}_j \frac{1}{\omega_j^2} \ddot{p}_j(t) - \sum_{j=1}^r \{\phi\}_j \left[\left(\frac{2\beta_j}{\omega_j} \right) \dot{h}_j(t) + \frac{1}{\omega_j^2} \ddot{h}_j(t) \right] p_j(0) \\ &\quad - \sum_{j=1}^r \{\phi\}_j \left[\left(\frac{2\beta_j}{\omega_j} \right) \int_0^t h_j(t-\tau) \dot{p}_j(\tau) d\tau + \left(\frac{1}{\omega_j^2} \right) \int_0^t \dot{h}_j(t-\tau) \ddot{p}_j(\tau) d\tau \right]. \end{aligned} \quad (4.13)$$

Eliminating the second and third summation terms from equation (4.12) and (4.13), one obtains:

$$\{X(t)\}_1 = \{X(t)\}_0 + \left[[K]^{-1} \{Q(t)\} - \sum_{j=1}^r \{\phi\}_j \left(\frac{1}{\omega_j^2} \right) p_j(t) \right] . \quad (4.14)$$

This relates the classical truncated mode displacement solution $\{X(t)\}_0$ to the first order solution $\{X(t)\}_1$. Obviously, the terms in parentheses represent the first order pseudo-static contribution of the higher modes to the response. Equation (4.14) is nothing but an alternative form of the classical mode acceleration approach. Actually it is just the modified mode displacement approach developed in chapter 2. This was also obtained by Leger and Wilson [26] through a quite different analysis. An advantage of the form of equation (4.14) over the classical mode acceleration form, is that here the improved response is expressed in terms of the response obtained by the classical truncated mode displacement approach. Also in equation (4.14), the absence of any force derivative terms is noted. This was, however, not the case in the formulation developed by Leung [28] and Camarda et. al. [10]. This absence of derivative terms simplifies the analysis.

4.4 Second Order Force Derivative Approach

To further improve the truncated mode solution, equation (4.10) is integrated by parts again. After some rearrangements of terms and simplification (see appendix B) it can be shown that

$$\begin{aligned} \{X(t)\} &= \sum_{j=1}^n \{\phi\}_j \left(\frac{1}{\omega_j^2} \right) p_j(t) - \sum_{j=1}^n \{\phi\}_j \left(\frac{2\beta_j}{\omega_j^3} \right) \dot{p}_j(t) \\ &\quad - \sum_{j=1}^n \{\phi\}_j \left[\left(\frac{2\beta_j}{\omega_j} \right) h_j(t) + \left(\frac{1}{\omega_j^2} \right) \dot{h}_j(t) \right] p_j(0) \end{aligned}$$

$$\begin{aligned}
& + \sum_{j=1}^n \{\phi\}_j \left[\left(\frac{4\beta_j^2 - 1}{\omega_j^2} \right) h_j(t) + \left(\frac{2\beta_j}{\omega_j^3} \right) \dot{h}_j(t) \right] \dot{p}_j(0) \\
& + \sum_{j=1}^n \{\phi\}_j \left[\left(\frac{4\beta_j^2 - 1}{\omega_j^2} \right) \int_0^t h_j(t-\tau) \tilde{p}_j(\tau) d\tau + \left(\frac{2\beta_j}{\omega_j^3} \right) \int_0^t \dot{h}_j(t-\tau) \tilde{p}_j(\tau) d\tau \right].
\end{aligned} \tag{4.15}$$

The first summation term is expressed as a static solution in equation (4.11). To avoid the use of the higher modes in the calculation of the second summation term, one can also express it in terms of the matrices $[K]$ and $[C]$ as follows:

$$\sum_{j=1}^n \{\phi\}_j \left(\frac{2\beta_j}{\omega_j^3} \right) \dot{p}_j(t) = \sum_{j=1}^n \{\phi\}_j \left(\frac{1}{\omega_j^2} \right) (2\beta_j \omega_j) \left(\frac{1}{\omega_j^2} \right) \dot{p}_j(t) = [K]^{-1} [C] [K]^{-1} \{\dot{Q}(t)\}. \tag{4.16}$$

Substituting equations (4.11) and (4.16) into equation (4.15), and then performing the truncation of modes in the remaining terms, one obtains the second order estimate of the response as follows:

$$\begin{aligned}
\{X(t)\}_2 &= [K]^{-1} \{Q(t)\} - [K]^{-1} [C] [K]^{-1} \{\dot{Q}(t)\} \\
&- \sum_{j=1}^r \{\phi\}_j \left[\left(\frac{2\beta_j}{\omega_j} \right) h_j(t) + \left(\frac{1}{\omega_j^2} \right) \dot{h}_j(t) \right] p_j(0) \\
&+ \sum_{j=1}^r \{\phi\}_j \left[\left(\frac{4\beta_j^2 - 1}{\omega_j^2} \right) h_j(t) + \left(\frac{2\beta_j}{\omega_j^3} \right) \dot{h}_j(t) \right] \dot{p}_j(0) \\
&+ \sum_{j=1}^r \{\phi\}_j \left[\left(\frac{4\beta_j^2 - 1}{\omega_j^2} \right) \int_0^t h_j(t-\tau) \tilde{p}_j(\tau) d\tau + \left(\frac{2\beta_j}{\omega_j^3} \right) \int_0^t \dot{h}_j(t-\tau) \tilde{p}_j(\tau) d\tau \right].
\end{aligned} \tag{4.17}$$

It is also observed that if the summations in equation (4.15) are only extended up to r , it becomes equal to $\{X(t)\}_0$. That is,

$$\begin{aligned}
\{X(t)\} &= \sum_{j=1}^r \{\phi\}_j \left(\frac{1}{\omega_j^2} \right) p_j(t) - \sum_{j=1}^r \{\phi\}_j \left(\frac{2\beta_j}{\omega_j^3} \right) \dot{p}_j(t) \\
&- \sum_{j=1}^r \{\phi\}_j \left[\left(\frac{2\beta_j}{\omega_j} \right) h_j(t) + \left(\frac{1}{\omega_j^2} \right) \dot{h}_j(t) \right] p_j(0) \\
&+ \sum_{j=1}^r \{\phi\}_j \left[\left(\frac{4\beta_j^2 - 1}{\omega_j^2} \right) h_j(t) + \left(\frac{2\beta_j}{\omega_j^3} \right) \dot{h}_j(t) \right] \dot{p}_j(0)
\end{aligned}$$

$$+ \sum_{j=1}^r \{\phi\}_j \left[\left(\frac{4\beta_j^2 - 1}{\omega_j^2} \right) \int_0^t h_j(t - \tau) \bar{p}_j(\tau) d\tau + \left(\frac{2\beta_j}{\omega_j^3} \right) \int_0^t \dot{h}_j(t - \tau) \bar{p}_j(\tau) d\tau \right]. \quad (4.18)$$

Eliminating the last three summation terms from equations (4.17) and (4.18) one obtains

$$\begin{aligned} \{X(t)\}_2 &= \{X(t)\}_0 + [K]^{-1} \{Q(t)\} - \sum_{j=1}^r \{\phi\}_j \left(\frac{1}{\omega_j^2} \right) p_j(t) \\ &\quad - [K]^{-1} [C] [K]^{-1} \{\dot{Q}(t)\} + \sum_{j=1}^r \{\phi\}_j \left(\frac{2\beta_j}{\omega_j^3} \right) \dot{p}_j(t). \end{aligned} \quad (4.19)$$

This equation expresses the second order estimate of the response in terms of the classical truncated mode displacement estimate plus some terms which represent the first and second order pseudostatic contributions of the higher modes. It is also noted that the first three terms are the same as $\{X(t)\}_1$. The remaining two terms represent the improvement over $\{X(t)\}_1$ due to consideration of the force derivative terms which are evaluated by a simple static type of analysis.

4.5 N^{th} Order Force Derivative Approach

Equation (4.19) will now be generalized to the N^{th} order estimate of the response by successive integration by parts N times. After some algebra and simplification (see appendix B), it can be shown that

$$\begin{aligned} \{X(t)\} &= \sum_{j=1}^n \{\phi\}_j \left[\sum_{k=1}^N \Upsilon_{j,k} \overset{<k-1>}{p}_j(t) \right] \\ &\quad + \sum_{j=1}^n \{\phi\}_j \left[\sum_{k=1}^N \left(\omega_j^2 \Upsilon_{j,k+1} h_j(t) - \Upsilon_{j,k} \dot{h}_j(t) \right) \overset{<k-1>}{p}_j(t) \right] \\ &\quad + \sum_{j=1}^n \{\phi\}_j \left[\omega_j^2 \Upsilon_{j,N+1} \int_0^t h_j(t - \tau) \overset{<N>}{p}_j(t) d\tau - \Upsilon_{j,N} \int_0^t \dot{h}_j(t - \tau) \overset{<N>}{p}_j(\tau) d\tau \right], \end{aligned} \quad (4.20)$$

where a number between angles, at the top of a variable, indicates the number of time derivatives, and the coefficients $\Upsilon_{j,k}$ are defined in appendix B by a second order recursive formula as:

$$\Upsilon_{j,k} = -\frac{2\beta_j}{\omega_j} \Upsilon_{j,k-1} - \frac{1}{\omega_j^2} \Upsilon_{j,k-2} \quad , \quad \Upsilon_{j,0} = 0 \quad , \quad \Upsilon_{j,-1} = -1 . \quad (4.21)$$

As it was done for the first and second order cases earlier, it is indeed possible to express the first summation in equation (4.20) in terms of the mass, stiffness and damping matrices by introducing the matrix $[F]_k$:

$$\sum_{j=1}^n \{\phi\}_j \left[\sum_{k=1}^N \Upsilon_{j,k} \frac{\langle k-1 \rangle}{p_j(t)} \right] = \sum_{k=1}^N [F]_k \frac{\langle k-1 \rangle}{\{Q(t)\}} , \quad (4.22)$$

where $[F]_k$ is a type of flexibility matrix, herein called the k^{th} pseudo-flexibility matrix, and it is defined by the following expression:

$$[F]_k = \sum_{j=1}^n \{\phi\}_j \Upsilon_{j,k} \{\phi\}_j^T , \quad (4.23)$$

which, in terms of the structural matrices, can be expressed by the following recursive formula (appendix C):

$$[F]_k = -[K]^{-1} \{ [C] [F]_{k-1} + [M] [F]_{k-2} \} \quad , \quad [F]_0 = [0] \quad , \quad [F]_1 = [K]^{-1} . \quad (4.24)$$

Substituting equation (4.22) into equation (4.20) and considering the modal summation only up to r modes in the second and third summation terms, we obtain the N^{th} order approximation of the response as

$$\begin{aligned} \{X(t)\}_N = & \sum_{k=1}^N [F]_k \frac{\langle k-1 \rangle}{\{Q(t)\}} + \sum_{j=1}^r \{\phi\}_j \left[\sum_{k=1}^N \left(\omega_j^2 \Upsilon_{j,k+1} h_j(t) - \Upsilon_{j,k} \dot{h}_j(t) \right) \frac{\langle k-1 \rangle}{p_j(t)} \right]_{t=0} \\ & + \sum_{j=1}^r \{\phi\}_j \left[\omega_j^2 \Upsilon_{j,N+1} \int_0^t h_j(t-\tau) \frac{\langle N \rangle}{p_j(\tau)} d\tau - \Upsilon_{j,N} \int_0^t \dot{h}_j(t-\tau) \frac{\langle N \rangle}{p_j(\tau)} d\tau \right] . \end{aligned} \quad (4.25)$$

One can also obtain $\{X(t)\}_0$ from equation (4.20) by carrying out the modal summation up to r modes. Subtracting such an expression of $\{x(t_0)\}$ from equation (4.25) one obtains

$$\{X(t)\}_N = \{X(t)\}_0 + \sum_{k=1}^N [F]_k \{Q(t)\}^{<k-1>} - \sum_{k=1}^N \sum_{j=1}^r \{\phi\}_j \Upsilon_{j,k} \{p_j(t)\}^{<k-1>} \quad (4.26)$$

Since $p_j(t) = \{\phi_j\}^T \{Q(t)\}$, one can also write equation (4.26) as:

$$\{X(t)\}_N = \{X(t)\}_0 + \sum_{k=1}^N \{X_h(t)\}_k, \quad (4.27)$$

where

$$\{X_h(t)\}_k = \overbrace{\left([F]_k - \sum_{j=1}^r \{\phi\}_j \Upsilon_{j,k} \{\phi\}_j^T \right)}^{[F_h]_k} \{Q(t)\}^{<k-1>}. \quad (4.28)$$

$\{X_h(t)\}_k$ can now be interpreted as the k^{th} order pseudo-static contribution of the higher modes to the response. It can be shown that as $N \rightarrow \infty$, the vector $\{X(t)\}_N$ approaches the correct response $\{X(t)\}$.

Equation (4.28) is not quite suitable for numerical work. It is better to obtain the matrix shown in the parentheses of equation (4.28) directly, and not as a difference of two matrices. This matrix will be denoted as $[F_h]_k$ where the superscript h signifies that this is the contribution from the "higher" modes. Using the definition of $[F]_k$ given by equation (4.23) and substituting in equation (4.28), one obtains:

$$[F_h]_k = [F]_k - \sum_{j=1}^r \{\phi\}_j \Upsilon_{j,k} \{\phi\}_j^T = \sum_{j=r+1}^n \{\phi\}_j \Upsilon_{j,k} \{\phi\}_j^T. \quad (4.29)$$

Since $[F_h]_k$ is defined in terms of higher modal vectors, it will be called as the k^{th} pseudo flexibility matrix associated with higher modes. It can be easily shown (appendix C) that this matrix is obtained by the following recursive formula, without

explicitly using the higher modes:

$$\begin{aligned} [F_h]_k &= -[K]^{-1} ([C] [F_h]_{k-1} + [M] [F_h]_{k-2}) \\ [F_h]_0 &= [0] \quad , \quad [F_h]_1 = [K]^{-1} - \sum_{j=1}^r \{\phi\}_j \left(\frac{1}{\omega_j^2} \right) \{\phi\}_j^T . \end{aligned} \quad (4.30)$$

The substitution of $[F_h]_k$, in equation (4.28), by the expression given in equation (4.30), provides the N^{th} order estimate of the response as:

$$\{X(t)\}_N = \{X(t)\}_0 + \sum_{k=1}^N [F_h]_k \{Q(t)\}^{<k-1>} \quad (4.31)$$

Equation (4.31) defines the procedure for calculating the improved estimate of the response, using only the first r modes. An observation of the recursive formula for $[F_h]_k$, suggests that this matrix need not be defined explicitly, rather, each term of the summation can be obtained by successive solutions of simultaneous equations. However, depending upon how many successive steps are required in the calculation of each summation term for $k = 1, \dots, N$, it may be computationally more efficient to store $[K]^{-1}$ once and utilize it whenever needed.

For the convergence of the summation terms in equation (4.31), it is necessary that all structural frequencies, which are lower than the highest frequency component in the input, are included in calculating $\{X(t)\}_0$. That is, the summation term in equation (4.31) only represents the contribution from the modal frequencies which are larger than the highest frequency in the input.

A response quantity, $R(t)$, linearly related to $\{X(t)\}$ can be easily approximated as:

$$R(t) = \{\mathcal{R}\}^T \{X(t)\} \approx \{\mathcal{R}\}^T \{X(t)\}_N , \quad (4.32)$$

where $\{\mathcal{R}\}$ is the vector containing the coefficients of the linear transformation.

The characteristics of the second and fourth order force derivative approaches, with regard to their effectiveness and limitations for calculating the time history response, have been thoroughly explored by Camarda et al [10] for different deterministic forcing functions. Though they presented an alternative formulation, their results are expected to possess the same characteristics as the results obtained by the N^{th} order formulation proposed here, since the latter is just an extension of Camarda et al's formulation but expressed in a different way. That is, the results will depend upon the frequency characteristics of the sustained loads, the duration of the transient loads and the response quantity being calculated. Here, these characteristics will not be investigated. Rather, the effectiveness of this approach for calculating the stationary response for stochastically stationary loads is examined.

4.6 Random Response: Auto-Correlation Function of $R(t)$

For a random forcing function vector, one can use equation (4.32) to obtain the auto-correlation function of the response quantity $R(t)$ as:

$$E[R(t_1) R(t_2)] = \{\mathcal{R}\}^T E[\{X(t_1)\}_N \{X(t_2)\}_N^T] \{\mathcal{R}\} , \quad (4.33)$$

where $E[.]$ denotes the expected value of the quantity in the brackets. Here equation (4.33) will be explicitly evaluated for only proportional load. That is, for the forcing function vector $\{Q(t)\}$ defined as:

$$\{Q(t)\} = \{Q_0\} q(t) \quad (4.34)$$

where $q(t)$ represents a common time variation of all forces and $\{Q_0\}$ is the amplitude vector. Here $q(t)$ will be assumed to be a zero mean stationary random process, de-

finable by its spectral density function $\Phi_q(\omega)$ which is related to the auto-correlation function of $q(t)$ as:

$$C_{00}(t_1 - t_2) = E [q(t_1) q(t_2)] = \int_{-\infty}^{\infty} \Phi_q(\omega) e^{i\omega(t_1 - t_2)} d\omega . \quad (4.35)$$

Using equation (4.9) in (4.31) and, in turn, (4.31) into (4.32), the expression of the response $R(t)$ for this proportional loading can be written as:

$$R(t) = \sum_{j=1}^r \{\mathcal{R}\}^T \{\phi\}_j \int_0^t h_j(t - \tau) \{\phi\}_j^T \{Q_0\} q(\tau) d\tau + \sum_{k=1}^N \{\mathcal{R}\}^T [F_h]_k \{Q_0\} \overset{<k-1>}{q(t)} , \quad (4.36)$$

or in a more compact form

$$R(t) = \sum_{j=1}^r \rho_j \gamma_j \int_0^t h_j(t - \tau) q(\tau) d\tau + \sum_{k=1}^N \{\mathcal{R}\}^T \{U_h\}_k \overset{<k-1>}{q(t)} , \quad (4.37)$$

where ρ_j is the j^{th} modal response quantity, γ_j is the j^{th} modal participation factor, and $\{U_h\}_k$ is the k^{th} pseudo-static response of the higher modes to the amplitude vector. These quantities are defined, respectively, as:

$$\rho_j = \{\mathcal{R}\}^T \{\phi\}_j ; \quad \gamma_j = \{\phi\}_j^T \{Q_0\} ; \quad \{U_h\}_k = [F_h]_k \{Q_0\} . \quad (4.38)$$

It is noted that, like $[F_h]_k$, $\{U_h\}_k$ can also be defined recursively as the solution of the following simultaneous equation:

$$\begin{aligned} [K] \{U_h\}_k &= -[C] \{U_h\}_{k-1} - [M] \{U_h\}_{k-2} \\ \{U_h\}_0 &= \{0\} , \quad [K] \{U_h\}_1 = \{Q_0\} - [K] \sum_{j=1}^r \left(\frac{1}{\omega_j^2} \right) \{\phi\}_j \gamma_j \end{aligned} \quad (4.39)$$

From equation (4.37), the auto-correlation function for $R(t)$ can be expressed as:

$$\begin{aligned} E[R(t_1) R(t_2)] &= E \left[\left(\sum_{j=1}^r \rho_j \gamma_j \int_0^{t_1} h_j(t_1 - \tau_1) q(\tau_1) d\tau_1 + \sum_{k=1}^N \{\mathcal{R}\}^T \{U_h\}_k \overset{<k-1>}{q(t_1)} \right) \right. \\ &\quad \times \left. \left(\sum_{l=1}^r \rho_l \gamma_l \int_0^{t_2} h_l(t_2 - \tau_2) q(\tau_2) d\tau_2 + \sum_{m=1}^N \{\mathcal{R}\}^T \{U_h\}_m \overset{<m-1>}{q(t_2)} \right) \right] , \end{aligned} \quad (4.40)$$

and after expanding this equation and distributing the expected values, it becomes

$$E[R(t_1) R(t_2)] = \Xi_r(t_1, t_2) + \Psi_N(t_1, t_2) + \Delta_N(t_1, t_2) , \quad (4.41)$$

where the quantity $\Xi_r(t_1, t_2)$ contains the terms associated to the retained modes and it is due to the truncated mode displacement approach, $\Psi_N(t_1, t_2)$ contains the terms associated to all N pseudostatic contributions of the truncated modes, and $\Delta_N(t_1, t_2)$ possesses the terms associated to the correlation between the dynamic response of the retained modes and all N pseudostatic contributions of the truncated modes. These three quantities are defined as follows:

$$\Xi_r(t_1, t_2) = \sum_{j=1}^r \sum_{l=1}^r \rho_j \rho_l \gamma_j \gamma_l \int_0^{t_1} \int_0^{t_2} h_j(t_1 - \tau_1) h_l(t_2 - \tau_2) C_{00}(\tau_1 - \tau_2) d\tau_1 d\tau_2 \quad (4.42)$$

$$\Psi_N(t_1, t_2) = \sum_{k=1}^N \sum_{m=1}^N \alpha_k \alpha_m C_{k-1, m-1}(t_1, t_2) , \quad (4.43)$$

$$\begin{aligned} \Delta_N(t_1, t_2) = & \sum_{m=1}^N \sum_{j=1}^r \alpha_m \rho_j \gamma_j \int_0^{t_1} h_j(t_1 - \tau_1) C_{0, m-1}(\tau_1, t_2) d\tau_1 \\ & + \sum_{k=1}^N \sum_{l=1}^r \alpha_k \rho_l \gamma_l \int_0^{t_2} h_j(t_2 - \tau_2) C_{k-1, 0}(t_1, \tau_2) d\tau_2 . \end{aligned} \quad (4.44)$$

where

$$\alpha_k = \{\mathcal{R}\}^T \{U_h\}_k , \quad (4.45)$$

and the cross-correlation function of the m^{th} and k^{th} derivative of $q(t)$ is defined as:

$$C_{k, m}(t_1, t_2) = E \left[\overset{<k>}{q(t_1)} \overset{<m>}{q(t_2)} \right] = \frac{\partial^{k+m} C_{00}(t_1, t_2)}{\partial t_1^k \partial t_2^m} . \quad (4.46)$$

4.7 Random Response: Stationary Mean Square Value of $R(t)$

For a stationary input $q(t)$, with power spectral density function $\Phi_q(\omega)$, the response statistics of a linear system are also stationary. In particular, the stationary

mean square value of the response $R(t)$ can be obtained by considering the limit of equation (4.41) as $t_1 = t_2 = t \rightarrow \infty$. Here, this limiting process will be performed independently on each term of equation (4.41). During this process it will be useful to consider the following relationships:

$$C_{k,m}(t_1, t_2) = E \left[\frac{\langle k \rangle}{q(t_1)} \frac{\langle m \rangle}{q(t_2)} \right] = \int_{-\infty}^{\infty} \Phi_{\frac{\langle k \rangle}{q(t_1)} \frac{\langle m \rangle}{q(t_2)}}(\omega) e^{i\omega(t_1-t_2)} d\omega, \quad (4.47)$$

where it can be easily shown that:

$$\Phi_{\frac{\langle k \rangle}{q(t_1)} \frac{\langle m \rangle}{q(t_2)}}(\omega) = (i\omega)^k (-i\omega)^m \Phi_q(\omega) = i^{k-m} \omega^{k+m} \Phi_q(\omega). \quad (4.48)$$

4.7.1 Contribution of the Retained Modes

The limit of $\Xi_r(t_1, t_2)$ as $t_1 = t_2 = t \rightarrow \infty$ is denoted as Ξ_r , and has already been developed in chapter 2 to get

$$\begin{aligned} \Xi_r &= \sum_{j=1}^r \rho_j^2 \gamma_j^2 I_j(0) \\ &+ 2 \sum_{j=1}^{r-1} \sum_{k=j+1}^r \rho_j \rho_k \gamma_j \gamma_k \left[T_{jk}^I I_j(0) + T_{jk}^{II} (I_j(2) - I_k(2)) + T_{jk}^{III} I_k(0) \right], \end{aligned} \quad (4.49)$$

where $I_j(s)$ denotes the following frequency integral

$$I_j(s) = \int_{-\infty}^{\infty} \omega^s \Phi_g(\omega) |H_j^c(\omega)|^2 d\omega, \quad (4.50)$$

and $H_j^c(\omega) = [\omega_j^2 - \omega^2 + 2i\beta_j \omega_j \omega]^{-1}$ is the stationary complex frequency response function of a single-degree-of-freedom oscillator with frequency ω_j and damping ratio β_j . The partial fraction coefficients T_{jk}^I , T_{jk}^{II} and T_{jk}^{III} are provided in equations (2.61–1.65).

4.7.2 Contribution Due to the Correlation Between Retained and Truncated Modes

To obtain the limit of $\Psi_N(t_1, t_2)$ as $t_1 = t_2 = t \rightarrow \infty$, first equation (4.47) is substituted into equation (4.43) (with the appropriate subscripts), to get

$$\Psi_N(t_1, t_2) = \sum_{k=1}^N \sum_{m=1}^N \alpha_k \alpha_m i^{k-m} \int_{-\infty}^{\infty} \omega^{k+m-2} \Phi_g(\omega) e^{i\omega(t_1-t_2)} d\omega . \quad (4.51)$$

At the limit, $\Psi_N(t_1, t_2)$ is denoted as Ψ_N and its expression is

$$\Psi_N = \sum_{k=1}^N \sum_{m=1}^N i^{k+3m} \alpha_k \alpha_m I_*(k+m-2) , \quad (4.52)$$

where it should be noticed that $i^{k-m} = i^{k+3m}$, and $I_*(s)$ is the following frequency integral:

$$I_*(s) = \int_{-\infty}^{\infty} \omega^s \Phi_g(\omega) d\omega . \quad (4.53)$$

To compact even further the notation, equation (4.52) can be written as

$$\Psi_N = \sum_{k=1}^N \sum_{m=1}^N i^{k+3m} \psi_{k,m} , \quad (4.54)$$

where $\psi_{j,k}$ is given by

$$\psi_{k,m} = \psi_{m,k} = \alpha_k \alpha_m I_*(k+m-2) . \quad (4.55)$$

The calculation of Ψ_N can be performed with significant numerical advantage by recognizing the symmetry and pattern of the terms involved in the summation process. First it should be noticed that $I_*(s) = 0$ for s being an odd number. In that case, the integrand is an odd function which will be integrated from $-\infty$ to ∞ . Therefore, for various values of k and m , the entries in the summation of equation

(4.54) are shown in the following $(N \times N)$ matrix

$$\begin{array}{ccccccc}
\psi_{1,1} & 0 & -\psi_{1,3} & 0 & \psi_{1,5} & 0 & -\psi_{1,7} & \dots \\
0 & \psi_{2,2} & 0 & -\psi_{2,4} & 0 & \psi_{2,6} & 0 & \dots \\
-\psi_{1,3} & 0 & \psi_{3,3} & 0 & -\psi_{3,5} & 0 & \psi_{3,7} & \dots \\
0 & -\psi_{2,4} & 0 & \psi_{4,4} & 0 & -\psi_{4,6} & 0 & \dots \\
\psi_{1,5} & 0 & -\psi_{3,5} & 0 & \psi_{5,5} & 0 & -\psi_{5,7} & \dots \\
0 & \psi_{2,6} & 0 & -\psi_{4,6} & 0 & \psi_{6,6} & 0 & \dots \\
-\psi_{1,7} & 0 & \psi_{3,7} & 0 & -\psi_{5,7} & 0 & \psi_{7,7} & \dots \\
\vdots & \vdots & \vdots & \vdots & \vdots & \vdots & \vdots & \ddots
\end{array}$$

For increasing values of N the elements in the leading $(N \times N)$ matrix are required to be summed up in equation (4.54) to obtain Ψ_N . This summation can be given by the following recursive formula:

$$\Psi_N = \Psi_{N-1} + \psi_{N,N} + 2 \sum_{j=1}^{J_N} (-1)^j \psi_{(N-2j),N} \quad , \quad \Psi_0 = 0 \quad , \quad J_N = \frac{2N-3-(-1)^N}{4} . \quad (4.56)$$

4.7.3 Contribution of the Truncated Modes

Similarly, appropriate substitutions of equation (4.47) into equation (4.44) produces

$$\begin{aligned}
\Delta_N(t_1, t_2) = & \\
& + \sum_{m=1}^N \sum_{j=1}^r \alpha_m \rho_j \gamma_j \int_0^{t_1} h_j(t_1 - \tau_1) i^{-(m-1)} \int_{-\infty}^{\infty} \omega^{m-1} \Phi_q(\omega) e^{i\omega(\tau_1 - t_2)} d\omega d\tau_1 \\
& + \sum_{k=1}^N \sum_{l=1}^r \alpha_k \rho_l \gamma_l \int_0^{t_2} h_j(t_2 - \tau_2) i^{k-1} \int_{-\infty}^{\infty} \omega^{k-1} \Phi_q(\omega) e^{i\omega(t_1 - \tau_2)} d\omega d\tau_2 . \quad (4.57)
\end{aligned}$$

After a change of variables ($u = t_1 - \tau_1$) and ($v = t_2 - \tau_2$) and some rearrangement, equation (4.57) becomes

$$\Delta_N(t_1, t_2) = \sum_{m=1}^N \sum_{j=1}^r i^{-(m-1)} \alpha_m \rho_j \gamma_j \int_{-\infty}^{\infty} \omega^{m-1} \Phi_q(\omega) e^{i\omega(t_1 - t_2)} \mathcal{H}_j^c(\omega, t_1) d\omega$$

$$+ \sum_{k=1}^N \sum_{l=1}^r i^{k-1} \alpha_k \rho_l \gamma_l \int_{-\infty}^{\infty} \omega^{k-1} \Phi_q(\omega) e^{i\omega(t_1-t_2)} \mathcal{H}_l^{cc}(\omega, t_2) d\omega , \quad (4.58)$$

where $\mathcal{H}_j^c(\omega, t_1)$ and $\mathcal{H}_l^{cc}(\omega, t_2)$ are complex and conjugate transient frequency response functions of single-degree-of-freedom oscillators:

$$\mathcal{H}_j^c(\omega, t_1) = \int_0^{t_1} h_j(u) e^{-i\omega u} du \quad , \quad \mathcal{H}_l^{cc}(\omega, t_2) = \int_0^{t_2} h_l(v) e^{i\omega v} dv . \quad (4.59)$$

At the limit, as $t_1 = t_2 = t \rightarrow \infty$, $\Delta_N(t_1, t_2)$ is denoted as Δ_N and its expression is

$$\begin{aligned} \Delta_N &= \sum_{m=1}^N \sum_{j=1}^r i^{-(m-1)} \alpha_m \rho_j \gamma_j \int_{-\infty}^{\infty} \omega^{m-1} \Phi_q(\omega) H_j^c(\omega) d\omega \\ &+ \sum_{k=1}^N \sum_{l=1}^r i^{k-1} \alpha_k \rho_l \gamma_l \int_{-\infty}^{\infty} \omega^{k-1} \Phi_q(\omega) H_j^{cc}(\omega) d\omega . \end{aligned} \quad (4.60)$$

By renaming the index m as k and l as j , and considering that $i^{-(k-1)} = (-1)^{k-1} i^{k-1}$, the above equation becomes

$$\Delta_N = \sum_{k=1}^N \sum_{j=1}^r i^{k-1} \alpha_k \rho_j \gamma_j \int_{-\infty}^{\infty} \omega^{k-1} \Phi_q(\omega) \left[(-1)^{k-1} H_j^c(\omega) + H_j^{cc}(\omega) \right] d\omega . \quad (4.61)$$

For convenience of analysis, equation (4.61) can be written in terms of somewhat simpler integrals. For this purpose, $H_j^c(\omega)$ and $H_j^{cc}(\omega)$ are multiplied and divided by their respective conjugates to get (after some rearrangement):

$$\begin{aligned} \Delta_N &= \sum_{k=1}^N \sum_{j=1}^r i^{k-1} \alpha_k \rho_j \gamma_j \left\{ \left[(-1)^{k-1} + 1 \right] \left[\omega_j^2 I_j(k-1) - I_j(k+1) \right] \right. \\ &\quad \left. + i 2 \left[(-1)^k + 1 \right] \beta_j \omega_j I_j(k) \right\} . \end{aligned} \quad (4.62)$$

Where the quantities $i^{k-1} = (-1)^{(k-1)/2}$ and $i^k = (-1)^{k/2}$ can be substituted in equation (4.62) to get

$$\begin{aligned} \Delta_N &= \sum_{k=1}^N \sum_{j=1}^r \alpha_k \rho_j \gamma_j \left\{ (-1)^{(k-1)/2} \left[1 - (-1)^k \right] \left[\omega_j^2 I_j(k-1) - I_j(k+1) \right] \right. \\ &\quad \left. + 2 (-1)^{k/2} \left[1 + (-1)^k \right] \beta_j \omega_j I_j(k) \right\} , \end{aligned} \quad (4.63)$$

which can be compacted to the following expression:

$$\Delta_N = \sum_{k=1}^N \{s_k \delta_k + s'_k \delta'_k\} , \quad (4.64)$$

or in recursive form:

$$\Delta_N = \Delta_{N-1} + s_N \delta_N + s'_N \delta'_N , \quad \Delta_0 = 0 . \quad (4.65)$$

where

$$\delta_k = \alpha_k \sum_{j=1}^r \rho_j \gamma_j \left[\omega_j^2 I_j(k-1) - I_j(k+1) \right] , \quad (4.66)$$

$$\delta'_k = 2 \alpha_k \sum_{j=1}^r \rho_j \gamma_j \beta_j \omega_j I_j(k) , \quad (4.67)$$

$$s_k = (-1)^{(k-1)/2} \left[1 - (-1)^k \right] , \quad (4.68)$$

$$s'_k = (-1)^{k/2} \left[1 + (-1)^k \right] . \quad (4.69)$$

The quantities s_k and s'_k can only take two values: ± 2 and 0. It can be noticed that their zero value also coincides with the zero value of their respective factors δ_k and δ'_k , which are zero because of the integration of odd functions from $-\infty$ to ∞ . The first seven values of Δ_k are provided in table 4.1 for illustrative purposes.

Table 4.1: First seven values of Δ_k

k	Δ_k
1	$2 \delta_1$
2	$2 (\delta_1 - \delta'_2)$
3	$2 (\delta_1 - \delta'_2 - \delta_3)$
4	$2 (\delta_1 - \delta'_2 - \delta_3 + \delta'_4)$
5	$2 (\delta_1 - \delta'_2 - \delta_3 + \delta'_4 + \delta_5)$
6	$2 (\delta_1 - \delta'_2 - \delta_3 + \delta'_4 + \delta_5 - \delta'_6)$
7	$2 (\delta_1 - \delta'_2 - \delta_3 + \delta'_4 + \delta_5 - \delta'_6 - \delta_7)$

4.7.4 Final Expression for $E[R^2(t)]$

The expression of the mean square value of the response $R(t)$ is given by

$$\lim_{t_1=t_2=t \rightarrow \infty} E[R(t_1) R(t_2)] = E[R^2(t)] = \Xi_r + \Psi_N + \Delta_N . \quad (4.70)$$

Therefore, substitution of equation (4.49), (4.52) and (4.63) into equation (4.70) renders

$$\begin{aligned} E[R^2(t)] &= \sum_{k=1}^N \sum_{m=1}^N i^{k+3m} \alpha_k \alpha_m I_*(k+m-2) + \sum_{j=1}^r \rho_j^2 \gamma_j^2 I_j(0) \\ &+ 2 \sum_{j=1}^{r-1} \sum_{k=j+1}^r \rho_j \rho_k \gamma_j \gamma_k \left[T_{jk}^I I_j(0) + T_{jk}^{II} (I_j(2) - I_k(2)) + T_{jk}^{III} I_k(0) \right] \\ &+ \sum_{k=1}^N \sum_{j=1}^r \alpha_k \rho_j \gamma_j \left\{ (-1)^{(k-1)/2} \left[1 - (-1)^k \right] \left[\omega_j^2 I_j(k-1) - I_j(k+1) \right] \right. \\ &\quad \left. + 2(-1)^{k/2} \left[1 + (-1)^k \right] \beta_j \omega_j I_j(k) \right\} , \end{aligned} \quad (4.71)$$

or the recursive expressions for Ψ_N and Δ_N , given in equations (4.56) and (4.65), can be especially helpful when one is interested in examining the effect of increasing number of integration by parts on the convergence of the calculated response. In such a study, the values of these quantities calculated in the previous step are directly used in the current step. In this case, the expression for $E[R^2(t)]$ is simply indicated as

$$\begin{aligned} E[R^2(t)] &= \Psi_N + \Delta_N + \sum_{j=1}^r \rho_j^2 \gamma_j^2 I_j(0) \\ &+ 2 \sum_{j=1}^{r-1} \sum_{k=j+1}^r \rho_j \rho_k \gamma_j \gamma_k \left[T_{jk}^I I_j(0) + T_{jk}^{II} (I_j(2) - I_k(2)) + T_{jk}^{III} I_k(0) \right] \end{aligned} \quad (4.72)$$

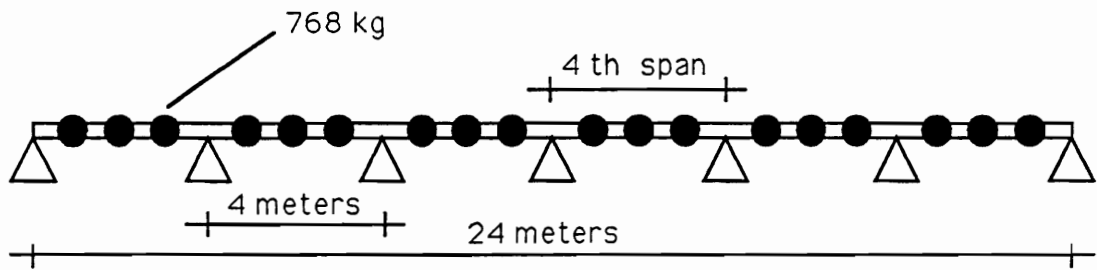
In principle, other statistics of the response quantity $R(t)$ can be similarly obtained. However in this work, only the mean square value has been calculated for the example problem by utilizing equation (4.71), and the effect of increasing the number of integrations by parts on the calculated response is shown.

4.8 Numerical Results

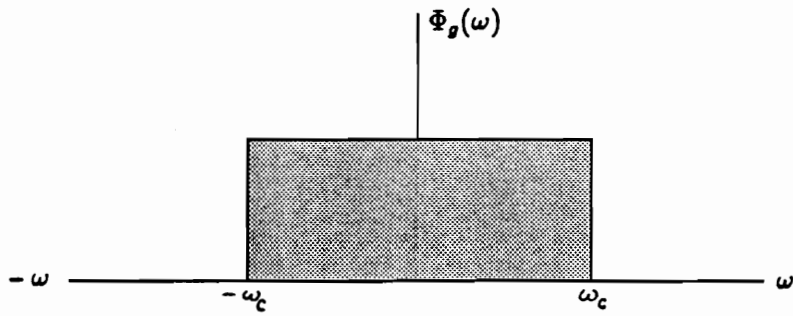
To verify the effectiveness of the proposed approach, the example problems of a multi-span beam are considered. There are six spans and each is four meters long. The moment of inertia of the beam about the axis of bending is 2700 cm^4 , the area is 43.68 cm^2 , the modulus of elasticity is $206 \times 10^9 \text{ N/m}^2$ and the mass density is 0.00786 kg/cm^3 . The beam also has concentrated masses of 768 kg at each meter. For dynamic analysis, each span was subdivided into four beam elements, each of length 1 m . The consistent mass matrix was used in the analysis. The beam was discretized in 43 degrees of freedom, with vertical displacement and rotational degrees of freedom at each node. Figure 4.1 shows some beam details.

The forcing function was due to a uniform support motion at all supports. The time variation of the motion is random and is characterized by a band-limited white noise with the cut-off frequency $\pm\omega_c$, shown in figure 4.1 (B). For this random process, the derivatives of all order exist in the mean square sense. As the convergence to the final result is affected by the frequency characteristic of the force, several cut-off frequencies values of the force spectral density function have been considered. Herein, the numerical results for the bending moment in the beam at the middle of the 4th span (from the left) are obtained.

The mean square value of the bending moment is obtained by (1) the classical mode displacement approach with truncated modes and with all modes, (2) by the mode acceleration approach with the same number of modes as the number used in the truncated mode displacement approach and (3) by the proposed approach. In the proposed approach, the increasing number of integration by parts are used to show



a) Beam layout



b) Forcing function spectral density function

Figure 4.1: (A) Schematic of the multi-span beam and (B) Band-limited white noise spectral density input considered in the analysis.

the convergence to the final results. The numerical value obtained with the complete set of modes is taken as the bench mark value. The response values obtained by the other methods are presented as ratios to the correct bench mark value. Thus, a ratio close to 1 indicates nearly perfect results.

The energy dissipation in the system is defined through the modal damping ratio, β_j . It is assumed that each mode used in the analysis has a damping ratio of 5% of the critical value. This characteristic could also be defined through a system damping matrix. However, for the formulation developed herein it is required that such a damping matrix be classical.

In order to utilize the recursive relationships of equations (4.30) and (4.39) we need to have the explicit form of the damping matrix. The method proposed presupposes that not all modal vectors will be available. In such a case, one can construct a damping matrix, with prescribed damping ratios for the first r modes but with increasing or decreasing damping or a combination of these for the truncated modes as shown in appendix D. Such a damping matrix can be defined as follows:

$$\begin{aligned}
 [C] &= [M] [F_l] [D_l] [F_l]^T [M] \\
 &+ \bar{c}_1 \left([K] - [M] [F_l] [\Lambda_l] [F_l]^T [M] \right) \\
 &+ \bar{c}_2 \left([M] - [M] [F_l] [F_l]^T [M] \right)
 \end{aligned} \tag{4.73}$$

where $[\Phi_l]$ is a $(n \times r)$ modal matrix containing only the first r modes; \bar{c}_1 and \bar{c}_2 are two constants which can be adjusted to obtain the damping ratios in the truncated modes within a desired range; the diagonal matrix $[D_l]$ is of size $(r \times r)$ with its elements defined as $(2\beta_j\omega_j)$; and $[\Lambda_l]$ is also a diagonal matrix of size $(r \times r)$ containing the first r eigenvalues ($\lambda_j = \omega_j^2$). It is simple to see that a damping matrix

constructed according to equation (4.73) will have the preselected damping ratios β_j in the first r modes. The damping ratios in the higher modes, though not explicitly used in the approach proposed, will vary according to the following equation:

$$\beta_j = \frac{1}{2} \left[\bar{c}_1 \omega_j + \frac{\bar{c}_2}{\omega_j} \right] \quad , \quad j = r + 1, r + 2, \dots, n \quad (4.74)$$

Equations (4.73) and (4.74) are simple generalizations of the formulation by Craig [15], which now includes a combination of increasing and decreasing modal damping ratios.

While performing numerical analysis with equation (4.71) or (4.72), sensitivity of the results to numerical roundoff errors was noticed. For large k and m values, the frequency integrals $I(m)$ and $I_j(m)$ start to become large. At the same time, however, the coefficients $\alpha_k = \{\mathcal{R}\}^T \{U_h\}_k$ tend to become small with increasing value of the index k ; it happens because, the vector $\{U_h\}_k$ is obtained by successive solution of equation (4.39) which, in principle, involves successive inversions of the $[K]$ matrix. The product of α_k with the frequency integral, however, diminishes with increasing k , as in most cases the contribution of the higher order integration-by-parts term usually also diminishes. The problem of rapid increase in the frequency integral values and commensurate decrease in the values of α_k can be balanced by considering the normalized values of the frequency integrals as follows:

$$\hat{I}_*(2m) = \int_{-1}^1 \omega^{2m} \hat{\Phi}_q(\omega) d\omega \quad , \quad \hat{I}_j(2m) = \int_{-1}^1 \omega^{2m} |\hat{H}_j^c(\omega)|^2 \hat{\Phi}_q(\omega) d\omega \quad , \quad (4.75)$$

where now

$$\hat{\Phi}_q(\omega) = \Phi_q(\omega_c \omega) \quad , \quad |\hat{H}_j^c(\omega)|^2 = \left[\left\{ \left(\frac{\omega_j}{\omega_c} \right)^2 - \omega^2 \right\}^2 + 4\beta_j^2 \left(\frac{\omega_j}{\omega_c} \right)^2 \right]^{-1} \quad (4.76)$$

where ω_c is the cut-off frequency of the spectral density function. Consistent with

this change in the frequency integral, the corresponding value of $\hat{\alpha}_k$ is defined as:

$$\hat{\alpha}_k = \{\mathcal{R}\} \{\hat{U}_h\}_k^T \quad (4.77)$$

with the vector $\{\hat{U}_h\}_k$ obtained as a solution of the following recursive equation:

$$\begin{aligned} [K] \{\hat{U}_h\}_k &= -\omega_c [C] \{\hat{U}_h\}_{k-1} - \omega_c^2 [M] \{\hat{U}_h\}_{k-2} \\ \{\hat{U}_h\}_0 &= \{0\} \quad , \quad [K] \{\hat{U}_h\}_1 = \omega_c^2 \{Q_0\} - [K] \sum_{j=1}^r \left(\frac{\omega_c}{\omega_j} \right)^2 \{\phi\}_j \gamma_j . \end{aligned} \quad (4.78)$$

In terms of these new $\hat{\alpha}_k$ and the frequency integrals, the expression for the mean square response in equation (4.72) becomes:

$$\begin{aligned} E[R^2(t)] &= \hat{\Psi}_N + \hat{\Delta}_N + \sum_{j=1}^r \rho_j^2 \gamma_j^2 \hat{I}_j(0) \\ &+ 2 \sum_{j=1}^{r-1} \sum_{k=j+1}^r \rho_j \rho_k \gamma_j \gamma_k \left[T_{jk}^I \hat{I}_j(0) + \omega_c^2 T_{jk}^{II} (\hat{I}_j(2) - \hat{I}_k(2)) + T_{jk}^{III} \hat{I}_k(0) \right] , \end{aligned} \quad (4.79)$$

with

$$\begin{aligned} \hat{\Psi}_N &= \hat{\Psi}_{N-1} + \hat{\psi}_{N,N} + 2 \sum_{j=1}^{J_N} (-1)^j \hat{\psi}_{N-2j,N} , \quad , \quad \hat{\Psi}_0 = 0 \\ J_N &= \frac{2N - 3 - (-1)^N}{4} , \quad \hat{\psi}_{k,m} = \hat{\alpha}_k \hat{\alpha}_m \hat{I}_*(k+m-2) , \end{aligned} \quad (4.80)$$

and

$$\begin{aligned} \hat{\Delta}_N &= \hat{\Delta}_{N-1} + s_N \hat{\delta}_N + s'_N \hat{\delta}'_N , \quad \hat{\Delta}_0 = 0 \\ \hat{\delta}_N &= \hat{\alpha}_N \sum_{j=1}^r \rho_j \gamma_j \left[(\omega_j/\omega_c)^2 \hat{I}_j(N-1) - \hat{I}_j(N+1) \right] \\ \hat{\delta}'_N &= \hat{\alpha}_N \sum_{j=1}^r \rho_j \gamma_j \left[2\beta_j (\omega_j/\omega_c) \hat{I}_j(N) \right] . \end{aligned} \quad (4.81)$$

In the numerical work it was observed that the use of equation (4.79) provided stable numerical values, especially for large N .

In figure 4.2 is shown the normalized mean square value of the bending moment at the middle of the fourth span, obtained by the proposed approach, for an increasing number of integration by parts. The normalization is with respect to the exact mean square value obtained with the complete set of modes. For the results of this figure, the cut-off frequency of the spectral density function of the force is 45 rad/s. The first three frequencies of the structure are 51.34, 55.30 and 65.78 rad/s. Since all structural frequencies are higher than the cut-off frequency, one need not consider any modes in the proposed analysis. Here in this figure, the results obtained by the proposed method with no modes (curve I) and with two modes (curve II) are shown. It is relevant to mention here that the normalized response obtained by truncated mode displacement approach with only two modes was about 8%.

From curve I, which corresponds to the case with no modes used in the analysis, it is seen that the first integration by parts (which is also the same as the mode acceleration approach) captures about 81% of the total response. More response can also be captured by including more integration-by-parts terms and it takes about 18 of these terms to capture the full response (within 0.1% of the total response). This number of integration-by-parts can be reduced by reducing the ratio of the input cut-off frequency to the frequency of the first truncated modes. This ratio is denoted by r_c in this and other figures. In this particular case this ratio is 0.876. For a given input cut-off frequency, this ratio can be decreased by including more modes in the calculation of the mode displacement part of the response, and thus reducing the number of modes to be truncated. This effect is clearly seen by the results represented by curve II, where now two modes have been included in the analysis and the remaining modes are to be truncated. In this case, two modes and one integration by parts term (mode acceleration formulation) captures about 96%

of the total response; the remaining 4% can be captured by nine integration by parts terms. In this case the ratio of the cut-off frequency to the first truncated frequency, which now is the third structural frequency, is 0.684.

In figure 4.3 are shown results similar to those shown in figure 4.2, but for the input cut-off frequency of 50 rad/s, which is now very close to the first structural frequency, with the frequency ratio of 0.974. Since the cut-off frequency is still smaller than all structural frequencies, one need not use any modes in the proposed approach. Curve I shows these results. It is noted that the first integration by parts (mode acceleration formulation), but with no modes, can now capture only 73% of the total response. This value can be improved again by including more integration by parts terms, and it requires about 27 integrations to achieve convergence to within 0.1% of the total response. Here again, this number of the integration by parts terms can increase significantly if the ratio of the cut-off frequency to the first truncated frequency is closer to 1. This is shown by curve II, where this ratio is now 0.9999; here, no mode included in the mode acceleration formulation captures about 70% of the total response, and the remaining 30% is captured by about 53 integration-by-parts terms.

In figure 4.4 are shown the results for a case in which the input cut-off frequency is now larger than the first structural frequency. This necessitates that at least the first mode be included in the analysis. Curve I shows the results for a cut-off frequency of 54 rad/s, which provides a frequency ratio of 0.976 with respect to the second modal frequency. Mode displacement formulation with one mode captures about 0% of the response, with two modes 19%, whereas one mode with one integration by parts (i. e. mode acceleration formulation) captures about 61%.

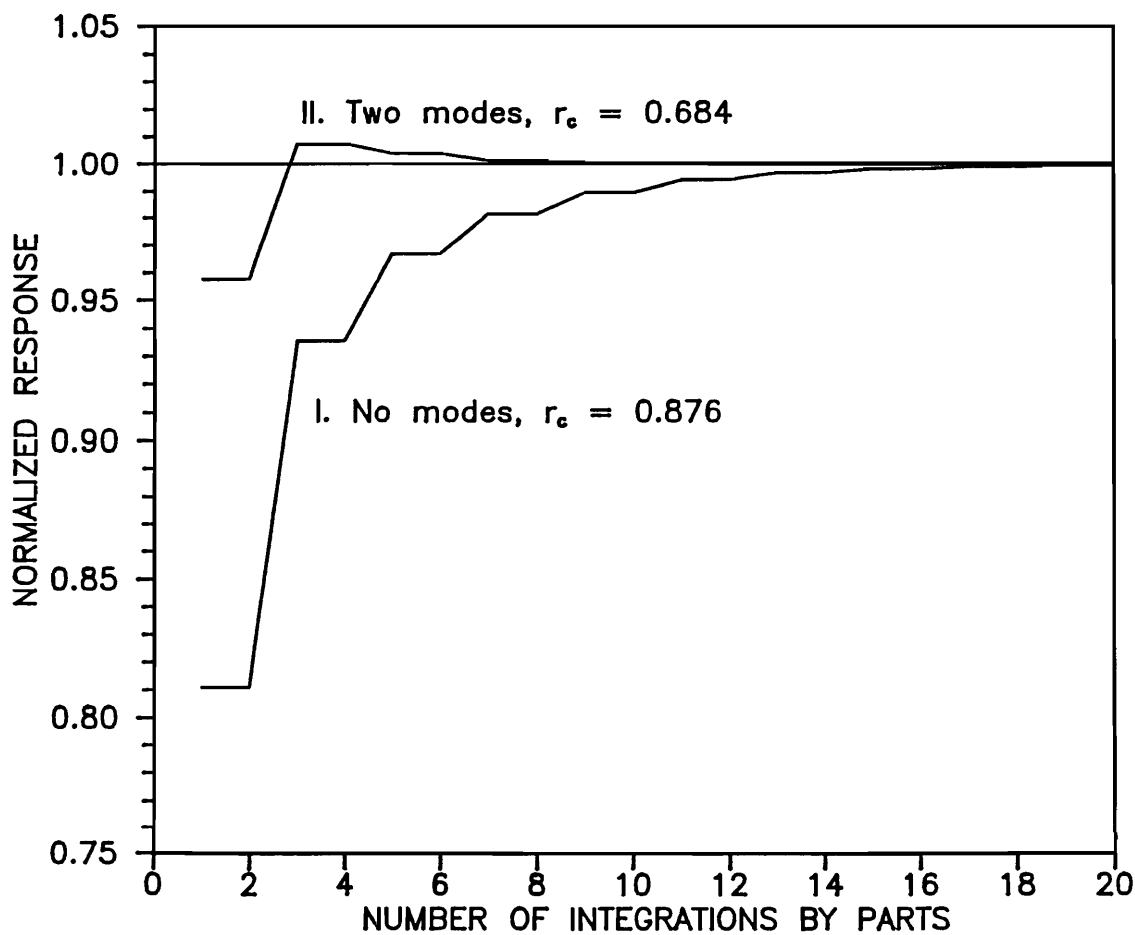


Figure 4.2: Convergence of the normalized mean square value of a bending moment with increasing number of integrations by parts: No modes within the input frequency range

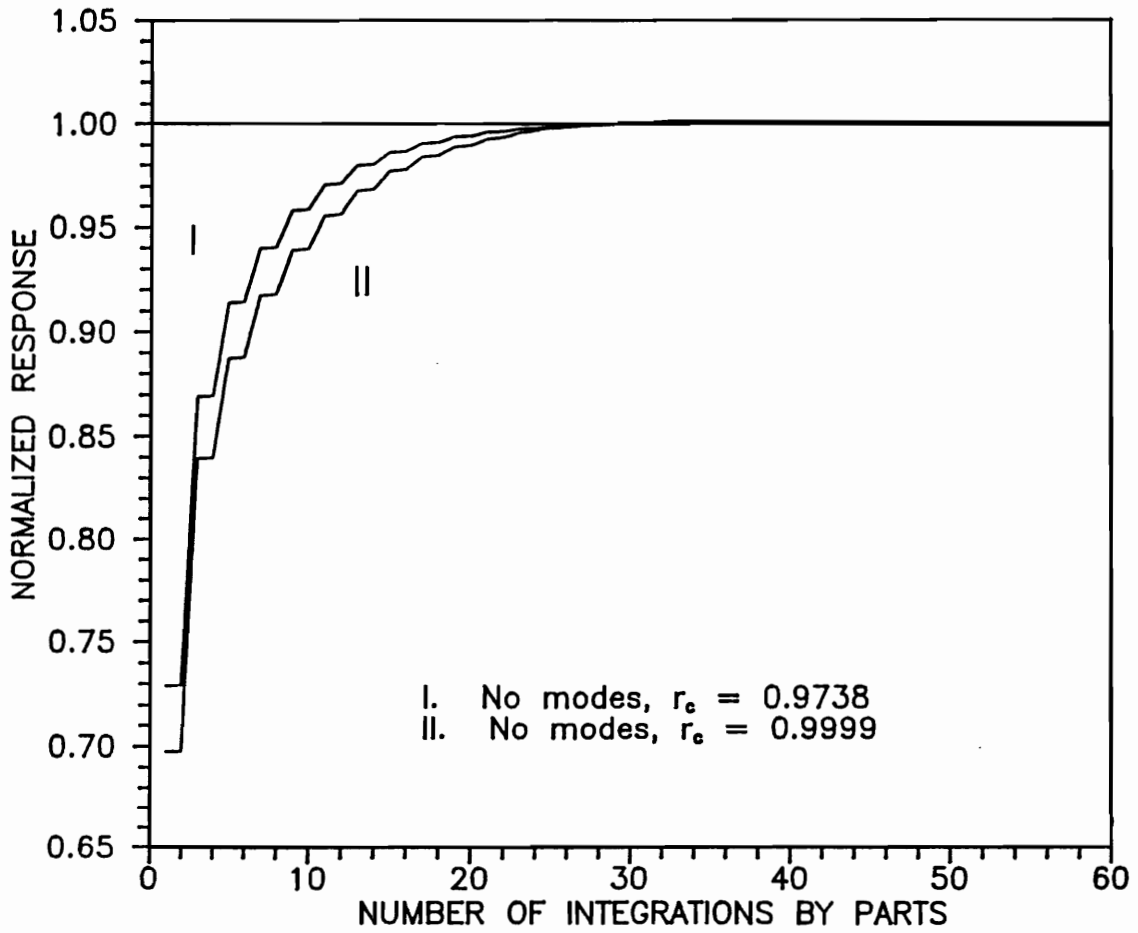


Figure 4.3: Convergence of the normalized mean square value of a bending moment with increasing number of integrations by parts: No modes within the input frequency range and higher values of the frequency ratio r_c .

Further improvements in the response estimates are again possible with increasing number of integration by parts. Curve II shows the effect of including one more mode in the analysis. Here the number of integrations required to capture the remaining response is about 15.

Figure 4.5 is similar to the previous figures but now the first five modes fall within the range of the input cut-off frequency (100 rad/s), and thus a minimum of five modes must be considered in the analysis. The convergence characteristics of the response is similar to those of the earlier cases.

A question which immediately arises is: How many integration by parts terms are necessary to achieve convergence to the total response? The answer to this query is probably as elusive as is the answer to the question: How many modes should one consider to capture the full response in the classical mode displacement approach? The total response being sought is not known a priori. One can thus only check for the mutual convergence of the results obtained with successively increased number of integration by parts. This, however, only checks for the flatness of the curves shown in the preceding figures. A problem arises here, as these curves are not monotonically increasing or decreasing to the final value of the response. Although the calculation of successive terms of the integration-by-parts scheme is very efficient, one can not indefinitely increase the number of integrations because of the accumulation of the round-off errors in the process of solving simultaneous equations successively.

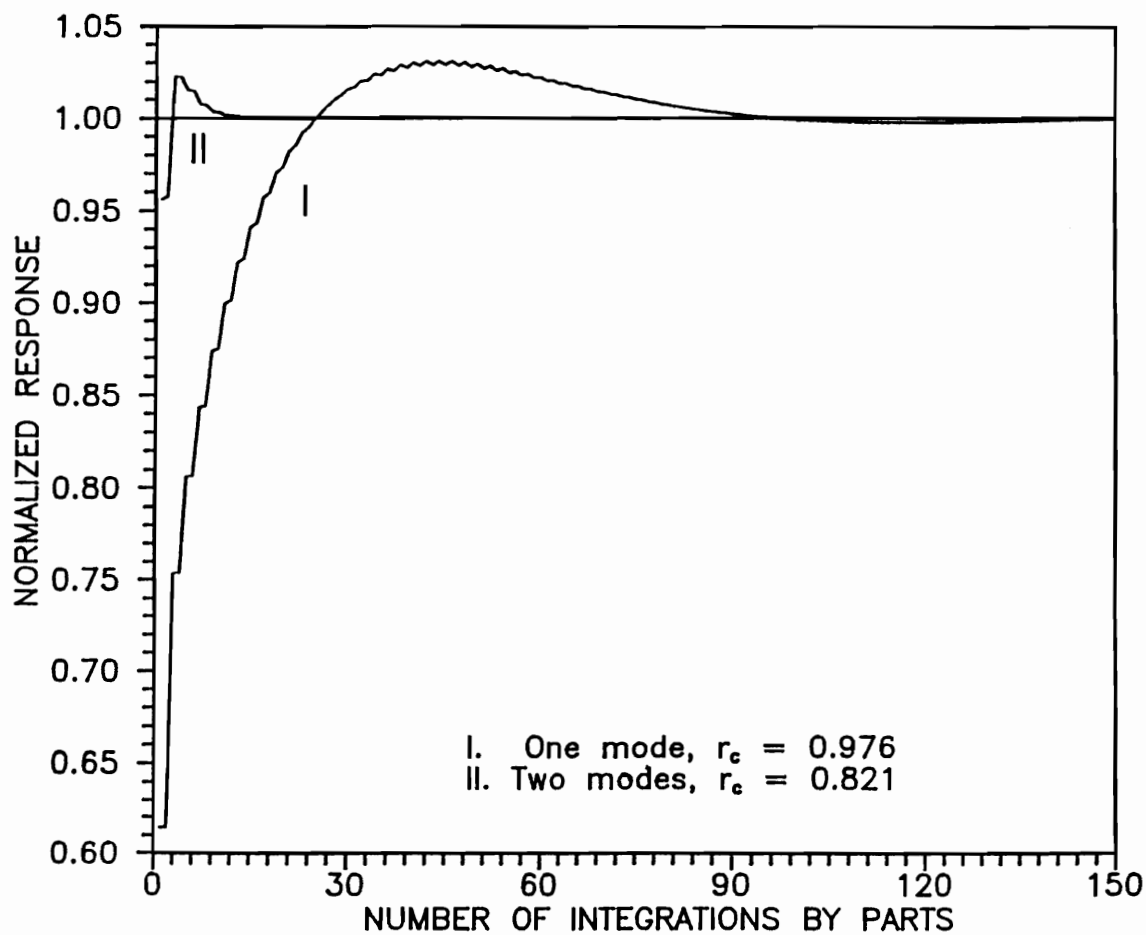


Figure 4.4: Convergence of the normalized mean square value of a bending moment with increasing number of integrations by parts: The first mode is within the input frequency range

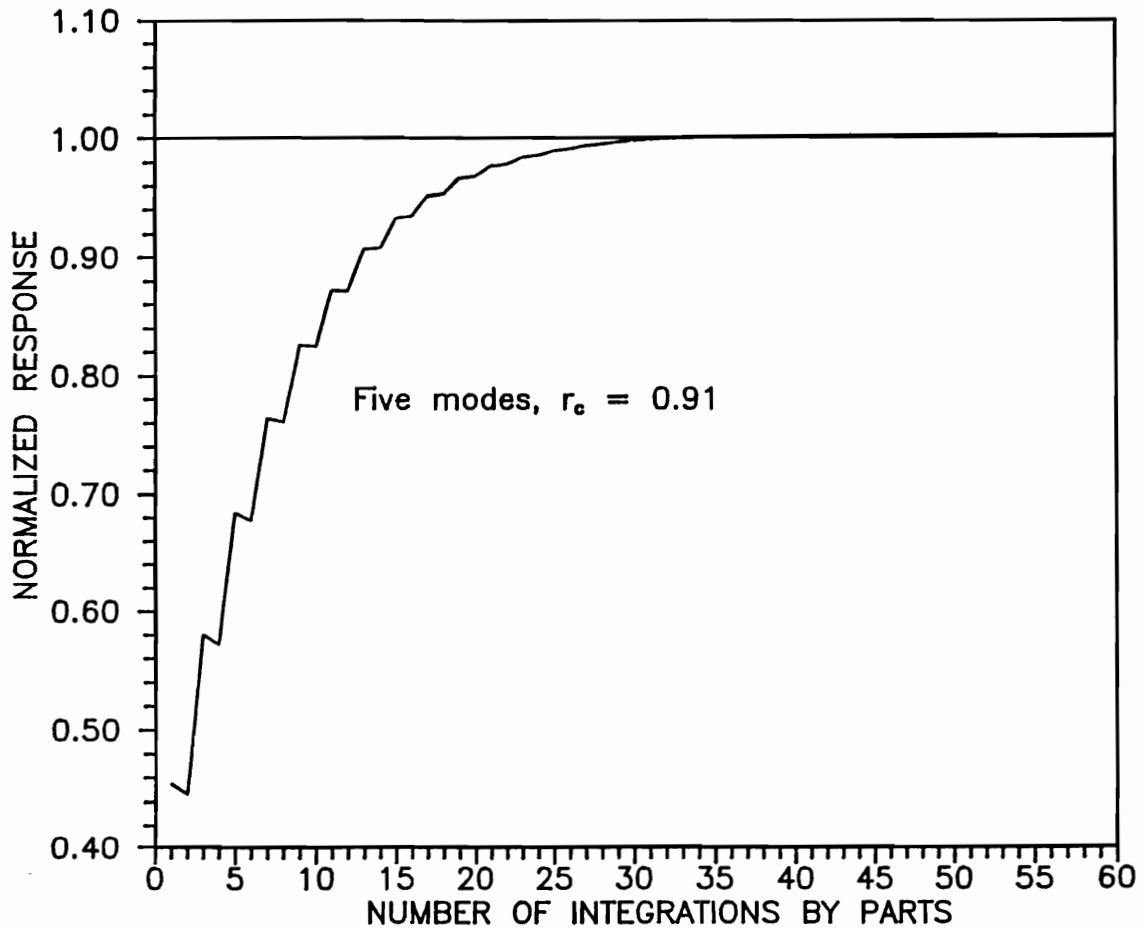


Figure 4.5: Convergence of the normalized mean square value of a bending moment with increasing number of integrations by parts: The first five modes are within the input frequency range

4.9 Conclusions

An N^{th} order force derivative approach is presented to reduce the error due to truncation of modes in modal analysis of structures. In this method the response is expressed in terms of a dynamic part and a pseudostatic part. The dynamic part is the same as used in the classical (truncated) mode displacement formulation. The pseudostatic part represents a correction which accounts for the contribution of the truncated modes. By increasing the order of the force derivatives in the approach, the contribution of higher modes can be more accurately calculated. In this chapter, this contribution is calculated without evaluating any convolution integrals: rather, only a simple inversion of the system stiffness matrix or the solution of a system of linear equations is required for calculating this contribution. Simple recursive formulas are presented to facilitate the calculation of this contribution for successively increasing orders of the force derivative terms.

The formulation is used to calculate the second order statistics of the response for random forcing functions. The numerical results of an example problem show how the convergence to the correct response is achieved by increasing the order of the derivatives in the approach. It can be proved that as the order of the derivative is increased indefinitely the calculated response will approach the correct response in the limit. For practical applications, however, it may not be necessary to adopt very high order of derivatives in the approach. Of course, the approach is only applicable to differentiable forcing functions. Also, it is necessary that all structural modes below the highest frequency in the input be included in the calculation of the dynamic part. It is only the contribution of modes with frequencies higher than

the highest input frequency that can be improved by the force derivative approach. Furthermore, the greater the separation between the highest frequency of the input and the frequency of the lowest truncated mode, the faster is the convergence with increasing order of the highest derivative in the approach. This separation can obviously be increased by including more modes in the dynamic part of the response. This fact is also clearly shown by the numerical results presented herein.

Chapter 5

Response Spectrum Method for Hysteretic Shear Buildings

5.1 Introduction

Civil engineering structures, affected by strong earthquake induced ground motions, need to be properly designed to avoid the damages leading to their collapse and the consequent loss of lives. Several structural systems have been designed to withstand such seismic forces elastically. That is, they are allowed to work within the elastic range of its constitutive materials. This design philosophy may, however, result in large and expensive structural members. To reduce the size of structural members, it is a common practice in building designs to permit some yielding of members. Structures so designed, dissipate vibratory energy through the hysteretic behavior of structural members subjected to cyclic loading caused by earthquake induced dynamic loads. As a result of this energy dissipation, these structures have slender structural members and are less expensive than those that behave elastically. However, it is understood that the structure may be partially damaged whenever

a design level earthquake would occur. The maximum amount of damage to be tolerated, is determined by the maximum ductility levels to be reached during a design earthquake.

For the calculation of design forces for such yielding structures, in a dynamic earthquake environment, the use of response modification factors, which depend upon the type of construction, has been suggested in some recent codes such as ATC 3 [2] and NEHRP [35]. The recommendations have also been made to include such behavior through the use of the inelastic ground response spectra developed for different ductility ratios. All these methods, however, provide just approximate solutions and have been proposed primarily to simplify the analysis. It is always possible to accurately evaluate the nonlinear behavior by using a step-by-step procedure for a given ground motion time history of the design earthquake. However, to use this approach it is necessary to employ several ground acceleration time histories as base inputs. Such analyses can become quite involved and cumbersome; they are not suitable for design purposes.

For multi-degree-of-freedom linear structures, a faster approach, known as the response spectrum method, is commonly utilized to calculate response for design purposes. It makes use of the smoothed response spectra of the design ground motion [38, 2, 35]. These spectra, define the random inputs in terms of the maximum responses of different single-degree-of-freedom oscillators. Multi-degree-of-freedom elastic structures can be easily decomposed into a set of single-degree-of-freedom oscillators by using modal analysis. The modal response combination rules such as those described in chapters 2 and 3 can be used to calculate the design response. Such approach, however, can only be used with linear systems.

This study presents a response spectrum method which can provide approximate, but still reasonably accurate values of design response for nonlinear structures with hysteretic elements. To be able to develop this response spectrum approach, the nonlinear equations of motion are first linearized using the stochastic equivalent linearization technique. The equivalent linear system of equations are then solved by a generalized modal analysis approach employing the adjoint sets of system eigenproperties. In this approach the seismic design inputs, commonly defined in terms of pseudo acceleration and relative velocity ground response spectra, can now be used. In addition to these conventionally used spectra, the need for defining the seismic input in terms of the relative displacement spectrum of a massless oscillator is also identified.

In this chapter, this approach is first developed for structures that can be modeled as *shear buildings* with one nonlinear hysteretic element for each story of the building structure. In the following chapter this approach is extended further for *two dimensional structural frames* with concentrated plastic hinges.

5.2 The Shear Building Model

The response of most structural buildings with rigid floor slabs, when subjected to horizontal seismic excitation, can be well approximated by just considering a few degrees of freedom at each floor level. Since these structures consist mainly of several stiff horizontal slabs connected by flexible columns and or shear walls, it is possible to allow just three degrees of freedom per floor, two horizontal translations and one rotation about the vertical axis, to obtain a good approximation to the response. In

some structures the mass centers of each floor coincide with the respective stiffness centers and the rotational degree of freedom can be avoided allowing the two translational components to be studied independently. In this case, just one horizontal translation per floor will suffice to study the response in one direction. This simplified model is widely known as shear building. Such models have been commonly used in earthquake engineering studies of multi-story building structures. In this chapter, we have also used this model to represent multi-story building structures.

5.3 Governing Equations

Figure 5.1 (on page 144) shows a schematic of a shear structure where the floor masses m_i have been concentrated at the story levels and are interconnected by elements that represent the columns and or shear walls of the actual structure. The relative displacement of the i^{th} mass with respect to the ground is indicated by x_i and the deformation of the i^{th} connecting element (or interstory drift) is denoted as $u_i = x_i - x_{i-1}$. It will be assumed that the i^{th} element, when dynamically deformed, provides stiffness forces s_i and damping forces d_i .

Using Newton's law the equation of motion for the i^{th} mass can be written

$$s_{i+1} - s_i + d_{i+1} - d_i = m_i \ddot{x}_i^a \quad (5.1)$$

where \ddot{x}_i^a is the absolute acceleration of the i^{th} floor. The damping force d_i is assumed to be viscous and is thus proportional to the drift velocity through the damping coefficient c_i :

$$d_i = c_i \dot{u}_i = c_i (\dot{x}_i - \dot{x}_{i-1}). \quad (5.2)$$

The model for the restoring stiffness force depends upon the constitutive characteristics of the structural materials. For structures with material deformation within the linear elastic range the stiffness force is simply given by

$$s_i = k_i u_i = k_i (x_i - x_{i-1}) \quad (5.3)$$

where k_i is the elastic stiffness coefficient. To represent the inelastic behavior here we will use the model proposed by Wen [57] which consists of an elastic part in parallel with an hysteretic part:

$$s_i = \alpha_i k_i (x_i - x_{i-1}) + (1 - \alpha_i) k_i v_i \quad (5.4)$$

where k_i is now the initial stiffness parameter of the hysteretic model, α_i is the proportionate contribution of the linear elastic part ($0 < \alpha_i < 1$), and v_i is the auxiliary variable (auxiliary drift) of the hysteretic part. The deformation variable u_i is assumed to be related to the auxiliary variable v_i by the Bouc-Wen [9, 56, 57] hysteretic constitutive model of the following form:

$$\dot{v}_i = \mathcal{A}_i \dot{u}_i - \mathcal{B}_i \dot{u}_i |v_i|^{\eta_i} - \mathcal{C}_i v_i |\dot{u}_i| |v_i|^{\eta_i-1}. \quad (5.5)$$

This ingenious differential equation was first proposed by Bouc [9] and has been extensively used by Wen [56, 57, 58], Baber and Wen [5, 6, 7] and many others in their studies of stochastic response of engineering structures. It can represent a wide variety of hysteretic characteristics depending upon the values of their parameters [5, 30]. Also, deterioration and pinching effects may be modeled by the introduction of additional parameters [4]. The meaning of the different parameters involved in equation (5.5) are discussed in appendix E.

The figure in appendix E shows the general shape of the hysteresis loop which has been adopted in the numerical examples. To model the softening behavior of the

which nonzero entries have the following pattern:

$$[C] = \begin{bmatrix} (c_1 + c_2) & -c_2 & & & \\ -c_2 & (c_2 + c_3) & -c_3 & & \\ & \ddots & \ddots & \ddots & \\ & & c_{n-1} & (c_{n-1} + c_n) & -c_n \\ & & & -c_n & c_n \end{bmatrix}. \quad (5.9)$$

The linear part of the stiffness matrix is denoted by $[K^\alpha]$ and its structure is

$$[K^\alpha] = \begin{bmatrix} (k_1^\alpha + k_2^\alpha) & -k_2^\alpha & & & \\ -k_2^\alpha & (k_2^\alpha + k_3^\alpha) & -k_3^\alpha & & \\ & \ddots & \ddots & \ddots & \\ & & k_{n-1}^\alpha & (k_{n-1}^\alpha + k_n^\alpha) & -k_n^\alpha \\ & & & -k_n^\alpha & k_n^\alpha \end{bmatrix} \quad (5.10)$$

where $k_i^\alpha = \alpha_i k_i$. Matrix $[H^\alpha]$ contains the hysteretic elements with following arrangement:

$$[H^\alpha] = \begin{bmatrix} h_1^\alpha & -h_2^\alpha & & & \\ & h_2^\alpha & -h_3^\alpha & & \\ & & \ddots & \ddots & \\ & & & h_{n-1}^\alpha & -h_n^\alpha \\ & & & & h_n^\alpha \end{bmatrix} \quad (5.11)$$

where $h_i^\alpha = (1 - \alpha_i)k_i$.

The n dynamic equilibrium conditions expressed by equation (5.8) contain n unknowns in vector $\{X\}$ plus n unknowns in $\{V\}$. Additional n equations are provided by the constitutive equations of each deforming element, equation (5.5).

The assembled constitutive equations for all n connecting elements, together with the equations of motion, fully describe the dynamic response of an inelastically behaving shear building subjected to ground excitation. To develop a response spectrum approach, the constitutive equations (5.5) must be linearized. The linearization procedures have been widely used in practice since the first proposal by Krylov and Bogoliubov [25]. The book by Roberts and Spanos [40] provides an excellent description of this technique. The analytical form of the Bouc-Wen model is especially

which nonzero entries have the following pattern:

$$[C] = \begin{bmatrix} (c_1 + c_2) & -c_2 & & & \\ -c_2 & (c_2 + c_3) & -c_3 & & \\ & \ddots & \ddots & \ddots & \\ & & c_{n-1} & (c_{n-1} + c_n) & -c_n \\ & & & -c_n & c_n \end{bmatrix}. \quad (5.9)$$

The linear part of the stiffness matrix is denoted by $[K^\alpha]$ and its structure is

$$[K^\alpha] = \begin{bmatrix} (k_1^\alpha + k_2^\alpha) & -k_2^\alpha & & & \\ -k_2^\alpha & (k_2^\alpha + k_3^\alpha) & -k_3^\alpha & & \\ & \ddots & \ddots & \ddots & \\ & & k_{n-1}^\alpha & (k_{n-1}^\alpha + k_n^\alpha) & -k_n^\alpha \\ & & & -k_n^\alpha & k_n^\alpha \end{bmatrix} \quad (5.10)$$

where $k_i^\alpha = \alpha_i k_i$. Matrix $[H^\alpha]$ contains the hysteretic elements with following arrangement:

$$[H^\alpha] = \begin{bmatrix} h_1^\alpha & -h_2^\alpha & & & \\ & h_2^\alpha & -h_3^\alpha & & \\ & & \ddots & \ddots & \\ & & & h_{n-1}^\alpha & -h_n^\alpha \\ & & & & h_n^\alpha \end{bmatrix} \quad (5.11)$$

where $h_i^\alpha = (1 - \alpha_i)k_i$.

The n dynamic equilibrium conditions expressed by equation (5.8) contain n unknowns in vector $\{X\}$ plus n unknowns in $\{V\}$. Additional n equations are provided by the constitutive equations of each deforming element, equation (5.5).

The assembled constitutive equations for all n connecting elements, together with the equations of motion, fully describe the dynamic response of an inelastically behaving shear building subjected to ground excitation. To develop a response spectrum approach, the constitutive equations (5.5) must be linearized. The linearization procedures have been widely used in practice since the first proposal by Krylov and Bogoliubov [25]. The book by Roberts and Spanos [40] provides an excellent description of this technique. The analytical form of the Bouc-Wen model is especially

suitable for stochastic linearization processes. The equivalent linear form of equation (5.5) is defined by the following expression:

$$\dot{v}_i = a_i \dot{u}_i + b_i v_i = a_i (\dot{x}_i - \dot{x}_{i-1}) + b_i v_i \quad , \quad i = 1, \dots, n \quad (5.12)$$

where a_i and b_i are the coefficients of linearization, yet to be defined. Assembling equation (5.12) for all deformable elements, we can rewrite them in the following form:

$$\{\dot{V}\} = [A] \{\dot{X}\} + [B] \{V\} \quad (5.13)$$

where matrix $[B]$ is diagonal and matrix $[A]$ has the following structure:

$$[A] = \begin{bmatrix} a_1 & & & & \\ -a_2 & a_2 & & & \\ & \ddots & \ddots & & \\ & & & -a_n & a_n \end{bmatrix} . \quad (5.14)$$

Equations (5.8) and (5.13) constitute the equivalent linear system of governing equations. The linearization coefficients a_i and b_i are chosen such that they minimize the mean square value of the error introduced by the linearization itself. This leads to expressions of the coefficients as functions of the response statistics of the actual nonlinear system which are not known a priori. Simplified closed form expressions can be obtained for a_i and b_i in terms of the response statistics if the response can be assumed to be Gaussian. See Atalik and Utku [3]. In appendix F, it is shown that these coefficients are:

$$a_i = \mathcal{A}_i - \sigma_{v_i}^{\eta_i} \sqrt{2^{\eta_i} / \pi} \left[\left(\frac{\eta_i - 1}{2} \right)! B_i + (\eta_i)! C_i \rho_i^{\eta_i} \Sigma_{a_i} \right] , \quad (5.15)$$

$$b_i = -\sigma_{v_i}^{\eta_i-1} \sigma_{\dot{u}_i} \sqrt{2^{\eta_i} / \pi} \left[\eta_i \rho_i \left(\frac{\eta_i - 1}{2} \right)! B_i + (\eta_i)! C_i \rho_i^{\eta_i-1} \Sigma_{b_i} \right] , \quad (5.16)$$

where η_i is the exponent of the model in equation (5.5) which is a positive odd integer, σ_* expresses the standard deviation of the subscripted variable $*$, ρ_i is the

correlation coefficient between \dot{u}_i and v_i , and Σ_{a_i} and Σ_{b_i} are defined by the following summations:

$$\Sigma_{a_i} = \sum_{j=0}^{(\eta_i-1)/2} \frac{[(\eta_i - 2j - 1) / 2]!}{j! (\eta_i - 2j)!} \frac{(1 - \rho_i^2)^j}{(2 \rho_i)^{2j}}, \quad (5.17)$$

$$\Sigma_{b_i} = \sum_{j=0}^{(\eta_i-1)/2} \frac{[(\eta_i - 2j - 1) / 2]!}{j! (\eta_i - 2j - 1)!} \frac{(1 - \rho_i^2)^j}{(2 \rho_i)^{2j}}. \quad (5.18)$$

Other expressions for these coefficients have also been obtained, [57, 11, 4].

Since the response statistics $\sigma_{\dot{u}_i}$, σ_{v_i} and ρ_i are still unknown, which in turn can be obtained only after the determination of the linearization coefficients, an iterative approach has to be implemented to solve this problem. Till now, several investigators have used the *Fixed Point* iterative scheme which can be described as follows: the first iteration starts with some assumed values of the linearization coefficients then the response statistics of the linearized system are determined, which in turn are used in equations (5.15) and (5.16) to obtain a new set of coefficients to be compared against the initial ones. If the comparison does not satisfy some tolerance requirement, the newly obtained coefficients can be used to initiate the next iteration. This scheme was observed to be rather slow to converge. Here, therefore, a faster approach has also been used, which is based on a modification of the well known *Newton method* [13]. Some further details of these methods are provided in section 5.7.

5.4 Solution of the Linearized Governing Equations

To solve the linearized governing equations (5.8) and (5.13) they will be combined into a system of first order equations

$$[L_1] \{\dot{Y}\} + [L_2] \{Y\} = \{F\} \quad (5.19)$$

where vectors $\{Y\}$ and $\{F\}$ have dimension $3n$ and are defined as

$$\{Y\} = \begin{Bmatrix} \{X\} \\ \{\dot{X}\} \\ \{V\} \end{Bmatrix}, \quad \{F\} = \begin{Bmatrix} \{0\} \\ -[M] \{\mathcal{I}\} \ddot{x}_g \\ \{0\} \end{Bmatrix}. \quad (5.20)$$

The dimension of matrices $[L_1]$ and $[L_2]$ is $(3n \times 3n)$ and they are given by:

$$[L_1] = \begin{bmatrix} [I] & [0] & [0] \\ [0] & [M] & [0] \\ [0] & [0] & [I] \end{bmatrix}, \quad [L_2] = \begin{bmatrix} [0] & -[I] & [0] \\ [K] & [C] & [H] \\ [0] & -[A] & -[B] \end{bmatrix} \quad (5.21)$$

where $[0]$ and $[I]$ are the $(n \times n)$ null and identity matrices respectively.

Since $[L_2]$ is a general nonsymmetric matrix, to decouple equation (5.19) it is necessary to obtain its right and left *complex* eigenproperties by solving the corresponding right and left eigenproblems:

$$[L_2][\Phi] = [L_1][\Phi][\Lambda] \quad , \quad [\Psi]^T [L_2] = [\Lambda][\Psi]^T [L_1] \quad (5.22)$$

where $[\Lambda]$ is a diagonal matrix the entries of which contain the $3n$ eigenvalues λ_i ordered by increasing modulus with λ_1 at entry (1,1); $[\Phi]$ and $[\Psi]$ are the right and left modal matrices respectively, which have been normalized with respect to matrix $[L_1]$ so the following conditions are satisfied:

$$[\Psi]^T [L_1] [\Phi] = [I] \quad , \quad [\Psi]^T [L_2] [\Phi] = [\Lambda]. \quad (5.23)$$

The columns of matrices $[\Phi]$ and $[\Psi]$ are ordered in accordance to the entries of matrix $[\Lambda]$, that is, the i^{th} columns of $[\Phi]$ and $[\Psi]$ contain respectively the i^{th} right eigenvector $\{\Phi\}_i$ and the i^{th} left eigenvector $\{\Psi\}_i$. The solution of each eigenproblem will provide n real and n pairs of complex conjugate eigenvalues with their corresponding real and complex eigenvectors. To distinguish between real and complex quantities the real eigenproperties will be indicated by a superscript r whereas the complex and complex conjugates by the superscripts c and cc respectively. All real eigenvalues as well as the real part of all complex eigenvalues are positive. We will write the n pairs of complex conjugate eigenvalues as [43]

$$\lambda_j^c = \beta_j \omega_j + i \omega_j \sqrt{1 - \beta_j^2} \quad , \quad \lambda_j^{cc} = \beta_j \omega_j - i \omega_j \sqrt{1 - \beta_j^2} \quad , \quad j = 1, \dots, n \quad (5.24)$$

where, β_j is the equivalent damping ratio and ω_j is the equivalent frequency for the j^{th} pair of complex conjugate modes. Equations (5.24) can be solved for ω_j and β_j to obtain:

$$\omega_j = |\lambda_j^c| \quad , \quad \beta_j = Re(\lambda_j^c) / \omega_j \quad , \quad j = 1, \dots, n \quad (5.25)$$

Equation (5.19) can be uncoupled by using the following transformation of coordinates:

$$\{Y\} = [\Phi] \{Z\} = \sum_{j=1}^{3n} \{\Phi\}_j z_j(t) \quad , \quad (5.26)$$

where $z_j(t)$ is the j^{th} component of vector $\{Z\}$. Substitution of equation (5.26) into equation (5.19) and then premultiplication by $[\Psi]^T$ provides the following set of uncoupled equations:

$$\{\dot{Z}\} + [\Lambda] \{Z\} = [\Psi]^T \{F\} \quad . \quad (5.27)$$

Thus, the n uncoupled equations are

$$\dot{z}_j(t) + \lambda_j z_j(t) = -\gamma_j \bar{x}_g(t) \quad , \quad j = 1, \dots, 3n \quad (5.28)$$

where γ_j is the j^{th} modal participation factor defined as

$$\gamma_j = \{\Psi\}_j^T \begin{Bmatrix} \{0\} \\ [M] \{\mathcal{I}\} \\ \{0\} \end{Bmatrix}. \quad (5.29)$$

The solution of the first order differential equation (5.28) for zero initial condition can be written as:

$$z_j(t) = -\gamma_j \int_0^t e^{-\lambda_j(t-\tau)} \tilde{x}_g(\tau) d\tau, \quad j = 1, \dots, 3n. \quad (5.30)$$

By performing the linear transformation indicated in equation (5.26), the l^{th} component of the response vector $\{Y\}$ can be written

$$y_l(t) = - \sum_{j=1}^{3n} q_{lj} \int_0^t e^{-\lambda_j(t-\tau)} \tilde{x}_g(\tau) d\tau; \quad l = 1, \dots, 3n \quad (5.31)$$

where $q_{lj} = \phi_{lj} \gamma_j$ and ϕ_{lj} is the (l, j) component of the right modal matrix $[\Phi]$.

Equation (5.31) defines the deterministic response of the linearized system of governing equations. The formulation to the response statistics of equation (5.19), for random ground motions, is presented in the following section.

5.5 Response Covariance Matrix of the Linearized System

To obtain the linearization coefficients, we will need some elements of the correlation matrix of the response vector $\{Y(t)\}$. Such matrix is denoted here as $[\mathcal{Y}(t_1, t_2)]$ and its (l, m) typical element can be defined as:

$$\mathcal{Y}_{lm}(t_1, t_2) = E[y_l(t_1) y_m(t_2)]. \quad (5.32)$$

To define this correlation in terms of the input motion and the eigenproperties we use equation (5.31) to obtain:

$$\mathcal{Y}_{lm}(t_1, t_2) = \sum_{j=1}^{3n} \sum_{k=1}^{3n} q_{lj} q_{mk} \int_0^{t_1} \int_0^{t_2} e^{-\lambda_j(t_1-\tau_1)} e^{-\lambda_k(t_2-\tau_2)} E[\tilde{x}_g(\tau_1) \tilde{x}_g(\tau_2)] d\tau_1 d\tau_2. \quad (5.33)$$

As considered in the previous chapters, we will assume the ground motion to be a stationary random process with power spectral density function $\Phi_g(\omega)$. Its autocorrelation function can then be written [29]

$$E[\tilde{x}_g(\tau_1) \tilde{x}_g(\tau_2)] = \int_{-\infty}^{\infty} \Phi_g(\omega) e^{i\omega(\tau_1-\tau_2)} d\omega. \quad (5.34)$$

Substitution of equation (5.34) into equation (5.33) and integration of the time integrals provides

$$\mathcal{Y}_{lm}(t_1, t_2) = \sum_{j=1}^{3n} \sum_{k=1}^{3n} q_{lj} q_{mk} \int_{-\infty}^{\infty} \Phi_g(\omega) \left(\frac{e^{i\omega t_1} - e^{-\lambda_j t_1}}{\lambda_j + i\omega} \right) \left(\frac{e^{-i\omega t_2} - e^{-\lambda_k t_2}}{\lambda_k - i\omega} \right) d\omega \quad (5.35)$$

For large values of t_1 and t_2 , this response correlation will also approach stationarity, as shown in previous chapters. For a finite value of the time difference, $\Delta t = t_1 - t_2$. This stationary correlation can be expressed as:

$$\mathcal{Y}_{lm}(\Delta t) = \int_{-\infty}^{\infty} \Phi_g(\omega) e^{i\omega \Delta t} \left(\sum_{j=1}^{3n} \frac{q_{lj}}{\lambda_j + i\omega} \right) \left(\sum_{k=1}^{3n} \frac{q_{mk}}{\lambda_k - i\omega} \right) d\omega. \quad (5.36)$$

The evaluation of the frequency integration for real and imaginary eigenproperties requires a different treatment. It is, therefore, necessary to consider these separately in the summations appearing in equations (5.36) as:

$$\sum_{j=1}^{3n} \frac{q_{lj}}{\lambda_j + i\omega} = \sum_{j=1}^n \frac{q_{lj}^r}{\lambda_j^r + i\omega} + \sum_{j=1}^n \left(\frac{q_{lj}^c}{\lambda_j^c + i\omega} + \frac{q_{lj}^{cc}}{\lambda_j^{cc} + i\omega} \right), \quad (5.37)$$

where the quantities q_{lj}^r are obtained from only the real eigenproperties, and q_{lj}^c and q_{lj}^{cc} from the complex and complex conjugate eigenproperties. Equation (5.37) can

be written in terms of the real and imaginary components of q_{lj}^c as

$$\sum_{j=1}^{3n} \frac{q_{lj}}{\lambda_j + i\omega} = \sum_{j=1}^n \frac{q_{lj}^r}{\lambda_j^r + i\omega} + \sum_{j=1}^n \left[\frac{(\lambda_j^{cc} + i\omega)(\delta_{lj} + i\varepsilon_{lj}) + (\lambda_j^c + i\omega)(\delta_{lj} - i\varepsilon_{lj})}{(\lambda_j^c + i\omega)(\lambda_j^{cc} + i\omega)} \right] \quad (5.38)$$

where

$$\delta_{lj} = \text{Re}(q_{lj}^c) \quad , \quad \varepsilon_{lj} = \text{Im}(q_{lj}^c) . \quad (5.39)$$

By substituting for λ_j^c and λ_j^{cc} from equation (5.24), equation (5.38) can be rewritten as:

$$\sum_{j=1}^{3n} \frac{q_{lj}}{\lambda_j + i\omega} = \sum_{j=1}^n q_{lj}^r G_j^c(\omega) + 2 \sum_{j=1}^n p_{lj}^c(\omega) H_j^c(\omega) \quad (5.40)$$

where $G_j^c(\omega)$ is the complex frequency response function of a first order system, defined as:

$$\dot{z}_j + \lambda_j^r z_j = e^{i\omega t} \quad , \quad z_j = G_j^c(\omega) e^{i\omega t} \quad , \quad G_j^c(\omega) = [\lambda_j^r + i\omega]^{-1} ; \quad (5.41)$$

and $H_j^c(\omega)$ is the complex frequency response function of a damped single-degree-of-freedom oscillator with natural frequency ω_j and damping ratio β_j ; defined in chapter 2 by equation (2.37). The other quantities appearing in (5.40) are defined as:

$$p_{lj}^c(\omega) = \zeta_{lj} + i \delta_{lj} \omega \quad , \quad \zeta_{lj} = \frac{\text{Re}(q_{lj}^c \lambda_j^{cc})}{2} = \omega_j (\beta_j \delta_{lj} + \varepsilon_{lj} \sqrt{1 - \beta_j^2}) . \quad (5.42)$$

The second summation term in equation (5.36) can be similarly rearranged to provide:

$$\sum_{k=1}^{3n} \frac{q_{mk}}{\lambda_k - i\omega} = \sum_{k=1}^n q_{mk}^r G_k^{cc}(\omega) + 2 \sum_{k=1}^n p_{mk}^{cc}(\omega) H_k^{cc}(\omega) , \quad (5.43)$$

where the quantities in (6.49) with superscript cc are the complex conjugates of the respective quantities defined in equations (5.41) through (5.42). After substitution of equations (5.40) and (5.43) into equation (5.36), with some further rearrangement of terms, the cross covariance term at $\Delta t = 0$ can be expressed as:

$$\mathcal{Y}_{lm} = \int_{-\infty}^{\infty} \Phi_g(\omega) \left[\Sigma_{lm}^R(\omega) + 2 \Sigma_{lm}^{RC}(\omega) + 4 \Sigma_{lm}^C(\omega) \right] d\omega , \quad (5.44)$$

where

$$\Sigma_{lm}^R(\omega) = \sum_{j=1}^n \sum_{k=1}^n q_{lj}^r q_{mk}^r G_j^c(\omega) G_k^{cc}(\omega) , \quad (5.45)$$

$$\Sigma_{lm}^{RC}(\omega) = \sum_{j=1}^n \sum_{k=1}^n q_{lj}^r p_{mk}^{cc}(\omega) G_j^c(\omega) H_k^{cc}(\omega) + q_{mk}^r p_{lj}^c(\omega) G_k^{cc}(\omega) H_j^c(\omega) , \quad (5.46)$$

$$\Sigma_{lm}^C(\omega) = \sum_{j=1}^n \sum_{k=1}^n p_{lj}^c(\omega) p_{mk}^{cc}(\omega) H_j^c(\omega) H_k^{cc}(\omega) , \quad (5.47)$$

Since $\Phi_g(\omega)$ is an even function of ω , the integrand terms defined by odd functions of ω will vanish when integrated from $-\infty$ to ∞ .

To be able to express the integration in equation (5.44) in terms of just a few frequency integrals, the summation terms given by equations (5.45-5.47) will be considered independently for further simplification

5.5.1 Terms associated with only real eigenproperties: $\Sigma_{lm}^R(\omega)$.

By multiplying and dividing equation (5.45) by $G_j^{cc}(\omega) G_k^c(\omega)$ and after some readjustment of terms, we obtain

$$\Sigma_{lm}^R(\omega) = \sum_{j=1}^n \sum_{k=1}^n q_{lj}^r q_{mk}^r |G_j^c(\omega)|^2 |G_k^c(\omega)|^2 [(\omega^2 + \lambda_j^r \lambda_k^r) + i \omega (\lambda_j^r - \lambda_k^r)] \quad (5.48)$$

where $|G_\star^c(\omega)|^2 = [(\lambda_\star^r)^2 + \omega^2]^{-1}$ is an even function of ω . Since the imaginary part of equation (5.48) is an odd function of ω , its contribution will become zero when integrated in equation (5.44). Therefore, only the real part of this expression which generates a nonzero contribution will be considered. This part is re-written as:

$$Re[\Sigma_{lm}^R(\omega)] = \sum_{j=1}^n \sum_{k=1}^n q_{lj}^r q_{mk}^r |G_j^c(\omega)|^2 |G_k^c(\omega)|^2 (\omega^2 + \lambda_j^r \lambda_k^r) . \quad (5.49)$$

The product term in equation (5.42) can be expressed as a sum of two terms by partial fractions (see Case I in appendix A) as:

$$Re[\Sigma_{lm}^R(\omega)] = \sum_{j=1}^n \sum_{k=1}^n T_{lmjk}^I |G_j^c(\omega)|^2 + T_{lmkj}^I |G_k^c(\omega)|^2, \quad (5.50)$$

where the coefficients of the partial fractions, T_{lmjk}^I and T_{lmkj}^I , are:

$$T_{lmjk}^I = q_{lj}^r q_{mk}^r \frac{\lambda_j^r}{\lambda_k^r + \lambda_j^r}, \quad T_{lmkj}^I = q_{lj}^r q_{mk}^r \frac{\lambda_k^r}{\lambda_k^r + \lambda_j^r} \quad (5.51)$$

5.5.2 Terms associated with real and complex eigenproperties: $\Sigma_{lm}^{RC}(\omega)$.

The terms in equation (5.46) will now be simplified so that the product of the response functions are avoided. For this purpose, the subscripts j and k in the second term of equation (5.46) are interchanged to get

$$\Sigma_{lm}^{RC}(\omega) = \sum_{j=1}^n \sum_{k=1}^n q_{lj}^r p_{mk}^{cc}(\omega) G_j^c(\omega) H_k^{cc}(\omega) + q_{mj}^r p_{lk}^c(\omega) G_j^{cc}(\omega) H_k^c(\omega). \quad (5.52)$$

Multiplication and division of each term by the corresponding conjugates of the frequency response functions yield

$$\Sigma_{lm}^{RC}(\omega) = \sum_{j=1}^n \sum_{k=1}^n |G_j^c(\omega)|^2 |H_k^c(\omega)|^2 \left\{ q_{lj}^r \left[\frac{p_{mk}^{cc}(\omega)}{G_j^{cc}(\omega) H_k^c(\omega)} \right] + q_{mj}^r \left[\frac{p_{lk}^c(\omega)}{G_j^c(\omega) H_k^{cc}(\omega)} \right] \right\}. \quad (5.53)$$

In this equation the quantities enclosed by brackets are the only complex quantities. The real and imaginary parts of $p_{mk}^{cc}(\omega)/[G_j^{cc}(\omega) H_k^c(\omega)]$, which are even and odd function of ω , respectively, are explicitly defined as:

$$\begin{aligned} Re \left[\frac{p_{mk}^{cc}(\omega)}{G_j^{cc}(\omega) H_k^c(\omega)} \right] &= (\zeta_{mk} \lambda_j^r - \delta_{mk} \omega^2) (\omega_k^2 - \omega^2) + 2\beta_k \omega_k (\zeta_{mk} + \delta_{mk} \lambda_j^r) \omega^2 \\ &= \delta_{mk} \omega^4 + \chi_{mjk} \omega^2 + \zeta_{mk} \lambda_j^r \omega_k^2, \end{aligned} \quad (5.54)$$

$$Im \left[\frac{p_{mk}^{cc}(\omega)}{G_j^{cc}(\omega) H_k^c(\omega)} \right] = 2\beta_k \omega_k (\zeta_{mk} \lambda_j^r \omega - \delta_{mk} \omega^3) - (\zeta_{mk} + \delta_{mk} \lambda_j^r) (\omega_k^2 \omega - \omega^3). \quad (5.55)$$

where χ_{mjk} is given by

$$\chi_{mjk} = (2\beta_k \omega_k - \lambda_j^r) \zeta_{mk} + (2\beta_k \omega_k \lambda_j^r - \omega_k^2) \delta_{mk}. \quad (5.56)$$

and its imaginary part, can be expressed by the following odd function of ω :

Similarly, the real and imaginary components of the remaining complex factor in equation (4.57) can be defined as:

$$Re \left[\frac{p_{lk}^c(\omega)}{G_j^c(\omega) H_k^{cc}(\omega)} \right] = \delta_{lk} \omega^4 + \chi_{ljk} \omega^2 + \zeta_{lk} \lambda_j^r \omega_k^2, \quad (5.57)$$

$$Im \left[\frac{p_{lk}^c(\omega)}{G_j^c(\omega) H_k^{cc}(\omega)} \right] = -2\beta_k \omega_k (\zeta_{lk} \lambda_j^r \omega - \delta_{lk} \omega^3) + (\zeta_{lk} + \delta_{lk} \lambda_j^r) (\omega_k^2 \omega - \omega^3). \quad (5.58)$$

In this case also the real and imaginary parts are even and odd functions of ω respectively. Again at this stage, the complex terms can be completely dropped from any further consideration since they provide zero contributions to equation (5.44) when integrated from $-\infty$ to ∞ . Thus, considering only the real parts in equation (4.57), we write we write

$$Re \left[\Sigma_{lm}^{RC}(\omega) \right] = \sum_{j=1}^n \sum_{k=1}^n |G_j^c(\omega)|^2 |H_k^c(\omega)|^2 P_{lmjk}(\omega) \quad (5.59)$$

where $P_{lmjk}(\omega)$ is a fourth degree polynomial in ω

$$P_{lmjk}(\omega) = (q_{lj}^r \delta_{mk} + q_{mj}^r \delta_{lk}) \omega^4 + (q_{lj}^r \chi_{mjk} + q_{mj}^r \chi_{ljk}) \omega^2 + (q_{lj}^r \zeta_{mk} + q_{mj}^r \zeta_{lk}) \lambda_j^r \omega_k^2. \quad (5.60)$$

The product $|G_j^c(\omega)|^2 |H_k^c(\omega)|^2 P_{lmjk}(\omega)$ can now be expanded into partial fractions (see Case II in appendix A) to provide:

$$Re \left[\Sigma_{lm}^{RC}(\omega) \right] = \sum_{j=1}^n \sum_{k=1}^n T_{lmjk}^{II} |G_j^c(\omega)|^2 + (T_{lmjk}^{III} + \omega^2 T_{lmjk}^{IV}) |H_k^c(\omega)|^2 \quad (5.61)$$

where the coefficients T_{lmjk}^{II} , T_{lmjk}^{III} and T_{lmjk}^{IV} are

$$T_{lmjk}^{II} = \left\{ \left[(q_{lj}^r \chi_{mjk} + q_{mj}^r \chi_{ljk}) - (\lambda_j^r)^2 (q_{lj}^r \delta_{mk} + q_{mj}^r \delta_{lk}) \right] (\lambda_j^r)^2 - (q_{lj}^r \zeta_{mk} + q_{mj}^r \zeta_{lk}) \lambda_j^r \omega_k^2 \right\} \left\{ 4 \beta_k^2 \omega_k^2 (\lambda_j^r)^2 - [(\lambda_j^r)^2 + \omega_k^2]^2 \right\}^{-1} \quad (5.62)$$

$$T_{lmjk}^{III} = \left\{ [\omega_k^2 (4 \beta_k^2 - 2) - (\lambda_j^r)^2] (q_{lj}^r \zeta_{mk} + q_{mj}^r \zeta_{lk}) \lambda_j^r \omega_k^2 - \omega_k^4 \left[(q_{lj}^r \chi_{mjk} + q_{mj}^r \chi_{ljk}) - (\lambda_j^r)^2 (q_{lj}^r \delta_{mk} + q_{mj}^r \delta_{lk}) \right] \right\} \left\{ 4 \beta_k^2 \omega_k^2 (\lambda_j^r)^2 - [(\lambda_j^r)^2 + \omega_k^2]^2 \right\}^{-1} \quad (5.63)$$

$$T_{lmjk}^{IV} = (q_{lj}^r \delta_{mk} + q_{mj}^r \delta_{lk}) - T_{lmjk}^{II} \quad (5.64)$$

5.5.3 Terms associated with only complex eigenproperties: $\Sigma_{lm}^C(\omega)$.

Here we will work with equation (5.47) to identify inconsequential odd terms and then express it as a sum of $|H_\star^c(\omega)|^2$ and no their product.

To achieve this Equation (5.47) is first decomposed into two parts. The first part contains only those terms with $j = k$ (diagonal terms) and the second part contains the remaining terms with $j \neq k$ (off-diagonal terms) as:

$$\Sigma_{lm}^C(\omega) = \sum_{j=1}^n p_{lj}^c(\omega) p_{mj}^{cc}(\omega) |H_j^c(\omega)|^2 + \sum_{j=1}^n \sum_{\substack{k=1 \\ k \neq j}}^n p_{lj}^c(\omega) p_{mk}^{cc}(\omega) H_j^c(\omega) H_k^{cc}(\omega). \quad (5.65)$$

The real and imaginary parts of the single summation terms can be easily identified by expanding the product $p_{lj}^c(\omega) p_{mj}^{cc}(\omega)$ into its real and imaginary parts. Again, at this stage the odd parts can be ignored as explained before. The remaining real part can now be expressed as:

$$Re \left[\sum_{j=1}^n p_{lj}^c(\omega) p_{mj}^{cc}(\omega) |H_j^c(\omega)|^2 \right] = \sum_{j=1}^n (\zeta_{lj} \zeta_{mj} + \delta_{lj} \delta_{mj} \omega^2) |H_j^c(\omega)|^2 \quad (5.66)$$

To simplify, the double summation term of equation (5.65), it is first multiplied and divided by the complex conjugates of the frequency response functions. At this stage again the imaginary part can be completely deleted for obvious reasons explained earlier. The remaining real part of a product term can be written as:

$$Re \left[p_{lj}^c(\omega) p_{mk}^{cc}(\omega) H_j^c(\omega) H_k^{cc}(\omega) \right] = \hat{P}_{lmjk}(\omega) |H_j^c(\omega)|^2 |H_k^c(\omega)|^2, \quad (5.67)$$

where $\hat{P}_{lmjk}(\omega)$ is a sixth degree polynomial in ω :

$$\begin{aligned} \hat{P}_{lmjk}(\omega) = & [\delta_{lj}\delta_{mk}] \omega^6 + [(4\beta_j\beta_k\omega_j\omega_k - \omega_j^2 - \omega_k^2)\delta_{lj}\delta_{mk} + \zeta_{lj}\zeta_{mk} \\ & + 2(\zeta_{mk}\delta_{lj} - \zeta_{lj}\delta_{mk})(\beta_k\omega_k - \beta_j\omega_j)] \omega^4 + [(4\beta_j\beta_k\omega_j\omega_k - \omega_j^2 - \omega_k^2)\zeta_{lj}\zeta_{mk} \\ & + \delta_{lj}\delta_{mk}\omega_j^2\omega_k^2 + 2\omega_j\omega_k(\zeta_{mk}\delta_{lj} - \zeta_{lj}\delta_{mk})(\beta_j\omega_k - \beta_k\omega_j)] \omega^2 \\ & + [\zeta_{lj}\zeta_{mk}\omega_j^2\omega_k^2] \omega^0 \end{aligned} \quad (5.68)$$

It is relevant to mention that the above polynomial is symmetric with respect to the indexes j and k . That is, $\hat{P}_{lmjk}(\omega) = \hat{P}_{lmkl}(\omega)$. This symmetry reduces by half the number of calculations required for the off-diagonal terms.

By using equations (5.66) and (5.67), and the symmetry of $\hat{P}_{lmjk}(\omega)$, this real component of equation (5.47) can be written as

$$Re \left[\Sigma_{lm}^C(\omega) \right] = \sum_{j=1}^n (\zeta_{lj}\zeta_{mj} + \delta_{lj}\delta_{mj}\omega^2) |H_j^c(\omega)|^2 + 2 \sum_{j=1}^{n-1} \sum_{k=j+1}^n \hat{P}_{lmjk}(\omega) |H_j^c(\omega)|^2 |H_k^c(\omega)|^2. \quad (5.69)$$

Finally, the product in the double summation term of equation (5.69) can be expressed as a sum by partial fractions (see Case III in appendix A) to provide the following equation:

$$\begin{aligned} Re \left[\Sigma_{lm}^C(\omega) \right] = & \sum_{j=1}^n (\zeta_{lj}\zeta_{mj} + \delta_{lj}\delta_{mj}\omega^2) |H_j^c(\omega)|^2 \\ & + 2 \sum_{j=1}^{n-1} \sum_{k=j+1}^n (T_{lmjk}^V + \omega^2 T_{lmjk}^{VI}) |H_j^c(\omega)|^2 + (T_{lmjk}^{VII} + \omega^2 T_{lmjk}^{VIII}) |H_k^c(\omega)|^2, \end{aligned} \quad (5.70)$$

where the coefficients T_{lmjk}^V , T_{lmjk}^{VI} , T_{lmjk}^{VII} and T_{lmjk}^{VIII} are given by

$$\begin{aligned}
T_{lmjk}^V &= \left\{ 2 \eta_{lmjk} \left[1 - \Omega_{jk}^2 + 2 (\beta_j^2 \Omega_{jk}^2 - \beta_k^2) \right] - \mu_{lmjk} (\Omega_{jk}^2 - \Omega_{jk}^{-2}) \right\} \Delta_{jk}^{-1} \\
T_{lmjk}^{VI} &= \left\{ \eta_{lmjk} (\Omega_{jk}^2 - \Omega_{jk}^{-2}) - 2 \Omega_{jk}^{-2} \mu_{lmjk} \left[1 - \Omega_{jk}^2 + 2 (\beta_k^2 \Omega_{jk}^2 - \beta_j^2) \right] \right\} \omega_j^{-2} \Delta_{jk}^{-1} \\
T_{lmjk}^{VII} &= \zeta_{lj} \zeta_{mk} \Omega_{jk}^{-2} - T_{lmjk}^V \Omega_{jk}^{-4} \\
T_{lmjk}^{VIII} &= \delta_{lj} \delta_{mk} - T_{lmjk}^{VI}, \tag{5.71}
\end{aligned}$$

with

$$\Omega_{jk} = \omega_j / \omega_k \tag{5.72}$$

$$\begin{aligned}
\mu_{lmjk} &= \zeta_{lj} \zeta_{mk} (\Omega_{jk}^2 - 1) + \omega_j^2 \delta_{lj} \delta_{mk} \left[(1 - 4\beta_j^2) \Omega_{jk}^2 + 4\beta_j \beta_k \Omega_{jk} - 1 \right] \\
&+ 2 \omega_j \Omega_{jk} (\delta_{lj} \zeta_{mk} - \delta_{mk} \zeta_{lj}) (\beta_k - \beta_j \Omega_{jk}) \tag{5.73}
\end{aligned}$$

$$\begin{aligned}
\eta_{lmjk} &= \zeta_{lj} \zeta_{mk} \left[1 - 4\beta_j^2 + 4\beta_j \beta_k \Omega_{jk} - \Omega_{jk}^2 \right] + \omega_j^2 \delta_{lj} \delta_{mk} (1 - \Omega_{jk}^2) \\
&+ 2 \omega_j (\delta_{lj} \zeta_{mk} - \delta_{mk} \zeta_{lj}) (\beta_j - \beta_k \Omega_{jk}) \tag{5.74}
\end{aligned}$$

$$\begin{aligned}
\Delta_{jk} &= 16 (\beta_j^2 + \beta_k^2 - \beta_j^4 - \beta_k^4) - \Omega_{jk}^4 - \Omega_{jk}^{-4} - 6 \\
&+ 4 (\Omega_{jk}^2 + \Omega_{jk}^{-2}) \left[1 - 2 (\beta_j^2 + \beta_k^2 - 2\beta_j^2 \beta_k^2) \right] \tag{5.75}
\end{aligned}$$

5.5.4 Final Expression for each Component of the Covariance Matrix

Since only the real parts of Σ_{lm}^R , Σ_{lm}^{RC} and Σ_{lm}^C need to be used in equation (5.44), it can be expressed in terms of simple frequency integrals as:

$$\begin{aligned}
\mathcal{Y}_{lm} &= \sum_{j=1}^n \sum_{k=1}^n \left(T_{lmjk}^I J_j + T_{lmkj}^I J_k \right) + 2 \sum_{j=1}^n \sum_{k=1}^n \left(T_{lmjk}^{II} J_j + T_{lmjk}^{III} I_k^d + T_{lmjk}^{IV} I_k^v \right) \\
&+ 4 \sum_{j=1}^n \left(\zeta_{lj} \zeta_{mj} I_j^d + \delta_{lj} \delta_{mj} I_J^v \right)
\end{aligned}$$

$$+ 8 \sum_{j=1}^{n-1} \sum_{k=j+1}^n \left(T_{lmjk}^V I_j^d + T_{lmjk}^{VI} I_j^v + T_{lmjk}^{VII} I_k^d + T_{lmjk}^{VIII} I_k^v \right) . \quad (5.76)$$

where J_j , I_j^d , and I_j^v are frequency integrals defined as

$$J_j = \int_{-\infty}^{\infty} \Phi_g(\omega) |G_j^c(\omega)|^2 d\omega ; , \quad (5.77)$$

$$I_j^d = \int_{-\infty}^{\infty} \Phi_g(\omega) |H_j^c(\omega)|^2 d\omega \quad , \quad I_j^v = \int_{-\infty}^{\infty} \Phi_g(\omega) \omega^2 |H_j^c(\omega)|^2 d\omega . \quad (5.78)$$

I_j^d and I_j^v were defined in chapter 2 as the mean square values of relative displacement and velocity response of a single-degree-of-freedom oscillator excited by ground motion. J_j is the mean square value of the response of a first order system, with parameter λ_j^r , excited by ground motion.

For some commonly used forms of spectral density functions these integrals may be obtained in closed-form. Appendix G provides some closed-form expressions for white noise and Kanai-Tajimi type of seismic inputs.

5.6 Response Spectrum Method

The objective of a response spectrum method is to express the maximum value of a design quantity by an appropriate combination of the maximum modal responses. These maximum responses, of the individual modes, are defined in terms of the input response spectra.

Any design quantity of interest $R(t)$, which is a linear combination of the response vector $\{Y(t)\}$ may be written

$$R(t) = \{\mathcal{R}\}^T \{Y(t)\} , \quad (5.79)$$

where $\{\mathcal{R}\}$ contains the coefficients of the linear transformation. For linear systems subjected to zero mean stationary inputs, the mean square value of R coincides with its covariance

$$\sigma_R^2 = E[R^2(t)] = \{\mathcal{R}\}^T E[\{Y(t)\}\{Y(t)\}^T] \{\mathcal{R}\} = \{\mathcal{R}\}^T [\mathcal{Y}] \{\mathcal{R}\}, \quad (5.80)$$

where $[\mathcal{Y}]$ is the covariance matrix of the response vector $\{Y(t)\}$. The (l, m) element of this covariance matrix is \mathcal{Y}_{lm} , which is defined in equations (5.76-5.78).

The maximum value of R , denoted as \mathcal{M}_R , can be approximated for some small probability of exceedance by scaling its standard deviation with an appropriate peak factor \mathcal{P}_R :

$$\mathcal{M}_R \approx \mathcal{P}_R \sigma_R, \quad (5.81)$$

Using equations (5.81) and (5.80) the squared maximum value can be approximated as

$$\mathcal{M}_R^2 \approx \{\mathcal{R}\}^T (\mathcal{P}_R^2 [\mathcal{Y}]) \{\mathcal{R}\}. \quad (5.82)$$

This equation expresses the maximum value of R as a function of the scaled stationary covariance matrix $\mathcal{P}_R^2[\mathcal{Y}]$. Therefore, it is of primary interest to relate the integral inputs used for \mathcal{Y}_{lm} in equations (5.76-5.78) with the ground inputs defined by the response spectra.

Approximate expressions for the frequency integrals in equations (5.77) and (5.78) can be obtained in terms of the response spectrum values and their respective peak factors:

$$J_j \approx \left(\frac{\mathcal{M}_j}{\mathcal{P}_j} \right)^2, \quad I_j^d \approx \left(\frac{\mathcal{M}_{d_j}}{\mathcal{P}_{d_j}} \right)^2, \quad I_j^v \approx \left(\frac{\mathcal{M}_{v_j}}{\mathcal{P}_{v_j}} \right)^2, \quad (5.83)$$

where \mathcal{M}_j is the spectrum value of the first order oscillator, and \mathcal{M}_{d_j} and \mathcal{M}_{v_j} are

the values of the relative displacement and relative velocity spectra, respectively, of the second order oscillator.

In terms of these frequency integrals we can define $(\mathcal{P}_R^2 \mathcal{Y}_{lm})$ as

$$\begin{aligned}
\mathcal{P}_R^2 \mathcal{Y}_{lm} \approx & \mathcal{P}_R^2 \left[\sum_{j=1}^n \sum_{k=1}^n \left(T_{lmjk}^I \frac{\mathcal{M}_j^2}{\mathcal{P}_j^2} + T_{lmkj}^I \frac{\mathcal{M}_k^2}{\mathcal{P}_k^2} \right) \right. \\
& + 2 \sum_{j=1}^n \sum_{k=1}^n \left(T_{lmjk}^{II} \frac{\mathcal{M}_j^2}{\mathcal{P}_j^2} + T_{lmjk}^{III} \frac{\mathcal{M}_{d_k}^2}{\mathcal{P}_{d_k}^2} + T_{lmjk}^{IV} \frac{\mathcal{M}_{v_k}^2}{\mathcal{P}_{v_k}^2} \right) \\
& + 4 \sum_{j=1}^n \left(\zeta_{lj} \zeta_{mj} \frac{\mathcal{M}_{d_j}^2}{\mathcal{P}_{d_j}^2} + \delta_{lj} \delta_{mj} \frac{\mathcal{M}_{v_j}^2}{\mathcal{P}_{v_j}^2} \right) \\
& \left. + 8 \sum_{j=1}^{n-1} \sum_{k=j+1}^n \left(T_{lmjk}^V \frac{\mathcal{M}_{d_j}^2}{\mathcal{P}_{d_j}^2} + T_{lmjk}^{VI} \frac{\mathcal{M}_{v_j}^2}{\mathcal{P}_{v_j}^2} + T_{lmjk}^{VII} \frac{\mathcal{M}_{d_k}^2}{\mathcal{P}_{d_k}^2} + T_{lmjk}^{VIII} \frac{\mathcal{M}_{v_k}^2}{\mathcal{P}_{v_k}^2} \right) \right]. \quad (5.84)
\end{aligned}$$

However, if we assume all the peak factors to be equal, equation (5.84) simplifies to:

$$\begin{aligned}
\mathcal{P}_R^2 \mathcal{Y}_{lm} \approx & \sum_{j=1}^n \sum_{k=1}^n \left(T_{lmjk}^I \mathcal{M}_j^2 + T_{lmkj}^I \mathcal{M}_k^2 \right) \\
& + 2 \sum_{j=1}^n \sum_{k=1}^n \left(T_{lmjk}^{II} \mathcal{M}_j^2 + T_{lmjk}^{III} \mathcal{M}_{d_k}^2 + T_{lmjk}^{IV} \mathcal{M}_{v_k}^2 \right) \\
& + 4 \sum_{j=1}^n \left(\zeta_{lj} \zeta_{mj} \mathcal{M}_{d_j}^2 + \delta_{lj} \delta_{mj} \mathcal{M}_{v_j}^2 \right) \\
& + 8 \sum_{j=1}^{n-1} \sum_{k=j+1}^n \left(T_{lmjk}^V \mathcal{M}_{d_j}^2 + T_{lmjk}^{VI} \mathcal{M}_{v_j}^2 + T_{lmjk}^{VII} \mathcal{M}_{d_k}^2 + T_{lmjk}^{VIII} \mathcal{M}_{v_k}^2 \right). \quad (5.85)
\end{aligned}$$

Substitution of equation (5.85) in equation (5.82) provides the squared design response value of interest. The numerical results have been obtained both from equation (5.84) and (5.85), that is, with and without the assumption of equal peak factors.

5.7 Summary of the Iterative Scheme

As it has been mentioned, the numerical solution of the proposed equivalent linear approximation to the hysteretic response, requires an iterative scheme. This

is due to the definition of the linearization coefficients as functions of the unknown response statistics.

Several iterative schemes may be adopted to reach the desired convergence. In particular, the fixed point [13] procedure has commonly been considered by several investigators. The fixed point approach is based on the solution of the following equations:

$$F_i^a(a_j, b_j) = a_i \quad , \quad F_i^b(a_j, b_j) = b_i \quad , \quad i, j = 1, \dots, n . \quad (5.86)$$

The functions F_i^a and F_i^b express the linearization coefficients as functions of the coefficients themselves. In the current problem, these functions can be defined only numerically. That is, equations (5.15-5.18) provide the coefficients a_i and b_i in terms of the response statistics, which are given by the appropriate elements of the covariance matrix. In turn, the components of the covariance matrix are functions of the eigenproperties of the linearized governing equations, which involve the linearization coefficients.

By considering equations (5.86), the fixed point scheme provides the following recursive formulas:

$$a_i^{(k+1)} = F_i^a(a_j^{(k)}, b_j^{(k)}) \quad , \quad b_i^{(k+1)} = F_i^b(a_j^{(k)}, b_j^{(k)}) \quad , \quad i, j = 1, \dots, n . \quad (5.87)$$

where the iteration steps are indicated by superscripts. Thus, the coefficients at step $(k + 1)$ are functions of the coefficients at the previous step (k) .

The different tasks required by each step, of the fixed point iterative scheme, can be summarized as follows:

1. Start with some assumed values of the linearization coefficients. For this purpose it is useful to notice that the linearization coefficients for a linear system are $a_i = 1$ and $b_i = 0$ for $i = 1, \dots, n$.
2. Assemble matrices $[A]$ and $[B]$, and modify accordingly matrix $[L_2]$.
3. Obtain the right and left eigenproperties corresponding to the homogeneous version of equation (5.19). Calculate the quantities required to determine all partial fraction coefficients.
4. Determine the response statistics by calculating only the necessary elements of the covariance matrix. For inputs defined in terms of power spectral density functions (Kanai-Tajimi), use equations (5.76-5.78). For inputs defined by ground response spectra, use equation (5.84). The latter requires the use of the peak factors associated to the ground motion.
5. Calculate the new linearization coefficients by using equations (5.15-5.18).
6. Compare the newly obtained coefficients with the initial coefficients. If the comparison satisfies some tolerance requirements, the process can be finished. Otherwise, the new coefficients are utilized to initiate the next iteration at step number 2.
7. After achieving convergence, the standard deviation of any quantity R , linearly related to the response vector $\{Y\}$, can be obtained by using just the covariance matrix: $\sigma_R = \sqrt{\{\mathcal{R}\}^T [\mathcal{Y}] \{\mathcal{D}\}}$. The maximum value of R requires the knowledge of its associated peak factor: $\mathcal{M}_R \approx \sqrt{\{\mathcal{R}\}^T (\mathcal{P}_R^2 [\mathcal{Y}]) \{\mathcal{R}\}}$.

To attain convergence, the fixed point approach requires the satisfaction of the

conditions given in reference [13]. The convergence of this scheme is *linear* because the error corresponding to the $(k + 1)^{th}$ step depends linearly on the error of the $(k)^{th}$ step. However, this type of convergence is characterized by its slow progress. Alternatively, the Newton method can be employed to accelerate convergence. It possesses the faster *quadratic* convergence. However, this method presents some drawbacks. It requires initial guesses not far from the actual values, and also the jacobian of F_i^a and F_i^b need to be provided. In the present problem only a numerical jacobian can be calculated.

The numerical solution of the examples presented in this work have used both iterative methods. For this purpose, the fixed point iteration has been fully implemented in a Fortran code, and a subroutine provided by the IMSL package [22, 34] has been employed to apply a modified version of the Newton method. Both approaches has been used independently or the fixed point iteration has been used first, to obtain an approximation to the convergence values, and a later refinement has been carried out by the Newton method.

5.8 Interstory Shear Responses

For the design of columns in a story it is of interest to calculate the interstory shear force. The shear force s_i affecting the column members between the i^{th} and the $i - 1^{th}$ floors, is given by equation (5.4). Also, it can be written in terms of the response vector $\{Y\}$ as

$$s_i = \{\mathcal{R}\}^T \{Y\} = k_i [\alpha_i (x_i - x_{i-1}) + (1 - \alpha_i) v_i] . \quad (5.88)$$

The mean square value (or covariance for zero mean processes) corresponding to this shear force can be obtained by using equation (5.80), or by calculating the expected value for the square of equation (5.88):

$$E[s_i^2] = k_i^2 E[\{\alpha_i(x_i - x_{i-1}) + (1 - \alpha_i)v_i\}^2], \quad (5.89)$$

which yields

$$\begin{aligned} E[s_i^2] = & k_i^2 \left\{ \alpha_i^2 (E[x_i^2] - 2 E[x_i x_{i-1}] + E[x_{i-1}^2]) \right. \\ & \left. + 2 \alpha_i (1 - \alpha_i) (E[x_i v_i] - E[x_{i-1} v_i]) + (1 - \alpha_i)^2 E[v_i^2] \right\}, \quad (5.90) \end{aligned}$$

where all the expected values of the right hand side are defined by the covariance matrix $[Y]$.

The maximum value of s_i can be obtained by amplifying the root mean square value by its peak factor. To simplify the calculations, the peak factors can be assumed to be equal as done in the derivation of equation (5.85). The calculation of peak factors by a procedure such as Davenport's approach [16], requires the calculation of the mean square value of the derivative of s_i with respect to time. From equation (5.88) this derivative can be defined as:

$$\dot{s}_i = k_i [\alpha_i (\dot{x}_i - \dot{x}_{i-1}) + (1 - \alpha_i) \dot{v}_i]. \quad (5.91)$$

It can be noticed that \dot{s}_i is a function of \dot{v}_i , which is not contained in the response vector $\{Y\}$. However, it can be expressed in terms of the components of $\{Y\}$ by using the equivalent linear constitutive law given in equation (5.12). Thus, \dot{s}_i becomes

$$\dot{s}_i = k_i [\alpha_i (\dot{x}_i - \dot{x}_{i-1}) + (1 - \alpha_i) \{a_i (\dot{x}_i - \dot{x}_{i-1}) + b_i v_i\}]. \quad (5.92)$$

From equation (5.92) we can obtain the mean square value as:

$$E[\dot{s}_i^2] = k_i^2 \left\{ [\alpha_i + a_i (1 - \alpha_i)]^2 (E[\dot{x}_i^2] - 2 E[\dot{x}_i \dot{x}_{i-1}] + E[\dot{x}_{i-1}^2]) \right. \quad (5.93)$$

$$+(1 - \alpha_i)^2 b_i^2 E[v_i^2] + 2 [\alpha_i + a_i (1 - \alpha_i)] (1 - \alpha_i) b_i (E[\dot{x}_i v_i] - E[\dot{x}_{i-1} v_i]) \},$$

where all the expected values on the right hand side are now defined in term of the elements of the covariance matrix $[\mathcal{Y}]$.

If Davenport's formula is used to calculate the peak factor then the mean of maximum values of s_i , is denoted as \mathcal{M}_{s_i} , and can be obtained from:

$$\mathcal{M}_{s_i} = \left(\sqrt{2 \ln(\wp T_d)} + \frac{0.5772}{\sqrt{2 \ln(\wp T_d)}} \right) \sigma_{s_i} \quad (5.94)$$

where

$$\sigma_{s_i} = \sqrt{E[s_i^2]} \quad , \quad \sigma_{\dot{s}_i} = \sqrt{E[\dot{s}_i^2]} \quad , \quad \wp = \frac{\sigma_{\dot{s}_i}}{\pi \sigma_{s_i}} \quad (5.95)$$

and T_d is the duration time for the strong motion part (stationary part) of the design earthquake.

5.9 Absolute Acceleration Response of a Floor

For design of light secondary systems it is of interest to calculate the absolute acceleration of a floor and floor response spectra. The vector of absolute floor acceleration can be defined by

$$\{\ddot{X}^a\} = \{\ddot{X}\} + \{I\} \ddot{x}_g(t) \quad (5.96)$$

Since the acceleration vectors $\{\ddot{X}\}$ and $\{\ddot{X}^a\}$ are not included in the response vector $\{Y\}$, it is necessary to express them as functions of the quantities contained in $\{Y\}$ to avoid the calculation of new responses. For this purpose, the relative acceleration vector $\{\ddot{X}\}$ is obtained by derivating once with respect to time the part

of the response vector $\{Y\}$ that contains the relative velocity vector.

$$\{\ddot{X}\} = \frac{d}{dt}\{\dot{X}\} = \frac{d}{dt}\{\bar{Y}\} \quad (5.97)$$

where $\{\bar{Y}\}$ is the middle third part of $\{Y\}$ containing just the elements $n+1, \dots, 2n$. By considering equation (5.26), the response vector $\{Y\}$ may be written as a linear combination of the principal coordinates, so the relative acceleration vector becomes

$$\{\ddot{X}\} = \frac{d}{dt} \sum_{j=1}^{3n} \{\bar{\phi}\}_j z_j(t) = \sum_{j=1}^{3n} \{\bar{\phi}\}_j \dot{z}_j(t) \quad (5.98)$$

where $\{\bar{\phi}\}_j$ is the middle third part of the j^{th} right eigenvector. The decoupled equations (5.28) can be solved for $\dot{z}_j(t)$ to obtain

$$\dot{z}_j(t) = -[\lambda_j z_j(t) + \gamma_j \ddot{x}_g(t)] \quad (5.99)$$

which can be substituted into equation (5.98) to get

$$\{\ddot{X}\} = -\sum_{j=1}^{3n} \lambda_j z_j(t) \{\bar{\phi}\}_j - \ddot{x}_g(t) \sum_{j=1}^{3n} \gamma_j \{\bar{\phi}\}_j. \quad (5.100)$$

Now, it will be proved that the factor $\sum_{j=1}^{3n} \gamma_j \{\bar{\phi}\}_j$ is equal to the influence vector $\{\mathcal{I}\}$. For this, consider the $3n$ vectors $\{\phi\}_j$ which are linearly independent and form a base for the $3n$ dimensional space. Since any vector belonging to such space can be obtained as a linear combination of the base vectors, the following equation can be written

$$\begin{Bmatrix} \{0\} \\ \{\mathcal{I}\} \\ \{0\} \end{Bmatrix} = \sum_{j=1}^{3n} \varrho_j \{\phi\}_j \quad (5.101)$$

where the coefficients ϱ_j can be determined by premultiplying both sides of equation (5.101) by $\{\Psi\}_k^T [L_1]$

$$\{\Psi\}_k^T [L_1] \begin{Bmatrix} \{0\} \\ \{\mathcal{I}\} \\ \{0\} \end{Bmatrix} = \sum_{j=1}^{3n} \varrho_j \{\Psi\}_k^T [L_1] \{\phi\}_j. \quad (5.102)$$

The left hand side of this equation is equal to the k^{th} participation factor (see equation (5.29))

$$\{\Psi\}_k^T \begin{bmatrix} [I] & [0] & [0] \\ [0] & [M] & [0] \\ [0] & [0] & [I] \end{bmatrix} \begin{Bmatrix} \{0\} \\ \{\mathcal{I}\} \\ \{0\} \end{Bmatrix} = \{\Psi\}_k^T \begin{Bmatrix} \{0\} \\ [M] \{\mathcal{I}\} \\ \{0\} \end{Bmatrix} = \gamma_k . \quad (5.103)$$

On the other hand, by considering the orthonormal property given by equation (5.23), the right hand side of equation (5.102) equals the coefficient ϱ_k . Therefore, $\varrho_k = \gamma_k$ and the influence vector in equation (5.101) becomes

$$\{\mathcal{I}\} = \sum_{j=1}^{3n} \gamma_j \{\bar{\phi}\}_j \quad (5.104)$$

which proves the initial hypothesis.

Substitution of equation (5.104) into equation (5.100) produces the following expression for the relative acceleration

$$\{\ddot{X}\} = - \sum_{j=1}^{3n} \lambda_j z_j(t) \{\bar{\phi}\}_j - \ddot{x}_g(t) \{\mathcal{I}\} . \quad (5.105)$$

and a new substitution of this equation into equation (5.96) provides the final expression of the absolute acceleration vector as a function of the eigenproperties and the principal coordinates

$$\{\ddot{X}^a\} = - \sum_{j=1}^{3n} \lambda_j z_j(t) \{\bar{\phi}\}_j \quad (5.106)$$

To obtain the maximum acceleration of a floor, we will first obtain its mean square value. The correlation matrix $[\ddot{X}^a(t_1, t_2)]$, corresponding to the absolute acceleration vector, can be defined by the following expected value by using equation (5.106)

$$[\ddot{X}^a(t_1, t_2)] = E[\{\ddot{X}^a(t_1)\} \{\ddot{X}^a(t_2)\}^T] = \sum_{j=1}^{3n} \sum_{k=1}^{3n} \lambda_j \lambda_k \{\bar{\phi}\}_j \{\bar{\phi}\}_k^T E[z_j(t_1) z_k(t_2)] . \quad (5.107)$$

The diagonal elements of this matrix defines the autocorrelation function of absolute acceleration for various floors. This autocorrelation function for the f^{th} floor can be written as:

$$\tilde{\chi}_{ff}^a(t_1, t_2) = E[\tilde{x}_f^a(t_1) \tilde{x}_f^a(t_2)] = \sum_{j=1}^{3n} \sum_{k=1}^{3n} \lambda_j \lambda_k \bar{\phi}_{fj} \bar{\phi}_{fk} E[z_j(t_1) z_k(t_2)] . \quad (5.108)$$

Equation (5.30) allows to write the cross correlation of $z_j(t_1)$ and $z_k(t_2)$, required in equation (5.108) as

$$E[z_j(t_1) z_k(t_2)] = \gamma_j \gamma_k \int_0^{t_1} \int_0^{t_2} e^{-\lambda_j(t_1-\tau_1)} e^{-\lambda_k(t_2-\tau_2)} E[\tilde{x}_g(\tau_1) \tilde{x}_g(\tau_2)] d\tau_1 d\tau_2 . \quad (5.109)$$

Substituting for the correlation function of ground acceleration in terms of spectral density function we obtain:

$$E[z_j(t_1) z_k(t_2)] = \gamma_j \gamma_k \int_0^{t_1} \int_0^{t_2} \int_{-\infty}^{\infty} \Phi_g(\omega) e^{i\omega(\tau_1-\tau_2)} e^{-\lambda_j(t_1-\tau_1)} e^{-\lambda_k(t_2-\tau_2)} d\tau_1 d\tau_2 d\omega . \quad (5.110)$$

For large t_1 and t_2 and finite $t_1 - t_2 = \Delta t$, it is simple to show that

$$E[z_j(t_1) z_k(t_2)] = \gamma_j \gamma_k \int_{-\infty}^{\infty} \frac{\Phi_g(\omega) e^{i\omega(\Delta t)}}{(\lambda_j + i\omega)(\lambda_k - i\omega)} d\omega . \quad (5.111)$$

From equation (5.111) one can identify the cross power spectral density function of the principal coordinates, here denoted by $\Phi_{z_j z_k}(\omega)$, as

$$\Phi_{z_j z_k}(\omega) = \frac{\gamma_j \gamma_k \Phi_g(\omega)}{(\lambda_j + i\omega)(\lambda_k - i\omega)} . \quad (5.112)$$

Substituting equation (5.111) into equation (5.108) and setting $\Delta t = 0$, we obtain the mean square value of the absolute acceleration of the f^{th} floor as:

$$\tilde{\chi}_{ff}^a = \int_{-\infty}^{\infty} \Phi_g(\omega) \left[\sum_{j=1}^{3n} \frac{\hat{q}_{fj}}{(\lambda_j + i\omega)} \right] \left[\sum_{k=1}^{3n} \frac{\hat{q}_{fk}}{(\lambda_k - i\omega)} \right] d\omega , \quad (5.113)$$

where \hat{q}_{fj} is defined as

$$\hat{q}_{fj} = \lambda_j \bar{\phi}_{fj} \gamma_j , \quad f = 1, \dots, n , \quad j = 1, \dots, 3n \quad (5.114)$$

For a fixed value of f , there are $3n$ quantities \hat{q}_{fj} , of which n are real values denoted as \hat{q}_{fj}^r and the remaining $2n$ are n pairs of complex conjugate values denoted as \hat{q}_{fj}^c and \hat{q}_{fj}^{cc} . Denoting the real and imaginary parts of \hat{q}_{fj}^c as

$$\hat{q}_{fj}^c = \hat{\delta}_{fj} + i \hat{\epsilon}_{fj} . \quad (5.115)$$

Substituting for the eigenvalues λ_j in terms of real and imaginary parts, the summation factors in equation (5.113) can be written as:

$$\sum_{j=1}^{3n} \frac{\hat{q}_{fj}}{\lambda_j + i\omega} = \sum_{j=1}^n \hat{q}_{fj}^r G_j^c(\omega) + 2 \sum_{j=1}^n \hat{p}_{fj}^c(\omega) H_j^c(\omega) \quad (5.116)$$

$$\sum_{k=1}^{3n} \frac{\hat{q}_{fk}}{\lambda_k - i\omega} = \sum_{k=1}^n \hat{q}_{fk}^r G_k^{cc}(\omega) + 2 \sum_{k=1}^n \hat{p}_{fk}^{cc}(\omega) H_k^{cc}(\omega) . \quad (5.117)$$

where $G_j^c(\omega)$ and $H_j^c(\omega)$ have been defined by equations (5.41) and (2.37) and the complex quantity \hat{p}_{fj}^c is given by

$$\hat{p}_{fj}^c(\omega) = \hat{\zeta}_{fj} + i \hat{\delta}_{fj} \omega \quad , \quad \hat{\zeta}_{fj} = \omega_j \left(\beta_j \hat{\delta}_{fj} + \hat{\epsilon}_{fj} \sqrt{1 - \beta_j^2} \right) . \quad (5.118)$$

Substituting equations (5.116) and (5.117) in equation (5.113) we obtain

$$\begin{aligned} \tilde{\chi}_{ff}^a = & \int_{-\infty}^{\infty} \Phi_g(\omega) \left(\sum_{j=1}^n \hat{q}_{fj}^r G_j^c(\omega) + 2 \sum_{j=1}^n \hat{p}_{fj}^c(\omega) H_j^c(\omega) \right) \\ & \times \left(\sum_{k=1}^n \hat{q}_{fk}^r G_k^{cc}(\omega) + 2 \sum_{k=1}^n \hat{p}_{fk}^{cc}(\omega) H_k^{cc}(\omega) \right) d\omega . \end{aligned} \quad (5.119)$$

This expression is very similar to equation (5.44). It can therefore, be simplified similarly to express this in terms of frequency integrals and real quantities as:

$$\begin{aligned} \tilde{\chi}_{ff}^a = & \sum_{j=1}^n \sum_{k=1}^n \left(\hat{T}_{ffjk}^I J_j + \hat{T}_{ffkj}^I J_k \right) + 2 \sum_{j=1}^n \sum_{k=1}^n \left(\hat{T}_{ffjk}^{II} J_j + \hat{T}_{ffjk}^{III} I_k^d + \hat{T}_{ffjk}^{IV} I_k^v \right) \\ & + 4 \sum_{j=1}^n \left(\hat{\zeta}_{fj}^2 I_j^d + \hat{\delta}_{fj}^2 I_j^v \right) \\ & + 8 \sum_{j=1}^{n-1} \sum_{k=j+1}^n \left(\hat{T}_{ffjk}^V I_j^d + \hat{T}_{ffjk}^{VI} I_j^v + \hat{T}_{ffjk}^{VII} I_k^d + \hat{T}_{ffjk}^{VIII} I_k^v \right) . \end{aligned} \quad (5.120)$$

where J_j , I_j^d , and I_j^v are the frequency integrals defined by equations (5.77) and (5.78). For some commonly used spectral density function, they can be evaluated easily (see appendix G). They can also be expressed in terms of ground response spectra by utilizing the proper peak factor values, as explained before. The partial fraction coefficients $\hat{T}_{ffjk}^I - \hat{T}_{ffjk}^{VIII}$ have similar expressions as those corresponding to the coefficients $T_{lmjk}^I - T_{lmjk}^{VIII}$ (see equations (5.51), (5.62-5.64) and (5.71)):

$$\hat{T}_{ffjk}^I = \hat{q}_{fj}^r \hat{q}_{fk}^r \frac{\lambda_j^r}{\lambda_k^r + \lambda_j^r}, \quad \hat{T}_{ffkj}^I = \hat{q}_{fj}^r \hat{q}_{fk}^r \frac{\lambda_k^r}{\lambda_k^r + \lambda_j^r} \quad (5.121)$$

$$\begin{aligned} \hat{T}_{ffjk}^{II} = & 2 \left\{ \left[\hat{q}_{fj}^r \hat{\chi}_{fjk} - (\lambda_j^r)^2 \hat{q}_{fj}^r \hat{\delta}_{fk} \right] (\lambda_j^r)^2 \right. \\ & \left. - \hat{q}_{fj}^r \hat{\zeta}_{fk} \lambda_j^r \omega_k^2 \right\} \left\{ 4 \beta_k^2 \omega_k^2 (\lambda_j^r)^2 - [(\lambda_j^r)^2 + \omega_k^2]^2 \right\}^{-1} \end{aligned} \quad (5.122)$$

$$\begin{aligned} \hat{T}_{ffjk}^{III} = & 2 \left\{ [\omega_k^2 (4 \beta_k^2 - 2) - (\lambda_j^r)^2] \hat{q}_{fj}^r \hat{\zeta}_{fk} \lambda_j^r \omega_k^2 - \omega_k^4 \left[\hat{q}_{fj}^r \hat{\chi}_{fjk} - (\lambda_j^r)^2 \hat{q}_{fj}^r \hat{\delta}_{fk} \right] \right\} \\ & \times \left\{ 4 \beta_k^2 \omega_k^2 (\lambda_j^r)^2 - [(\lambda_j^r)^2 + \omega_k^2]^2 \right\}^{-1} \end{aligned} \quad (5.123)$$

$$\hat{T}_{ffjk}^{IV} = 2 \hat{q}_{fj}^r \hat{\delta}_{fk} - \hat{T}_{ffjk}^{II} \quad (5.124)$$

$$\hat{T}_{ffjk}^V = \left\{ 2 \hat{\eta}_{ffjk} \left[1 - \Omega_{jk}^2 + 2 (\beta_j^2 \Omega_{jk}^2 - \beta_k^2) \right] - \hat{\mu}_{ffjk} (\Omega_{jk}^2 - \Omega_{jk}^{-2}) \right\} \Delta_{jk}^{-1} \quad (5.125)$$

$$\begin{aligned} \hat{T}_{ffjk}^{VI} = & \left\{ \hat{\eta}_{ffjk} (\Omega_{jk}^2 - \Omega_{jk}^{-2}) - 2 \Omega_{jk}^{-2} \hat{\mu}_{ffjk} \left[1 - \Omega_{jk}^2 + 2 (\beta_k^2 \Omega_{jk}^2 - \beta_j^2) \right] \right\} \omega_j^{-2} \Delta_{jk}^{-1} \\ & (5.126) \end{aligned}$$

$$\hat{T}_{ffjk}^{VII} = \hat{\zeta}_{fj} \hat{\zeta}_{fk} \Omega_{jk}^{-2} - \hat{T}_{ffjk}^V \Omega_{jk}^{-4} \quad (5.127)$$

$$\hat{T}_{ffjk}^{VIII} = \hat{\delta}_{fj} \hat{\delta}_{fk} - \hat{T}_{ffjk}^{VI} \quad (5.128)$$

where the variables Ω_{jk} and Δ_{jk} were defined in equations (5.72) and (5.75) and the auxiliary variables $\hat{\chi}_{fjk}$, $\hat{\mu}_{ffjk}$ and $\hat{\eta}_{ffjk}$ are

$$\hat{\chi}_{fjk} = (2 \beta_k \omega_k - \lambda_j^r) \hat{\zeta}_{fk} + (2 \beta_k \omega_k \lambda_j^r - \omega_k^2) \hat{\delta}_{fk}. \quad (5.129)$$

$$\begin{aligned}\hat{\mu}_{ffjk} &= \hat{\zeta}_{fj}\hat{\zeta}_{fk}(\Omega_{jk}^2 - 1) + \omega_j^2\hat{\delta}_{fj}\hat{\delta}_{fk} \left[(1 - 4\beta_j^2)\Omega_{jk}^2 + 4\beta_j\beta_k\Omega_{jk} - 1 \right] \\ &+ 2\omega_j\Omega_{jk}(\hat{\delta}_{fj}\hat{\zeta}_{fk} - \hat{\delta}_{fk}\hat{\zeta}_{fj})(\beta_k - \beta_j\Omega_{jk})\end{aligned}\quad (5.130)$$

$$\begin{aligned}\hat{\eta}_{ffjk} &= \hat{\zeta}_{fj}\hat{\zeta}_{fk} \left[1 - 4\beta_j^2 + 4\beta_j\beta_k\Omega_{jk} - \Omega_{jk}^2 \right] + \omega_j^2\hat{\delta}_{fj}\hat{\delta}_{fk}(1 - \Omega_{jk}^2) \\ &+ 2\omega_j(\hat{\delta}_{fj}\hat{\zeta}_{fk} - \hat{\delta}_{fk}\hat{\zeta}_{fj})(\beta_j - \beta_k\Omega_{jk}).\end{aligned}\quad (5.131)$$

To obtain the maximum value of floor acceleration, the root mean square value obtained from (5.120) can be amplified by its peak factor. The peak factor can be calculated by a suitable formula such as Davenport's formula. Or to simplify the calculation all peak factors can be set equal to calculate the maximum floor acceleration in terms of ground response spectra.

5.10 Floor Response Spectra

To obtain floor response spectra, we need to obtain the maximum acceleration of a single degree of freedom oscillator subjected to the acceleration of the floor at its base. The equation of motion of a single-degree-of-freedom oscillator attached to the f^{th} floor of a shear building can be written as

$$\ddot{x}_o + 2\beta_o\omega_o\dot{x}_o + \omega_o^2x_o = -\ddot{x}_f^a, \quad (5.132)$$

where the subscript o indicates variables that are associated to such oscillator, x_o is the relative displacement of the oscillator with respect to the f^{th} floor and \ddot{x}_f^a is the absolute acceleration of such floor. \ddot{x}_f^a can be obtained from equation (5.106)

$$\ddot{x}_f^a = -\sum_{j=1}^{3n} \lambda_j z_j(t) \bar{\phi}_{fj}. \quad (5.133)$$

Thus, the equation of motion of the oscillator becomes

$$\ddot{x}_o + 2\beta_o \omega_o \dot{x}_o + \omega_o^2 x_o = \sum_{j=1}^{3n} \lambda_j z_j(t) \bar{\phi}_{fj}, \quad (5.134)$$

and its solution for zero initial conditions is

$$x_o(t) = \sum_{j=1}^{3n} \lambda_j \bar{\phi}_{fj} \int_0^t h_o(t-\tau) z_j(\tau) d\tau. \quad (5.135)$$

The absolute acceleration of oscillator o is defined as:

$$\ddot{x}_o^a = \ddot{x}_o + \ddot{x}_f^a = -2\beta_o \omega_o \dot{x}_o - \omega_o^2 x_o. \quad (5.136)$$

Using equation (5.136), we can define the autocorrelation formula of oscillator acceleration as:

$$\begin{aligned} E[\ddot{x}_o^a(t_1) \ddot{x}_o^a(t_2)] &= \omega_o^4 E[x_o(t_1) x_o(t_2)] + 4\beta_o^2 \omega_o^2 E[\dot{x}_o(t_1) \dot{x}_o(t_2)] \\ &+ 2\beta_o \omega_o^3 (E[\dot{x}_o(t_1) x_o(t_2)] + E[x_o(t_1) \dot{x}_o(t_2)]) \end{aligned} \quad (5.137)$$

where the four expected values will now be considered independently.

By using equation (5.135) the auto correlation function of relative displacements becomes

$$\begin{aligned} E[x_o(t_1) x_o(t_2)] &= \sum_{j=1}^{3n} \sum_{k=1}^{3n} \lambda_j \bar{\phi}_{fj} \lambda_k \bar{\phi}_{fk} \\ &\times \int_0^{t_1} \int_0^{t_2} h_o(t_1 - \tau_1) h_o(t_2 - \tau_2) E[z_j(\tau_1) z_k(\tau_2)] d\tau_1 d\tau_2. \end{aligned} \quad (5.138)$$

For stationary inputs, and response, $E[z_j(\tau_1) z_k(\tau_2)]$ can be expressed by equation (5.111) as

$$E[z_j(\tau_1) z_k(\tau_2)] = \int_{-\infty}^{\infty} \Phi_{z_j z_k}(\omega) e^{i\omega(\tau_1 - \tau_2)} d\omega \quad (5.139)$$

where $\Phi_{z_j z_k}(\omega)$ is given in equation (5.112). Substitution of equation (5.139) into (5.138) and considering large values of t_1 and t_2 , we can show that

$$E[x_o(t_1) x_o(t_2)] = \sum_{j=1}^{3n} \sum_{k=1}^{3n} \lambda_j \bar{\phi}_{fj} \lambda_k \bar{\phi}_{fk} \int_{-\infty}^{\infty} \Phi_{z_j z_k}(\omega) e^{i\omega(t_1 - t_2)} |H_o^c(\omega)|^2 d\omega, \quad (5.140)$$

where $H_o^c(\omega)$ is defined as

$$H_o^c(\omega) = \left[\omega_o^2 - \omega^2 + 2i\beta_o\omega_o\omega \right]^{-1}. \quad (5.141)$$

The remaining three expected values in equation (5.137) can be obtained by appropriate derivations of equation (5.140) with respect to time. Thus,

$$E[\dot{x}_o(t_1) \dot{x}_o(t_2)] = \sum_{j=1}^{3n} \sum_{k=1}^{3n} \lambda_j \bar{\phi}_{fj} \lambda_k \bar{\phi}_{fk} \int_{-\infty}^{\infty} \omega^2 \Phi_{z_j z_k}(\omega) e^{i\omega(t_1-t_2)} |H_o^c(\omega)|^2 d\omega. \quad (5.142)$$

$$E[\dot{x}_o(t_1) x_o(t_2)] = \sum_{j=1}^{3n} \sum_{k=1}^{3n} \lambda_j \bar{\phi}_{fj} \lambda_k \bar{\phi}_{fk} \int_{-\infty}^{\infty} (i\omega) \Phi_{z_j z_k}(\omega) e^{i\omega(t_1-t_2)} |H_o^c(\omega)|^2 d\omega, \quad (5.143)$$

and

$$E[x_o(t_1) \dot{x}_o(t_2)] = \sum_{j=1}^{3n} \sum_{k=1}^{3n} \lambda_j \bar{\phi}_{fj} \lambda_k \bar{\phi}_{fk} \int_{-\infty}^{\infty} (-i\omega) \Phi_{z_j z_k}(\omega) e^{i\omega(t_1-t_2)} |H_o^c(\omega)|^2 d\omega. \quad (5.144)$$

Substituting the above equations in equation (5.137) and setting $t_1 = t_2 = t$, we obtain the mean square value of the absolute acceleration of the oscillator as:

$$E[(\ddot{x}_o^a)^2] = \int_{-\infty}^{\infty} \Phi_g(\omega) (\omega_o^4 + 4\beta_o^2 \omega_o^2 \omega^2) \sum_{j=1}^{3n} \frac{\hat{q}_{fj}}{(\lambda_j + i\omega)} \sum_{k=1}^{3n} \frac{\hat{q}_{fk}}{(\lambda_k - i\omega)} |H_o^c(\omega)|^2 d\omega. \quad (5.145)$$

Where \hat{q}_{fj} and \hat{q}_{fk} were defined by equation (5.114). Substituting for the summation terms defined in equations (5.116) and (5.117), and after some rearrangement of terms we obtain

$$\begin{aligned} E[(\ddot{x}_o^a)^2] &= \int_{-\infty}^{\infty} \Phi_g(\omega) (\omega_o^4 + 4\beta_o^2 \omega_o^2 \omega^2) |H_o^c(\omega)|^2 \\ &\times \left[\hat{\Sigma}_{ff}^R(\omega) + 2\hat{\Sigma}_{ff}^{RC}(\omega) + 4\hat{\Sigma}_{ff}^C(\omega) \right] d\omega, \end{aligned} \quad (5.146)$$

where

$$\hat{\Sigma}_{ff}^R(\omega) = \sum_{j=1}^n \sum_{k=1}^n \hat{q}_{fj}^r \hat{q}_{fk}^r G_j^c(\omega) G_k^{cc}(\omega) \quad (5.147)$$

$$\hat{\Sigma}_{ff}^{RC}(\omega) = \sum_{j=1}^n \sum_{k=1}^n \hat{q}_{ff}^r \hat{p}_{fk}^{cc}(\omega) G_j^c(\omega) H_k^{cc}(\omega) + \hat{q}_{fk}^r \hat{p}_{jj}^c(\omega) G_k^{cc}(\omega) H_j^c(\omega) \quad (5.148)$$

$$\hat{\Sigma}_{ff}^C(\omega) = \sum_{j=1}^n \sum_{k=1}^n \hat{p}_{jj}^c(\omega) \hat{p}_{fk}^{cc}(\omega) H_j^c(\omega) H_k^{cc}(\omega) \quad (5.149)$$

$G_j^c(\omega)$, $H_j^c(\omega)$ and \hat{p}_{jj}^c have been defined by equations (5.41), (2.37) and (5.118) respectively.

Since equations (5.146-5.149) have a structure similar to equations (5.44-5.47), the analysis used to simplify these equations can also be used here to simplify the expression for $E[(\tilde{x}_o^a)^2]$ in terms of real quantities only and the frequency integrals. After some pages of algebra, the mean square value of the oscillator acceleration can be written as:

$$E[(\tilde{x}_o^a)^2] = \sum_{i=1}^7 [E_{of}^{(i)}] , \quad (5.150)$$

where

$$E_{of}^{(1)} = \sum_{j=1}^n \sum_{k=1}^n \hat{S}_{fkjo}^{(1)} J_j + \hat{S}_{fkjo}^{(2)} I_o^d + \hat{S}_{fkjo}^{(3)} I_o^v , \quad (5.151)$$

$$E_{fo}^{(2)}(\omega) = \sum_{j=1}^n \sum_{k=1}^n \hat{S}_{fjko}^{(4)} J_k + \hat{S}_{fjko}^{(5)} I_o^d + \hat{S}_{fjko}^{(6)} I_o^v , \quad (5.152)$$

$$E_{fo}^{(3)}(\omega) = 2 \sum_{j=1}^n \sum_{k=1}^n \hat{S}_{fkjo}^{(7)} J_j + \hat{S}_{fkjo}^{(8)} I_o^d + \hat{S}_{fkjo}^{(9)} I_o^v , \quad (5.153)$$

$$E_{fo}^{(4)}(\omega) = 2 \sum_{j=1}^n \sum_{k=1}^n \hat{S}_{fjko}^{(10)} I_k^d + \hat{S}_{fjko}^{(11)} I_k^v + \hat{S}_{fjko}^{(12)} I_o^d + \hat{S}_{fjko}^{(13)} I_o^v , \quad (5.154)$$

$$E_{fo}^{(5)}(\omega) = 4 \sum_{j=1}^n \hat{S}_{fjjo}^{(14)} I_j^d + \hat{S}_{fjjo}^{(15)} I_j^v + \hat{S}_{fjjo}^{(16)} I_o^d + \hat{S}_{fjjo}^{(17)} I_o^v , \quad (5.155)$$

$$E_{fo}^{(6)}(\omega) = 8 \sum_{j=1}^{n-1} \sum_{k=j+1}^n \hat{S}_{fkjo}^{(18)} I_j^d + \hat{S}_{fkjo}^{(19)} I_j^v + \hat{S}_{fkjo}^{(20)} I_o^d + \hat{S}_{fkjo}^{(21)} I_o^v , \quad (5.156)$$

$$E_{fo}^{(7)}(\omega) = 8 \sum_{j=1}^{n-1} \sum_{k=j+1}^n \hat{S}_{fjko}^{(22)} I_k^d + \hat{S}_{fjko}^{(23)} I_k^v + \hat{S}_{fjko}^{(24)} I_o^d + \hat{S}_{fjko}^{(25)} I_o^v . \quad (5.157)$$

J_* , I_*^d and I_*^v are the frequency integrals defined by equations (5.77) and (5.78) with the appropriate change of subscripts. The factors of partial coefficients are defined in appendix A. As mentioned before, the frequency integrals can be expressed in terms of the spectral density functions or in terms of ground response spectra by using appropriate peak factor values.

Thus, equations (5.150-5.157) provide the mean square value of the absolute acceleration of oscillator "o" attached to the f^{th} floor. To obtain the maximum value of the oscillator acceleration, $\mathcal{M}_{\ddot{x}_o}$, the mean square value needs to be amplified by the peak factor of the acceleration. However, if the peak factors are assumed equal, the maximum values of the oscillator acceleration can be defined in terms of the ground response spectrum values as:

$$\mathcal{M}_{\ddot{x}_o} \approx \sqrt{\sum_{i=1}^7 [M_{fo}^{(i)}]}, \quad (5.158)$$

where

$$M_{fo}^{(1)} \approx \sum_{j=1}^n \sum_{k=1}^n \hat{S}_{fjko}^{(1)} \mathcal{M}_j^2 + \hat{S}_{fjko}^{(2)} \mathcal{M}_{d_o}^2 + \hat{S}_{fjko}^{(3)} \mathcal{M}_{v_o}^2, \quad (5.159)$$

$$M_{fo}^{(2)}(\omega) \approx \sum_{j=1}^n \sum_{k=1}^n \hat{S}_{fjko}^{(4)} \mathcal{M}_k^2 + \hat{S}_{fjko}^{(5)} \mathcal{M}_{d_o}^2 + \hat{S}_{fjko}^{(6)} \mathcal{M}_{v_o}^2, \quad (5.160)$$

$$M_{fo}^{(3)}(\omega) \approx 2 \sum_{j=1}^n \sum_{k=1}^n \hat{S}_{fjko}^{(7)} \mathcal{M}_j^2 + \hat{S}_{fjko}^{(8)} \mathcal{M}_{d_o}^2 + \hat{S}_{fjko}^{(9)} \mathcal{M}_{v_o}^2, \quad (5.161)$$

$$M_{fo}^{(4)}(\omega) \approx 2 \sum_{j=1}^n \sum_{k=1}^n \hat{S}_{fjko}^{(10)} \mathcal{M}_{d_k}^2 + \hat{S}_{fjko}^{(11)} \mathcal{M}_{v_k}^2 + \hat{S}_{fjko}^{(12)} \mathcal{M}_{d_o}^2 + \hat{S}_{fjko}^{(13)} \mathcal{M}_{v_o}^2, \quad (5.162)$$

$$M_{fo}^{(5)}(\omega) \approx 4 \sum_{j=1}^n \hat{S}_{fjjo}^{(14)} \mathcal{M}_{d_j}^2 + \hat{S}_{fjjo}^{(15)} \mathcal{M}_{v_j}^2 + \hat{S}_{fjjo}^{(16)} \mathcal{M}_{d_o}^2 + \hat{S}_{fjjo}^{(17)} \mathcal{M}_{v_o}^2, \quad (5.163)$$

$$M_{fo}^{(6)}(\omega) \approx 8 \sum_{j=1}^{n-1} \sum_{k=j+1}^n \hat{S}_{fjko}^{(18)} \mathcal{M}_{d_j}^2 + \hat{S}_{fjko}^{(19)} \mathcal{M}_{v_j}^2 + \hat{S}_{fjko}^{(20)} \mathcal{M}_{d_o}^2 + \hat{S}_{fjko}^{(21)} \mathcal{M}_{v_o}^2, \quad (5.164)$$

$$M_{fo}^{(7)}(\omega) \approx 8 \sum_{j=1}^{n-1} \sum_{k=j+1}^n \hat{S}_{fjko}^{(22)} \mathcal{M}_{d_k}^2 + \hat{S}_{fjko}^{(23)} \mathcal{M}_{v_k}^2 + \hat{S}_{fjko}^{(24)} \mathcal{M}_{d_o}^2 + \hat{S}_{fjko}^{(25)} \mathcal{M}_{v_o}^2. \quad (5.165)$$

It should be noticed that the expression for the maximum value of the absolute acceleration of the oscillator "o" is given in terms of: 1) the relative displacement spectrum \mathcal{M}_d , which can be easily obtained from the pseudo acceleration spectrum, 2) the relative velocity spectrum \mathcal{M}_v , which can be approximated by the pseudo velocity spectrum, and 3) the relative displacement spectrum of the massless oscillator \mathcal{M}_j . This last spectra is required whenever hysteretic behavior is involved in the analysis.

5.11 Numerical Results

In this section we present numerical results for two example problems of multi-story shear structures. The first structure is used to demonstrate the application of the response spectrum approach presented in the previous section. The formulation presented has also been used with the second structure, but in addition a numerical simulation study has also been conducted to ascertain the accuracy of the response calculated by the proposed equivalent linear approach.

Figure 5.1 shows the schematic of the first structure. The mass, stiffness and damping ratios for this structure are shown in table 5.1. Also all four interstory stiffness elements are assumed to behave nonlinearly. The parameters of these hysteretic elements are given in table 5.2.

The seismic input for this case is defined in terms of mean pseudo-acceleration and relative velocity response spectra of an ensemble of time histories. These spectra are shown in figure 5.2. We also need the spectra for the first order oscillator which is shown in figure 5.3 (A).

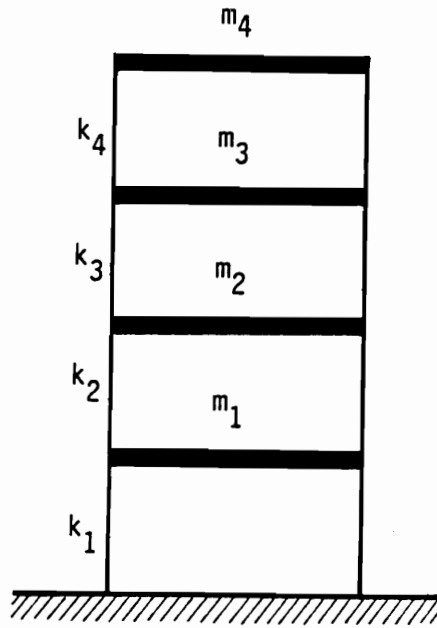


Figure 5.1: Schematic of the 4-story shear building.

Table 5.1: Structural characteristics of the 4-DOF structure

Story	4-DOF Structure		
	Mass	Elastic Stiffness	Modal Damping Ratio
	$kips\text{-}sec^2/in$	$kips/in$	(%)
1	3	3200	mode 1: 5
2	2	2400	mode 2: 5
3	2	1600	mode 3: 5
4	1	800	mode 4: 5

Table 5.2: Hysteretic parameters of the 4-DOF structure

Interstory	Parameters			
	α	η	\mathcal{A}	$\mathcal{B} = \mathcal{C}$
1	0.25	1	1	$(2u_y)^{-1}$
2	0.25	1	1	$(2u_y)^{-1}$
3	0.25	1	1	$(2u_y)^{-1}$
4	0.25	1	1	$(2u_y)^{-1}$

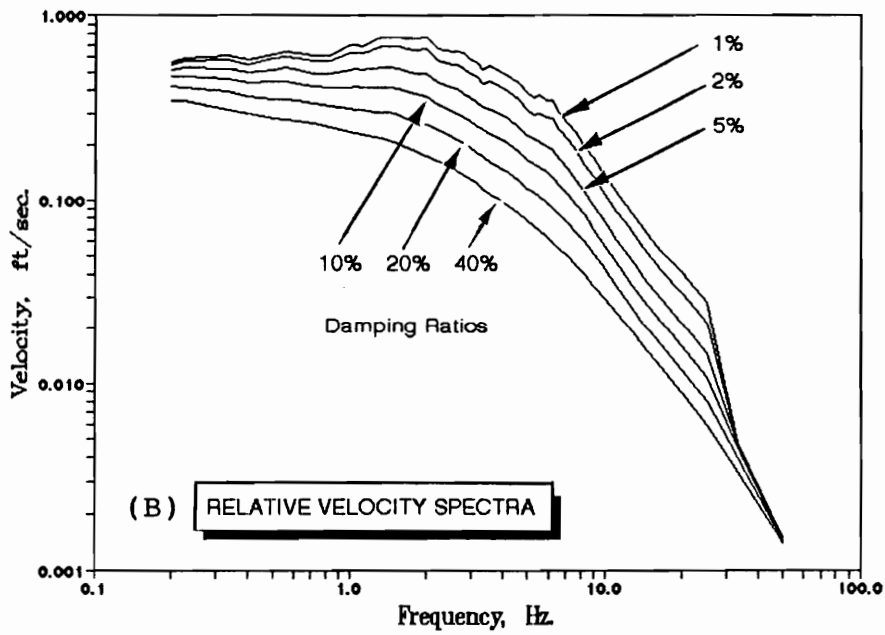
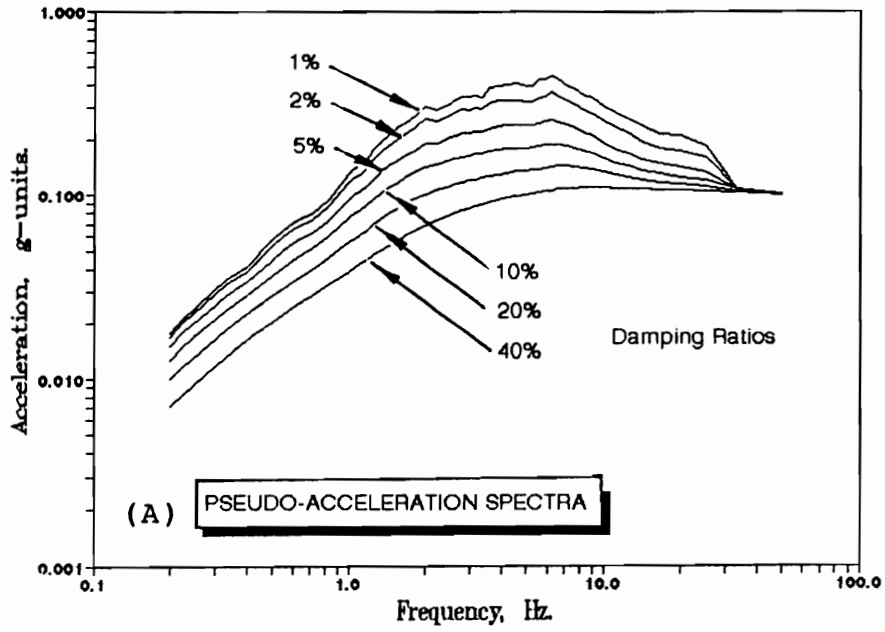


Figure 5.2: Ground response spectra for the second order oscillator: (A) Pseudo-acceleration spectra, (B) Relative velocity spectra.

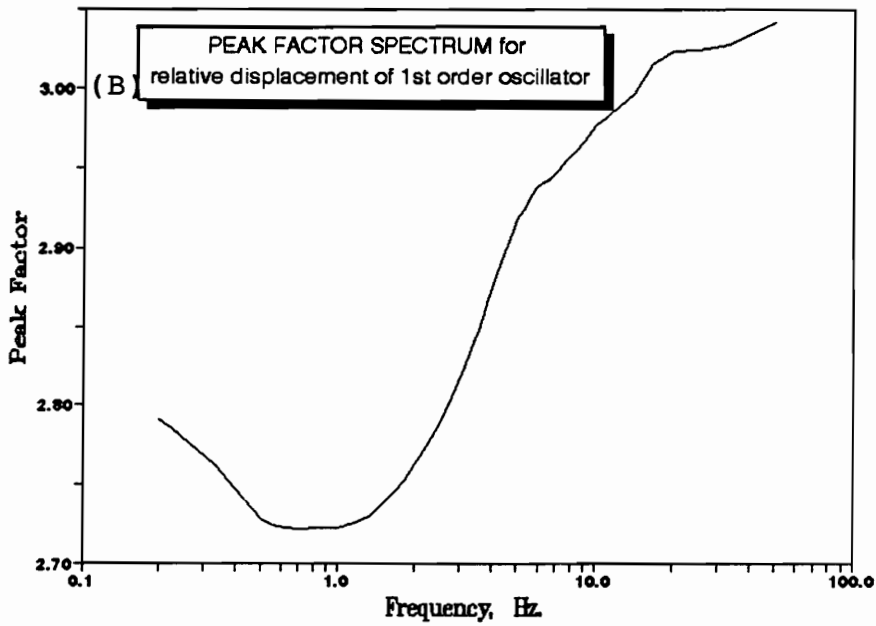
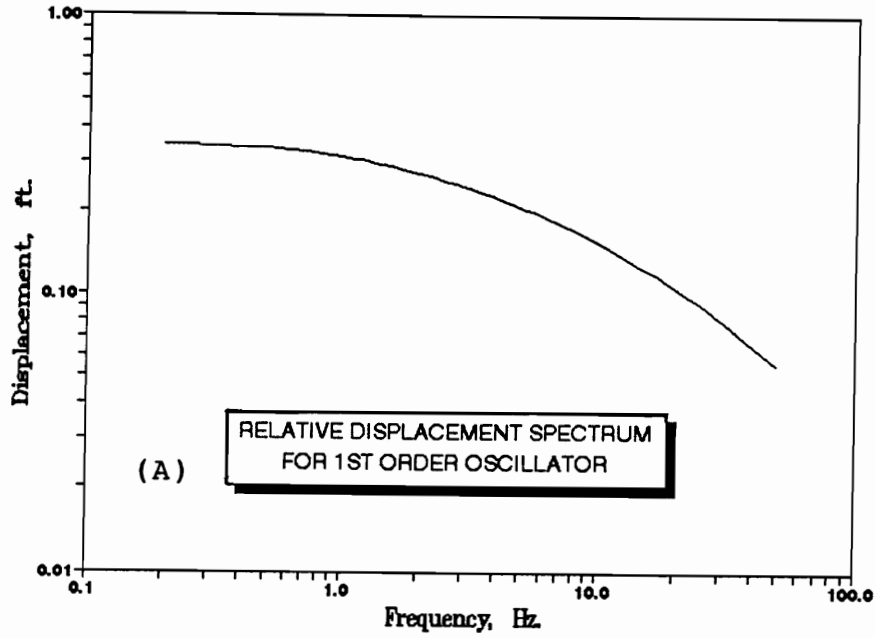


Figure 5.3: Spectra for the first order oscillator: (A) Ground response spectra for relative displacement, (B) Peak factors for relative displacements.

The calculation of the linearization coefficients requires the use of the spectra for the peak factors of the pseudo-acceleration, relative velocity and first order oscillator response. These peak factor spectra were obtained from the mean and standard deviation spectra of the maximum responses using the following formulas derived by Davenport [16]:

$$\mathcal{P}_z = \frac{\mu_{maz(z)}}{\sigma_z} = \left(\sqrt{2 \ln(\rho T_d)} + \frac{0.5772}{\sqrt{2 \ln(\rho T_d)}} \right), \quad (5.166)$$

$$\sigma_{maz(z)} = \frac{\pi \sigma_z}{\sqrt{6} \sqrt{2 \ln(\rho T_d)}}, \quad \rho = \frac{\sigma_{\dot{z}}}{\pi \sigma_z}. \quad (5.167)$$

These two equations define the mean and standard deviations of the maximum response in terms of the response standard deviation σ_z , zerocrossing rate ρ and duration of the response process T_d . Knowing $\mu_{maz(z)}$ and $\sigma_{maz(z)}$ for the input, and assuming a strong motion phase of 7 seconds, equations (5.166) and (5.167) were solved to obtain ρ and σ_z . These known values were then utilized to calculate the peak factor from equation (5.166). Figures 5.4 and 5.3 (B) show these peak factor spectra for the pseudo-acceleration, relative velocity and massless oscillator response.

In the following set of figures we show the maximum values of story shears and story ductilities. To obtain the maximum value of a response quantity, the standard deviation of the quantity obtained from equation (5.80) was amplified by its peak factor value. The peak factor of a response quantity was also calculated using equation (5.166).

Figure 5.5 shows the variation of the maximum shear force in each story with the maximum ground acceleration. The values of the ground response spectra have been appropriately scaled to vary the level of the maximum ground acceleration. The yield level for the interstory drifts is considered to be the same for all stories: $u_y = 0.4$ in.

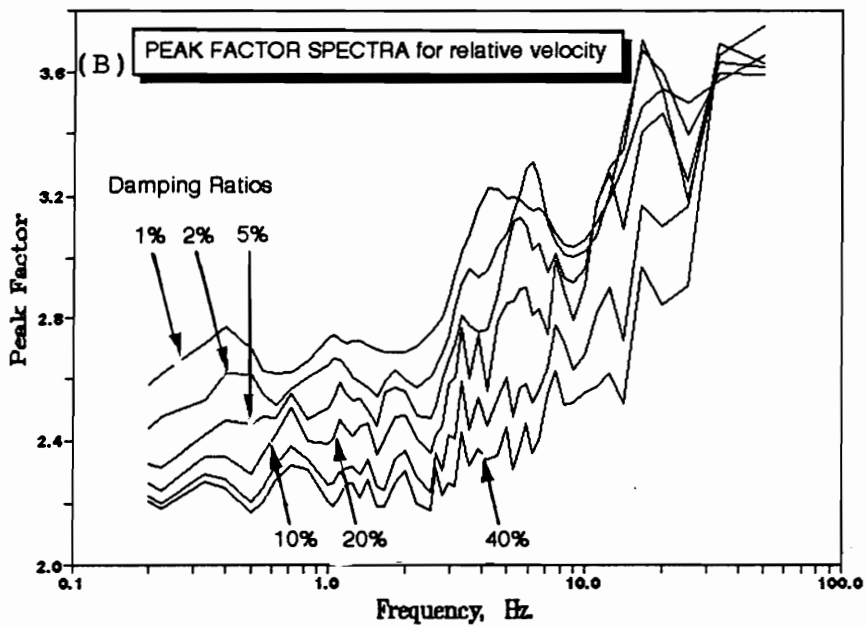
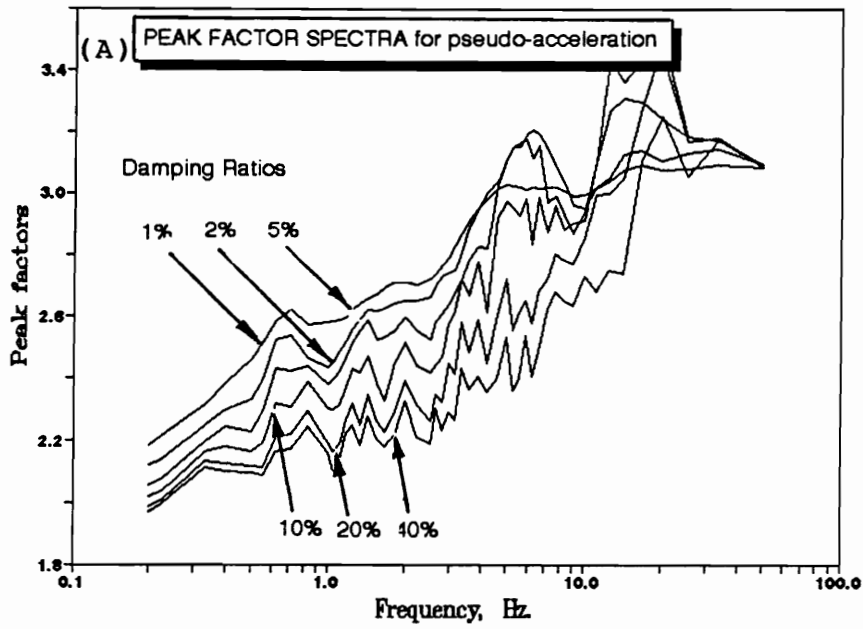


Figure 5.4: Peak factor spectra for the second order oscillator: A) Peak factors for pseudo-acceleration, B) Peak factors for relative velocity.

For comparison purposes, the figure also shows two straight lines that correspond to the interstory shears (for the first and fourth floor) of the same structure but with perfectly linear elastic behavior. As it is expected, the shear forces due to the inelastic behavior, follow curved paths which initial tangents (at zero acceleration) coincide with the straight lines of the elastic structure. It is seen that the structure has been excited well inside the plastic zone since the two tangent stiffness of the constitutive law intercept at the points with ordinates 1280, 960, 640, and 320 kips for the first, second, third and fourth floor respectively. This fact is best appreciated in figure 5.6 where the maximum interstory ductilities have been plotted against the maximum ground accelerations. The interstory ductility is defined here as the ratio between the maximum interstory drift and the yield level.

In the iterative process, it is important to have some idea about the values of the linearization coefficients a_i and b_i . Figures 5.7 and 5.8 show the different values of the linearization coefficients (at convergence) with increasing maximum ground acceleration. It is noted that for low levels of ground acceleration the structure behaves almost elastically. For those cases, the coefficients of linearization, denoted as $a_i, i = 1, \dots, n$ possess values close to 1, whereas the b_i coefficients have values near to zero. As the stiffness element goes into inelastic range, the value of the coefficient a_i becomes less than 1. After performing a parametric study, considering different shear buildings and different parameters of the Bouc-Wen model (with $B_i = C_i$), it has been observed that the a_i coefficients, for structures behaving well inside the plastic zone (high ductilities), never reach a value less than $n/(n+1)$. The knowledge of these minimum and maximum values is especially useful to provide an adequate initial guess for a_i at the start of the iteration process.

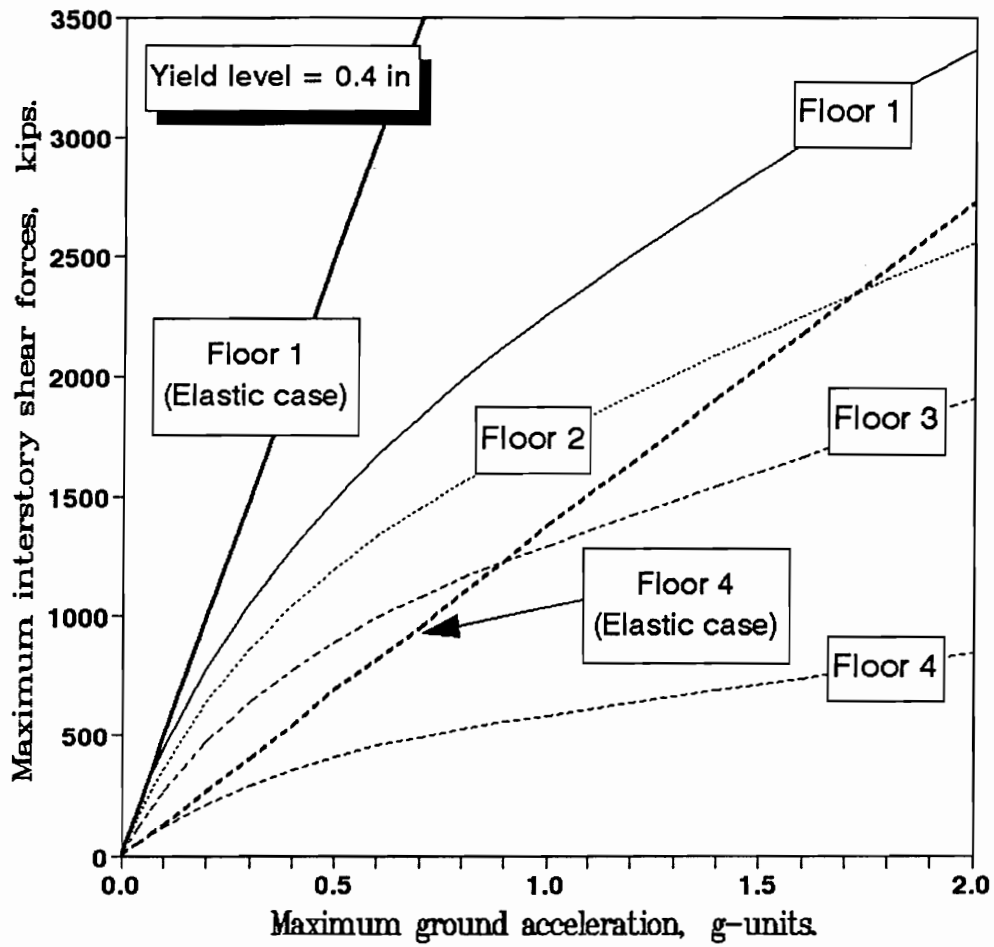


Figure 5.5: Maximum shear force vs. maximum ground acceleration in various stories of the structure .

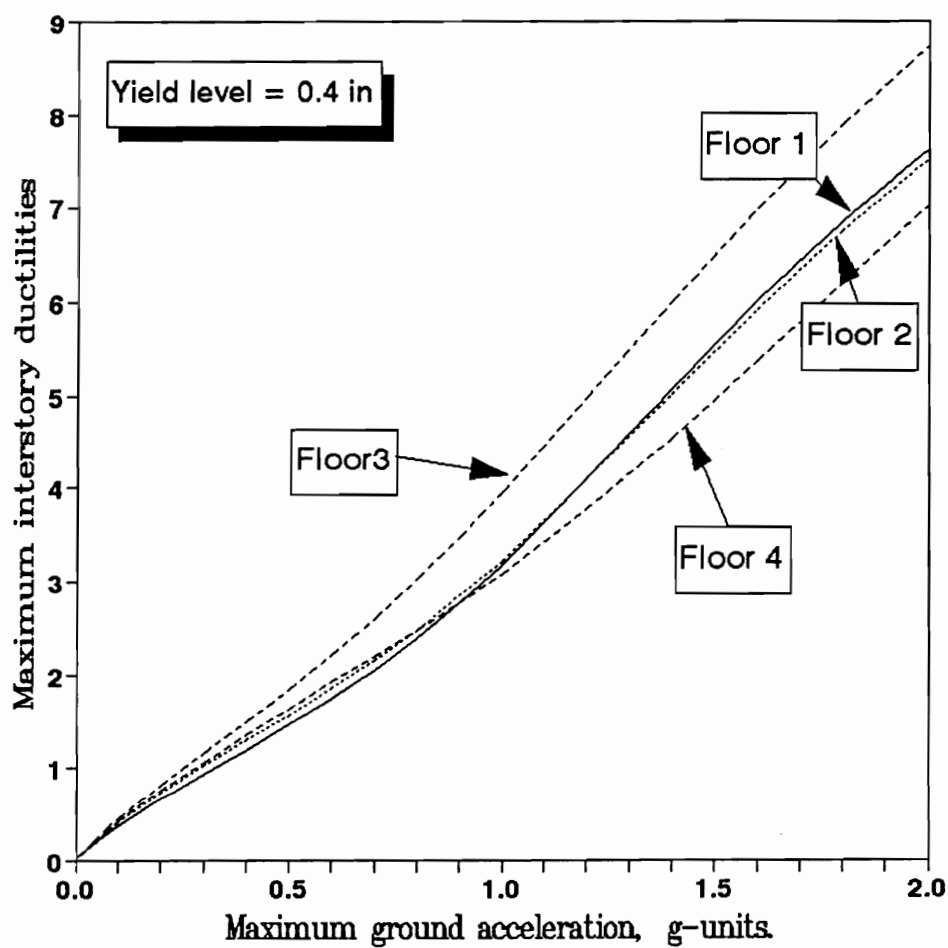


Figure 5.6: Maximum ductilities vs. maximum ground acceleration in various stories of the structure

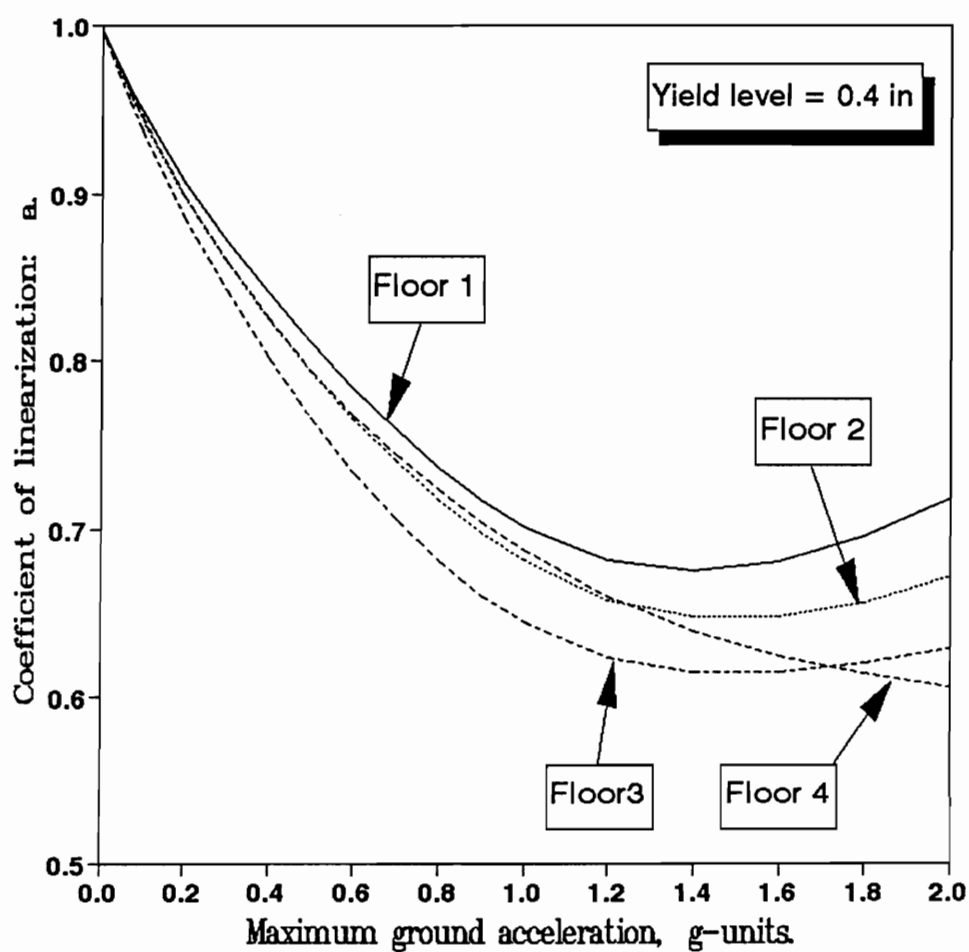


Figure 5.7: Coefficient of linearization a_i vs. maximum ground acceleration in various stories of the structure

Figure 5.8 shows that the coefficients b_i have negative values, but unlike the a_i coefficients, the parametric study was unable to provide a recognizable minimum value. However, it can be said that in general they increase their absolute value as the structure penetrates into the plastic zone.

Figure 5.9 shows the variation of the interstory shear forces with the yield level when the structure is subjected to the same maximum ground acceleration of 0.2 g. This is equivalent to change the constitutive law of the material. The purpose of doing this, is to check, at least qualitatively, the behavior of the equivalent linear structure. That is, for large values of yield level, the structure should behave as a linear elastic structure, and as the yield level decreases (or the ductilities increase) the structure should present plastic characteristics, such as a decrease in the maximum interstory shear forces. Both tendencies are clearly shown in this figure, where the shear forces approach the value corresponding to the elastic structure for high yield levels and they diminish as the ductilities increases (or yield levels decreases).

Figure 5.10 is basically the same figure 5.9 where now only the shear forces for the first and fourth floor have been plotted. The purpose of the figure is to show the different levels of shear forces as the exponent parameter η varies. As the yield levels increase the structure approaches the behavior of the corresponding elastic case (horizontal lines), but the approach is faster as the exponent parameter increases. This is in agreement with the effect of the exponent parameter of the Bouc-Wen model (see appendix E). However, for low yield levels (high ductilities) the curves cross and higher shear forces are provided by the lower exponents.

Next we present same results for the same structure but with nearly elasto-

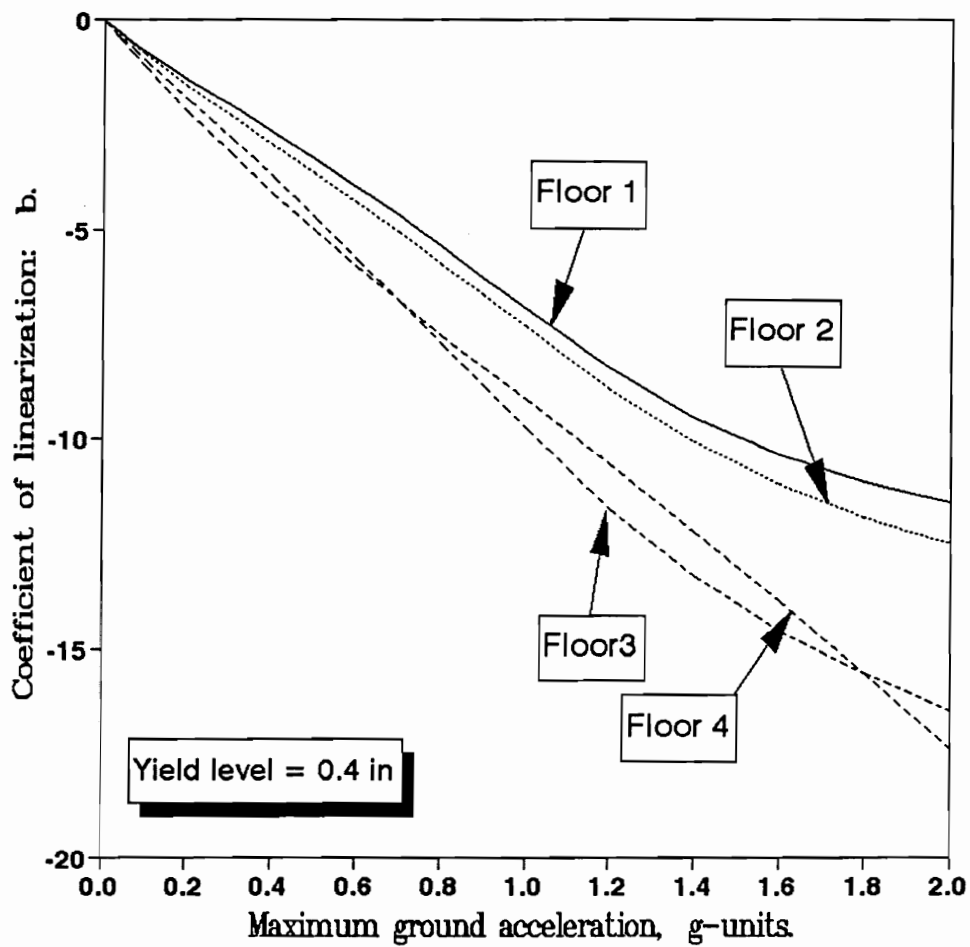


Figure 5.8: Coefficient of linearization b_i vs. maximum ground acceleration in various stories of the structure

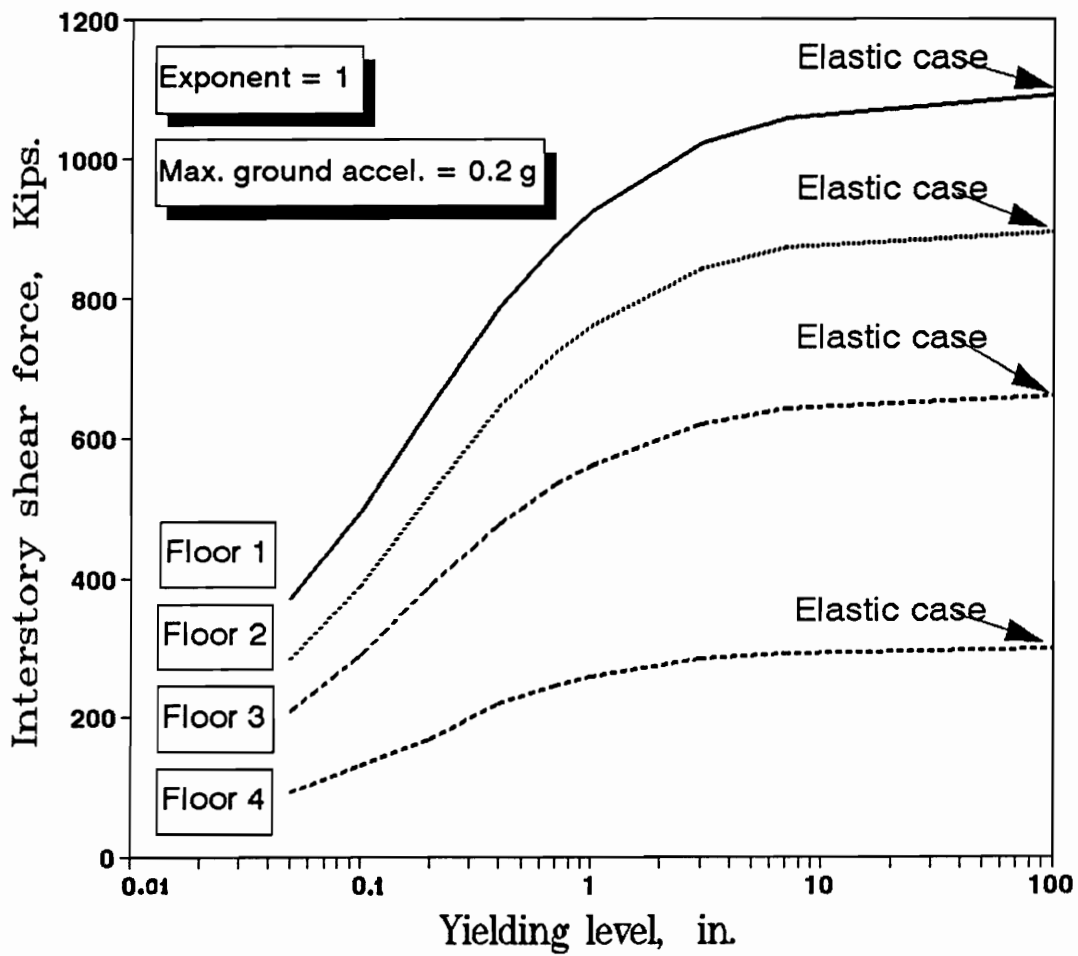


Figure 5.9: Maximum shear forces vs. yield level of interstory drifts for various stories of the structure

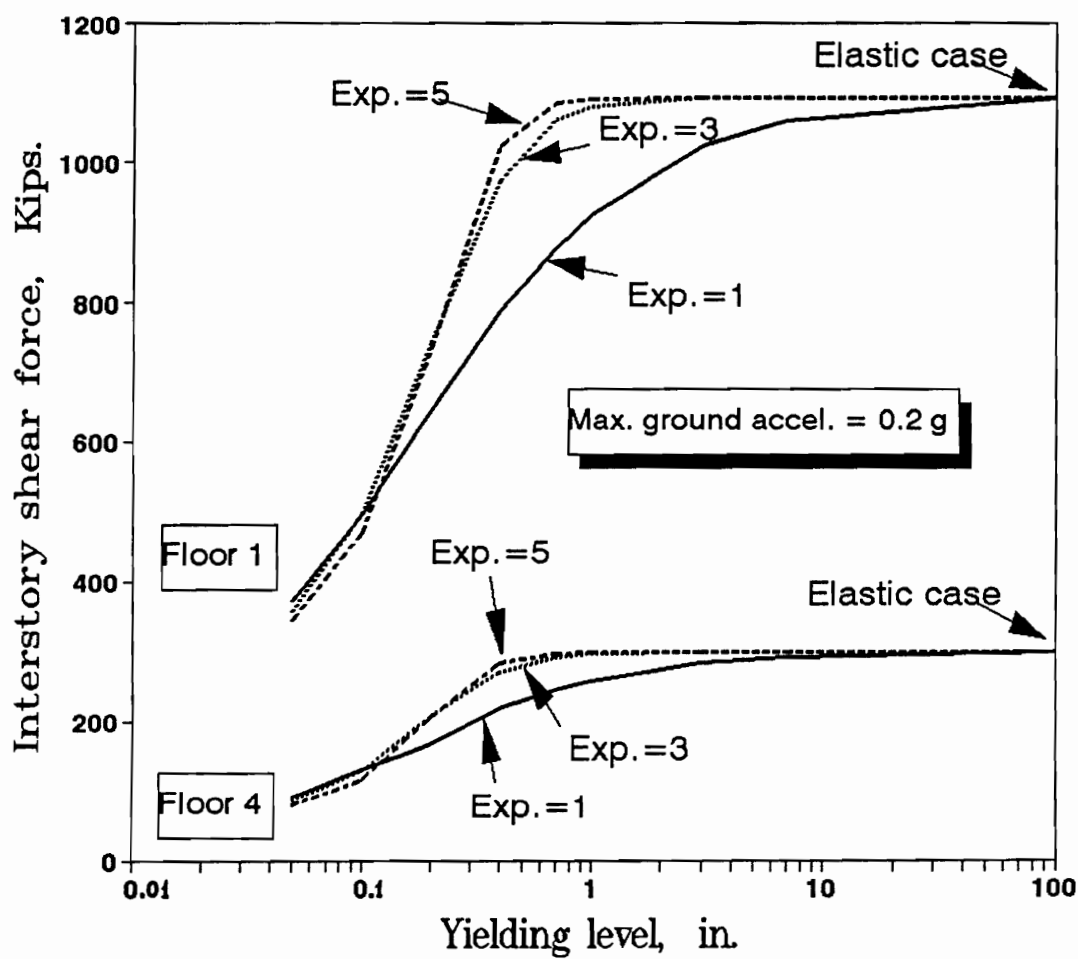


Figure 5.10: Maximum shear forces vs. yield level of interstory drifts for different values of the exponent parameter.

plastic behavior. This is achieved by choosing a small value for the post-yield stiffness parameter $\alpha = 0.05$ and a high value for the exponent $\eta = 9$. The hysteretic parameters for this structure are shown in table 5.3. The yield level parameter u_y has been assumed to be the same for different stiffness elements. The seismic inputs defined in terms of a Kanai-Tajimi type of spectral density function as well as ground response spectra have been used.

Table 5.3: Hysteretic parameters of the nearly elasto-plastic 4-DOF structure.

<i>Interstory</i>	<i>Parameters</i>			
	α	η	\mathcal{A}	$\mathcal{B} = \mathcal{C}$
1	0.05	9	1	$0.5 u_y^{-9}$
2	0.05	9	1	$0.5 u_y^{-9}$
3	0.05	9	1	$0.5 u_y^{-9}$
4	0.05	9	1	$0.5 u_y^{-9}$

The results shown in figures 5.11, 5.12, 5.13, 5.14, and 5.15 are for the structure with exponent parameter $\eta = 9$. The seismic input for these results is again defined in terms of the ground response spectra.

Figure 5.11 shows the maximum interstory ductility ratios as the maximum ground acceleration increases. The yield level is $u_y = 0.4$ in. This figure is similar to figure 5.6 but for different hysteretic parameters.

Figure 5.12 (A) shows the maximum accelerations of various floors for increasing levels of maximum ground acceleration. The story yield level was fixed at 0.4 in. Decreasing slope of the curves for various stories indicates the softening of the structure due to yielding at higher intensities of the ground motion. Part (B) shows again the same response, but now for a fixed level of ground motion intensity (0.4 g) and increasing value of yield levels. The response increases asymptotically to its

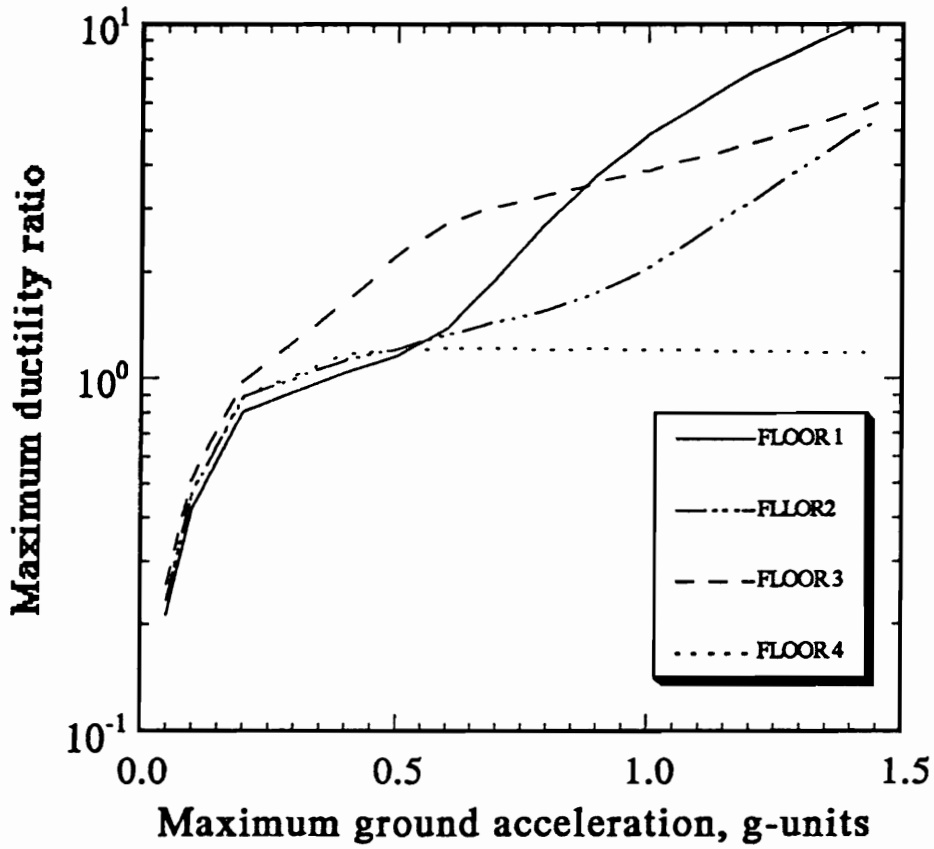


Figure 5.11: Maximum ductility ratios in various stories of the structure vs. maximum ground acceleration. (Yield level = 0.4 in; $\alpha = 0.05$; $\eta = 9$).

elastic response level as the yield level is increased. Thus, yielding in the supporting structure is seen to reduce the maximum acceleration which a supported secondary system will experience.

Figures 5.13, 6.14 and 6.15 show the frequency content of a floor acceleration in terms of floor response spectra for equipment damping ratio of 0.005. Figure 5.13 shows the floor response spectra obtained for floor 1, whereas figure 5.14 shows the floor response spectra for floor 4. The different yield levels are indicated by the letter Y. The elastic spectra is seen to provide the highest peaks always. For the lower floors, however, the valleys in the elastic spectra are also the lowest. Thus, the secondary systems at some frequencies may even experience a higher level of response when the supporting structure yields. But in general, the highest peaks in the floor response spectra are reduced by yielding. The floor spectra for decreasing yielding levels (increasing ductilities) are seen to flatten out, showing the effect of increased damping provided by the hysteresis cycles.

In figures 5.15 (A) and (B) we plot the ratio of the inelastic to elastic floor response spectra for floors 1 and 4 respectively. Several yielding levels are considered. It is seen that the inelastic floor response spectrum values are not always less than elastic floor spectrum values as ratios greater than one are also seen for some frequencies.

Figure 5.16 shows the root mean square value of the floor response spectra for floor 2 obtained for a Kanai-Tajimi type of spectral density function. For this particular case the exponent parameter has been changed to $\eta = 3$. Even though the ground motion is specified in a different form, this figure presents similar character-

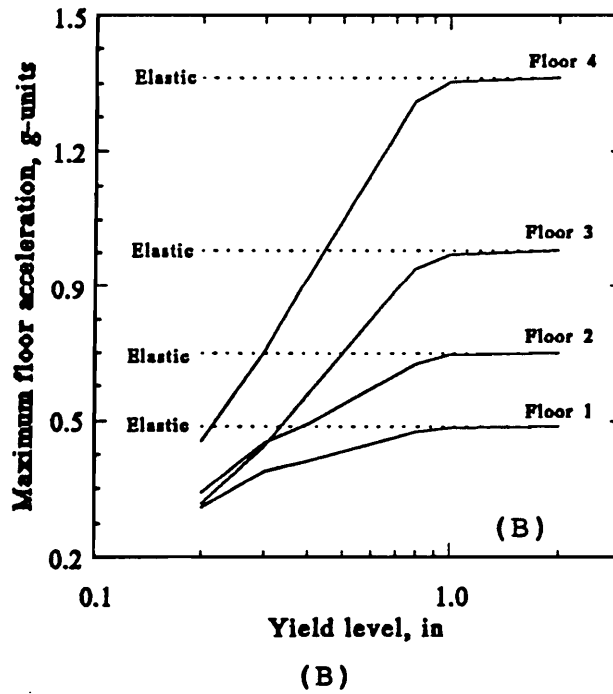
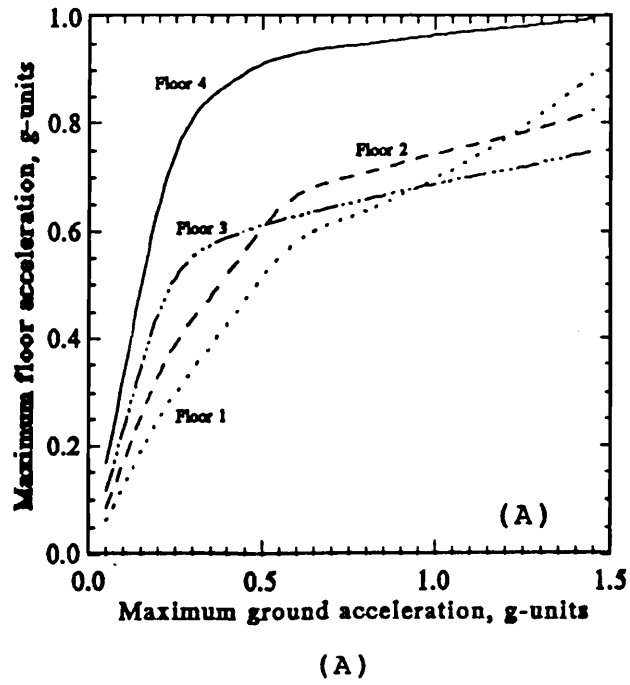


Figure 5.12: Maximum absolute accelerations for various floors of the structure vs. (A) maximum ground acceleration and (B) yield level ($\alpha = 0.05$; $\eta = 9$)

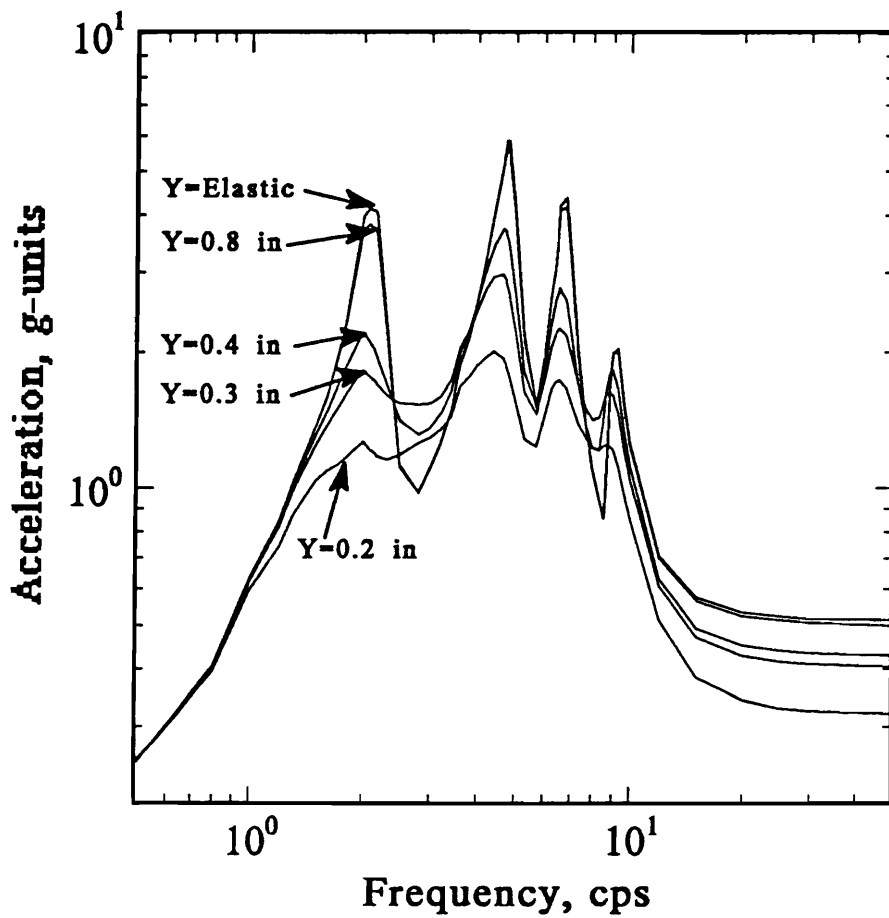


Figure 5.13: Floor response spectra of absolute acceleration in floor 1 for different yield levels. (Max. ground accel. = 0.4 g; $\alpha = 0.05$; $\eta = 9$; equip. damp. ratio = 0.005)

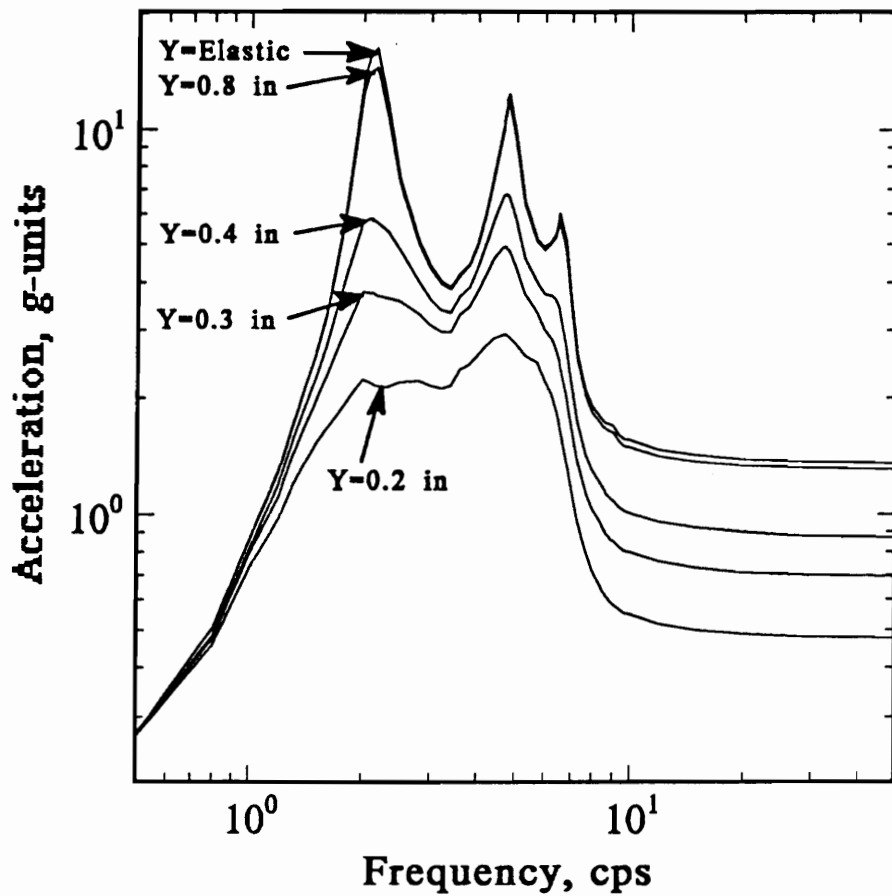


Figure 5.14: Floor response spectra of absolute acceleration in floor 4 for different yield levels. (Max. ground accel. = 0.4 g; $\alpha = 0.05$; $\eta = 9$; equip. damp. ratio = 0.005)

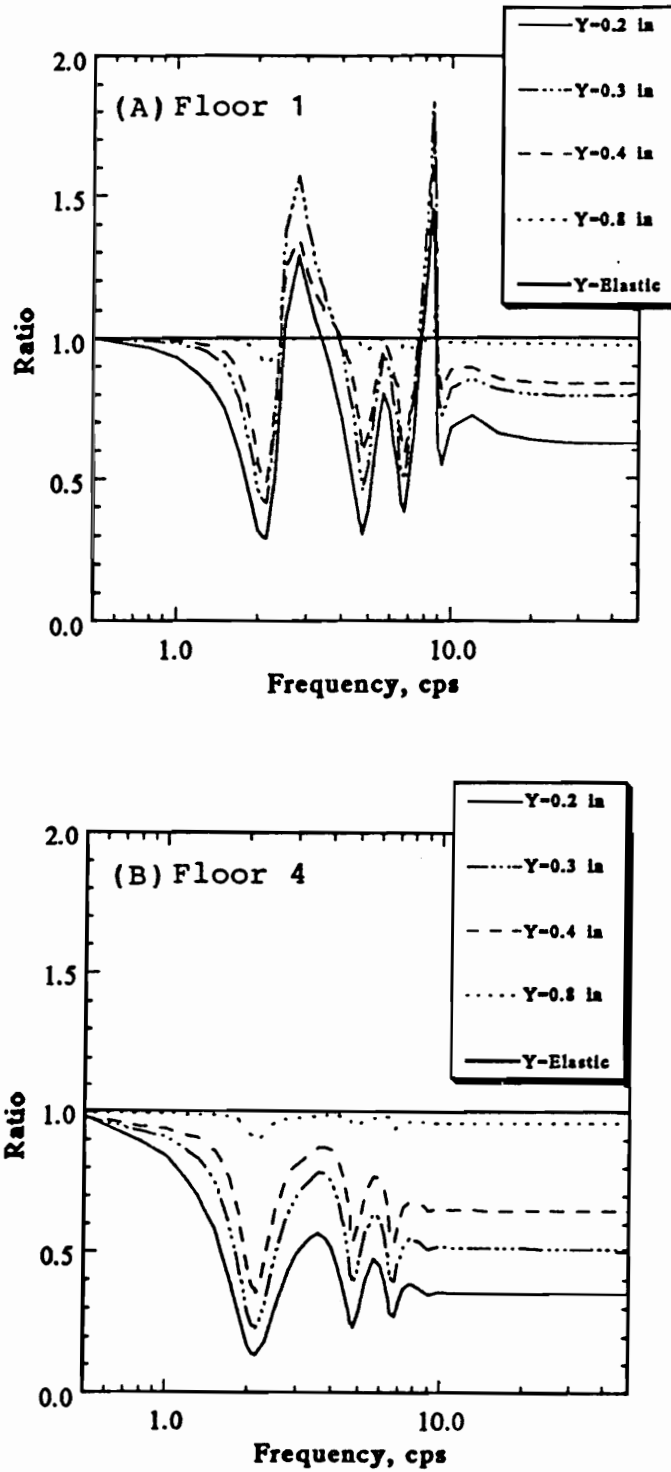


Figure 5.15: Floor response spectra ratios of absolute acceleration in (A) floor 1 and (B) floor 4 for different yield levels Y . (Max. ground accel. = 0.4 g; $\alpha = 0.05$; $\eta = 9$; equip. damp. ratio = 0.005)

istics to those of figures 5.14 and 5.15 for ground response spectra.

Next we present the results for a five-story shear building used in the work by Sewell et. al. [42]. Only the first interstory (bottom element) is considered to behave nonlinearly. The remaining elements were modeled as elastic by choosing a very high yield level. The corresponding structural characteristics and hysteretic parameters are given in tables 5.4 and 5.5 respectively.

Table 5.4: Structural characteristics of the 5-DOF structure.

Story	5-DOF Structure		
	Mass	Elastic Stiffness	Modal Damping Ratio
	lb-sec ² /in	lb/in	(%)
1	1	4500	mode 1: 5.00
2	1	4500	mode 2: 5.00
3	1	4500	mode 3: 6.68
4	1	4500	mode 4: 8.17
5	1	4500	mode 5: 9.15

Table 5.5: Hysteretic parameters of the 5-DOF structure.

Interstory	Parameters			
	α	η	\mathcal{A}	$B = C$
1	0.10	3	1	$(0.5(u_y)^{-3})$
2	Elastic	-	-	-
3	Elastic	-	-	-
4	Elastic	-	-	-
5	Elastic	-	-	-

The base input for the results of this structure was also defined by ground response spectra. The pseudo-acceleration, relative velocity and first order oscillator response spectra are shown in figure 5.17 and 5.18 (A). They represent the mean of the maximum values obtained for 100 synthetically generated accelerograms. These

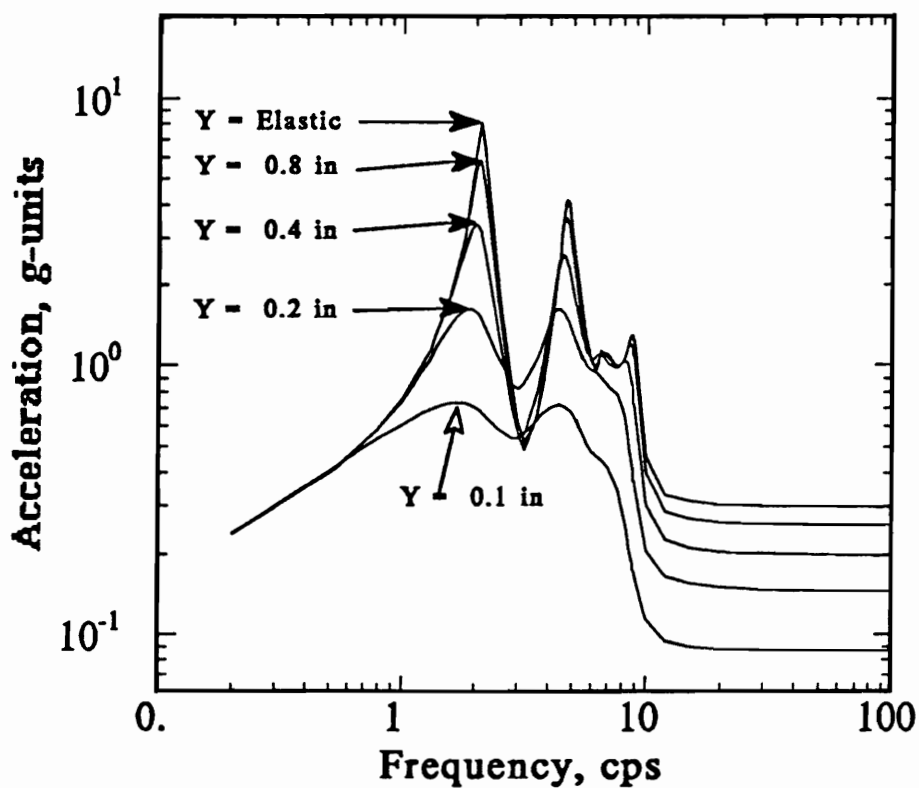


Figure 5.16: Floor response spectra for the root mean square value of absolute acceleration in floor 2 for different yield levels Y . (Max. ground accel. = 0.4 g; $\alpha = 0.05$; $\eta = 3$; equip. damp. ratio = 0.005)

acceleration time histories are also used in the simulation study later on. The peak factor spectra for these inputs were also obtained as described previously. The strong motion phase duration used to calculate the peak factor values from equations (5.166) and (5.167) was 11 seconds. They are shown in figures 5.19 and 5.18 (B).

Figure 5.20 shows the normalized modal damping ratios of the equivalent linear structure with the variation of the yield level (ductility) when the maximum ground acceleration is 0.53 g and the exponent parameter is 3. The damping ratios have been normalized with respect to the five modal damping ratios corresponding to the elastic structure and given in table 6.3. It is observed that as the yield level decreases, the equivalent damping ratios increase. These increments are logically expected since the statistically equivalent linear structures have to dissipate energy to approach the behavior of the real nonlinear structures, and the only form of dissipation allowed to linear structures is through viscous damping. Also it is observed that the lower modes are associated with larger increments of the damping ratio values. This is due to the fact that the only nonlinear element is in the first interstory and its corresponding drift is mainly due to the contribution of the first mode.

Figure 5.21 shows the behavior of the equivalent normalized frequencies with respect to the yield level. They have been normalized with respect to the frequencies of the elastic case. It can be seen that they decrease as the behavior of the structure change from elastic to plastic, but for high ductilities ratios (low yield levels) they began to increase again. For some structural cases and some model parameters, they become even higher than the frequencies due to the elastic behavior.

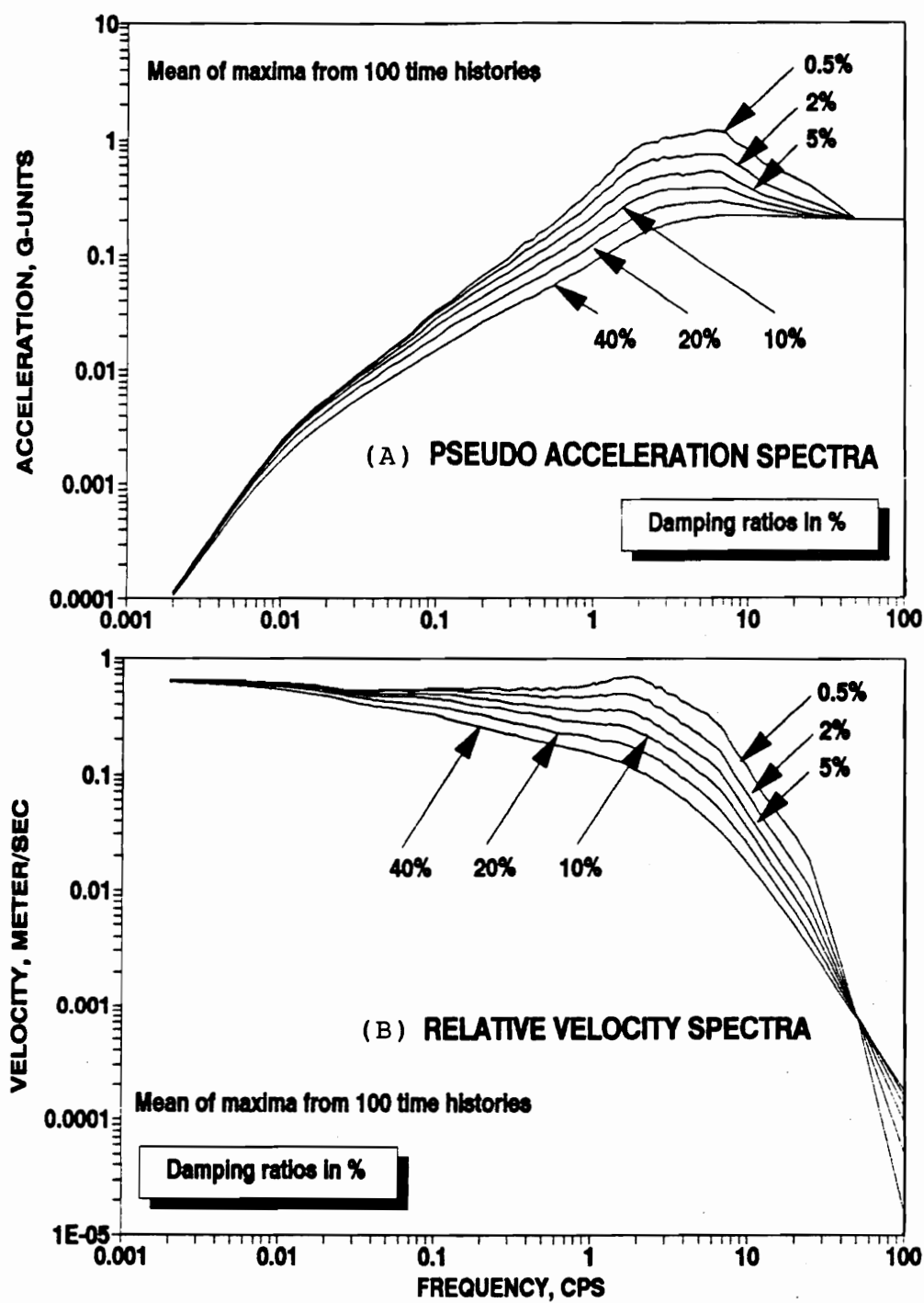


Figure 5.17: Ground response spectra for the second order oscillator: (A) Pseudo-acceleration spectra, (B) Relative velocity spectra.

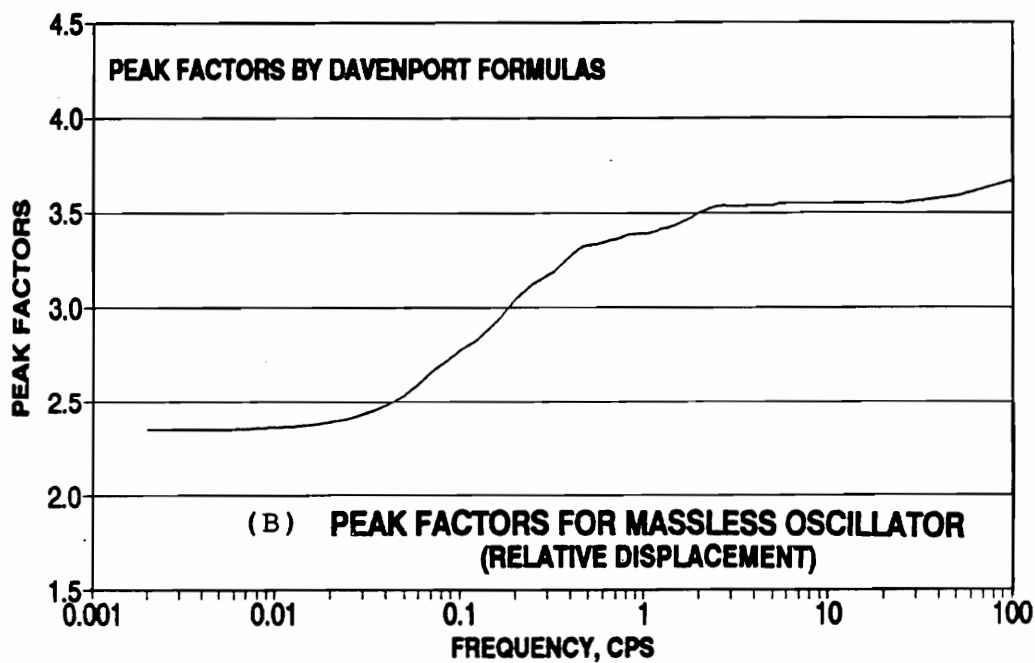
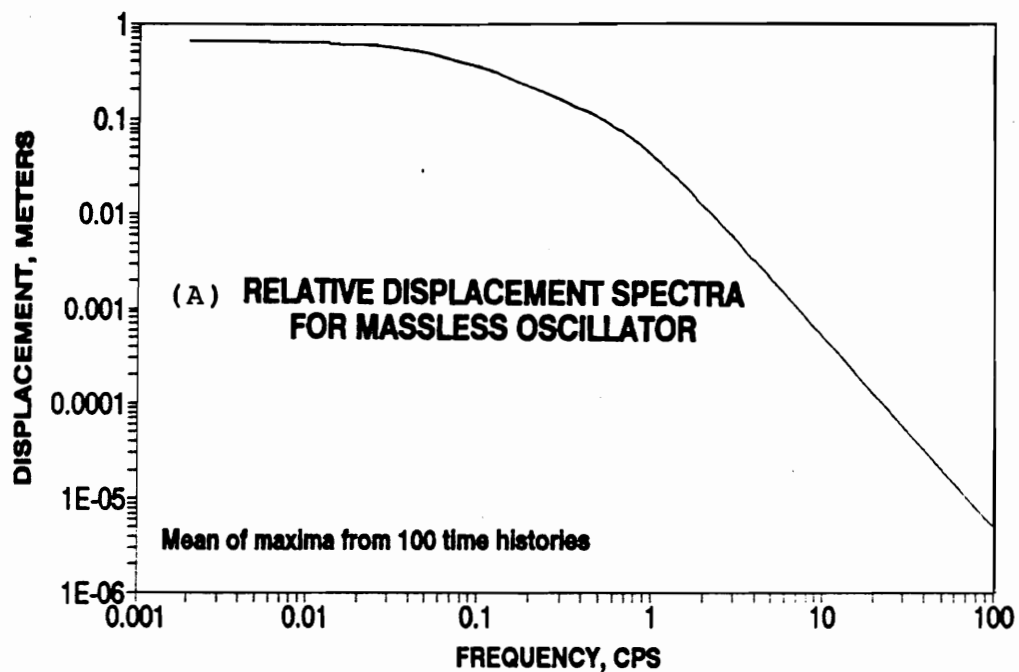


Figure 5.18: Spectra for the first order oscillator: (A) Ground response spectra for relative displacement, (B) Peak factors for relative displacements.

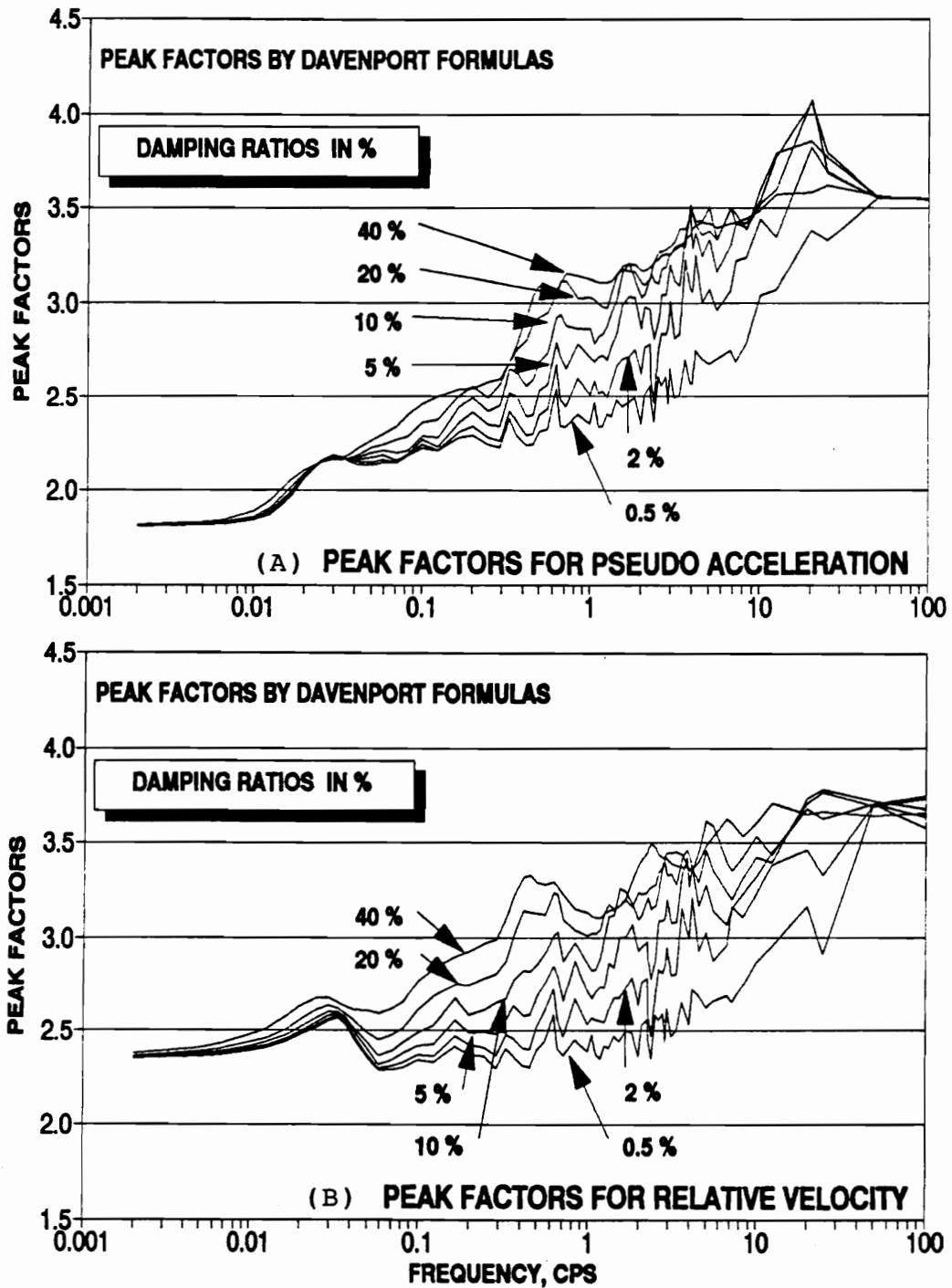


Figure 5.19: Peak factor spectra for the second order oscillator: A) Peak factors for pseudo-acceleration, B) Peak factors for relative velocity.

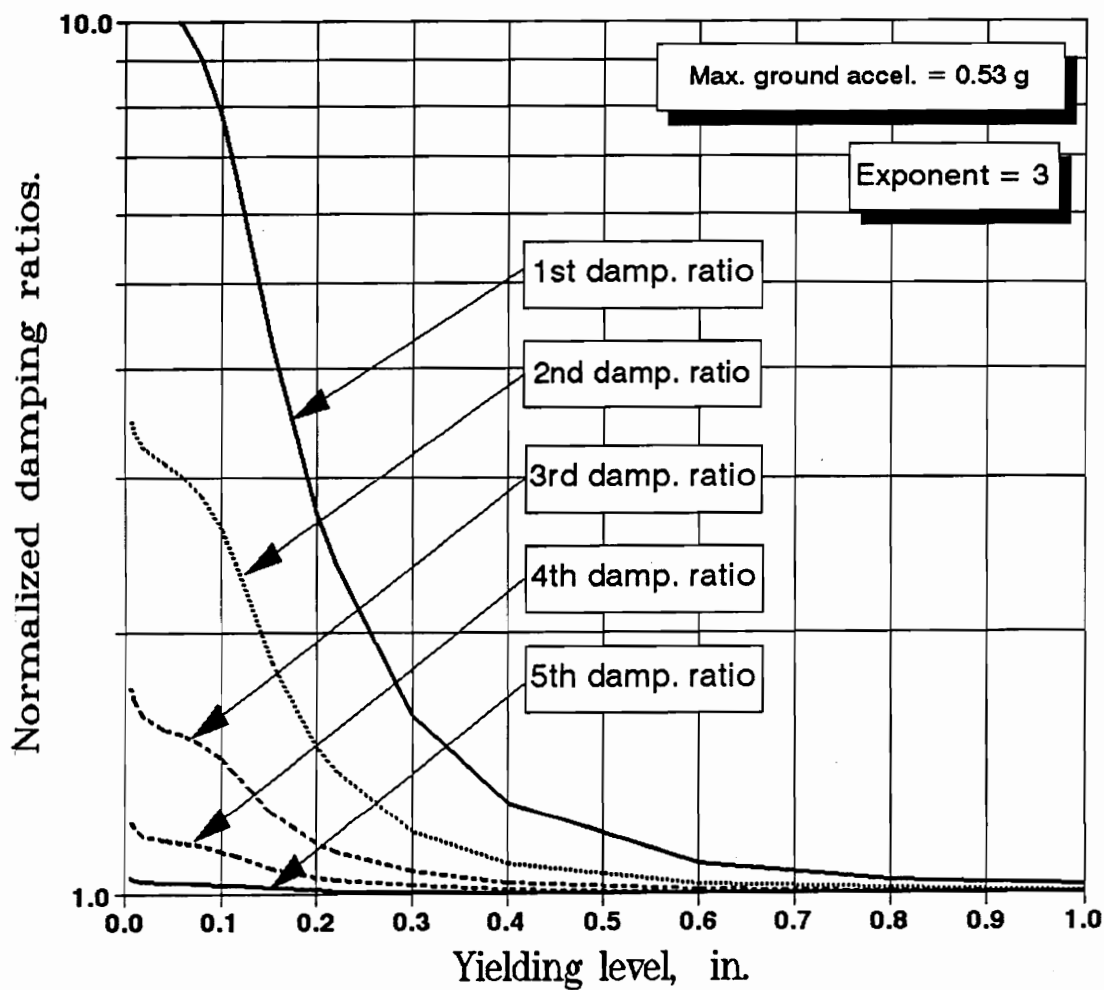


Figure 5.20: Normalized damping ratios (with respect to the elastic case) vs. yield level of interstory drifts for various modes of the structure

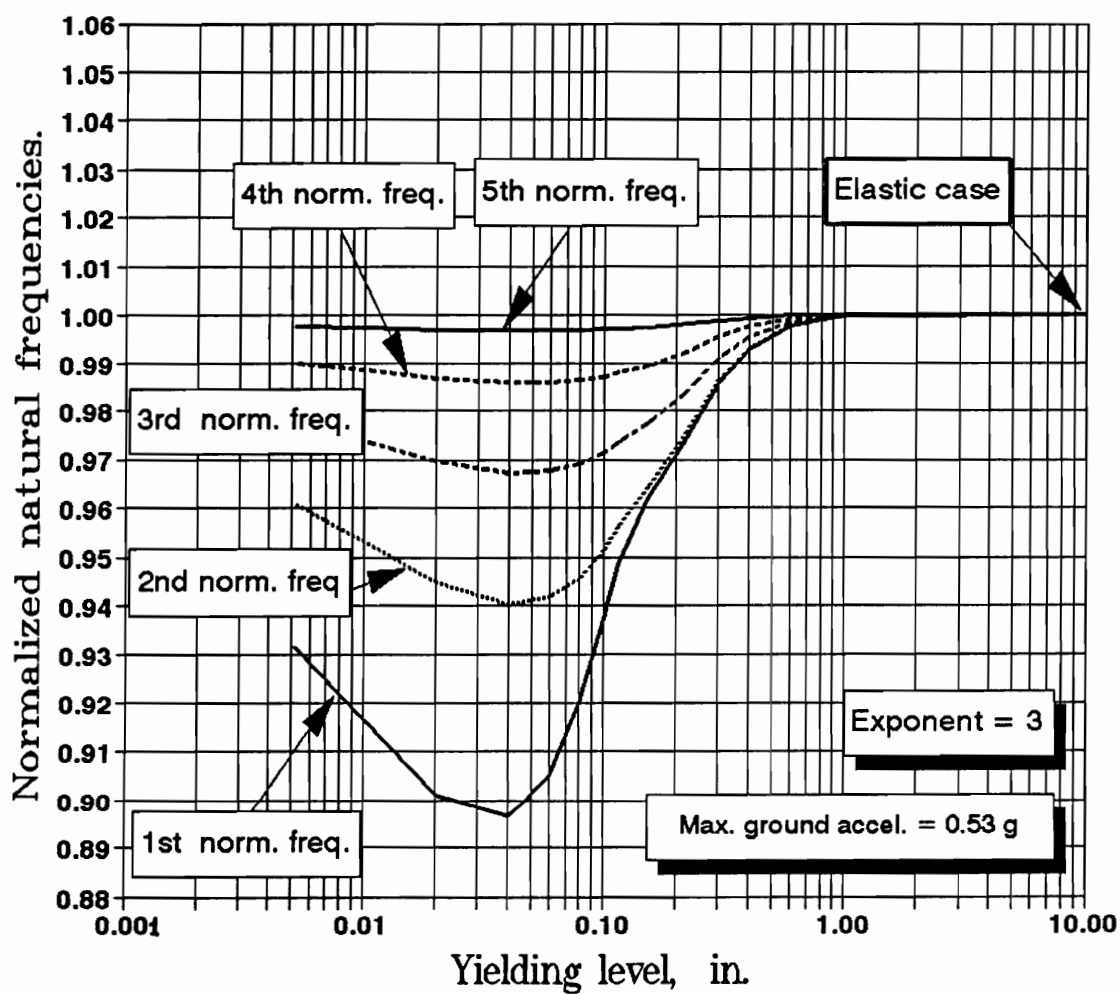


Figure 5.21: Normalized frequencies (with respect to the elastic case) vs. yield level of interstory drifts for various modes of the structure

Simulation study

The purpose of this simulation study is to compare the design response obtained by the proposed response spectrum approach with the average of maximum responses obtained by 100 time history analyses of the nonlinear equations of motion. The study used the same 100 artificially generated time histories of ground acceleration which were employed to generate the ground response spectra used to obtain the results in figures 5.20 and 5.21.

Three different cases of structures were analyzed by time history analysis: 1) the perfectly elastic case, 2) a moderate plastic case with ductility ratio equal to 2, and 3) a highly plastic case with ductility ratio of 4. To achieve this ductilities, several trial and error cases were considered with different yield levels till the desired maximum ductility ratio was obtained. The maximum ductilities were determined by using the assumption of equal peak factors. Thus, for the first interstory, the maximum ductilities of 2 and 4 corresponded to yield levels of $u_y = 0.24585$ and $u_y = 0.13574$ inches respectively. Table 5.6 provides the equivalent frequencies and damping ratios corresponding to the stochastically equivalent linear structures

First, we compare the interstory shear responses. The design values provided by the proposed approach were also calculated by assuming equal peak factors. Therefore, equation (5.82) has been used. The corresponding components of the linear transformation vector \mathcal{R} can be deduced from equation (5.88). Thus, the maximum shear forces were calculated by the following expression:

$$\begin{aligned} \mathcal{M}_{si}^2 = & k_i^2 \left\{ \alpha_i^2 \left(\mathcal{P}_{si}^2 E[x_i^2] - 2 \mathcal{P}_{si}^2 E[x_i x_{i-1}] + \mathcal{P}_{si}^2 E[x_{i-1}^2] \right) \right. \\ & \left. + 2 \alpha_i (1 - \alpha_i) \left(\mathcal{P}_{si}^2 E[x_i v_i] - \mathcal{P}_{si}^2 E[x_{i-1} v_i] \right) + (1 - \alpha_i)^2 \mathcal{P}_{si}^2 E[v_i^2] \right\} , \end{aligned} \quad (5.168)$$

Table 5.6: Equivalent frequencies and damping ratios of the stochastically equivalent linear structures

Case	Mode	Modal Characteristics	
		Equiv. Frequency Hz	Equiv. Damp. Ratio %
Elastic	1	3.039	5.00
"	2	8.870	5.00
"	3	13.983	6.68
"	4	17.963	8.17
"	5	20.488	9.15
Duct. 2	1	2.987	8.69
"	2	8.729	6.07
"	3	13.834	7.14
"	4	17.868	8.35
"	5	20.459	9.12
Duct. 4	1	2.920	22.06
"	2	8.547	9.41
"	3	13.661	8.32
"	4	17.770	8.73
"	5	20.432	9.27

where the amplified expected values are given by equation (5.85).

Table 5.7 lists the maximum values and the relative percent error of the interstory shears for floors 1, 3 and 5 obtained by the proposed response spectrum approach and by the time history analyses. The relative percent error is defined as:

$$\text{Percent error} = 100 \frac{(\text{Resp. spec. value}) - (\text{Time hist. value})}{(\text{Time hist. value})}. \quad (5.169)$$

Also, table 5.7 contains a column with relative errors marked with a superscripted asterisk. These errors were calculated by replacing the quantities $\mathcal{P}_{i,i}^2 E[v_i^2]$ by the square of the yielding levels when the former were bigger than the latter. This is a clear error introduced by the Gaussian equivalent linearization since the auxiliary variables should not take values greater than its ultimate value. For models with parameters $\mathcal{A}_i = 1$ such limiting values are equal to the yield levels of the principal variables.

Table 5.7: Comparison of interstory shears obtained by the proposed response spectrum approach and by time history simulation

<i>Case</i>	<i>Interstory</i>	<i>Maximum Interstory Shears</i>			
		<i>Response Spectra lb</i>	<i>Time History lb</i>	<i>Relative Error %</i>	<i>Relative Error* %</i>
Elastic	1	2210	2102	5.1	-
"	3	1640	1587	3.3	-
"	5	619	608	1.8	-
Duct. 2	1	1742	1283	35.7	-0.2*
"	3	1287	1057	21.7	21.7*
"	5	487	490	-0.6	-0.6*
Duct. 4	1	1124	915	22.8	-13.0*
"	3	834	729	14.5	14.5*
"	5	320	385	-17.0	-17.0*

It is observed that the responses calculated by the response spectrum approach

present differences with the values obtained by the time history analysis. Even for the elastic cases, some differences, though small, still persist. In general the response spectrum approaches formulated with the assumption of large stationary strong motion phases, provide conservative values for elastic responses since the real and artificial time histories have shorter strong motion phases. From the analysis of just this example it is difficult to predict tendencies for the plastic cases since in some stories the error is bigger for ductility 2, and in another floors it is bigger for ductility 4. Also the sign of the error changes. However, after introducing the above mentioned limitation for the value of $\mathcal{P}_{s,i}^2 E[v_i^2]$, the error associated to the hysteretic element of the first interstory decreases. This suggests that the error is due to the assumption of Gaussianness in the probability density functions of the nonlinear structure. As expected, the errors at the interstories 3 and 5 do not diminish because they are modeled to behave linearly. Since no adjustment to limit the value of $\mathcal{P}_{s,i}^2 E[v_i^2]$ are needed for these stories, the errors in the shear values are not affected.

Finally, the floor response spectra calculated by the proposed approach are compared with those floor spectra generated by the time history analysis. In all cases, the floor spectra have been calculated for equipment with 5% of critical damping, and three different structures have been considered: 1) the elastic structure, 2) the structure with ductility 2, and 3) the structure with ductility 4. Figures 5.22, 5.23 and 5.24 show the floor spectra for stories 1, 3 and 5 respectively. Part (A) of these figures shows the spectra calculated by the proposed response spectrum approach whereas part (B) shows the spectra calculated by the simulation analysis.

As it was observed by Sewell et. al. [42] the floor spectra of nonlinear structures at the high frequency range may show peaks higher than the peaks associated to

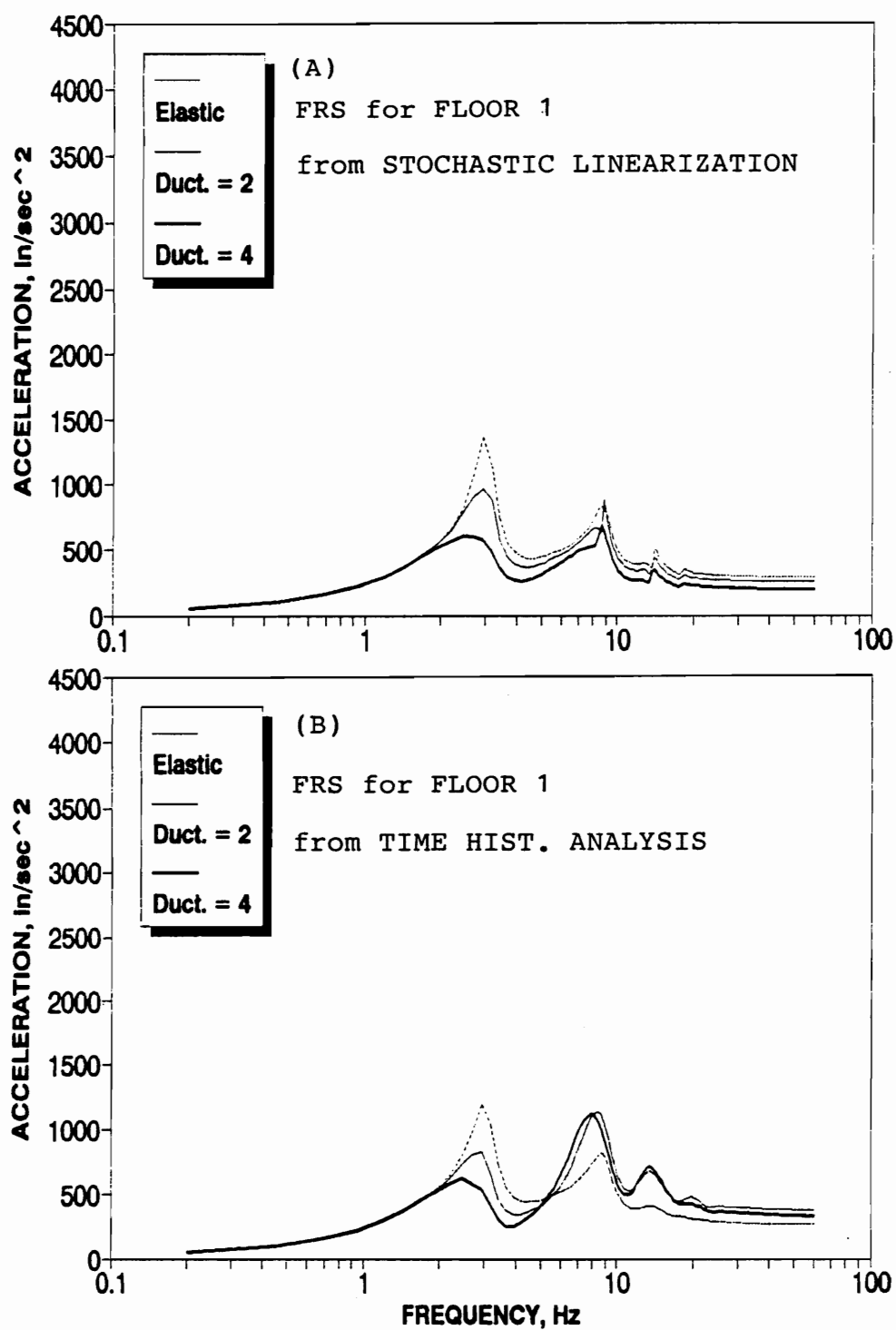


Figure 5.22: Floor response spectra of absolute acceleration for floor 1 (equip. damp. ratio = 5%). (A) Stochastic equivalent linearization, (B) Time history analysis.

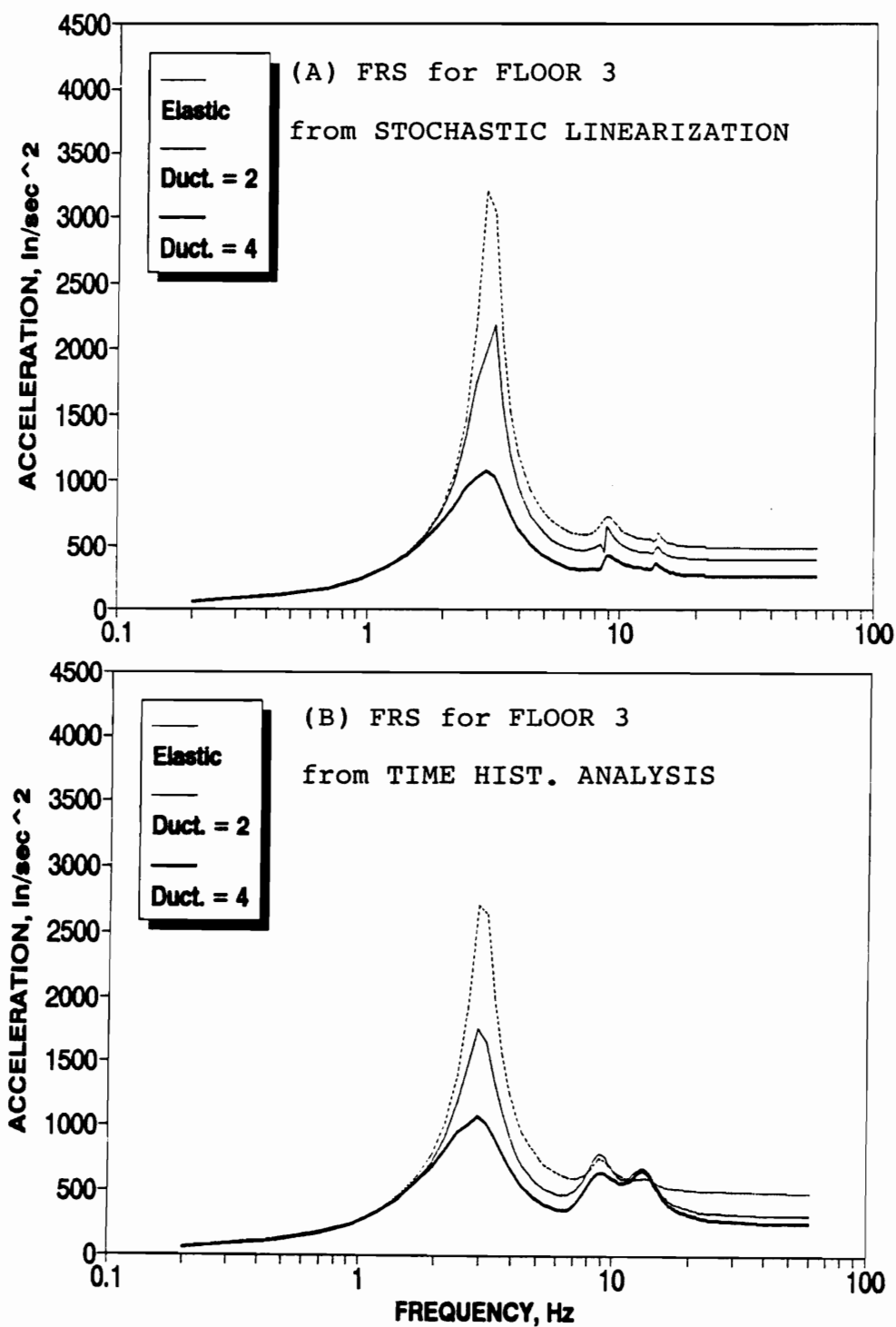


Figure 5.23: Floor response spectra of absolute acceleration for floor 3 (equip. damp. ratio = 5%). (A) Stochastic equivalent linearization, (B) Time history analysis.

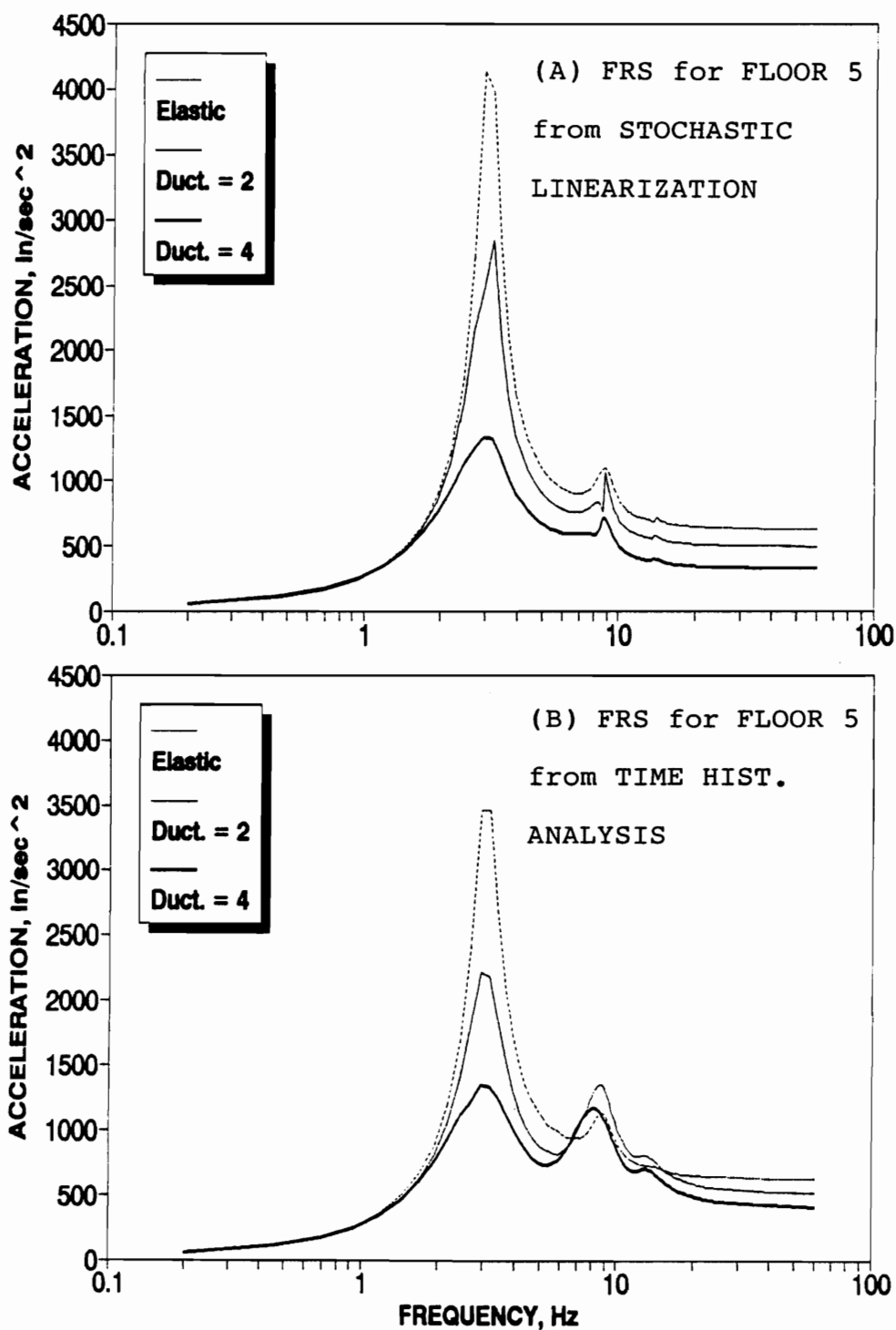


Figure 5.24: Floor response spectra of absolute acceleration for floor 5 (equip. damp. ratio = 5%). (A) Stochastic equivalent linearization, (B) Time history analysis.

elastic structures. This is, however, not captured by the proposed approach. This fact can be better seen from the figures 5.25, 5.26 and 5.27, where we have plotted the inelastic to elastic spectrum values for the three floors. It is seen that the inelastic spectra calculated by the proposed approach are always lower than the elastic spectra in the high frequency range.

In table 5.8 we compare the magnitudes of the floor spectra obtained by the proposed approach and time history analysis for the three floors. Table 5.8 shows the percent error at the vicinity of the first two peaks. These errors have been calculated by using equation (5.169). It can be noticed that, for the low frequency range, that is for the first peak of these spectra, the magnitudes calculated by the proposed approach show slightly conservative results for ductility 2, and a small error for ductility 4. However, for peaks in the high frequency range, the results provided by the proposed approach differs from the time history results.

It is believed that the main cause of error in the stochastic equivalent linearization technique is due to the assumption of Gaussianness in the density functions of the nonlinear systems. Such assumption directly affects the characteristics of the equivalent linear system since the linearization coefficients are calculated as functions of the response statistics, which are assumed to be Gaussian. In figures 5.28 and 5.29 we compare the joint density functions of the normalized auxiliary variable (with respect to the yield level) and the normalized interstory drift velocity (with respect to its maximum value), obtained in the simulation study, with the assumed Gaussian distributions. Part (A) shows the density function obtained in the simulation study whereas part (B) shows the gaussian density function determined by the statistics of the equivalent linear system. The assumed Gaussian distributions

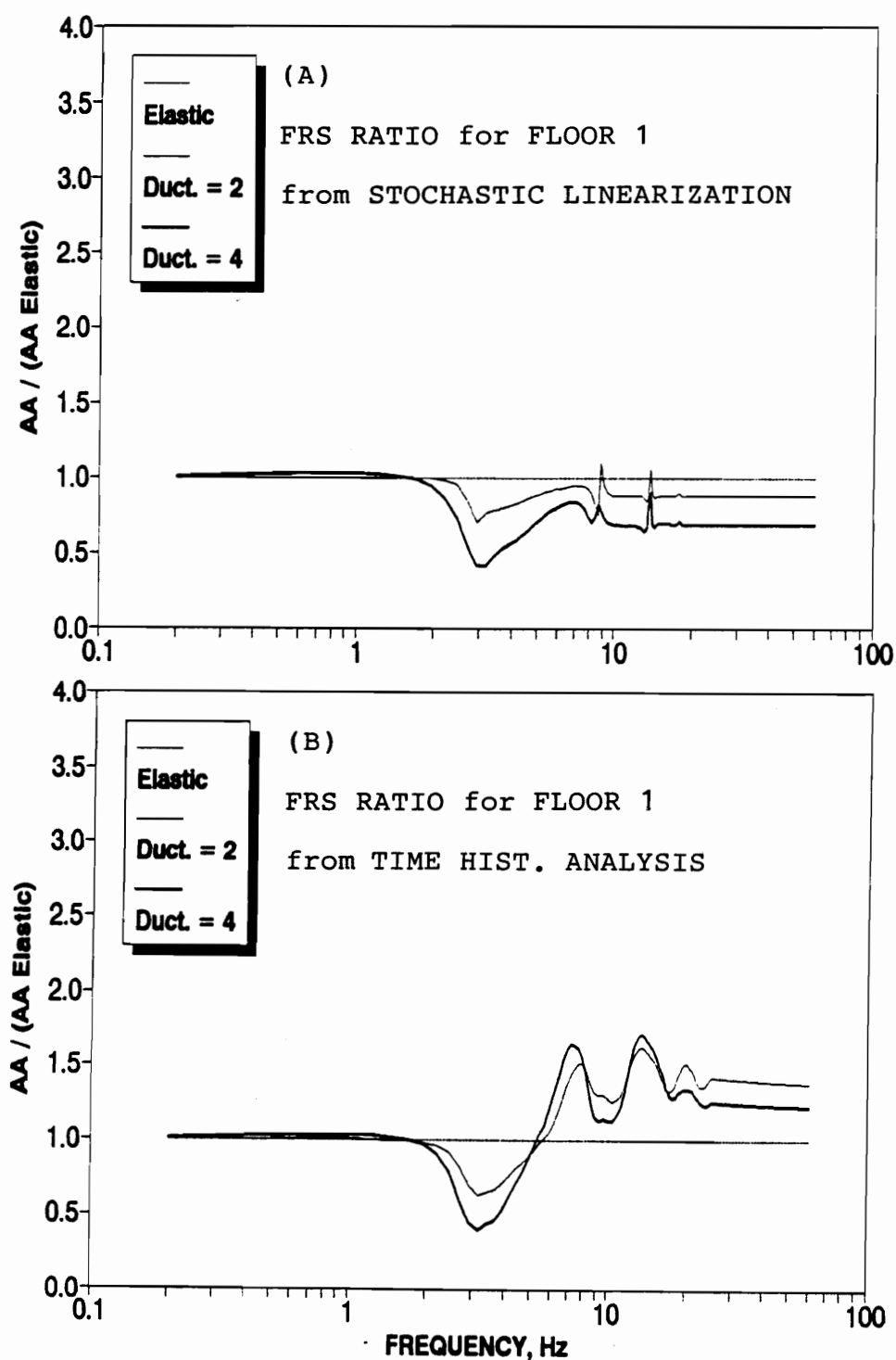


Figure 5.25: Floor response spectra ratio of absolute acceleration for floor 1 (equip. damp. ratio = 5%). (A) Stochastic equivalent linearization, (B) Time history analysis.

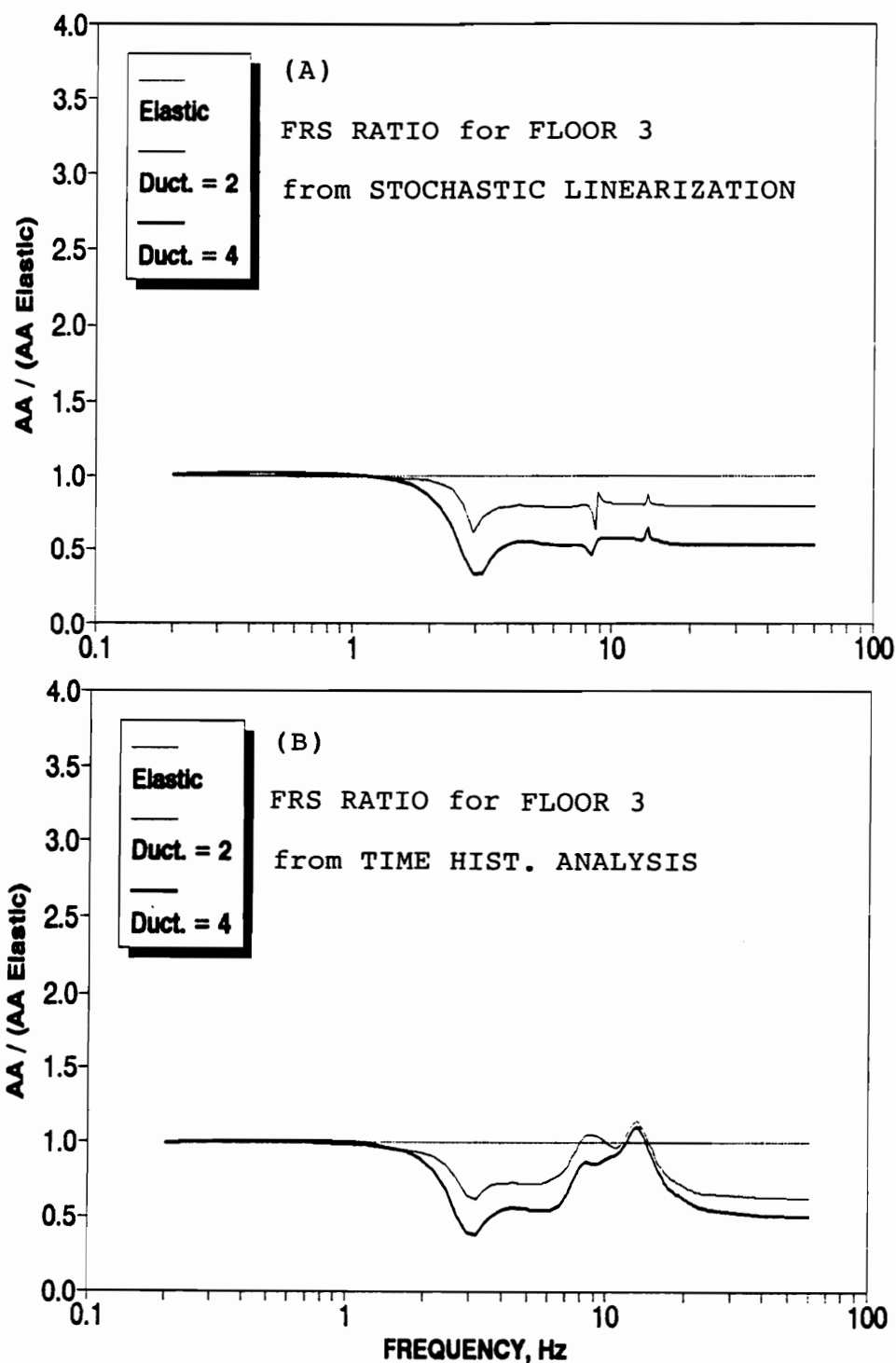


Figure 5.26: Floor response spectra ratio of absolute acceleration for floor 3 (equip. damp. ratio = 5%). (A) Stochastic equivalent linearization, (B) Time history analysis.

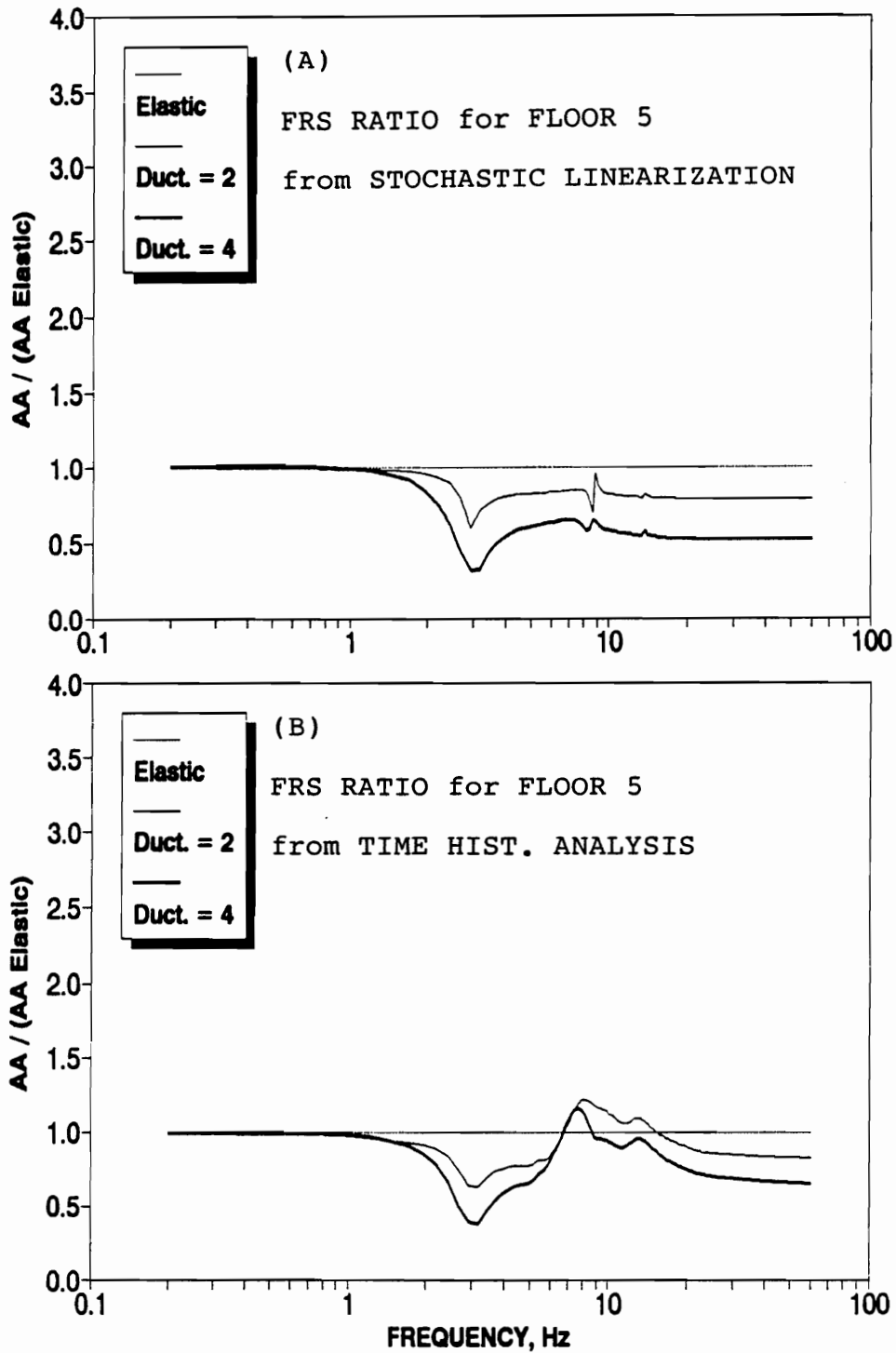


Figure 5.27: Floor response spectra ratio of absolute acceleration for floor 5 (equip. damp. ratio = 5%). (A) Stochastic equivalent linearization, (B) Time history analysis.

Table 5.8: Percent error in the floor spectra at the vicinity of the first and second peaks

Freq. Hz	PERCENT ERROR NEAR FIRST PEAK								
	Floor 1			Floor 3			Floor 5		
	Elas.	Du. 2	Du. 4	Elas.	Du. 2	Du. 4	Elas.	Du. 2	Du. 4
2.432	3.5	7.8	-2.9	5.4	13.0	-0.6	6.0	14.0	0.1
2.680	9.0	13.4	2.2	12.8	19.1	1.5	13.4	20.7	1.6
2.928	14.0	15.9	5.8	18.8	12.7	-0.2	19.4	12.3	-1.5
3.176	10.1	34.3	14.5	14.4	32.2	1.8	15.0	30.8	-1.1
3.424	2.4	22.1	14.5	3.5	15.5	-1.9	3.7	13.6	-5.5
Freq. Hz	PERCENT ERROR NEAR SECOND PEAK								
	Floor 1			Floor 3			Floor 5		
	Elas.	Du. 2	Du. 4	Elas.	Du. 2	Du. 4	Elas.	Du. 2	Du. 4
8.384	0.4	-41.5	-44.6	-3.6	-30.0	-48.4	-5.1	-38.3	-46.8
8.632	0.9	-43.5	-32.2	-2.9	-41.3	-40.3	-4.2	-44.1	-37.6
8.880	0.8	-16.9	-31.6	-2.4	-16.6	-35.0	-4.0	-21.5	-35.3
9.128	0.2	-27.3	-35.8	-2.9	-21.1	-35.1	-4.3	-28.4	-37.9
9.376	-1.0	-31.5	-38.5	-3.4	-23.1	-35.8	-5.8	-31.1	-39.9

are shown truncated at the limiting value of the auxiliary variable for comparison purposes only. The actual range of this variable is, however, unlimited. Figure 5.28 is for the first interstory element when the ductility ratio is 2, and figure 6.33 is also for the first element but when the ductility is 4. It is seen, especially in figure 5.29, that the actual density functions of the nonlinear system strongly differ from the assumed Gaussian ones. They differ not only on the shape but also on their domains.

5.12 Conclusions

The response of shear buildings with material nonlinearities has been studied. A response spectrum method is presented to obtain the force and displacement re-

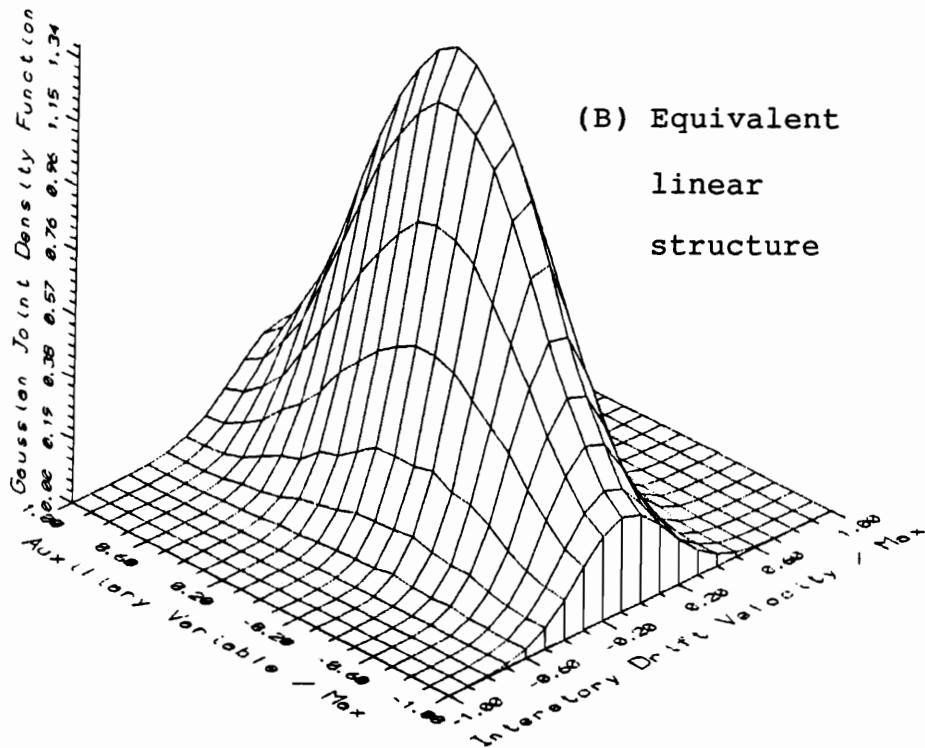
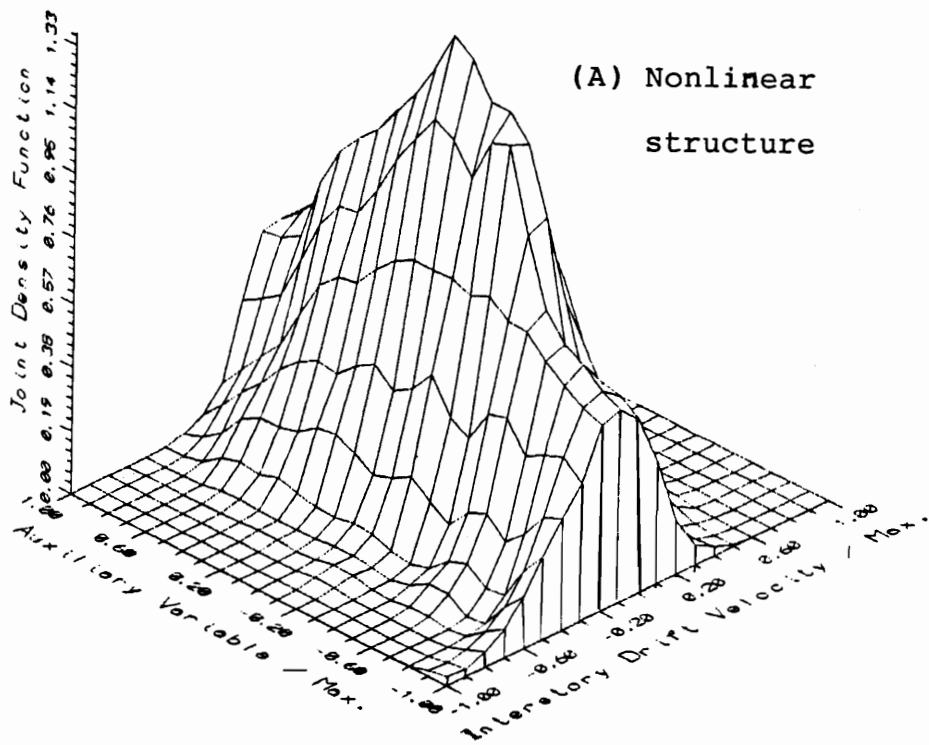


Figure 5.28: Joint probability density functions for the normalized auxiliary variable and the normalized interstory drift velocity for floor 1 and ductility 2

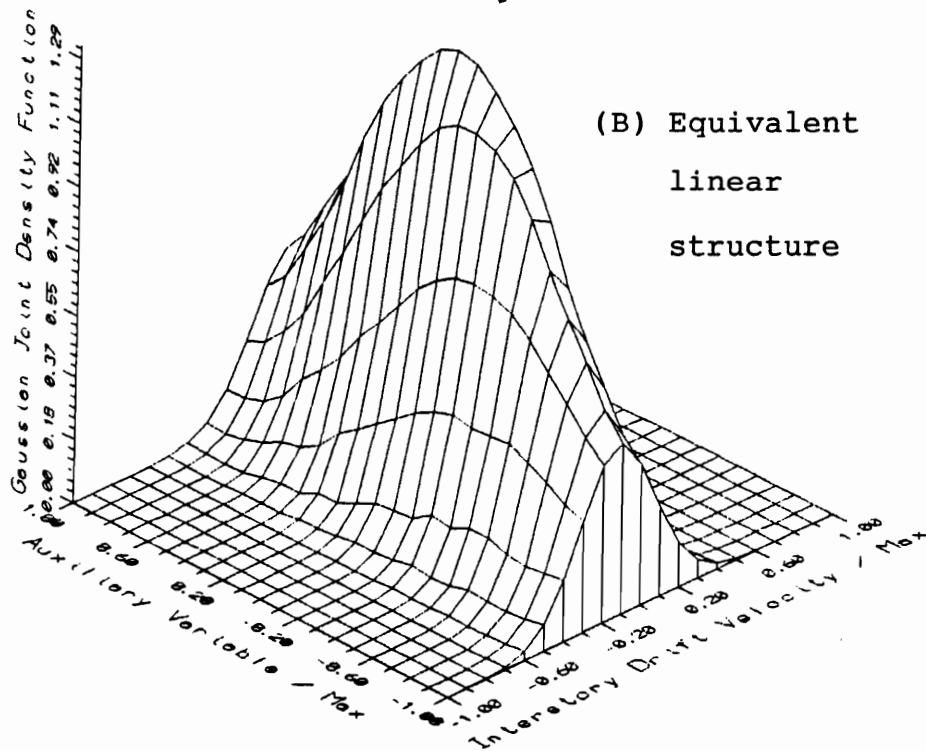
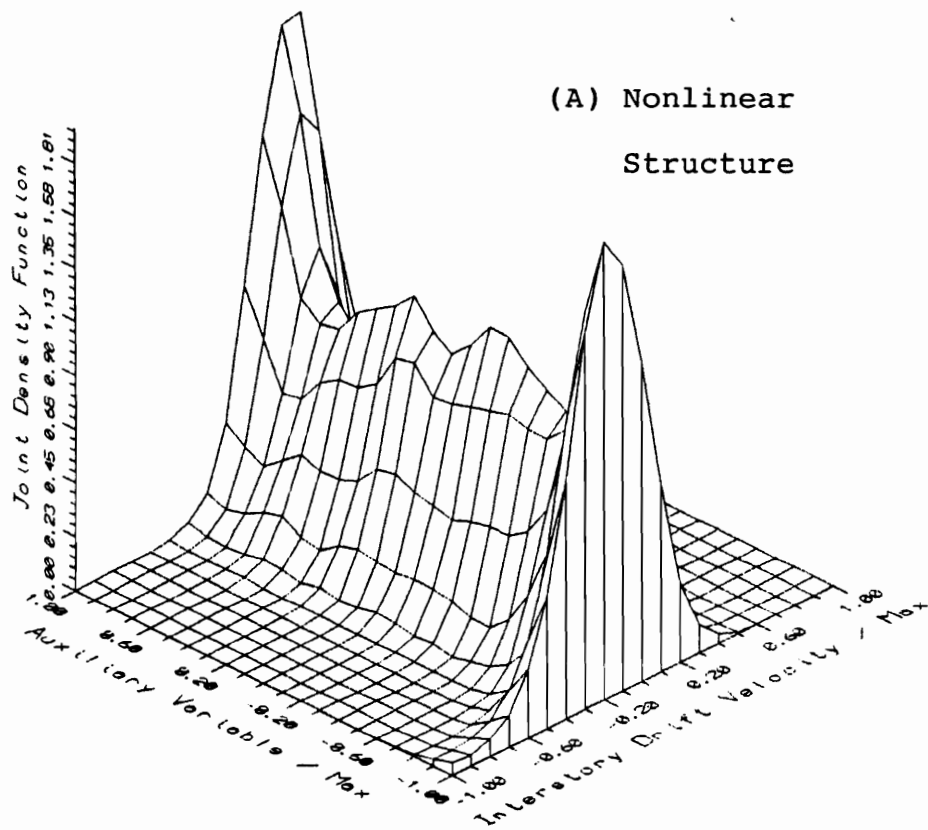


Figure 5.29: Joint probability density functions for the normalized auxiliary variable and the normalized interstory drift velocity for floor 1 and ductility 4

sponse of nonlinear primary structures. The formulation has also been provided to calculate the maximum floor acceleration as well as the floor response spectra. An iterative stochastic linearization is used to provide equivalent linear systems associated with the nonlinear structures. The linearized equations of motion are solved by the successful utilization of a generalized modal analysis approach which allows the use of ground response spectra in the calculation of response. The proposed response spectrum method is based on the classical mode displacement combination rule of structural dynamics, and employs the commonly used pseudo-acceleration and relative velocity ground response spectra plus a new spectrum associated with the response of a first order oscillators.

Several numerical results have been presented to study the response characteristics of the equivalent linear systems. It has been observed that the behavior of such nonlinear systems is in general well described by the resulting equivalent linear structures. To facilitate the initial guess of the linearization coefficients, upper bounds have been provided to both of them, and also a lower bound to the a_i coefficients is presented in terms of the exponent parameter η of the constitutive model. The Newton's method have been successfully used, in addition to the fixed point iterations, to improve the convergence rate of the iterative process.

To examine the accuracy of the proposed equivalent linear response spectrum approach, a simulation study has been performed. It involved 100 artificially generated earthquakes, which were applied to three different structures with the same characteristics but with different degrees of plasticity. The comparison of the responses obtained by the equivalent linear and by the time history analysis shows that there are discrepancies in the two values, although qualitatively the two re-

sponses are similar. In majority of cases, however, the equivalent linear approach was seen to provide a more conservative value of response.

The proposed response spectrum method to generate in-structure response spectra has also been compared against the simulation study. In these cases the proposed approach provided conservative results for equipment in the low frequency range. However, in the high frequency range the, responses were in general lower than the results obtained by the simulation study.

An analysis of the assumptions adopted by the proposed approach suggests that the main cause of the observed errors is most probable due to the assumed shape of the probability density functions used in the linearization process. It is presumed that the errors may be decreased by employing a suitable non-Gaussian linearization technique.

Finally it is relevant to mention that the proposed approach is computationally very efficient, especially when compared against the time history analyses. This suggests that the proposed method can be used as a powerful tool for the iterative design tasks. However, if a more accurate value of response is desired then time history analysis with several ground motion accelerograms may be necessary.

Chapter 6

Response Spectrum Method for 2D Frames with Plastic Hinges

6.1 Introduction

In this chapter, we present a formulation to incorporate the nonlinear plastic hinges which can develop at the joints in two dimensional frames during a strong seismic excitation. This formulation is used to develop a response spectrum method employing the general modal analysis approach presented in chapter 6.

The main difference between this chapter and chapter 5 are found on the structural localization of the inelastic zones. The potential hinges are assumed to be developed at specific regions of the different frame members. On the other hand, the shear building elements were considered to have the inelastic characteristics distributed along all their length.

The incorporation of plastic hinges results in a softening model of the total structural stiffness, which will depend not only on the level of deformation but also

on the load history. This hysteretic behavior is due to the hysteretic characteristics assigned to the plastic hinges. Again the Bouc-Wen [9, 56, 57] constitutive law is used to model the inelastic behavior of plastic hinges. The nonlinear equations of motion are linearized by the stochastic linearization approach. The resulting linearized governing equations are generalizations of the works by Casciati and Faravelli [11, 12] and Baber and Wen [8]. The linearization process is iterative involving repetitive modal analyses and combinations of modal responses. Thus, the methodology used in this chapter is closely related to that applied on chapter 5. However, the formulation to include the plastic hinges and the governing equations are quite different.

6.2 Equations of Motion

The equations of motion of an n -degree-of-freedom structural frame with inelastic stiffness, and subjected to ground acceleration $\ddot{x}_g(t)$, can be written as:

$$[M] \{\ddot{X}(t)\} + [C] \{\dot{X}(t)\} + [K]_* \{X(t)\} = -[M] \{\mathcal{I}\} \ddot{x}_g(t) \quad (6.1)$$

where $\{X(t)\}$ is the vector containing the n nodal displacements with respect to the undeformed state fixed to the ground, $[M]$ and $[C]$ are the $(n \times n)$ mass and damping matrices respectively, $[K]_*$ is the $(n \times n)$ inelastic tangent stiffness matrix, and $\{\mathcal{I}\}$ is the influence vector. In this chapter, all the quantities related to inelastic behavior will be identified by a subscripted asterisk.

It is assumed that the mass and damping matrices remain linear and constant during all the deformation process. In particular, a lumped mass or a consistent mass matrix can be used. Also, the system can be modeled by a classical or a non-classical damping matrix. The term involving the inelastic stiffness matrix $[K]_*$, provides the

only inelastic restoring forces of the present model:

$$\{F(t)\}_* = [K]_* \{X(t)\} \quad (6.2)$$

To model the restoring forces due to inelastic stiffnesses, their behavior is compared against that of forces corresponding to perfectly elastic stiffness. It can be observed that, for a fixed displacement configuration, an elastic structure generates larger restoring forces than an structure with the same geometric characteristics but with inelastic behavior. Therefore, the inelastic restoring forces corresponding to a particular set of displacements, may be calculated by an appropriate reduction of the elastic forces associated to the same displacements. The present study models these reductions in the forces by considering the development of plastic hinges at specific sections of the structural elements. That is, any rotation at the hinges involves a relaxation of the deformations associated to the remaining elastic part of the element. Consequently, the restoring elastic forces are reduced to become the inelastic restoring forces. In this chapter, the rotations at the plastic hinges are often called *imposed* rotations because their effects are equivalent to the effects caused by imposing hypothetical external forces.

The inelastic restoring forces, thus, can be expressed by the difference between the elastic forces and those forces associated to the imposed rotations as:

$$\{F(t)\}_* = [K] \{X(t)\} - [P] \{\Theta(t)\} , \quad (6.3)$$

where $[K]$ is the $(n \times n)$ constant elastic stiffness matrix. $[P]$ is an $(n \times m)$ matrix relating the m imposed rotations, one at each plastic hinge, with the total n nodal forces. $\{\Theta(t)\}$ is the vector containing the imposed rotations at the m plastic hinges.

The equations of motion can be rewritten by substituting equation (6.3) into equation (6.1) as:

$$[M] \{\ddot{X}(t)\} + [C] \{\dot{X}(t)\} + [K] \{X(t)\} - [P] \{\Theta(t)\} = -[M] \{\mathcal{I}\} \ddot{x}_g(t). \quad (6.4)$$

The vector $\{\Theta(t)\}$ incorporates m additional unknowns, which not only depend on the time, but also on the amplitude of the excitation, on the material characteristics of the plastic hinges, and on the load history. Consequently, the problem requires m additional constitutive equations to become determinate.

To develop the extra equations it is necessary to use some concepts concerning the mechanics of the frame element with potential hinges. Therefore, the following section presents the matrix equations that define such element, as well as the procedure to assemble the different element matrices to obtain the global governing equations.

6.3 Plane Frame Element with Plastic Hinges

The well known two dimensional elastic frame element is modified here to incorporate two potential plastic hinges. However, a similar three dimensional element can be easily developed by following the concepts expressed in this section. To simplify the analysis, the hinges are assumed to be localized at both ends of the element. However, some eccentricities can be allowed by adding simple geometric considerations. Also, the element requiring just one potential hinge (cantilevered beam), are not explicitly developed in this work, but it can easily be done following the formulation given for the element with two potential hinges.

The element mass matrix and the element damping matrix are assumed to remain constant during the inelastic process and their formulation is available in several books on structural dynamics. In particular, the damping matrices corresponding to the numerical examples of this chapter, were obtained by using the eigenproperties of the undamped linear structure and assumed damping ratios (see equation (D.6) in appendix D).

Some known characteristics of the 2D elastic frame element are recalled in the next subsection, and the formulation leading to the inelastic nodal forces as well as to the constitutive equations is presented in the subsequent two subsections.

6.3.1 2D Elastic Frame Element

For the 2D elastic frame element, the relation between nodal forces and nodal displacements through the elastic stiffness matrix is well known. However, the relation between equivalent efforts and the corresponding axial and flexural deformations are not commonly used. Since the latter are employed in this work to formulate an inelastic element, it is considered appropriate to provide in this section all the relations among forces, displacements, efforts and deformations of the elastic element.

Figure 6.1 (A) shows a 2D elastic frame element at an angle φ^e with the global X axis. The element is denoted as e , and it possesses three degrees of freedom at each node, two translational and one rotational. They are denoted as x_1^e , x_2^e , and x_3^e at the initial node, and x_4^e , x_5^e , and x_6^e at the final node. The (6×6) elastic stiffness

matrix $[k^e]$ of the e^{th} element can be written in standard form as:

$$[k^e] = \begin{bmatrix} k_1^e & & & & & \\ k_4^e & k_2^e & & & & \\ k_6^e & k_5^e & k_3^e & & & \\ -k_1^e & -k_4^e & -k_6^e & k_1^e & & \\ -k_4^e & -k_2^e & -k_5^e & k_4^e & k_2^e & \\ k_6^e & k_5^e & \frac{-k_3^e}{2} & -k_6^e & -k_5^e & k_3^e \end{bmatrix}, \quad \text{Symm.} \quad (6.5)$$

where the six different quantities required in equation (6.5) are

$$k_1^e = A^e E^e (L^e)^{-1} \cos^2 \varphi^e + 12 E^e I^e (L^e)^{-3} \sin^2 \varphi^e, \quad (6.6)$$

$$k_2^e = A^e E^e (L^e)^{-1} \sin^2 \varphi^e + 12 E^e I^e (L^e)^{-3} \cos^2 \varphi^e, \quad (6.7)$$

$$k_3^e = 4 E^e I^e (L^e)^{-1}, \quad (6.8)$$

$$k_4^e = (A^e E^e (L^e)^{-1} - 12 E^e I^e (L^e)^{-3}) \cos \varphi^e \sin \varphi^e, \quad (6.9)$$

$$k_5^e = 6 E^e I^e (L^e)^{-2} \cos \varphi^e, \quad (6.10)$$

$$k_6^e = -6 E^e I^e (L^e)^{-2} \sin \varphi^e. \quad (6.11)$$

The element quantities A^e , I^e , E^e and L^e are, respectively, the cross section area, the area moment of inertia, the modulus of elasticity and the length of the e^{th} element. Here it is assumed that shear deformations are negligible.

Figures 6.1 (A) and (B) show the six nodal displacements x_i^e , and the corresponding six nodal forces f_i^e . The elastic constitutive relation between these nodal quantities is given by

$$\{f^e\} = [k^e] \{x^e\}. \quad (6.12)$$

However, the element only possesses axial and flexural deformations, and just three quantities are needed to completely determine its deformed state. Those are the axial deformation d_A^e (along the length), the flexural deformation $d_{R_i}^e$ (rotation), at

its initial node, and the flexural deformation $d_{R_f}^e$, at the final node. The deformation vector $\{d^e\}$ groups these three quantities in that order. Figure 6.1 (C) shows the element e in its undeformed and deformed configurations, as well as the nodal displacements and the equivalent nodal deformations.

For small deformations, which also implies a small change of the element direction (small angle $\Delta\varphi^e$), the deformation vector is linearly related to the vector containing the six nodal displacements. Such linear relations are now deduced for each deformation quantity. The quantity d_A^e , which equals the difference in length between the deformed and the undeformed element, can be approximated by the total displacement of the final node minus the total displacement of the initial node, both projected in the direction of the undeformed element. Thus,

$$d_A^e \approx L_{deformed}^e - L^e = x_4^e \cos \varphi^e + x_5^e \sin \varphi^e - x_1^e \cos \varphi^e - x_2^e \sin \varphi^e . \quad (6.13)$$

The deformation $d_{R_i}^e$ is equal to the rotation of the cross section at the initial node with respect to the deformed direction of the element. From figure 6.1 (C), the following relation can be written

$$d_{R_i}^e = x_3^e - \Delta\varphi^e . \quad (6.14)$$

Similarly, the rotation of the section at the final nodes is

$$d_{R_f}^e = x_6^e - \Delta\varphi^e . \quad (6.15)$$

The small angle $\Delta\varphi^e$ can be expressed in terms of the nodal displacements by using simple geometric relations. Thus, from figure 6.1 (C) it can be inferred that

$$\tan(\Delta\varphi^e + \varphi^e) = \frac{Y_f + x_5^e - Y_i - x_2^e}{X_f + x_4^e - X_i - x_1^e} \approx \frac{\Delta\varphi^e + \tan \varphi^e}{1 - \Delta\varphi^e \tan \varphi^e} \quad (6.16)$$

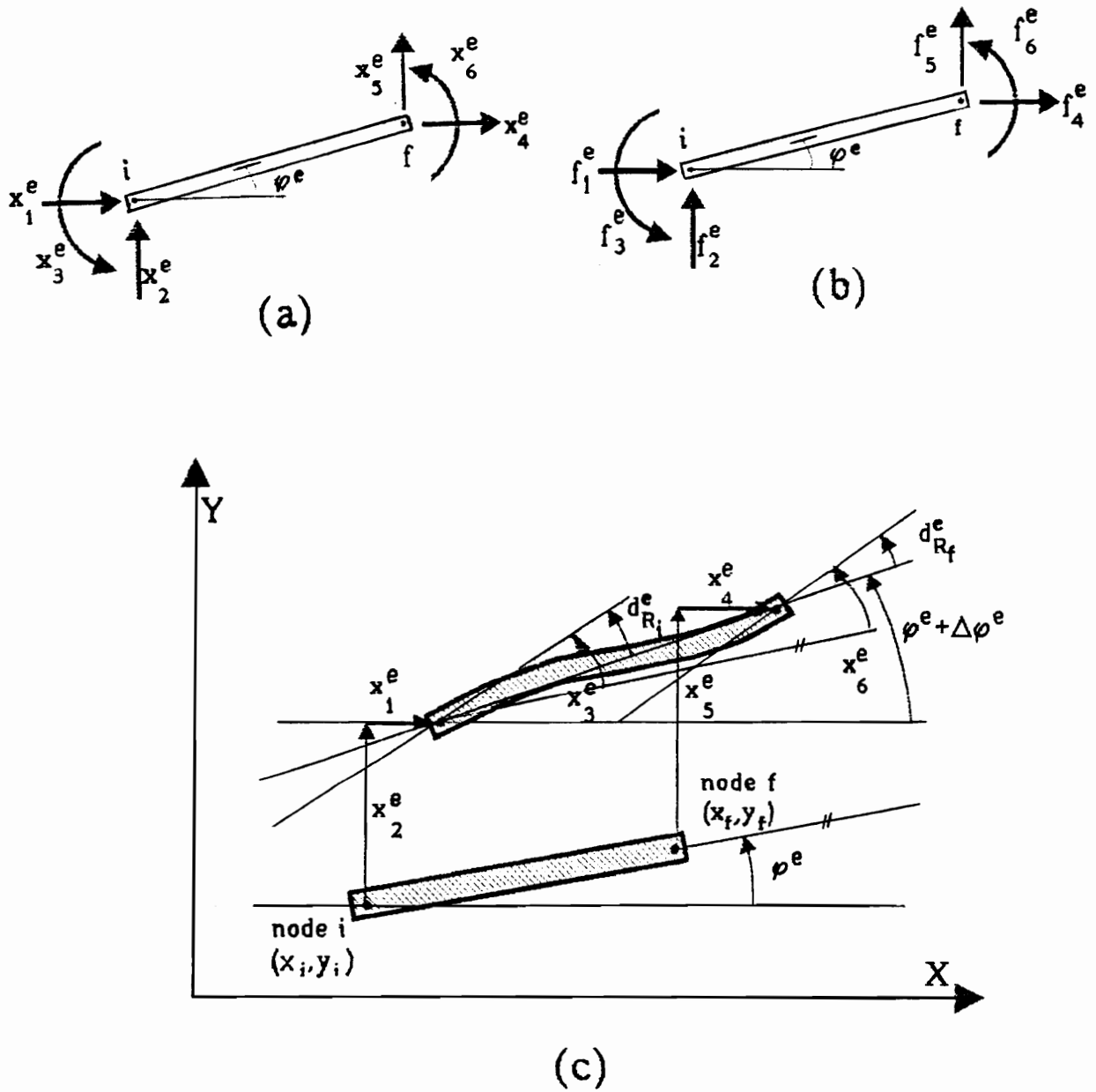


Figure 6.1: Two dimensional elastic frame element: (A) Nodal displacements, (B) Nodal forces, (C) Undeformed and deformed states

where (X_i, Y_i) and (X_f, Y_f) are the global nodal coordinates of the undeformed element. In this equation, $(\tan \Delta\varphi^e)$ has been approximated by $\Delta\varphi^e$. The right hand side of equation (6.16) can be multiplied and divided by $(\cos \varphi^e)$ to get

$$\frac{Y_f + x_5^e - Y_i - x_2^e}{X_f + x_4^e - X_i - x_1^e} \approx \frac{\Delta\varphi^e \cos \varphi^e + \sin \varphi^e}{\cos \varphi^e - \Delta\varphi^e \sin \varphi^e} . \quad (6.17)$$

After some rearrangement, and taking into account the following identities

$$(Y_f - Y_i) \cos \varphi^e - (X_f - X_i) \sin \varphi^e = 0 , \quad (6.18)$$

$$(X_f - X_i) \cos \varphi^e + (Y_f - Y_i) \sin \varphi^e = L^e , \quad (6.19)$$

equation (6.16) can be rewritten as:

$$(x_5^e - x_2^e) \cos \varphi^e + (x_4^e - x_1^e) \sin \varphi^e \approx \Delta\varphi^e [(x_4^e - x_1^e) \cos \varphi^e + (x_5^e - x_2^e) \sin \varphi^e + L^e] , \quad (6.20)$$

With the help of equation (6.13), equation (6.20) can be expressed in term of d_A^e as:

$$\Delta\varphi^e + \Delta\varphi^e d_A^e (L^e)^{-1} \approx [(x_5^e - x_2^e) \cos \varphi^e - (x_4^e - x_1^e) \sin \varphi^e] (L^e)^{-1} . \quad (6.21)$$

Since $\Delta\varphi^e d_A^e (L^e)^{-1}$ is a second order differential, it can be neglected to get

$$\Delta\varphi^e \approx [(x_5^e - x_2^e) \cos \varphi^e - (x_4^e - x_1^e) \sin \varphi^e] (L^e)^{-1} . \quad (6.22)$$

Substitution of equation (6.22) into equations (6.14) and (6.15) provides the expressions of $d_{R_i}^e$ and $d_{R_f}^e$ as linear functions of the nodal displacements:

$$d_{R_i}^e = x_3^e - [(x_5^e - x_2^e) \cos \varphi^e - (x_4^e - x_1^e) \sin \varphi^e] (L^e)^{-1} , \quad (6.23)$$

and

$$d_{R_f}^e = x_6^e - [(x_5^e - x_2^e) \cos \varphi^e - (x_4^e - x_1^e) \sin \varphi^e] (L^e)^{-1} . \quad (6.24)$$

Equations (6.13), (6.23) and (6.24) can be written in matrix form as

$$\begin{Bmatrix} d_A^e \\ d_{R_i}^e \\ d_{R_f}^e \end{Bmatrix} = \begin{bmatrix} -\cos \varphi^e & -\sin \varphi^e & 0 & \cos \varphi^e & \sin \varphi^e & 0 \\ -\frac{\sin \varphi^e}{L^e} & \frac{\cos \varphi^e}{L^e} & 1 & \frac{\sin \varphi^e}{L^e} & -\frac{\cos \varphi^e}{L^e} & 0 \\ -\frac{\sin \varphi^e}{L^e} & \frac{\cos \varphi^e}{L^e} & 0 & \frac{\sin \varphi^e}{L^e} & -\frac{\cos \varphi^e}{L^e} & 1 \end{bmatrix} \begin{Bmatrix} x_1^e \\ x_2^e \\ x_3^e \\ x_4^e \\ x_5^e \\ x_6^e \end{Bmatrix}, \quad (6.25)$$

or in a shorter notation

$$\{d^e\} = [g^e] \{x^e\}, \quad (6.26)$$

where $[g^e]$ is the (3×6) geometric matrix containing the constant coefficients necessary to linearly transform the nodal displacements of element e into the corresponding element deformations. Equation (6.25) also appears in reference [23].

Each of the three element deformations can be considered to be caused by an associated effort. d_A^e is associated to the axial effort (force) ε_A^e , $d_{R_i}^e$ is associated to the flexural effort $\varepsilon_{M_i}^e$ (moment), and $d_{R_f}^e$ is associated to the flexural effort (moment) $\varepsilon_{M_f}^e$. The element vector denoted $\{\varepsilon^e\}$, contains these three efforts, which are shown in figure 6.2 (B).

The elastic constitutive relation between deformations and efforts can easily be deduced to get

$$\begin{Bmatrix} \varepsilon_A^e \\ \varepsilon_{M_i}^e \\ \varepsilon_{M_f}^e \end{Bmatrix} = \begin{bmatrix} k_A^e & 0 & 0 \\ 0 & k_3^e & k_3^e/2 \\ 0 & k_3^e/2 & k_3^e \end{bmatrix} \begin{Bmatrix} d_A^e \\ d_{R_i}^e \\ d_{R_f}^e \end{Bmatrix}, \quad (6.27)$$

where k_3^e is defined by equation (6.8), and k_A^e is the axial stiffness of the element

$$k_A^e = A^e E^e (L^e)^{-1}. \quad (6.28)$$

The (3×3) matrix in equation (6.27) is denoted as $[\hat{k}^e]$ and is the axial-flexural stiffness matrix of the element. So, by using a shorter notation, equation (6.27) can

be written as

$$\{\varepsilon^e\} = [\hat{k}^e] \{d^e\} . \quad (6.29)$$

The two matrices $[k^e]$ and $[\hat{k}^e]$ are related. The mathematical relationship can be obtained by considering the total internal energy for element e , which is the same for an element subjected to the six nodal forces or to the three equivalent element efforts that produce the same deformations. See figure 6.2 (A) and (B). Thus,

$$\text{Internal energy} = \frac{1}{2} \{x^e\}^T \{f^e\} = \frac{1}{2} \{d^e\}^T \{\varepsilon^e\} , \quad (6.30)$$

where equations (6.12) and (6.29) can be used to get

$$\{x^e\}^T [k^e] \{x^e\} = \{d^e\}^T [\hat{k}^e] \{d^e\} . \quad (6.31)$$

In this equation, $\{d^e\}$ (and its transpose) can be substituted by the expression given in equation (6.26) (and its transpose) to produce

$$\{x^e\}^T [k^e] \{x^e\} = \{x^e\}^T [g^e]^T [\hat{k}^e] [g^e] \{x^e\} . \quad (6.32)$$

From equation (6.32) we can infer that

$$[k^e] = [g^e]^T [\hat{k}^e] [g^e] . \quad (6.33)$$

Finally, the vectors $\{\varepsilon^e\}$ and $\{f^e\}$ can also be explicitly related. For this purpose consider equation (6.29), and substitute the vector $\{d^e\}$ by the expression given in equation (6.26) to get

$$\{\varepsilon^e\} = [\hat{k}^e] [g^e] \{x^e\} . \quad (6.34)$$

Premultiplication by $[g^e]^T$ gives

$$[g^e]^T \{\varepsilon^e\} = [g^e]^T [\hat{k}^e] [g^e] \{x^e\} = [k^e] \{x^e\} , \quad (6.35)$$

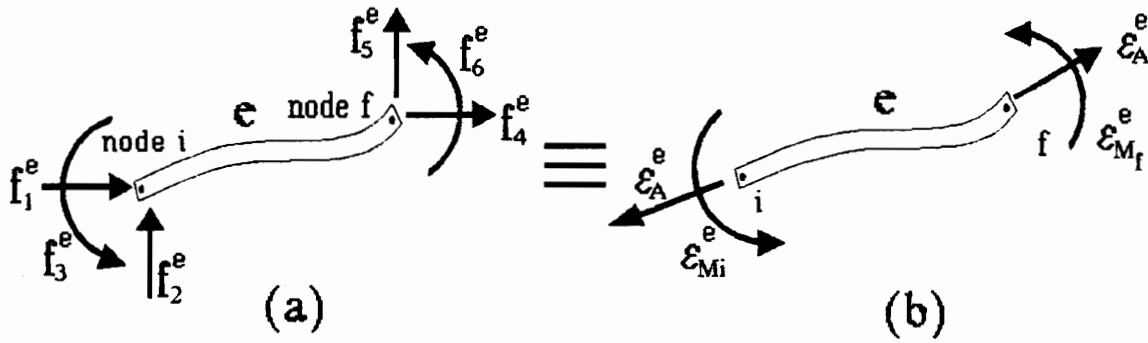


Figure 6.2: Deformed elastic element: (A) due to nodal forces, and (C) due to equivalent nodal efforts.

where $[k^e]\{x^e\} = \{f^e\}$, and equation (6.34) becomes

$$\{f^e\} = [g^e]^T \{\epsilon^e\}. \quad (6.36)$$

Equations (6.12), (6.26), (6.29) and (6.36) provide all the relationships between nodal forces, nodal displacements, axial and flexural deformations, and equivalent efforts corresponding to a 2D elastic frame element.

6.3.2 Inelastic Nodal Forces

The elastic element presented in the previous subsection is now modified to incorporate the inelastic behavior by adding two plastic hinges. The proposed element consists of three different parts, an elastic part located between the hinges, a

plastic hinge at the initial node and other plastic hinge at the final node. The plastic behavior of the two element hinges not necessarily has to be the same. To develop this element, the approach proposed in section 6.2 is followed. That is, for a given displacement configuration, the nodal forces acting at the ends of the elastic part, as a consequence of the inelastic behavior, are denoted as $\{f^e\}_*$ (inelastic nodal forces), and are obtained by decreasing the hypothetical elastic nodal forces $\{f^e\}$, associated to such deformations. The reduction is caused by the imposition of rotations at the plastic hinges. The amounts of the reduction depend on the magnitude of the imposed rotations as well as on the constitutive law of each hinge. Thus,

$$\{f^e\}_* = \{f^e\} - \{f^e\}_\theta, \quad (6.37)$$

where $\{f^e\}_\theta$ contains the six elastic nodal forces to be released due to the imposition of the rotations at the initial and final hinges of the element, θ_i^e and θ_f^e , respectively.

The forces $\{f^e\}_\theta$ can be written as functions of the imposed rotations. For this purpose, the rotations at the plastic hinges are considered to be transmitted to the ends of the remaining elastic part of the element as two flexural deformations with no axial effect. Thus, the elastic efforts to be released (due to these imposed "rotations") are the moments μ_i^e and μ_f^e , at the initial and final nodes respectively. They can be obtained by using equation (6.27):

$$\begin{Bmatrix} 0 \\ \mu_i^e \\ \mu_f^e \end{Bmatrix} = \begin{bmatrix} k_A^e & 0 & 0 \\ 0 & k_3^e & k_3^e/2 \\ 0 & k_3^e/2 & k_3^e \end{bmatrix} \begin{Bmatrix} 0 \\ \theta_i^e \\ \theta_f^e \end{Bmatrix}, \quad (6.38)$$

where the (3×3) matrix is $[\hat{k}^e]$. That is, the axial-flexural stiffness matrix of the element e .

As it is indicated in equation (6.36), the six nodal forces, equivalent to these

efforts, can be obtained by premultiplying them by $[g^e]^T$,

$$\{f^e\}_\theta = [g^e]^T \begin{Bmatrix} 0 \\ \mu_i^e \\ \mu_f^e \end{Bmatrix} = [g^e]^T [\hat{k}^e] \begin{Bmatrix} 0 \\ \theta_i^e \\ \theta_f^e \end{Bmatrix}. \quad (6.39)$$

Since the first components of the vectors in equation (6.39) are zero, the vectors and matrices used there can be reduced in size to write:

$$\{f^e\}_\theta = [g^e]_r^T \{\mu^e\} = [g^e]_r^T [\hat{k}^e]_r \{\theta^e\}, \quad (6.40)$$

where the subscript r indicates a reduced matrix. Thus, $[g^e]_r$ is a (2×6) matrix composed of the last two rows of $[g^e]$, $[\hat{k}^e]_r$ is a (2×2) matrix that results from not considering the first row and first column of $[\hat{k}^e]$, $\{\mu^e\}$ is a vector with just two components, the moments μ_i^e and μ_f^e , and $\{\theta^e\}$ is also a vector with two components, the imposed rotations θ_i^e and θ_f^e . The product $[g^e]_r^T [\hat{k}^e]_r$ is a (6×2) matrix that is denoted as $[p^e]$, and has the following components:

$$[p^e] = [g^e]_r^T [\hat{k}^e]_r = \begin{bmatrix} k_6^e & k_8^e \\ k_5^e & k_5^e \\ k_3^e & k_3^e/2 \\ -k_6^e & -k_6^e \\ -k_5^e & -k_5^e \\ k_3^e/2 & k_3^e \end{bmatrix}, \quad (6.41)$$

where k_3^e , k_5^e and k_6^e were given in equations (6.8), (6.10) and (6.11) respectively. Substitution of this expression into equation (6.40) produces

$$\{f^e\}_\theta = [p^e] \{\theta^e\}, \quad (6.42)$$

which expresses $\{f^e\}_\theta$ as a function of the imposed rotations at the plastic hinges. Finally, by substituting equations (6.12) and (6.42) into equation (6.37), the inelastic nodal forces become

$$\{f^e\}_* = [k^e] \{x^e\} - [p^e] \{\theta^e\}. \quad (6.43)$$

This equation shows that the nodal inelastic forces of the e^{th} element require the use of two element matrices, $[k^e]$ and $[p^e]$, which remain constant during the deformation process. This equation is the element version of the assembled expression given in equation (6.3).

To complete the definition of the inelastic element, it is necessary to satisfy two additional requirements. One is the equilibrium of moments at the interface sections that separate the elastic part of the element from the plastic hinges, and the other is to provide an appropriate inelastic constitutive law to model the relationship between the imposed rotations at the plastic hinges with the actual moments acting on those hinges. Both topics are covered in detail in the next subsection where the constitutive equations for each element and for the structure are presented.

Here the assemblage of equation (6.43) for all elements requires that the equilibrium of the inelastic nodal forces, as well as the compatibility of the nodal displacements, be satisfied. However, no compatibility is required between the imposed rotations of different elements.

The equilibrium of the inelastic nodal forces requires to balance all the contributions of the elements that share the same node with the external loads applied at such node. This is performed by superposing the rows of the equations (6.43) associated to all the elements that share the same node. On the other hand, the compatibility of the nodal displacements requires that all the elements, that share a particular node, have the same displacements at such node. This requirement is satisfied by adding the appropriate columns of the different stiffness matrices $[k^e]$ that are associated with the same nodal displacements. As a result, the assemblage

of matrix $[K]$ is performed in the same way as it is usually done for elastic structures, that is, by the adequate superposition of rows and columns of the different element matrices $[k^e]$. Whereas the assemblage of matrix $[P]$, is performed by superposing only the appropriate rows of the element matrices $[p^e]$.

6.3.3 Constitutive Equations

The constitutive equations of the e^{th} element, are based on the constitutive law selected to model the plastic behavior of the hinges, as well as on the satisfaction of equilibrium between the moments acting on the hinges and the end moments at the extremes of the elastic part of the element.

First, the moments at the ends of the elastic part of the element are considered. They can be expressed in terms of the nodal displacements at those ends, and in terms of the imposed rotations at the hinges. Such expressions can be obtained by recalling equation (6.37)

$$\{f^e\}_* = \{f^e\} - \{f^e\}_\theta, \quad (6.44)$$

where the vector $\{f^e\}_*$, containing the forces and moments at the ends of the elastic part, is modeled as the difference between hypothetical elastic forces $\{f^e\}$, and release forces $\{f^e\}_\theta$, due to the imposed rotations at the plastic hinges. The resulting deformed configuration can also be reproduced by applying equivalent axial-flexural efforts at the same nodes. That is,

$$\{\epsilon^e\}_* = \{\epsilon^e\} - \{\epsilon^e\}_\theta, \quad (6.45)$$

Where equation (6.29) can be invoked to write

$$\{\varepsilon^e\}_* = [\hat{k}^e] \{d^e\} - [\hat{k}^e] \begin{Bmatrix} 0 \\ \theta_i^e \\ \theta_f^e \end{Bmatrix}, \quad (6.46)$$

The vector, $\{d^e\}$ can now be substituted by its expression given in equation (6.26) to get

$$\{\varepsilon^e\}_* = [\hat{k}^e] [g^e] \{x^e\} - [\hat{k}^e] \begin{Bmatrix} 0 \\ \theta_i^e \\ \theta_f^e \end{Bmatrix}. \quad (6.47)$$

The last two components of the vector $\{\varepsilon^e\}_*$ contain the moments of interest, that is, the moments M_i^e and M_f^e at the elastic ends of the element. The part of vector $\{\varepsilon^e\}_*$ containing these moments is now denoted as $\{M^e\}_*$. Therefore, by disregarding the first component, equation (6.47) is reduced to get

$$\{M^e\}_* = \begin{Bmatrix} M_i^e \\ M_f^e \end{Bmatrix}_* = [\hat{k}^e]_r [g^e]_r \{x^e\} - [\hat{k}^e]_r \{\theta^e\}, \quad (6.48)$$

where all the quantities on the right hand side have been defined in the previous section. Also, from equation (6.41), it can be recognized that $[\hat{k}^e]_r [g^e]_r = [p^e]^T$, and $\{M^e\}_*$ is finally written as

$$\{M^e\}_* = [p^e]^T \{x^e\} - [\hat{k}^e]_r \{\theta^e\}. \quad (6.49)$$

On the other hand, the moments acting on the initial and final hinge of the element are denoted as $M_{H_i}^e$ and $M_{H_f}^e$, respectively. The inelastic moment-rotation relationship of the plastic hinges is modeled by the same Bouc-Wen's constitutive law that was used for shear buildings in the previous chapter (see also appendix E). The moments at the hinges are considered to be composed of an elastic part in parallel with an hysteretic part, as it was the case in equation (5.4). Thus,

$$M_{H_i}^e = \alpha_i^e k_{H_i}^e \theta_i^e + (1 - \alpha_i^e) k_{H_i}^e v_i^e, \quad (6.50)$$

$$M_{H,}^e = \alpha_f^e k_{I,}^e \theta_f^e + (1 - \alpha_f^e) k_{I,}^e v_f^e, \quad (6.51)$$

where $k_{I,}^e$ and $k_{I,}^e$ are the initial stiffness parameters of the initial and final hinges, α_i^e and α_f^e are the proportionate contributions of the linear elastic part for each hinge, and v_i^e and v_f^e are the auxiliary variables of the hysteretic part of each hinge. Equations (6.50) and (6.51) can be written in matrix form as:

$$\{M_H^e\} = [k_\alpha^e] \{\theta^e\} + [h_\alpha^e] \{v^e\}, \quad (6.52)$$

where the vector $\{M_H^e\}$ contains the two moments at the plastic hinges, the vector $\{v^e\}$ has both auxiliary variables, the vector $\{\theta^e\}$, as it was already specified, contains the imposed rotations at both hinges and the matrices $[k_\alpha^e]$ and $[h_\alpha^e]$ are (2×2) diagonal matrices defined as follows:

$$[k_\alpha^e] = \begin{bmatrix} \alpha_i^e k_{I,}^e & 0 \\ 0 & \alpha_f^e k_{I,}^e \end{bmatrix}, \quad [h_\alpha^e] = \begin{bmatrix} (1 - \alpha_i^e) k_{I,}^e & 0 \\ 0 & (1 - \alpha_f^e) k_{I,}^e \end{bmatrix}. \quad (6.53)$$

The auxiliary variables v_i^e and v_f^e are related to the principal variables θ_i^e and θ_f^e through the nonlinear Bouc-Wen differential equation (see appendix E) applied at both hinges:

$$\dot{v}_i^e = \mathcal{A}_i^e \dot{\theta}_i^e - B_i^e \dot{\theta}_i^e |v_i^e|^{\eta_i^e} - C_i^e v_i^e |\dot{\theta}_i^e| |v_i^e|^{\eta_i^e-1}, \quad (6.54)$$

$$\dot{v}_f^e = \mathcal{A}_f^e \dot{\theta}_f^e - B_f^e \dot{\theta}_f^e |v_f^e|^{\eta_f^e} - C_f^e v_f^e |\dot{\theta}_f^e| |v_f^e|^{\eta_f^e-1}, \quad (6.55)$$

where the model parameters \mathcal{A}_i^e , B_i^e , C_i^e and η_i^e , for the hinge at the initial node, and the corresponding set for the hinge at the final node, should be appropriately selected to model the desired characteristics of the hysteresis loops. In the next subsection, further consideration is provided to these parameters, as well as to other parameters necessary to completely determine a particular kind of hysteresis loops.

The nonlinear constitutive equations can be linearized to obtain an statistically equivalent set of linear equations. Thus, the linearized version of equations (6.54)

and (6.55) can be written in matrix form as

$$\{\dot{v}^e\} = [a^e] \{\dot{\theta}^e\} + [b^e] \{v^e\}, \quad (6.56)$$

where matrices $[a^e]$ and $[b^e]$ contains the linearization coefficients for the hinges of the e^{th} element. Both matrices are diagonal and have dimension (2×2) :

$$[a^e] = \begin{bmatrix} a_i^e & 0 \\ 0 & a_f^e \end{bmatrix}, \quad [b^e] = \begin{bmatrix} b_i^e & 0 \\ 0 & b_f^e \end{bmatrix}. \quad (6.57)$$

The constitutive equations at the plastic hinges have introduced the additional variables $\{v^e\}$ in their definition. As a result, it is necessary to provide extra conditions to completely determine the proposed inelastic element. These conditions are given by the satisfaction of equilibrium at the interface sections that separate the hinges from the elastic part of the element. Thus, the following moment equilibrium equation is written:

$$\{M^e\}_* = \{M_H^e\}, \quad (6.58)$$

where equations (6.49) and (6.52) are substituted to write

$$[p^e]^T \{x^e\} - [\hat{k}^e]_r \{\theta^e\} = [k_\alpha^e] \{\theta^e\} + [h_\alpha^e] \{v^e\}. \quad (6.59)$$

This equation is solved for $\{v^e\}$ to get

$$\{v^e\} = [h_\alpha^e]^{-1} \left\{ [p^e]^T \{x^e\} - ([\hat{k}^e]_r + [k_\alpha^e]) \{\theta^e\} \right\}, \quad (6.60)$$

and the first derivative of $\{v^e\}$ with respect to time is

$$\{\dot{v}^e\} = [h_\alpha^e]^{-1} \left\{ [p^e]^T \{\dot{x}^e\} - ([\hat{k}^e]_r + [k_\alpha^e]) \{\dot{\theta}^e\} \right\}. \quad (6.61)$$

Substitution of equations (6.60) and (6.61) into the linearized constitutive law, given in equation (6.56), provides

$$[h_\alpha^e]^{-1} \left\{ [p^e]^T \{\dot{x}^e\} - ([\hat{k}^e]_r + [k_\alpha^e]) \{\dot{\theta}^e\} \right\} = [a^e] \{\dot{\theta}^e\} + [b^e] [h_\alpha^e]^{-1} \left\{ [p^e]^T \{x^e\} - ([\hat{k}^e]_r + [k_\alpha^e]) \{\theta^e\} \right\}. \quad (6.62)$$

Premultiplication by $[h_\alpha^e]$ and after some rearrangement, this equation becomes

$$[p^e]^T \{\dot{x}^e\} - [j^e] \{\dot{\theta}^e\} - [u^e] \{x^e\} + [s^e] \{\theta^e\} = \{0\} \quad (6.63)$$

which is the linear constitutive equation for the e^{th} element. The new element matrices $[j^e]$, $[u^e]$ and $[s^e]$ are defined as follows

$$[j^e] = [\hat{k}^e]_r + [k_\alpha^e] + [h_\alpha^e] [a^e], \quad (6.64)$$

$$[u^e] = [b^e] [p^e]^T, \quad (6.65)$$

$$[s^e] = [b^e] ([\hat{k}^e]_r + [k_\alpha^e]) . \quad (6.66)$$

After performing the matrix operations indicated in equations (6.64), (6.65) and (6.66), the final components of these matrices are:

$$[j^e] = \begin{bmatrix} k_3^e + \alpha_i^e k_{I_i}^e + (1 - \alpha_i^e) k_{I_i}^e a_i^e & k_3^e/2 \\ k_3^e/2 & k_3^e + \alpha_f^e k_{I_f}^e + (1 - \alpha_f^e) k_{I_f}^e a_f^e \end{bmatrix} \quad (6.67)$$

$$[u^e] = \begin{bmatrix} k_6^e b_i^e & k_5^e b_i^e & k_3^e b_i^e & -k_6^e b_i^e & -k_5^e b_i^e & k_3^e b_i^e / 2 \\ k_6^e b_f^e & k_5^e b_f^e & k_3^e b_f^e & -k_6^e b_f^e & -k_5^e b_f^e & k_3^e b_f^e / 2 \end{bmatrix} \quad (6.68)$$

$$[s^e] = \begin{bmatrix} (k_3^e + \alpha_i^e k_{I_i}^e) b_i^e & k_3^e b_i^e / 2 \\ k_3^e b_f^e / 2 & (k_3^e + \alpha_f^e k_{I_f}^e) b_f^e \end{bmatrix} . \quad (6.69)$$

To assemble the element constitutive equations it is necessary to realize that, in equation (6.63), only the vectors $\{x^e\}$ and $\{\dot{x}^e\}$ contain the nodal displacements and velocities compatible with all the elements sharing the same node. On the other hand, the rotations at the plastic hinges are inherent to each element and need no compatibility among the different elements. Thus, the columns of the assembled matrix $[P]^T$, are constructed by adding up the contributions of the appropriate columns of those element matrices, $[p^e]^T$, that share the same nodal displacements. This is commonly known as column superposition. Similarly, the assembled matrix $[U]$ is constructed by column superposition of the element matrices $[u^e]$. The assembled

matrices $[J]$ and $[S]$ need no superposition at all of the elements matrices $[j^e]$ and $[s^e]$. They have just to be placed at the positions dictated by the vector containing the hinge rotations of all the elements or by the vector containing the hinge angular velocity, respectively.

The resulting assembled constitutive equation is

$$[P]^T \{\dot{X}\} - [J] \{\dot{\Theta}\} - [U] \{X\} + [S] \{\Theta\} = \{0\}. \quad (6.70)$$

The dimensions associated to the different matrices can be given in terms of the total number of degrees of freedom n and the total number of potential plastic hinges m , (two per element). Thus, $[P]^T$ and $[U]^T$ are $(m \times n)$ matrices, whereas $[J]^T$ and $[S]^T$ are $(m \times m)$ matrices.

To fully determine these constitutive equations, it is necessary to specify the parameters associated to the Bouc-Wen model. The following section analyzes these parameters and the associated conditions.

6.3.4 Parameters of the Constitutive Model

The parameters involved in the Bouc-Wen constitutive law, should be appropriately selected to model a particular hysteresis loop. Appendix E provides some relationships between the model parameters denoted as \mathcal{A} , \mathcal{B} , \mathcal{C} , η , and α with quantities that also characterize the shape of a particular hysteresis loop. The latter are the initial stiffness k_I , the postyielding or final stiffness k_F , the yielding displacement x_u and/or the yielding force F_u . These relationships are useful to determine the model parameters, and are presented here for the plastic hinges of the proposed element.

Each hinge of the e^{th} element may have different constitutive characteristics. To avoid the repetition of similar equations, this subsection provides only the expressions corresponding to a general hinge denoted as h , which can be the initial or final hinge of the e^{th} element.

In the previous subsection, the moments acting at the initial and final hinges have been given by equations (6.50) and (6.51), which for the general hinge can be written as

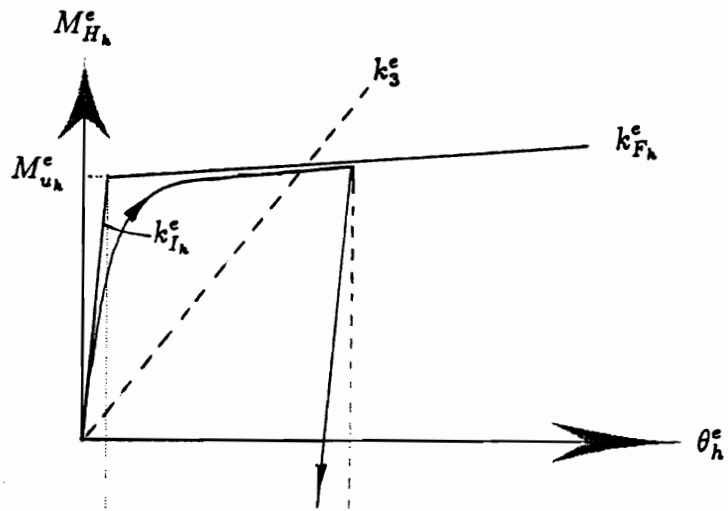
$$M_{H_h}^e = \alpha_h^e k_{I_h}^e \theta_h^e + (1 - \alpha_h^e) k_{I_h}^e v_h^e . \quad (6.71)$$

The moment $M_{H_h}^e$ is defined by two terms, one representing a proportional elastic contribution and the other representing a proportional inelastic contribution. The latter is due to the hysteretic behavior of the auxiliary variable v_h^e with respect to the principal variable θ_h^e . Figure 6.3 shows the relationships between auxiliary variable and hinge rotation, as well as the relationship between moment and rotation, both due to the use of the Bouc-Wen hysteretic model described in appendix E.

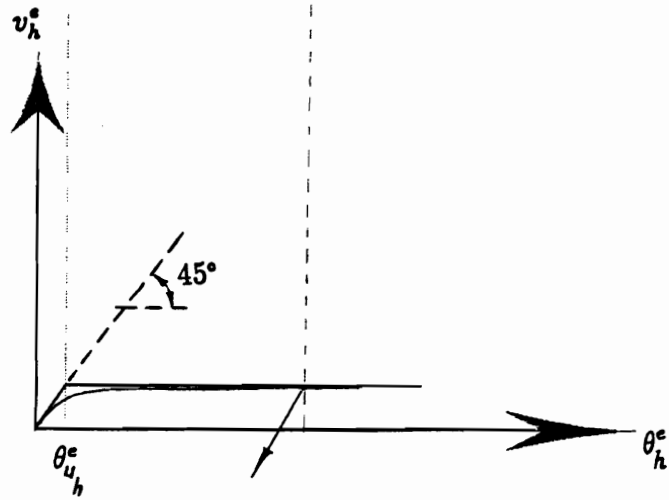
For the hinge at node h , the initial and final rotational stiffnesses are $k_{I_h}^e$ and $k_{F_h}^e$ respectively. It should be recalled that the Bouc-Wen model requires the quantity \mathcal{A}_h^e be equal to 1 for $k_{I_h}^e$ being the initial stiffness. For a perfectly plastic hinge the initial stiffness should be infinity and the post yielding stiffness (final stiffness) should be zero. An approximation to this ideal behavior can be obtained by defining the initial and final stiffnesses as

$$k_{I_h}^e = \bar{\beta}_h^e k_3^e \quad , \quad k_{F_h}^e = \bar{\alpha}_h^e k_3^e \quad (6.72)$$

where k_3^e is given in equation (6.8), $\bar{\beta}_h^e$ is a large number and $\bar{\alpha}_h^e$ is a small number.



(A)



(B)

Figure 6.3: Constitutive law of the plastic hinges: (A) Moment at the hinge vs. hinge rotation, (B) Auxiliary variable vs. hinge rotation

For $\mathcal{A}_h^e = 1$, α_h^e is the ratio between the final and initial stiffnesses,

$$\alpha_h^e = \frac{k_{F_h}^e}{k_{I_h}^e} = \frac{\bar{\alpha}_h^e}{\bar{\beta}_h^e}. \quad (6.73)$$

Therefore, the selection of the factors $\bar{\alpha}_h^e$ and $\bar{\beta}_h^e$, to model the initial and final stiffnesses in equations (6.72), determines automatically the coefficient α_h^e . The hinge moment $M_{H_h}^e$, can be written in terms of $\bar{\alpha}_h^e$, $\bar{\beta}_h^e$ and k_3^e by substituting equation (6.73) into (6.71):

$$M_{H_h}^e = \bar{\alpha}_h^e k_3^e \theta_h^e + (\bar{\beta}_h^e - \bar{\alpha}_h^e) k_3^e v_h^e, \quad (6.74)$$

and the element matrices $[j^e]$ and $[s^e]$ become:

$$[j^e] = \begin{bmatrix} k_3^e [1 + \bar{\alpha}_i^e + (\bar{\beta}_i^e - \bar{\alpha}_i^e) a_i^e] & k_3^e/2 \\ k_3^e/2 & k_3^e [1 + \bar{\alpha}_f^e + (\bar{\beta}_f^e - \bar{\alpha}_f^e) a_f^e] \end{bmatrix} \quad (6.75)$$

$$[s^e] = \begin{bmatrix} (1 + \bar{\alpha}_i^e) k_3^e b_i^e & k_3^e b_i^e/2 \\ k_3^e b_f^e/2 & (1 + \bar{\alpha}_f^e) k_3^e b_f^e \end{bmatrix}. \quad (6.76)$$

On the other, hand the parameters B_h^e and C_h^e can be chosen to be equal to a positive number to model a softening dissipative hysteresis loop, with curved loading paths and straight lines for the unloading paths. In appendix E it has been shown that for such characteristics, the parameter $B_h^e = C_h^e$ is given in term of the yielding rotation $\theta_{u_h}^e$ or in term of the yielding moment $M_{u_h}^e$ as

$$B_h^e = C_h^e = \frac{0.5}{(\theta_{u_h}^e)^{\eta_h^e}} = 0.5 \left(\frac{\bar{\beta}_h^e k_3^e}{M_{u_h}^e} \right)^{\eta_h^e}, \quad (6.77)$$

where $\theta_{u_h}^e$ and $M_{u_h}^e$ are the coordinates at the intersection point of the initial and final stiffnesses. These two quantities are linearly related by the following expression

$$M_{u_h}^e = k_{I_h}^e \theta_{u_h}^e = \bar{\beta}_h^e k_3^e \theta_{u_h}^e, \quad (6.78)$$

Finally, the only remaining parameter, η_h^e , is a positive integer that controls the sharpness of the transition from the initial to the final stiffness, and its value should

be specified by comparisons of the analytic model with the actual hysteresis loops obtained experimentally for a particular material and structure. In general, a value of 1 produces a smooth curved transition, and values of 9 or 11 model hysteresis loops that almost follow the initial and final tangent stiffnesses, by closely approaching their intersection point.

6.4 Response of the Linearized Governing Equations

The n equations of motion given in section 6.2 along with the m linearized constitutive equations presented in section 6.3.3 form the linearized governing equations of the present problem. They are rewritten here as

$$[M] \{\ddot{X}(t)\} + [C] \{\dot{X}(t)\} + [K] \{X(t)\} - [P] \{\Theta(t)\} = -[M] \{T\} \ddot{x}_g(t) \quad (6.79)$$

$$[P]^T \{\dot{X}(t)\} - [J] \{\dot{\Theta}(t)\} - [U] \{X(t)\} + [S] \{\Theta(t)\} = \{0\} . \quad (6.80)$$

where the global matrices $[J]$ and $[S]$ contain four linearization coefficients (a_i^ϵ , b_i^ϵ , a_i^ϵ and b_i^ϵ) for each of the total $m/2$ elements. That is, the system possesses $2m$ linearization coefficients (two per hinge).

The linearization coefficients can be determined by the same gaussian stochastic linearization scheme described in chapter 5. Thus, the resulting expressions, in terms of the response statistics, are:

$$a_h^\epsilon = \mathcal{A}_h^\epsilon - \sigma_{v_h^\epsilon}^{\eta_h^\epsilon} \sqrt{2\eta_h^\epsilon / \pi} \left[B_h^\epsilon \left(\frac{\eta_h^\epsilon - 1}{2} \right)! + C_h^\epsilon (\eta_h^\epsilon)! (\rho_h^\epsilon)^{\eta_h^\epsilon} \Sigma_{a_h^\epsilon} \right] , \quad (6.81)$$

$$b_h^\epsilon = - \sigma_{v_h^\epsilon}^{\eta_h^\epsilon - 1} \sigma_{\dot{\theta}_h^\epsilon} \sqrt{2\eta_h^\epsilon / \pi} \left[\eta_h^\epsilon \rho_h^\epsilon B_h^\epsilon \left(\frac{\eta_h^\epsilon - 1}{2} \right)! + C_h^\epsilon (\eta_h^\epsilon)! (\rho_h^\epsilon)^{\eta_h^\epsilon - 1} \Sigma_{b_h^\epsilon} \right] , \quad (6.82)$$

where η_h^ϵ is a positive odd integer, σ is the standard deviation of its subscripted variable, ρ_h^ϵ is the correlation coefficient between $\dot{\theta}_h^\epsilon$ and v_h^ϵ , and the quantities denoted by $\Sigma_{a_h^\epsilon}$ and $\Sigma_{b_h^\epsilon}$ are the following summations:

$$\Sigma_{a_h^\epsilon} = \sum_{j=0}^{(\eta_h^\epsilon-1)/2} \frac{[(\eta_h^\epsilon - 2j - 1)/2]!}{j! (\eta_h^\epsilon - 2j)!} \frac{[1 - (\rho_h^\epsilon)^2]^j}{(2\rho_h^\epsilon)^{2j}}, \quad (6.83)$$

$$\Sigma_{b_h^\epsilon} = \sum_{j=0}^{(\eta_h^\epsilon-1)/2} \frac{[(\eta_h^\epsilon - 2j - 1)/2]!}{j! (\eta_h^\epsilon - 2j - 1)!} \frac{[1 - (\rho_h^\epsilon)^2]^j}{(2\rho_h^\epsilon)^{2j}}. \quad (6.84)$$

Here, as it was the case in chapter 5, the response statistics, $\sigma_{v_h^\epsilon}$, $\sigma_{\dot{\theta}_h^\epsilon}$ and $\rho_h^\epsilon = E[v_h^\epsilon \dot{\theta}_h^\epsilon]/(\sigma_{v_h^\epsilon} \sigma_{\dot{\theta}_h^\epsilon})$, are not known a priori. As a consequence, an iterative scheme, similar to that described in 5.3, has to be implemented to determine them. In section 6.5, these quantities are further considered.

The governing equations can be written as a system of first order linear differential equations through the use of vector $\{Y(t)\}$, which has $2n + m$ components: n nodal displacements, n nodal velocities and m imposed rotations at the hinges (in that order).

$$\{Y(t)\}^T = \{\{X(t)\}^T, \{\dot{X}(t)\}^T, \{\Theta(t)\}^T\}. \quad (6.85)$$

Thus, equations (6.78) and (6.79) become

$$[L_1] \{\dot{Y}(t)\} + [L_2] \{Y(t)\} = \{F(t)\}. \quad (6.86)$$

Where $\{F(t)\}$ is the forcing vector which first n elements are zero, the following n elements are given in the vector $-[M]\{\mathcal{I}\}\ddot{x}_g(t)$, and the last m elements are also zero. The matrices $[L_1]$ and $[L_2]$ have dimension $(2n + m) \times (2n + m)$, and are defined as:

$$[L_1] = \begin{bmatrix} [I] & [0] & [0] \\ [0] & [M] & [0] \\ [0] & [0] & -[J] \end{bmatrix}, \quad [L_2] = \begin{bmatrix} [0] & -[I] & [0] \\ [K] & [C] & -[P] \\ -[R] & -[P]^T & [S] \end{bmatrix}. \quad (6.87)$$

The decoupling of these $(2n + m)$ equations is obtained by the same approach used for the $(3n)$ equations of section 5.3. That is, by using the properties associated to the right and left eigenanalysis, as well as the linear transformation of coordinates $\{Z(t)\} = [\Phi]\{Y(t)\}$, where $[\Phi]$ is the right modal matrix. The set of eigenvalues, corresponding to systems with subcritically damped modes, contains m real quantities and n pairs of complex conjugates. The real and imaginary parts of the complex eigenvalues are associated to the modal frequencies and damping ratios as indicated by equations (5.24) and (5.25). The resulting $(2n + m)$ decoupled equations are

$$\dot{z}_j(t) + \lambda_j z_j(t) = -\gamma_j \bar{x}_g(t) \quad , \quad j = 1, \dots, 2n + m \quad (6.88)$$

where γ_j is the j^{th} modal participation factor defined in term of the normalized j^{th} left eigenvector $\{\Psi\}_j$,

$$\gamma_j = \{\Psi\}_j^T \begin{Bmatrix} \{0\} \\ [M] \{I\} \\ \{0\} \end{Bmatrix} . \quad (6.89)$$

Finally, the deterministic solution of the first order uncoupled equations leads to the following expression for each component of the response vector $\{Y(t)\}$:

$$y_l(t) = - \sum_{j=1}^{2n+m} q_{lj} \int_0^t e^{-\lambda_j(t-\tau)} \bar{x}_g(\tau) d\tau \quad ; \quad l = 1, \dots, 2n + m \quad (6.90)$$

where q_{lj} is an auxiliary quantity involving the product of the (l, j) component of the right modal matrix and the j^{th} participation factor:

$$q_{lj} = \phi_{lj} \gamma_j . \quad (6.91)$$

6.5 Response Covariance Matrix and Response Spectrum Method

The covariance matrix $[\mathcal{Y}]$ of the response vector $\{Y(t)\}$ can be obtained by adopting the same assumptions and procedure presented in section 5.5. However, it should be noticed that here the quantity of real eigenvalues is m and not n . Consequently, the variables associated to that number should be appropriately considered.

Thus, the resulting expression for the (l, i) component of the covariance matrix is

$$\begin{aligned} \mathcal{Y}_{li} = & \sum_{j=1}^m \sum_{k=1}^m \left(T_{lij}^I J_j + T_{lik}^I J_k \right) + 2 \sum_{j=1}^m \sum_{k=1}^n \left(T_{lij}^{II} J_j + T_{lik}^{III} I_k^d + T_{lij}^{IV} I_k^v \right) \\ & + 4 \sum_{j=1}^n \left(\zeta_{lj} \zeta_{ij} I_j^d + \delta_{lj} \delta_{ij} I_j^v \right) \\ & + 8 \sum_{j=1}^{n-1} \sum_{k=j+1}^n \left(T_{lij}^V I_j^d + T_{lik}^{VI} I_j^v + T_{lij}^{VII} I_k^d + T_{lik}^{VIII} I_k^v \right) . \end{aligned} \quad (6.92)$$

where all the quantities involved have already been defined in chapter 5.

The response spectrum procedure, used in section 5.6, can also be applied here to approximate the (l, i) element of the covariance matrix $[\mathcal{Y}]$, as

$$\begin{aligned} \mathcal{Y}_{li} \approx & \sum_{j=1}^m \sum_{k=1}^m \left(T_{lij}^I \frac{\mathcal{M}_{x_j^I}^2}{\mathcal{P}_{x_j^I}^2} + T_{lik}^I \frac{\mathcal{M}_{x_k^I}^2}{\mathcal{P}_{x_k^I}^2} \right) \\ & + 2 \sum_{j=1}^m \sum_{k=1}^n \left(T_{lij}^{II} \frac{\mathcal{M}_{x_j^I}^2}{\mathcal{P}_{x_j^I}^2} + T_{lik}^{III} \frac{\mathcal{M}_{x_k^{II}}^2}{\mathcal{P}_{x_k^{II}}^2} + T_{lij}^{IV} \frac{\mathcal{M}_{x_k^{II}}^2}{\mathcal{P}_{x_k^{II}}^2} \right) \\ & + 4 \sum_{j=1}^n \left(\zeta_{lj} \zeta_{ij} \frac{\mathcal{M}_{x_j^{II}}^2}{\mathcal{P}_{x_j^{II}}^2} + \delta_{lj} \delta_{ij} \frac{\mathcal{M}_{x_j^{II}}^2}{\mathcal{P}_{x_j^{II}}^2} \right) \\ & + 8 \sum_{j=1}^{n-1} \sum_{k=j+1}^n \left(T_{lij}^V \frac{\mathcal{M}_{x_j^{II}}^2}{\mathcal{P}_{x_j^{II}}^2} + T_{lik}^{VI} \frac{\mathcal{M}_{x_j^{II}}^2}{\mathcal{P}_{x_j^{II}}^2} + T_{lij}^{VII} \frac{\mathcal{M}_{x_k^{II}}^2}{\mathcal{P}_{x_k^{II}}^2} + T_{lik}^{VIII} \frac{\mathcal{M}_{x_k^{II}}^2}{\mathcal{P}_{x_k^{II}}^2} \right) . \end{aligned} \quad (6.93)$$

The quantity $\mathcal{M}_{x_j^I}$ is the relative displacement response spectrum value of the massless oscillator, whereas $\mathcal{M}_{x_j^{II}}$ and $\mathcal{M}_{\dot{x}_j^{II}}$ are the response spectrum values corresponding to the relative displacement and relative velocity, respectively, of the second order oscillator. The quantities $\mathcal{P}_{x_j^I}$, $\mathcal{P}_{x_j^{II}}$, and $\mathcal{P}_{\dot{x}_j^{II}}$ are the peak factors associated to the above variables.

The response spectrum approach can also be used to obtain the maximum response value \mathcal{M}_R , of a certain response quantity $R(t)$, which is linearly related to the response vector $\{Y(t)\}$. That is,

$$\mathcal{M}_R \approx \sqrt{\{\mathcal{R}\}^T (\mathcal{P}_R^2 [\mathcal{Y}]) \{\mathcal{R}\}}. \quad (6.94)$$

where \mathcal{P}_R is the peak factor of the response $R(t)$, $\{\mathcal{R}\}$ is the constant vector corresponding to the linear transformation $R(t) = \{\mathcal{R}\}^T \{Y(t)\}$, and the (l, i) component of $\mathcal{P}_R^2[\mathcal{Y}]$ is approximated by assuming equal peak factors as

$$\begin{aligned} \mathcal{P}_R^2 \mathcal{Y}_{li} &\approx \sum_{j=1}^m \sum_{k=1}^m \left(T_{lijk}^I \mathcal{M}_{x_j^I}^2 + T_{likj}^I \mathcal{M}_{x_k^I}^2 \right) \\ &+ 2 \sum_{j=1}^m \sum_{k=1}^n \left(T_{lijk}^{II} \mathcal{M}_{x_j^I}^2 + T_{lijk}^{III} \mathcal{M}_{x_k^{II}}^2 + T_{lijk}^{IV} \mathcal{M}_{\dot{x}_k^{II}}^2 \right) \\ &+ 4 \sum_{j=1}^n \left(\zeta_{lj} \zeta_{mj} \mathcal{M}_{x_j^{II}}^2 + \delta_{lj} \delta_{mj} \mathcal{M}_{\dot{x}_j^{II}}^2 \right) \\ &+ 8 \sum_{j=1}^{n-1} \sum_{k=j+1}^n \left(T_{lijk}^V \mathcal{M}_{x_j^{II}}^2 + T_{lijk}^{VI} \mathcal{M}_{\dot{x}_j^{II}}^2 + T_{lijk}^{VII} \mathcal{M}_{x_k^{II}}^2 + T_{lijk}^{VIII} \mathcal{M}_{\dot{x}_k^{II}}^2 \right). \end{aligned} \quad (6.95)$$

The final expressions presented in this section are similar to those fully developed in chapter 5. However, the former can be easily deduced from the latter by considering m real eigenproperties in lieu of n , and by the adequate renaming of the subscripts.

6.6 Response Statistics Required by the Linearization Coefficients

Equations (6.81)–(6.84) provide the linearization coefficients as functions of the standard deviations and correlation coefficients corresponding to variables v_h^e and $\dot{\theta}_h^e$. Such variables are not contained in the response vector $\{Y(t)\}$. However, they are linear functions of its elements.

The auxiliary variables v_i^e and v_j^e , of the e^{th} element, are expressed in terms of the nodal displacements as well as of the rotations at the hinges, in equation (6.60). On the other hand, equation (6.63) can be solved for $\{\dot{\theta}^e\}$ to get

$$\{\dot{\theta}^e\} = [j^e]^{-1} [p^e]^T \{\dot{x}^e\} - [j^e]^{-1} [u^e] \{x^e\} + [j^e]^{-1} [s^e] \{\theta^e\}, \quad (6.96)$$

which is a linear function the nodal displacements, the nodal velocities, and the rotations at the hinges. The inverse of the (2×2) symmetric matrix $[j^e]$, can easily be written in terms of the elements of $[j^e]$ as

$$[j^e] = \begin{bmatrix} j_{11}^e & j_{12}^e \\ j_{12}^e & j_{22}^e \end{bmatrix}, \quad [j^e]^{-1} = \frac{1}{j_{11}^e j_{22}^e - (j_{12}^e)^2} \begin{bmatrix} j_{22}^e & -j_{12}^e \\ -j_{12}^e & j_{11}^e \end{bmatrix}. \quad (6.97)$$

For zero mean processes, the statistics $\sigma_{v_k^e}$, $\sigma_{\dot{\theta}_k^e}$ and ρ_h^e are defined as follows

$$\sigma_{v_k^e} = \sqrt{E[(v_k^e)^2]}, \quad \sigma_{\dot{\theta}_k^e} = \sqrt{E[(\dot{\theta}_k^e)^2]}, \quad \rho_h^e = \frac{E[v_h^e \dot{\theta}_h^e]}{\sigma_{v_k^e} \sigma_{\dot{\theta}_k^e}}. \quad (6.98)$$

The variances $\sigma_{v_k^e}^2$ and $\sigma_{\dot{\theta}_k^e}^2$ are the diagonal elements of the (2×2) covariance matrices $E[\{v^e\}\{v^e\}^T]$ and $E[\{\dot{\theta}^e\}\{\dot{\theta}^e\}^T]$, respectively. On the other hand, the expected values $E[v_h^e \dot{\theta}_h^e]$ are given by the diagonal elements of the (2×2) cross covariance matrix $E[\{v^e\}\{\dot{\theta}^e\}^T]$. Substitution of equations (6.60) and (6.96) into the above expected values, provides the expressions of these covariance matrices for the e^{th} element.

In particular, the covariance matrix of vector $\{v^e\}$ is

$$E \left[\{v^e\} \{v^e\}^T \right] = E \left[[h_\alpha^e]^{-1} \left\{ [p^e]^T \{x^e\} - [\hat{k}^e]_{r+\alpha} \{\theta^e\} \right\} \right. \\ \left. \times \left\{ \{x^e\}^T [p^e] - \{\theta^e\}^T [\hat{k}^e]_{r+\alpha} \right\} [h_\alpha^e]^{-1} \right] , \quad (6.99)$$

where the (2×2) symmetric matrix $[\hat{k}^e]_{r+\alpha}$ is given by

$$[\hat{k}^e]_{r+\alpha} = [\hat{k}^e]_r + [k_\alpha^e] \quad (6.100)$$

Distribution of the expected values in equation (6.99) produces

$$E \left[\{v^e\} \{v^e\}^T \right] = [h_\alpha^e]^{-1} \left\{ [p^e]^T [E_{xx}^e] [p^e] - [\hat{k}^e]_{r+\alpha} [E_{\theta x}^e] [p^e] - [p^e]^T [E_{x\theta}^e] [\hat{k}^e]_{r+\alpha} \right. \\ \left. + [\hat{k}^e]_{r+\alpha} [E_{\theta\theta}^e] [\hat{k}^e]_{r+\alpha} \right\} [h_\alpha^e]^{-1} , \quad (6.101)$$

where the element matrices $[E_{xx}^e]$ and $[E_{\theta\theta}^e]$, are the following covariance matrices:

$$[E_{xx}^e] = E[\{x^e\} \{x^e\}^T] , \quad [E_{\theta\theta}^e] = E[\{\theta^e\} \{\theta^e\}^T] ; \quad (6.102)$$

and $[E_{\theta x}^e]$ and $[E_{x\theta}^e]$ are the following cross covariance matrices:

$$[E_{\theta x}^e] = E[\{\theta^e\} \{x^e\}^T] , \quad [E_{x\theta}^e] = E[\{x^e\} \{\theta^e\}^T] . \quad (6.103)$$

Similarly, the matrices $E \left[\{\dot{\theta}^e\} \{\dot{\theta}^e\}^T \right]$ and $E \left[\{v^e\} \{\dot{\theta}^e\}^T \right]$ can be expressed as:

$$E \left[\{\dot{\theta}^e\} \{\dot{\theta}^e\}^T \right] = [j_\alpha^e]^{-1} \left\{ [u^e] \left([E_{xx}^e] [u^e]^T - [E_{x\dot{z}}^e] [p^e] - [E_{x\theta}^e] [s^e]^T \right) \right. \\ \left. + [p^e]^T \left(- [E_{\dot{z}x}^e] [u^e]^T + [E_{\dot{z}\dot{z}}^e] [p^e] + [E_{\dot{z}\theta}^e] [s^e]^T \right) \right. \\ \left. + [s^e] \left(- [E_{\theta x}^e] [u^e]^T + [E_{\theta\dot{z}}^e] [p^e] + [E_{\theta\theta}^e] [s^e]^T \right) \right\} [j_\alpha^e]^{-1} , \quad (6.104)$$

$$E \left[\{v^e\} \{\dot{\theta}^e\}^T \right] = [h_\alpha^e]^{-1} \left\{ [p^e]^T \left(- [E_{xx}^e] [u^e]^T + [E_{x\dot{z}}^e] [p^e] + [E_{x\theta}^e] [s^e]^T \right) \right. \\ \left. + [\hat{k}^e]_{r+\alpha} \left([E_{\theta x}^e] [u^e]^T - [E_{\theta\dot{z}}^e] [p^e] - [E_{\theta\theta}^e] [s^e]^T \right) \right\} [j_\alpha^e]^{-1} , \quad (6.105)$$

where the quantities $[E_{\star\bullet}^e]$ are covariance or cross covariance matrices of the vectors indicated by the subscripts \star and \bullet .

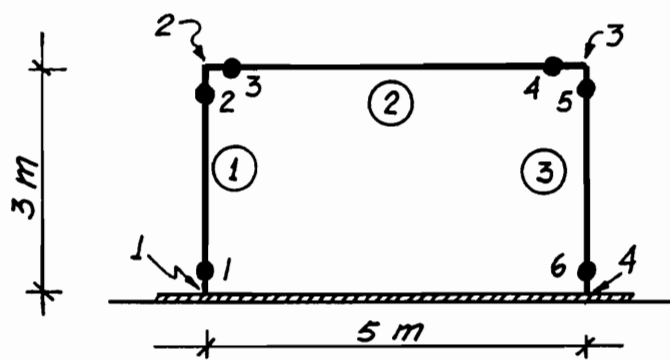
It can be seen that the matrices given by equations (6.101), (6.104) and (6.105), are linear combinations of the element matrices $[E_{\star\bullet}^e]$, which components are also components of the global response covariance matrix $[\mathcal{Y}]$. It should be noticed that these element matrices do not need to be calculated completely since only their diagonal elements are required by the expressions of the linearization coefficients.

6.7 Numerical Results

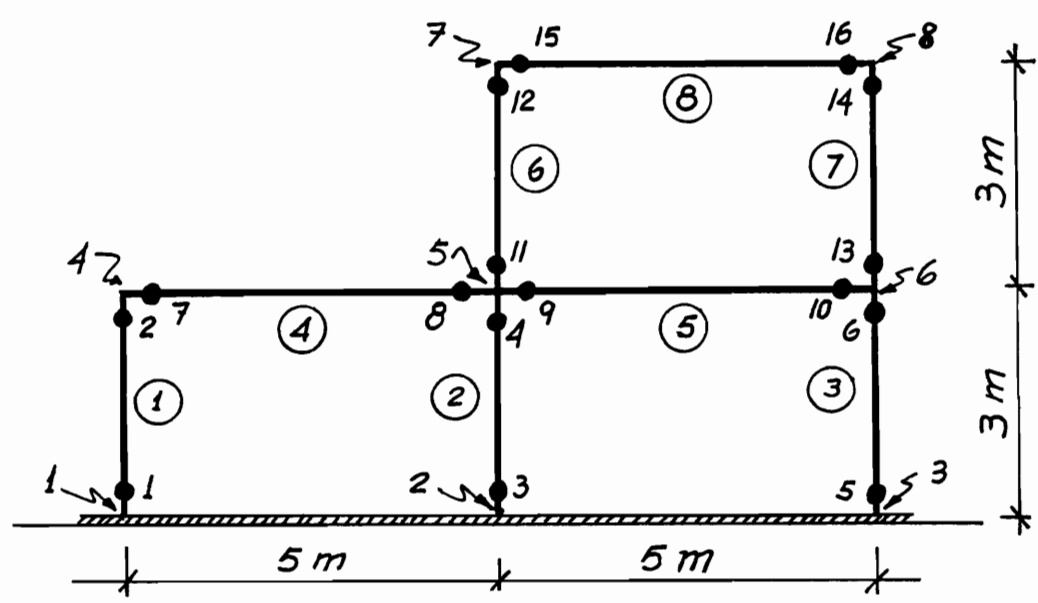
In this section we present numerical results obtained by the proposed approach. For presentation of these results, all calculated responses have been normalized with respect to the response values corresponding to a perfectly elastic structure.

Two different steel structures have been considered. Figures 6.4 (A) and (B) show their dimensions and finite element discretizations. The potential plastic hinges are indicated by filled circles and the different nodes are indicated by arrows.

The single-story structure has 6 degrees of freedom and it has been discretized by 3 frame elements with a total of 6 potential plastic hinges. Its three elements possess the same structural shape, S4x8.5. Due to the symmetry of this structure, it is especially useful to partially check the numerical results. The second structure is a two-story frame with 15 degrees of freedom and discretized by 8 elements with a total of 16 plastic hinges. The same shape used previously is also employed here for the elements 1, 4, 5, 6, 7 and 8, whereas for elements 2 and 3 the stronger S8x23



(A)



(B)

Figure 6.4: Schematic of the structures considered in the numerical results: (A) Single-story frame, (B) Two-story frame

shape is utilized.

The seismic excitation has been defined in two forms: (1) by the ground response spectra, used in chapter 5 and calculated for 100 artificial time histories, and (2) by a Kanai-Tajimi type of spectral density function. In both cases the maximum ground acceleration is 0.5 g.

Figures 6.5, 6.6, and 6.7 provide results for the single-story structure. All hinges are assumed to have the same constitutive characteristics. Thus, the following parameters have been chosen to model their a quasi-plastic constitutive: $\bar{\alpha}_h^e = 10^{-4}$, $\bar{\beta}_h^e = 10^4$, which provide the following stiffness ratio $\alpha_h^e = k_{F_h}^e/k_{I_h}^e = 10^{-8}$. The parameters \mathcal{A}_h^e are considered to be equal to 1, and the parameters $\mathcal{B}_h^e = \mathcal{C}_h^e$ are given by equation (6.77) in terms of the yielding moments at the hinges $M_{u_h}^e$. The exponent parameters are equal to 1.

Figure 6.5 shows the increase of the normalized equivalent damping ratios as the yielding moment at the plastic hinges is decreased. This decrement is equivalent to an increase in the ductilities. This fact has also been observed in the previous chapter for shear buildings, and it is due to the necessity of the equivalent linear structure to dissipate energy in order to approximate the actual nonlinear hysteretic structure. On the other hand, the frequencies of the equivalent linear structures remain almost constant as the yielding moment decreases.

Figure 6.6 shows some normalized maximum forces as the yielding moment at the plastic hinges is decreased. It is seen that these forces decrease as the ductility levels increase (or the yielding moments at the hinges diminish). This is in complete agreement with the behavior of plastic structures.

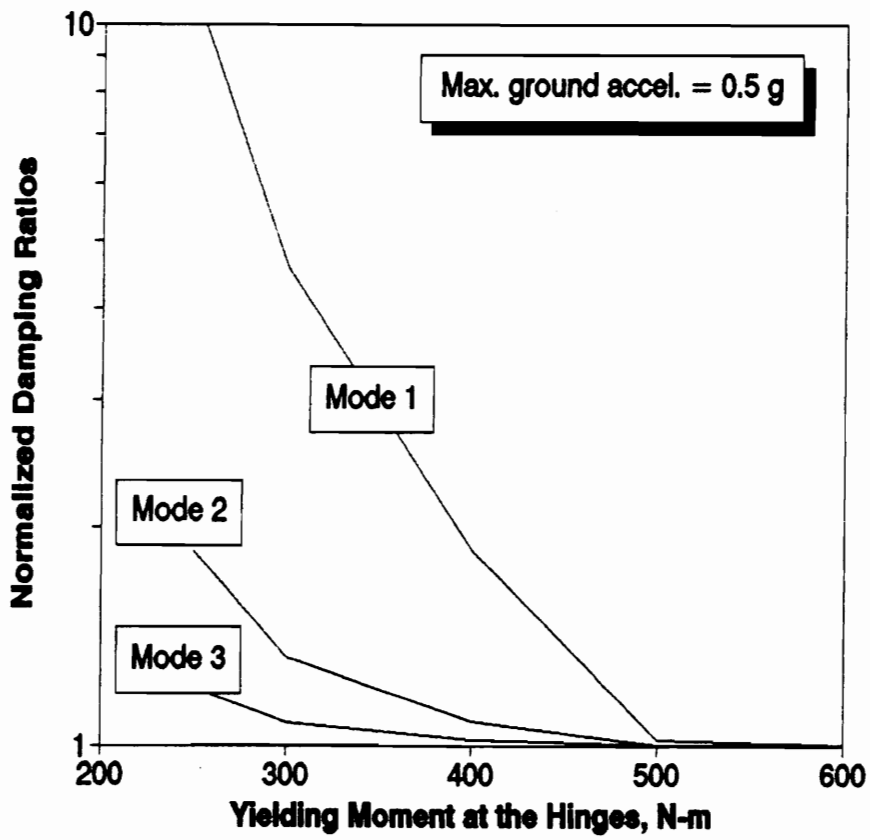


Figure 6.5: Normalized equivalent damping ratios of the single-story frame for different levels of yielding moment at the plastic hinges

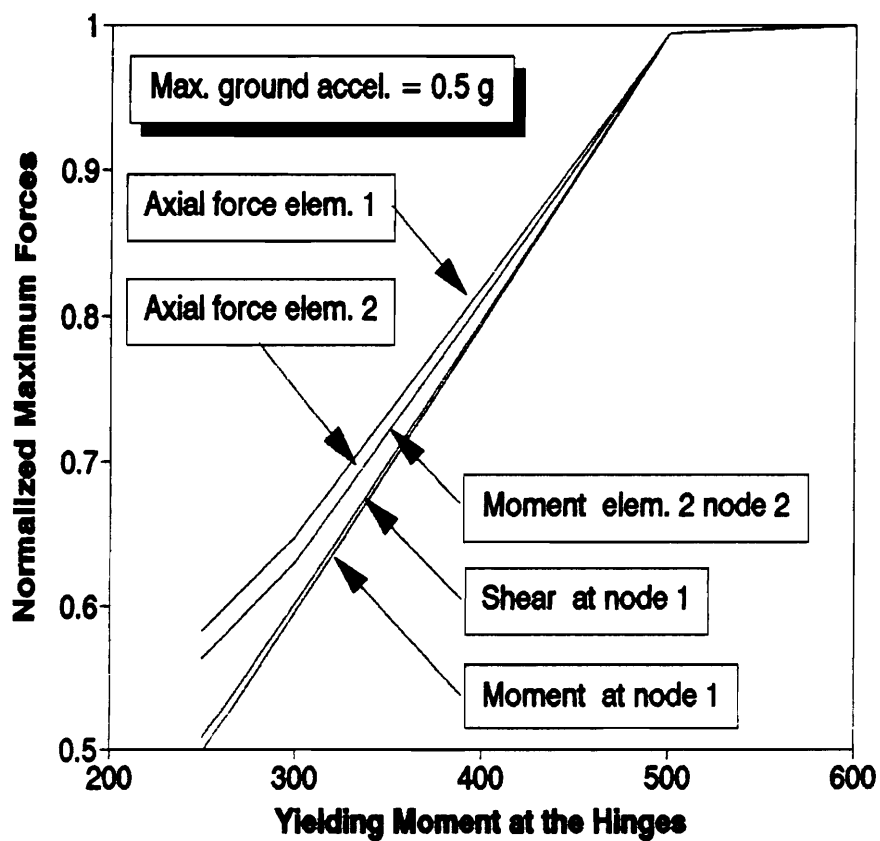


Figure 6.6: Normalized maximum shear forces of the single-story frame for different levels of yielding moment at the plastic hinges

Figure 6.7 is for a an excitation defined by a Kanai-Tajimi spectral density function. The normalized standard deviation of the horizontal drift is plotted against several values of the yielding moments at the plastic hinges. As expected, such drift increases as the structure penetrates into the plastic range.

A similar behavior has been observed for the two-story structure. In this case only the exponent parameter has been changed to 3. All other parameters remain the same as those used by the single-story structure. As the size of the structure and the ductilities increased, it became difficult to achieve convergence in the results. To facilitate the initial guess of the linearization coefficients, it is noted that the same limits provided in chapter 5 are still valid for the present case. Figure 6.8 shows the behavior of the linearization coefficient a_i^e for hinges 1, 3 and 5 as the yielding moment of the hinges is decreased. It is relevant to mention, that the ultimate lower values for these coefficients are still given in terms of the exponent parameter by the expression $\eta/(\eta + 1)$. In this case such limit is 0.75 and figure 6.8 clearly shows that fact.

Finally, figure 6.9 shows the variation of the shears forces at the base of elements 1, 3 and 5. Again, such forces decrease as the ductility increases.

6.8 Conclusions

A response spectrum approach has been presented to approximate the seismic design response of two-dimensional frames with potential plastic hinges. The nonlinearities are concentrated at determined regions, plastic hinges, and it is due to the nonlinear behavior of the materials. The Bouc-Wen constitutive law has been

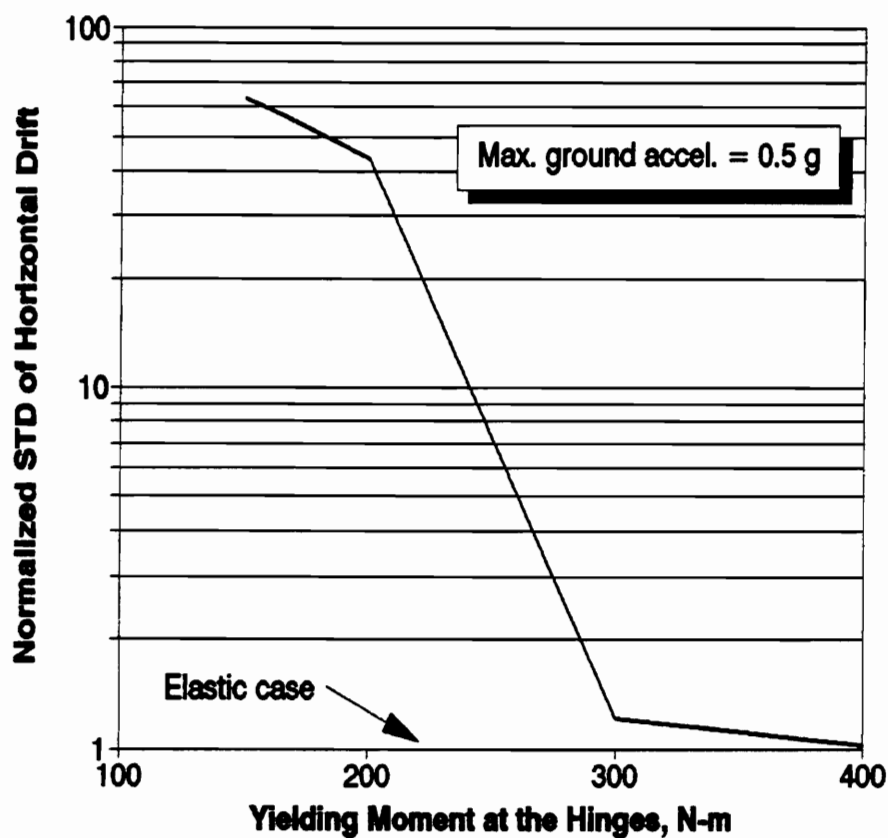


Figure 6.7: Normalized standard deviation of the horizontal drift of the single-story frame for different levels of yielding moment at the plastic hinges. The input is defined by a Kanai-Tajimi spectral density function

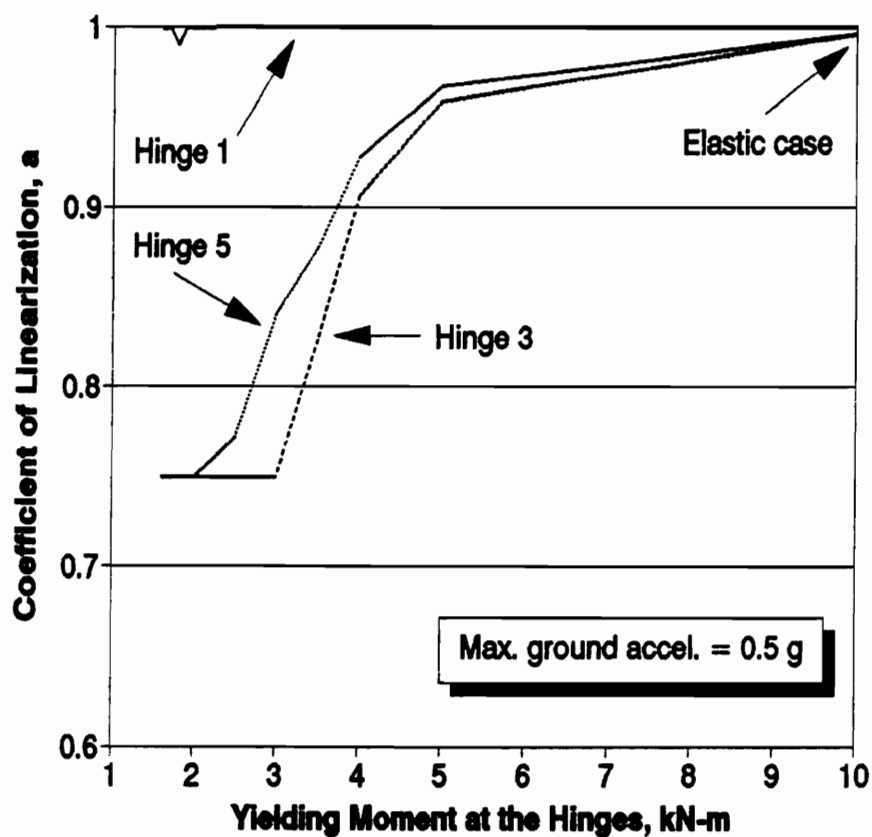


Figure 6.8: Coefficient of linearization, a_i , of the two-story frame for different levels of yielding moment at the plastic hinges

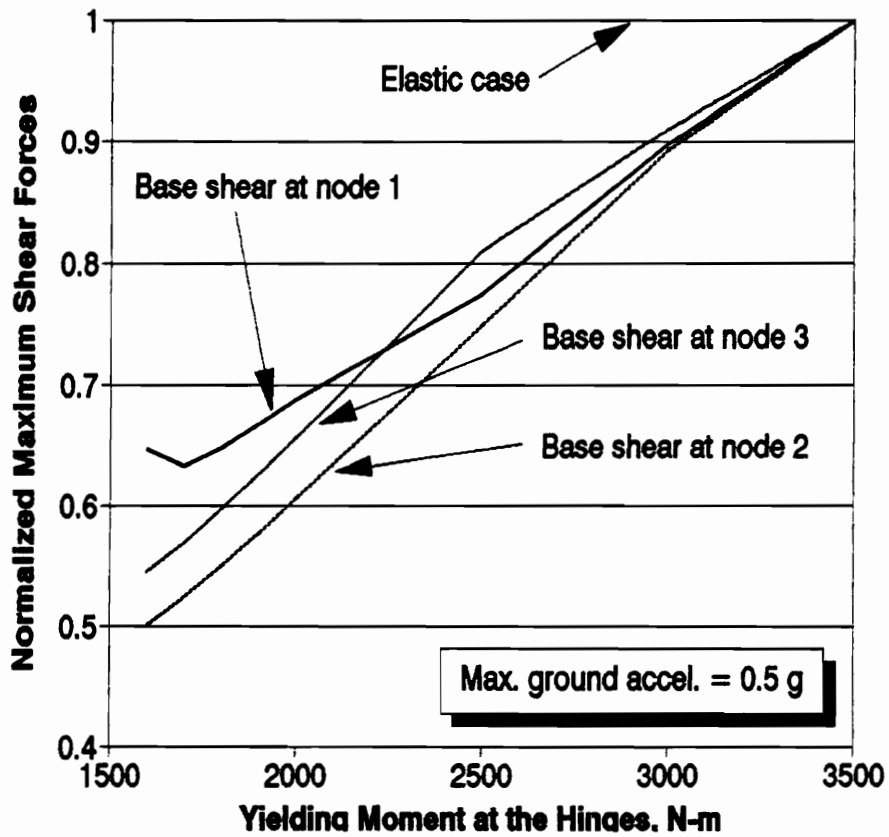


Figure 6.9: Normalized maximum shears forces at the base of the three columns of the two-story structure for different levels of yielding moment at the plastic hinges

proposed to model the plastic hinges.

The formulation leading to the proposed nonlinear equations of motion is provided in detail. Stochastic equivalent linearization is used to determine an equivalent system of linear equations which is solved by a generalized eigenanalysis. The real and complex eigenproperties are combined by the same modal combination rule presented in chapter 5 for shear buildings. As a consequence, the same ground response spectra are required. That is, the commonly used pseudo acceleration and relative velocity spectra of second order oscillators, as well as the relative displacement spectrum of the massless oscillator.

The numerical results show that the responses due to the actual nonlinear behavior can be approximated by the proposed approach. However, for larger size structures with large ductilities the convergence in the linearization process may become difficult to achieve. The qualitative characteristics of the response observed in the previous chapter were also observed here for the frames. The errors associated with the assumption of Gaussian density function for the response still remain in the response calculated in this chapter.

Chapter 7

Summary and Recommendations for Future Work

This work presents various approaches to calculate the stochastic and seismic design response of linear and nonlinear structures. The approaches developed for the linear structures are presented in chapters 2, 3 and 4 whereas those for nonlinear structures in chapter 5 and 6. The details of the formulation and more specific conclusions pertaining to the proposed approaches are presented in their respective chapters. Here we only summarize the work, provide general conclusions and suggest future extensions.

For linear structures, a response spectrum method, based on the proposed modified mode displacement technique is presented for classically damped as well as non-classically damped structures. The approach is especially designed to include the pseudostatic contribution of the truncated modes in the dynamic and stochastic analyses. The numerical results, as well as the comparison against commonly used methods show the ability of the technique to capture the contribution of the truncated modes without using them in the analysis. The proposed response spectrum

approaches combine the efficiency of the mode acceleration-based response spectrum approaches with the practical advantage of the mode displacement-based response spectrum approach. It uses the more common pseudo-acceleration response spectra in lieu of the relative acceleration spectra. Future work should be able to extend the approach to general systems like the linearized systems presented in chapters 5 and 6. Also its extension to the generation of in-structure response spectra for the calculation of secondary structures is feasible. A further generalization of this approach, to improve even further the calculation of the contribution of the truncated modes, is also presented in this work for structures subjected to stochastic loads defined in terms of power spectral density functions. This technique is called as the force derivative method since it is based on the successive integration by parts of the Duhamel integral of the response, and higher derivatives of the forcing function are required for each integration. It presents a fast calculation scheme due to the use of recursive formulas to calculate the boundary terms generated by the integrations by parts. Future work is expected to extend the approach to non-classically damped structures as well as to general structures.

For nonlinear structures, a response spectrum method is proposed to approximate the response of hysteretic shear buildings as well as of two-dimensional frames with plastic hinges. The approach is based in the well known stochastic linearization technique. The proposed method requires that the seismic input be defined in terms of pseudo-acceleration and relative velocity spectra as well as a response spectrum of the first order oscillator. The approach can be utilized as a useful numerical tool for preliminary evaluation of a design incorporating inelastic behavior of structures, especially for shear building structures. However, for two-dimensional frames with plastic hinges, difficulty in achieving convergence may be encountered in the cal-

ulation process. A simulation study provided a quantitative measure of the error introduced by the linearization technique. It is believed that the errors are primarily due to the assumption of Gaussian density functions for the responses. Future work using more realistic assumptions for the density functions are suggested to improve the accuracy of the equivalent linearization technique.

Although, the equivalent linear approach may not be able to provide very accurate values for the design response, compared to the time history analyses, the author feels that it still is the best workable tool for seismic evaluation of hysteretic structures.

Appendix A

Common Partial Fractions

A.1 Case I

This section determines the partial fraction coefficients $T_{jk}^{(1)}$ and $T_{jk}^{(2)}$ corresponding to the following expansion

$$P^I(\omega) |G_j^c(\omega)|^2 |G_k^c(\omega)|^2 = T_{jk}^{(1)} |G_j^c(\omega)|^2 + T_{jk}^{(2)} |G_k^c(\omega)|^2 , \quad (\text{A.1})$$

where $P^I(\omega)$ is a second degree polynomial in ω with coefficients denoted as p_i^I

$$P^I(\omega) = p_0^I + p_2^I \omega^2 , \quad (\text{A.2})$$

$G_j^c(\omega)$ is the stationary frequency response function of a first order oscillator (massless oscillator)

$$G_j^c(\omega) = [\lambda_j^r + i\omega]^{-1} \quad (\text{A.3})$$

with its squared modulus given by

$$|G_j^c(\omega)|^2 = G_j^c(\omega) G_j^{cc}(\omega) = [(\lambda_j^r)^2 + \omega^2]^{-1} . \quad (\text{A.4})$$

Equation (A.1) can be solved for $P^I(\omega)$ to get

$$P^I(\omega) = \frac{T_{jk}^{(1)}}{|G_k^c(\omega)|^2} + \frac{T_{jk}^{(2)}}{|G_j^c(\omega)|^2}. \quad (\text{A.5})$$

Substitution of equation (A.4) into (A.5) produces

$$P^I(\omega) = [T_{jk}^{(1)}(\lambda_k^r)^2 + T_{jk}^{(2)}(\lambda_j^r)^2]\omega^0 + [T_{jk}^{(1)} + T_{jk}^{(2)}]\omega^2. \quad (\text{A.6})$$

A system of two equations with two unknowns can be written by equating the coefficients of the terms with equal powers of ω in equations (A.2) and (A.6)

$$\begin{bmatrix} (\lambda_k^r)^2 & (\lambda_j^r)^2 \\ 1 & 1 \end{bmatrix} \begin{Bmatrix} T_{jk}^{(1)} \\ T_{jk}^{(2)} \end{Bmatrix} = \begin{Bmatrix} p_0^I \\ p_2^I \end{Bmatrix}. \quad (\text{A.7})$$

The determinant of which is

$$\Delta_{jk}^I = (\lambda_k^r)^2 - (\lambda_j^r)^2. \quad (\text{A.8})$$

Solving the above system, the coefficients $T_{jk}^{(1)}$ and $T_{jk}^{(2)}$ become

$$T_{jk}^{(1)} = [p_0^I - p_2^I(\lambda_j^r)^2](\Delta_{jk}^I)^{-1} \quad (\text{A.9})$$

$$T_{jk}^{(2)} = [p_2^I(\lambda_k^r)^2 - p_0^I](\Delta_{jk}^I)^{-1} = -[p_0^I - p_2^I(\lambda_k^r)^2](\Delta_{jk}^I)^{-1} \quad (\text{A.10})$$

Since $\Delta_{jk}^I = -\Delta_{kj}^I$, the coefficient $T_{jk}^{(2)}$ can also be written as

$$T_{jk}^{(2)} = T_{kj}^{(1)} \quad (\text{A.11})$$

It can be noticed that the partial fraction coefficients are not determined when the determinant is zero, that is when $|\lambda_j^r| = |\lambda_k^r|$.

A.2 Case II

This section provides the partial fraction coefficients $T_{jk}^{(3)}$, $T_{jk}^{(4)}$ and $T_{jk}^{(5)}$ corresponding to the following expansion

$$P^{II}(\omega) |G_j^c(\omega)|^2 |H_k^c(\omega)|^2 = T_{jk}^{(3)} |G_j^c(\omega)|^2 + (T_{jk}^{(4)} + \omega^2 T_{jk}^{(5)}) |H_k^c(\omega)|^2 \quad (\text{A.12})$$

where $P^{II}(\omega)$ is a fourth degree polynomial in ω with coefficients denoted as p_i^{II}

$$P^{II}(\omega) = p_0^{II} + p_2^{II} \omega^2 + p_4^{II} \omega^4, \quad (\text{A.13})$$

$G_j^c(\omega)$ and its squared modulus are respectively given by equations (A.3) and (A.4) respectively. Whereas $H_k^c(\omega)$, is the stationary frequency response function of a second order oscillator:

$$H_k^c(\omega) = [\omega_k^2 - \omega^2 + 2i\beta_k \omega_k \omega]^{-1}. \quad (\text{A.14})$$

with squared modulus

$$|H_k^c(\omega)|^2 = H_k^c(\omega) H_k^{cc}(\omega) = [\omega_k^4 + (4\beta_k^2 - 2)\omega_k^2 \omega^2 + \omega^4]^{-1}. \quad (\text{A.15})$$

From equation (A.12), $P^{II}(\omega)$ can be written as

$$P^{II}(\omega) = \frac{T_{jk}^{(3)}}{|H_k^c(\omega)|^2} + \frac{(T_{jk}^{(4)} + \omega^2 T_{jk}^{(5)})}{|G_j^c(\omega)|^2}, \quad (\text{A.16})$$

where substitution of equations (A.4) and (A.15) produces

$$\begin{aligned} P^{II}(\omega) = & [T_{jk}^{(3)} \omega_k^4 + T_{jk}^{(4)} (\lambda_j^r)^2] \omega^0 \\ & + [(4\beta_k^2 - 2) \omega_k^2 T_{jk}^{(3)} + T_{jk}^{(4)} + (\lambda_j^r)^2 T_{jk}^{(5)}] \omega^2 + [T_{jk}^{(3)} + T_{jk}^{(5)}] \omega^4, \end{aligned} \quad (\text{A.17})$$

A system of three equations with three unknowns can now be constructed by equating the coefficients of the terms with equal powers of ω in equations (A.13) and (A.17)

$$p_0^{II} = T_{jk}^{(3)} \omega_k^4 + T_{jk}^{(4)} (\lambda_j^r)^2, \quad (\text{A.18})$$

$$p_2^{II} = (4\beta_k^2 - 2)\omega_k^2 T_{jk}^{(3)} + T_{jk}^{(4)} + (\lambda_j^r)^2 T_{jk}^{(5)}, \quad (\text{A.19})$$

$$p_4^{II} = T_{jk}^{(3)} + T_{jk}^{(5)}. \quad (\text{A.20})$$

From equation (A.20) the coefficient $T_{jk}^{(5)}$ can be written as a function of the coefficient $T_{jk}^{(3)}$:

$$T_{jk}^{(5)} = p_4^{II} - T_{jk}^{(3)} \quad (\text{A.21})$$

and by substituting this equation into (A.18) and (A.19) the following system is written

$$\begin{bmatrix} [(4\beta_k^2 - 2)\omega_k^2 - (\lambda_j^r)^2] & 1 \\ \omega_k^4 & (\lambda_j^r)^2 \end{bmatrix} \begin{Bmatrix} T_{jk}^{(3)} \\ T_{jk}^{(4)} \end{Bmatrix} = \begin{Bmatrix} p_2^{II} - (\lambda_j^r)^2 p_4^{II} \\ p_0^{II} \end{Bmatrix}, \quad (\text{A.22})$$

with determinant given by

$$\begin{aligned} \Delta_{jk}^{II} &= [(4\beta_k^2 - 2)\omega_k^2 - (\lambda_j^r)^2] (\lambda_j^r)^2 - \omega_k^4 \\ &= 4\beta_k^2 \omega_k^2 (\lambda_j^r)^2 - [(\lambda_j^r)^2 + \omega_k^2]^2. \end{aligned} \quad (\text{A.23})$$

For $\lambda_j^r > 0$, $\omega_k > 0$ and $0 \leq \beta_k \leq 1$, the determinant will vanish only if $\beta_k = 1$ and $\lambda_j^r = \omega_k$. In such a case the partial fraction coefficients become undetermined. For nonzero determinant, the solution of the system provides

$$T_{jk}^{(3)} = \left[(p_2^{II} - (\lambda_j^r)^2 p_4^{II}) (\lambda_j^r)^2 - p_0^{II} \right] (\Delta_{jk}^{II})^{-1} \quad (\text{A.24})$$

$$T_{jk}^{(4)} = \left[\{(4\beta_k^2 - 2)\omega_k^2 - (\lambda_j^r)^2\} p_0^{II} - \{p_2^{II} - (\lambda_j^r)^2 p_4^{II}\} \omega_k^4 \right] (\Delta_{jk}^{II})^{-1} \quad (\text{A.25})$$

The remaining coefficient, $T_{jk}^{(5)}$, can be obtained by substituting equation (A.24) into equation (A.21).

If the original expression to be expanded were $P^{II}(\omega) |G_k^c(\omega)|^2 |H_j^c(\omega)|^2$, where the subscripts have been interchanged, the corresponding partial fraction coefficients $T_{kj}^{(3)}$, $T_{kj}^{(4)}$ and $T_{kj}^{(5)}$ can be obtained from equations (A.24), (A.25) and (A.21) by considering the appropriate change of subscripts $j \leftrightarrow k$.

A.3 Case III

This section presents the partial fraction coefficients $T_{jk}^{(6)}$, $T_{jk}^{(7)}$, $T_{jk}^{(8)}$ and $T_{jk}^{(9)}$ corresponding to the following expansion

$$P^{III}(\omega) |H_j^c(\omega)|^2 |H_k^c(\omega)|^2 = (T_{jk}^{(6)} + \omega^2 T_{jk}^{(7)}) |H_j^c(\omega)|^2 + (T_{jk}^{(8)} + \omega^2 T_{jk}^{(9)}) |H_k^c(\omega)|^2 \quad (\text{A.26})$$

where $P^{III}(\omega)$ is a sixth degree polynomial in ω with coefficients denoted as p_i^{III}

$$P^{III}(\omega) = p_0^{III} + p_2^{III} \omega^2 + p_4^{III} \omega^4 + p_6^{III} \omega^6, \quad (\text{A.27})$$

$H_k^c(\omega)$ and its squared modulus are given by equation (A.14) and (A.15) respectively.

From equation (A.26), $P^{III}(\omega)$ can be written as

$$P^{III}(\omega) = \frac{(T_{jk}^{(6)} + \omega^2 T_{jk}^{(7)})}{|H_k^c(\omega)|^2} + \frac{(T_{jk}^{(8)} + \omega^2 T_{jk}^{(9)})}{|H_j^c(\omega)|^2}, \quad (\text{A.28})$$

where equation (A.15) can be substituted to get

$$\begin{aligned} P^{III}(\omega) = & [T_{jk}^{(6)} \omega_k^4 + T_{jk}^{(8)} \omega_j^4] \omega^0 \\ & + [(4\beta_k^2 - 2) \omega_k^2 T_{jk}^{(6)} + T_{jk}^{(7)} \omega_k^4 + (4\beta_j^2 - 2) \omega_j^2 T_{jk}^{(8)} + T_{jk}^{(9)} \omega_j^4] \omega^2 \\ & + [T_{jk}^{(6)} + (4\beta_k^2 - 2) \omega_k^2 T_{jk}^{(7)} + T_{jk}^{(8)} + (4\beta_j^2 - 2) \omega_j^2 T_{jk}^{(9)}] \omega^4 \\ & + [T_{jk}^{(7)} + T_{jk}^{(9)}] \omega^6. \end{aligned} \quad (\text{A.29})$$

A system of four equations with the four coefficients as unknowns, can be written by equating the coefficients of the terms with equal powers of ω in equations (A.27) and (A.29)

$$p_0^{III} = T_{jk}^{(6)} \omega_k^4 + T_{jk}^{(8)} \omega_j^4 \quad (\text{A.30})$$

$$p_2^{III} = (4\beta_k^2 - 2) \omega_k^2 T_{jk}^{(6)} + \omega_k^4 T_{jk}^{(7)} + (4\beta_j^2 - 2) \omega_j^2 T_{jk}^{(8)} + \omega_j^4 T_{jk}^{(9)} \quad (\text{A.31})$$

$$p_4^{III} = T_{jk}^{(6)} + (4\beta_k^2 - 2)\omega_k^2 T_{jk}^{(7)} + T_{jk}^{(8)} + (4\beta_j^2 - 2)\omega_j^2 T_{jk}^{(9)} \quad (\text{A.32})$$

$$p_6^{III} = T_{jk}^{(7)} + T_{jk}^{(9)} . \quad (\text{A.33})$$

By using equations (A.30) and (A.33), the unknowns $T_{jk}^{(8)}$ and $T_{jk}^{(9)}$ can be written as functions of $T_{jk}^{(6)}$ and $T_{jk}^{(7)}$

$$T_{jk}^{(8)} = p_0^{III} \omega_j^{-4} - \Omega_{jk}^{-4} T_{jk}^{(6)} \quad (\text{A.34})$$

$$T_{jk}^{(9)} = p_6^{III} - T_{jk}^{(7)} , \quad (\text{A.35})$$

where $\Omega_{jk} = \omega_j/\omega_k$. These last two equations can now be substituted into equations (A.31) and (A.32), which are then divided by ω_k^2 to get the following (2×2) system of equations

$$\omega_k^{-2} [1 - \Omega_{jk}^{-4}] T_{jk}^{(6)} + 2 [(\Omega_{jk}^2 - 1) + 2(\beta_k^2 - \beta_j^2 \Omega_{jk}^2)] T_{jk}^{(7)} = \mu_{jk} \omega_j^{-2} \quad (\text{A.36})$$

$$2 [(\Omega_{jk}^{-2} - 1) + 2(\beta_k^2 - \beta_j^2 \Omega_{jk}^{-2})] T_{jk}^{(6)} + \omega_k^2 [1 - \Omega_{jk}^4] T_{jk}^{(7)} = \eta_{jk} , \quad (\text{A.37})$$

where the quantities μ_{jk} and η_{jk} are defined as

$$\mu_{jk} = \Omega_{jk}^2 [p_4^{III} - \omega_j^{-4} p_0^{III} - \omega_j^2 (4\beta_j^2 - 2) p_6^{III}] \quad (\text{A.38})$$

$$\eta_{jk} = \Omega_{jk}^2 \left[\frac{p_2^{III}}{\omega_j^2} - \omega_j^2 p_6^{III} - \omega_j^{-4} (4\beta_j^2 - 2) p_0^{III} \right] \quad (\text{A.39})$$

The (2×2) matrix of this system possesses the following determinant

$$\begin{aligned} \Delta_{jk}^{III} = & 16(\beta_j^2 + \beta_k^2 - \beta_j^4 - \beta_k^4) - \Omega_{jk}^4 - \Omega_{jk}^{-4} - 6 \\ & + 4(\Omega_{jk}^2 + \Omega_{jk}^{-2}) [1 - 2(\beta_j^2 + \beta_k^2 - 2\beta_j^2 \beta_k^2)] . \end{aligned} \quad (\text{A.40})$$

After solving equations (A.36) and (A.37), the coefficients $T_{jk}^{(6)}$ and $T_{jk}^{(7)}$ become

$$T_{jk}^{(6)} = \{2\eta_{jk} [1 - \Omega_{jk}^2 + 2(\beta_j^2 \Omega_{jk}^2 - \beta_k^2)] - \mu_{jk} (\Omega_{jk}^2 - \Omega_{jk}^{-2})\} (\Delta_{jk}^{III})^{-1} \quad (\text{A.41})$$

$$T_{jk}^{(7)} = \left\{ \eta_{jk} (\Omega_{jk}^2 - \Omega_{jk}^{-2}) - 2 \Omega_{jk}^{-2} \mu_{jk} [1 - \Omega_{jk}^2 + 2 (\beta_k^2 \Omega_{jk}^2 - \beta_j^2)] \right\} \omega_j^{-2} (\Delta_{jk}^{III})^{-1}. \quad (\text{A.42})$$

Which, in turn, can be substituted into equations (A.34) and (A.35) to get the remaining coefficients $T_{jk}^{(8)}$ and $T_{jk}^{(9)}$.

It should be noticed that for $\omega_j = \omega_k$ the determinant becomes

$$\Delta_{jk}^{III} = 16 (2 \beta_j^2 \beta_k^2 - \beta_j^4 - \beta_k^4). \quad (\text{A.43})$$

In addition, if $\beta_j = \beta_k$, then $\Delta_{jk}^{III} = 0$ and the partial fraction coefficients are undetermined.

A.4 Case IV

This case is just a particularization of Case III, but due to its widespread use in this study for the calculation of the stochastic response by the mode displacement, the modified mode displacement and the force derivative approaches, it has been considered convenient to analyze it as a different case. Thus, this section presents the partial fraction coefficients $T_{jk}^{(10)}$, $T_{jk}^{(11)}$, $T_{jk}^{(12)}$ and $T_{jk}^{(13)}$ associated to the following expansion

$$P^{IV}(\omega) |H_j^c(\omega)|^2 |H_k^c(\omega)|^2 = (T_{jk}^{(10)} + \omega^2 T_{jk}^{(11)}) |H_j^c(\omega)|^2 + (T_{jk}^{(12)} + \omega^2 T_{jk}^{(13)}) |H_k^c(\omega)|^2, \quad (\text{A.44})$$

where $H_k^c(\omega)$ and its squared modulus have been previously defined in equations (A.14) and (A.15) respectively. $P^{IV}(\omega)$ is a fourth degree polynomial in ω which coefficients are denoted as p_i^{IV}

$$P^{IV}(\omega) = p_0^{IV} + p_2^{IV} \omega^2 + p_4^{IV} \omega^4, \quad (\text{A.45})$$

with

$$p_0^{IV} = \omega_j^2 \omega_k^2, \quad p_2^{IV} = 4\beta_j \beta_k \omega_j \omega_k - \omega_j^2 - \omega_k^2, \quad p_4^{IV} = 1. \quad (\text{A.46})$$

These partial fractions can be obtained by considering the procedure presented in Case III for $p_6^{III} = 0$. Thus, the coefficients $T_{jk}^{(12)}$ and $T_{jk}^{(13)}$ are obtained by using equations (A.34) and (A.35) for this particular case:

$$T_{jk}^{(12)} = p_0^{IV} \omega_j^{-4} - \Omega_{jk}^{-4} T_{jk}^{(10)} = \Omega_j^{-2} - \Omega_{jk}^{-4} T_{jk}^{(10)}, \quad (\text{A.47})$$

$$T_{jk}^{(13)} = -T_{jk}^{(11)}, \quad (\text{A.48})$$

where $\Omega_{jk} = \omega_j / \omega_k$. On the other hand, the coefficients $T_{jk}^{(10)}$ and $T_{jk}^{(11)}$ are given by equations (A.38-A.42) after being particularized for this case. Thus,

$$\mu_{jk} = \Omega_{jk}^2 [p_4^{IV} - \omega_j^{-4} p_0^{IV}] = \Omega_{jk}^2 - 1, \quad (\text{A.49})$$

$$\eta_{jk} = \Omega_{jk}^2 \left[\frac{p_2^{IV}}{\omega_j^2} - \omega_j^{-4} (4\beta_j^2 - 2) p_0^{IV} \right] = 1 - 4\beta_j^2 + 4\beta_j \beta_k \Omega_{jk} - \Omega_{jk}^2, \quad (\text{A.50})$$

$$\begin{aligned} \Delta_{jk}^{III} &= 16(\beta_j^2 + \beta_k^2 - \beta_j^4 - \beta_k^4) - \Omega_{jk}^4 - \Omega_{jk}^{-4} - 6 \\ &+ 4(\Omega_{jk}^2 + \Omega_{jk}^{-2}) [1 - 2(\beta_j^2 + \beta_k^2 - 2\beta_j^2 \beta_k^2)], \end{aligned} \quad (\text{A.51})$$

$$T_{jk}^{(11)} = \{2\eta_{jk} [1 - \Omega_{jk}^2 + 2(\beta_j^2 \Omega_{jk}^2 - \beta_k^2)] - \mu_{jk} (\Omega_{jk}^2 - \Omega_{jk}^{-2})\} (\Delta_{jk}^{III})^{-1}, \quad (\text{A.52})$$

$$T_{jk}^{(12)} = \{\eta_{jk} (\Omega_{jk}^2 - \Omega_{jk}^{-2}) - 2\Omega_{jk}^{-2} \mu_{jk} [1 - \Omega_{jk}^2 + 2(\beta_k^2 \Omega_{jk}^2 - \beta_j^2)]\} \omega_j^{-2} (\Delta_{jk}^{III})^{-1}. \quad (\text{A.53})$$

The substitution of equations (A.49), (A.50) and (A.51) into equations (A.52) and (A.53), and some simplifications, render

$$T_{jk}^{(11)} = [(4\beta_j^2 - 1)\Omega_{jk}^4 + 4\beta_j \beta_k \Omega_{jk}^3 + \Omega_{jk}^2] d_{jk}^{-1}, \quad (\text{A.54})$$

$$T_{jk}^{(12)} = [\Omega_{jk}^2 - 1] \omega_k^{-2} d_{jk}^{-1}, \quad (\text{A.55})$$

where the quantity d_{jk} is

$$d_{jk} = \Omega_{jk}^4 + 4\beta_j \beta_k \Omega_{jk}^3 + (4\beta_j^2 + 4\beta_k^2 - 2) \Omega_{jk}^2 + 4\beta_j \beta_k \Omega_{jk} + 1 . \quad (\text{A.56})$$

Finally, the expression for $T_{jk}^{(12)}$ can be obtained by substituting equation (A.54) into (A.47). Thus,

$$T_{jk}^{(12)} = \left[\Omega_{jk}^2 + 4\beta_j \beta_k \Omega_{jk} + 4\beta_k^2 - 1 \right] d_{jk}^{-1} . \quad (\text{A.57})$$

Since $T_{jk}^{(13)} = -T_{jk}^{(11)}$, equations (A.54-A.57) completely determine the partial fraction coefficients for this particular case.

It can be noticed that all four coefficients $T_{jk}^{(10)}$, $T_{jk}^{(11)}$, $T_{jk}^{(12)}$ and $T_{jk}^{(13)}$ are also defined for the especial case in which $\omega_j = \omega_k$ and $\beta_j = \beta_k$. That is,

$$T_{jj}^{(10)} = T_{jj}^{(12)} = 1/2 \quad , \quad T_{jj}^{(11)} = T_{jj}^{(13)} = 0 . \quad (\text{A.58})$$

This warrants the determination of such coefficients even when the frequencies ω_j and ω_k are closely spaced.

Appendix B

Integration by parts of the Duhamel Integral

The Duhamel integral can be expressed as

$$D_0(t) = \int_0^t h(t-\tau) p(\tau) d\tau, \quad (\text{B.1})$$

where

$$h(t-\tau) = \frac{e^{-\beta\omega(t-\tau)}}{\omega_d} \sin[\omega_d(t-\tau)] \quad , \quad \omega_d = \omega \sqrt{1-\beta^2}. \quad (\text{B.2})$$

Successive integrations by parts of this integral provide several different expressions for the same quantity $D_0(t)$. Thus, if $D_1(t)$ denotes the result of the first integration by parts, $D_2(t)$ of the second, and $D_N(t)$ of the N^{th} integration, it is possible to write the following identities

$$D_0(t) = D_1(t) = D_2(t) = \dots = D_N(t). \quad (\text{B.3})$$

To perform such integrations it is useful to consider the following two well known indefinite integrals:

$$\int e^{ax} \sin(bx) dx = e^{ax} \frac{[a \sin(bx) - b \cos(bx)]}{(a^2 + b^2)}, \quad (\text{B.4})$$

$$\int e^{ax} \cos(bx) dx = e^{ax} \frac{[a \cos(bx) + b \sin(bx)]}{(a^2 + b^2)}, \quad (\text{B.5})$$

which are used to provide the subsequent two expressions:

$$\int h(t-\tau) d\tau = \left(\frac{\beta}{\omega}\right) h(t-\tau) + \left(\frac{1}{\omega^2}\right) \tilde{h}(t-\tau), \quad (\text{B.6})$$

$$\int \tilde{h}(t-\tau) d\tau = \left(\frac{\beta}{\omega}\right) \tilde{h}(t-\tau) + (\beta^2 - 1) h(t-\tau), \quad (\text{B.7})$$

where

$$\tilde{h}(t-\tau) = e^{-\beta\omega(t-\tau)} \cos[\omega_d(t-\tau)]. \quad (\text{B.8})$$

Thus, by considering equation (B.6), the first integration by parts becomes

$$\begin{aligned} D_1(t) &= \left[\left\{ \left(\frac{\beta}{\omega}\right) h(t-\tau) + \left(\frac{1}{\omega^2}\right) \tilde{h}(t-\tau) \right\} p(\tau) \right]_{\tau=0}^{\tau=t} \\ &\quad - \int_0^t \left\{ \left(\frac{\beta}{\omega}\right) h(t-\tau) + \left(\frac{1}{\omega^2}\right) \tilde{h}(t-\tau) \right\} \dot{p}(\tau) d\tau, \end{aligned} \quad (\text{B.9})$$

where the evaluation of the limits renders

$$\begin{aligned} D_1(t) &= \left(\frac{1}{\omega^2}\right) p(t) - \left\{ \left(\frac{\beta}{\omega}\right) h(t) + \left(\frac{1}{\omega^2}\right) \tilde{h}(t) \right\} p(0) \\ &\quad - \left(\frac{\beta}{\omega}\right) \int_0^t h(t-\tau) \dot{p}(\tau) d\tau - \left(\frac{1}{\omega^2}\right) \int_0^t \tilde{h}(t-\tau) \dot{p}(\tau) d\tau. \end{aligned} \quad (\text{B.10})$$

The expression for $D_2(t)$ can be obtained from equation (B.10) with the help of equations (B.6) and (B.7) as

$$\begin{aligned} D_2(t) &= \left(\frac{1}{\omega^2}\right) p(t) - \left\{ \left(\frac{\beta}{\omega}\right) h(t) + \left(\frac{1}{\omega^2}\right) \tilde{h}(t) \right\} p(0) \\ &\quad - \left(\frac{\beta}{\omega}\right) \left[\left\{ \left(\frac{\beta}{\omega}\right) h(t-\tau) + \left(\frac{1}{\omega^2}\right) \tilde{h}(t-\tau) \right\} \dot{p}(\tau) \right]_{\tau=0}^{\tau=t} \\ &\quad + \left(\frac{\beta}{\omega}\right) \int_0^t \left\{ \left(\frac{\beta}{\omega}\right) h(t-\tau) + \left(\frac{1}{\omega^2}\right) \tilde{h}(t-\tau) \right\} \ddot{p}(\tau) d\tau \\ &\quad - \left(\frac{1}{\omega^2}\right) \left[\left\{ \left(\frac{\beta}{\omega}\right) \tilde{h}(t-\tau) + (\beta^2 - 1) h(t-\tau) \right\} \dot{p}(\tau) \right]_{\tau=0}^{\tau=t} \\ &\quad + \left(\frac{1}{\omega^2}\right) \int_0^t \left\{ \left(\frac{\beta}{\omega}\right) \tilde{h}(t-\tau) + (\beta^2 - 1) h(t-\tau) \right\} \ddot{p}(\tau) d\tau, \end{aligned} \quad (\text{B.11})$$

and after evaluation of the limits $D_2(t)$ becomes

$$\begin{aligned}
D_2(t) &= \left(\frac{1}{\omega^2}\right) p(t) - \left(\frac{2\beta}{\omega^3}\right) \dot{p}(t) - \left\{ \left(\frac{\beta}{\omega}\right) h(t) + \left(\frac{1}{\omega^2}\right) \tilde{h}(t) \right\} p(0) \\
&+ \left\{ \left(\frac{2\beta^2 - 1}{\omega^2}\right) h(t) + \left(\frac{2\beta}{\omega^3}\right) \tilde{h}(t) \right\} \dot{p}(0) \\
&+ \left(\frac{2\beta^2 - 1}{\omega^2}\right) \int_0^t h(t-\tau) \ddot{p}(\tau) d\tau + \left(\frac{2\beta}{\omega^3}\right) \int_0^t \tilde{h}(t-\tau) \ddot{p}(\tau) d\tau .
\end{aligned} \tag{B.12}$$

The function $\tilde{h}(t)$ can be written in terms of $h(t)$ and its time derivative $\dot{h}(t)$ as

$$\tilde{h}(t) = \dot{h}(t) + \beta \omega h(t) . \tag{B.13}$$

Therefore, the substitution of equation (B.13) into equations (B.10) and (B.12) provides the following expressions for $D_1(t)$ and $D_2(t)$:

$$\begin{aligned}
D_1(t) &= \left(\frac{1}{\omega^2}\right) p(t) - \left\{ \left(\frac{2\beta}{\omega}\right) h(t) + \left(\frac{1}{\omega^2}\right) \dot{h}(t) \right\} p(0) \\
&- \left(\frac{2\beta}{\omega}\right) \int_0^t h(t-\tau) \dot{p}(\tau) d\tau - \left(\frac{1}{\omega^2}\right) \int_0^t \dot{h}(t-\tau) \dot{p}(\tau) d\tau .
\end{aligned} \tag{B.14}$$

$$\begin{aligned}
D_2(t) &= \left(\frac{1}{\omega^2}\right) p(t) - \left(\frac{2\beta}{\omega^3}\right) \dot{p}(t) - \left\{ \left(\frac{2\beta}{\omega}\right) h(t) + \left(\frac{1}{\omega^2}\right) \dot{h}(t) \right\} p(0) \\
&+ \left\{ \left(\frac{4\beta^2 - 1}{\omega^2}\right) h(t) + \left(\frac{2\beta}{\omega^3}\right) \dot{h}(t) \right\} \dot{p}(0) \\
&+ \left(\frac{4\beta^2 - 1}{\omega^2}\right) \int_0^t h(t-\tau) \ddot{p}(\tau) d\tau + \left(\frac{2\beta}{\omega^3}\right) \int_0^t \dot{h}(t-\tau) \ddot{p}(\tau) d\tau .
\end{aligned} \tag{B.15}$$

By a similar procedure it is possible to determine the remaining expressions $D_3(t)$, $D_4(t)$, ..., $D_N(t)$. Every new integration by parts provides new, and more intricate, boundary terms at $\tau = 0$ and at $\tau = t$. However, the coefficients involved on these terms are recursively related. This facilitates their calculation, and allows to write the following general expression after N integrations by parts:

$$D_N(t) = \sum_{k=1}^N \left(\frac{1}{\omega}\right)^{k+1} \hat{\Upsilon}_k^{<k-1>} p(t)$$

$$\begin{aligned}
& + \sum_{k=1}^N \left\{ \left(\frac{1}{\omega} \right)^k \hat{\Upsilon}_{k+1} h(t) - \left(\frac{1}{\omega} \right)^{k+1} \hat{\Upsilon}_k \dot{h}(t) \right\} \left[\frac{< k-1 >}{p(t)} \right]_{t=0} \\
& + \left(\frac{1}{\omega} \right)^N \hat{\Upsilon}_{N+1} \int_0^t h(t-\tau) \frac{< N >}{p(\tau)} d\tau - \left(\frac{1}{\omega} \right)^{N+1} \hat{\Upsilon}_N \int_0^t \dot{h}(t-\tau) \frac{< N >}{p(\tau)} d\tau,
\end{aligned} \tag{B.16}$$

where an upper number delimited by $< . >$ indicates the number of derivatives, with respect to time, of the lower variable. The coefficients $\hat{\Upsilon}_k$ can be determined by using the following second order recursion

$$\hat{\Upsilon}_k = -2\beta \hat{\Upsilon}_{k-1} - \hat{\Upsilon}_{k-2} \quad , \quad \hat{\Upsilon}_0 = 0 \quad , \quad \hat{\Upsilon}_{-1} = -1. \tag{B.17}$$

It can be noticed that the recursive coefficient $\hat{\Upsilon}_k$ depend only on the coefficient β , but to further simplify equation (B.16), it is possible to involve also the variable ω in the recursive formula. That is, a new recursive coefficient Υ_k is defined by the following product:

$$\Upsilon_k = \left(\frac{1}{\omega} \right)^{k+1} \hat{\Upsilon}_k, \tag{B.18}$$

and the resulting recursive relationship can be written as

$$\Upsilon_k = - \left(\frac{2\beta}{\omega} \right) \Upsilon_{k-1} - \left(\frac{1}{\omega^2} \right) \Upsilon_{k-2} \quad , \quad \Upsilon_0 = 0 \quad , \quad \Upsilon_{-1} = -1. \tag{B.19}$$

By using the recursive equation (B.19), the expression for $D_N(t)$ becomes

$$\begin{aligned}
D_N(t) = & \sum_{k=1}^N \Upsilon_k \frac{< k-1 >}{p(t)} + \sum_{k=1}^N \left[\omega^2 \Upsilon_{k+1} h(t) - \Upsilon_k \dot{h}(t) \right] \left[\frac{< k-1 >}{p(t)} \right]_{t=0} \\
& + \omega^2 \Upsilon_{N+1} \int_0^t h(t-\tau) \frac{< N >}{p(\tau)} d\tau - \Upsilon_N \int_0^t \dot{h}(t-\tau) \frac{< N >}{p(\tau)} d\tau.
\end{aligned} \tag{B.20}$$

Appendix C

Recursive Formula for Pseudo-Flexibility Matrices

C.1 Pseudo-Flexibility Matrices for all Modes

The dynamic behavior of a linear structural system, with n degrees of freedom and classical damping, is completely characterized by three well known ($n \times n$) structural matrices: the mass matrix $[M]$, the classical damping matrix $[C]$, and the stiffness matrix $[K]$. However, the force derivative method, proposed in chapter 4, makes use of the so called pseudo-flexibility matrices, which can be defined by a recursive relationship involving the previous three matrices. This appendix presents the formulation leading to such recursive expression.

The k^{th} pseudo-flexibility matrix is denoted here as $[F]_k$ and is defined by the following expression:

$$[F]_k = \sum_{j=1}^n \{\phi\}_j \Upsilon_{j,k} \{\phi\}^T = [\Phi] [\Upsilon]_k [\Phi]^T \quad (C.1)$$

where $[\Phi]$ is the normalized (with respect to the mass) modal matrix which columns

contain the n eigenvectors $\{\phi\}_j$, and $[\Upsilon]_k$ is a diagonal recursive matrix which j^{th} entry contains the recursive coefficient $\Upsilon_{j,k}$. These coefficients results from the integration by parts of the Duhamel integral and they are defined recursively (appendix B) in terms of the natural frequency ω_j and the damping ratio β_j as

$$\Upsilon_{j,k} = - \left(\frac{2\beta_j}{\omega_j} \right) \Upsilon_{j,k-1} - \left(\frac{1}{\omega_j^2} \right) \Upsilon_{j,k-2} \quad , \quad \Upsilon_{j,0} = 0 \quad , \quad \Upsilon_{j,-1} = -1 \quad . \quad (C.2)$$

The orthonormality eigenproperties of a classically damped linear system can be expressed as

$$[\Phi]^T [M] [\Phi] = [I] \quad , \quad [\Phi]^T [C] [\Phi] = [D] \quad , \quad [\Phi]^T [K] [\Phi] = [\Lambda] \quad , \quad (C.3)$$

where $[I]$ is the $(n \times n)$ identity matrix, $[D]$ is the diagonal modal damping matrix with its j^{th} entry given by $(2\beta_j \omega_j)$, and $[\Lambda]$ is the diagonal modal stiffness matrix which entries contain the n eigenvalues $\lambda_j = \omega_j^2$.

By considering the expressions in equation (C.3) it is possible to rewrite the recursive relationship of equation (C.2) in matrix form. That is,

$$[\Upsilon]_k = -[\Lambda]^{-1} \{ [D] [\Upsilon]_{k-1} + [\Upsilon]_{k-2} \} \quad , \quad [\Upsilon]_0 = [0] \quad , \quad [\Upsilon]_{-1} = -[I] \quad , \quad (C.4)$$

where $[\Lambda]^{-1}$ can be obtained from equation (C.3) as

$$[\Lambda]^{-1} = \begin{bmatrix} 1/\omega_1^2 & & & \\ & 1/\omega_2^2 & & \\ & & \ddots & \\ & & & 1/\omega_n^2 \end{bmatrix} = [\Phi]^{-1} [K]^{-1} [\Phi]^{-T} \quad , \quad (C.5)$$

and a matrix with the superscript $-T$ indicates the inverse of its transpose.

Equation (C.5) can be substituted into equation (C.1) to get the following recursive expression of $[F]_k$ in matrix form:

$$[F]_k = -[\Phi] [\Lambda]^{-1} \{ [D] [\Upsilon]_{k-1} + [I] [\Upsilon]_{k-2} \} [\Phi]^T$$

$$[F]_0 = [\Phi][\Upsilon]_0[\Phi]^T = [0] \quad , \quad [F]_{-1} = [\Phi][I][\Phi]^T = -[M]^{-1} . \quad (C.6)$$

Finally, the expressions for $[I]$ and $[D]$ in equation (C.3), and the expression of $[\Lambda]^{-1}$ in equation (C.5), can be substituted into equation (C.6) to get

$$\begin{aligned} [F]_k &= -[K]^{-1} \left\{ [C][\Phi][\Upsilon]_{k-1}[\Phi]^T + [M][\Phi][\Upsilon]_{k-2}[\Phi]^T \right\} \\ [F]_0 &= [0] \quad , \quad [F]_{-1} = -[M]^{-1} , \end{aligned} \quad (C.7)$$

where it can be recognized that $[\Phi][\Upsilon]_{k-1}[\Phi]^T$ and $[\Phi][\Upsilon]_{k-2}[\Phi]^T$ are equal to $[F]_{k-1}$ and to $[F]_{k-2}$ respectively. Thus, the expression for $[F]_k$ becomes

$$\begin{aligned} [F]_k &= -[K]^{-1} \left\{ [C][F]_{k-1} + [M][F]_{k-2} \right\} \\ [F]_0 &= [0] \quad , \quad [F]_{-1} = -[M]^{-1} . \end{aligned} \quad (C.8)$$

It should be noticed that the first pseudo-flexibility matrix is just the actual flexibility matrix. That is,

$$[F]_1 = -[K]^{-1} \left\{ [C][0] - [M][M]^{-1} \right\} = [K]^{-1} , \quad (C.9)$$

as a consequence, there is no need to invert the mass matrix since it is possible to calculate all $[F]_k$ for $k = 2, 3, \dots, N$ by initiating the recursion with $[F]_1 = [K]^{-1}$ and $[F]_0 = [0]$.

C.2 Pseudo-Flexibility Matrices for Lower and Higher Modes

The formulation of the previous section presents the recursive formulas necessary to generate a set of pseudo-flexibility matrices associated to all n structural

modes. However, the force derivative method, developed in chapter 4, requires the use of a different set of pseudo-flexibility matrices. That is, the pseudo-flexibility matrices associated only to the higher modes. This section presents the recursive formulas corresponding to two different sets of pseudo-flexibility matrices: (1) a set associated to the lower modes, $[F_l]_k$, and (2) a set associated to the higher (truncated) modes, $[F_h]_k$.

By assuming that the first r modes constitute the lower modes and the remaining $n - r$ modes are the higher modes, it is possible to rewrite equation (C.1) as

$$[F]_k = \sum_{j=1}^r \{\phi\}_j \Upsilon_{j,k} \{\phi\}^T + \sum_{j=r+1}^n \{\phi\}_j \Upsilon_{j,k} \{\phi\}^T = [F_l]_k + [F_h]_k \quad (C.10)$$

where the pseudo-flexibility matrices associated to the lower and higher modes are defined, respectively, as

$$[F_l]_k = \sum_{j=1}^r \{\phi\}_j \Upsilon_{j,k} \{\phi\}^T = [\Phi_l] [\Upsilon_l]_k [\Phi_l]^T, \quad (C.11)$$

$$[F_h]_k = \sum_{j=r+1}^n \{\phi\}_j \Upsilon_{j,k} \{\phi\}^T = [\Phi_h] [\Upsilon_h]_k [\Phi_h]^T. \quad (C.12)$$

The dimensions of the different matrices involved in equations (C.11) and (C.12) are presented in table C.2.

Substitution of equation (C.10) for the subscripts k , $k - 1$, $k - 2$, 0 and 1 into equations (C.8) and (C.9) produces

$$\begin{aligned} [F]_k &= [F_l]_k + [F_h]_k \\ &= -[K]^{-1} \{ [C] ([F_l]_{k-1} + [F_h]_{k-1}) + [M] ([F_l]_{k-2} + [F_h]_{k-2}) \} \\ [F]_1 &= [F_l]_1 + [F_h]_1, \quad [F]_0 = [F_l]_0 + [F_h]_0, \end{aligned} \quad (C.13)$$

Table C.1: Dimensions of the matrices associates to the lower and higher modes

<i>Matrix</i>	<i>Dimension</i>
$[\Phi_\ell] = [\{\phi\}_1, \{\phi\}_2, \dots, \{\phi\}_r]$	$n \times r$
$[\Phi_h] = [\{\phi\}_{r+1}, \{\phi\}_{r+2}, \dots, \{\phi\}_n]$	$n \times (n - r)$
$[\Upsilon_\ell]$ diagonal (first r elements)	$r \times r$
$[\Upsilon_h]$ diagonal (last $(n - r)$ elements)	$(n - r) \times (n - r)$
$[F_\ell]$	$n \times n$
$[F_h]$	$n \times n$

where

$$[F_\ell]_1 = [\Phi_\ell] [\Upsilon_\ell]_1 [\Phi_\ell]^T = \sum_{j=1}^r \{\phi\}_j \left(\frac{1}{\omega_j^2} \right) \{\phi\}_j^T \quad (C.14)$$

$$[F_h]_1 = [F]_1 - [F_\ell]_1 = [K]^{-1} - \sum_{j=1}^r \{\phi\}_j \left(\frac{1}{\omega_j^2} \right) \{\phi\}_j^T \quad (C.15)$$

$$[F]_0 = [F_\ell]_0 = [F_h]_0 = [0] . \quad (C.16)$$

Equation (C.15) can be easily splited in the following two expressions:

$$\begin{aligned} [F_\ell]_k &= -[K]^{-1} \{ [C] [F_\ell]_{k-1} + [M] [F_\ell]_{k-2} \} \\ [F_\ell]_1 &= \sum_{j=1}^r \{\phi\}_j \left(\frac{1}{\omega_j^2} \right) \{\phi\}_j^T \quad , \quad [F_\ell]_0 = [0] , \end{aligned} \quad (C.17)$$

$$\begin{aligned} [F_h]_k &= -[K]^{-1} \{ [C] [F_h]_{k-1} + [M] [F_h]_{k-2} \} \\ [F_h]_1 &= [K]^{-1} - \sum_{j=1}^r \{\phi\}_j \left(\frac{1}{\omega_j^2} \right) \{\phi\}_j^T \quad , \quad [F_h]_0 = [0] . \end{aligned} \quad (C.18)$$

Equation (C.17) is the recursive relationship that defines the pseudo-flexibility matrices associated to the lower modes and equation (C.18) is the recursive formula to generate the pseudo-flexibility matrices associates to the higher (truncated) modes. In both cases the matrices are expressed in terms of the retained lower eigenproperties and in terms of the complete mass, stiffness and damping matrices of the system.

Appendix D

Calculation of a Classical Damping Matrix from a Truncated Modal Analysis

In general, the dynamic analysis of classically damped linear structures does not require the knowledge of the damping matrix $[C]$. If modal analysis is used on a system with n degrees of freedom, only the values of $r \leq n$ damping ratios are needed to apply the modal combination rule leading to the dynamic response. However, some calculation procedures require the complete knowledge of the damping matrix, i.e. any direct integration scheme, or the force derivative method developed in chapter 4. In particular, the latter uses the damping matrix for the calculation of the recursive pseudostatic contributions of the truncated (higher) modes. This appendix presents a generalization of the procedure given by Craig [15] to approximate the complete damping matrix in terms of the retained eigenproperties as well as the mass and stiffness matrices: $[M]$ and $[K]$.

The orthonormal modal properties of these systems can be written as:

$$[\Phi]^T [M] [\Phi] = [I] , \quad (D.1)$$

$$[\Phi]^T [C] [\Phi] = [D] = \begin{bmatrix} 2\beta_1\omega_1 & & & 0 \\ & 2\beta_2\omega_2 & & \\ & & \ddots & \\ 0 & & & 2\beta_n\omega_n \end{bmatrix} , \quad (D.2)$$

$$[\Phi]^T [K] [\Phi] = [\Lambda] = \begin{bmatrix} \omega_1^2 & & & 0 \\ & \omega_2^2 & & \\ & & \ddots & \\ 0 & & & \omega_n^2 \end{bmatrix} , \quad (D.3)$$

where β_j and ω_j are the j^{th} modal damping ratio and modal frequency respectively, $[I]$ is the $(n \times n)$ identity matrix, $[\Phi]$ is the modal matrix which columns contain the modal vectors $\{\phi\}_j$, and the diagonal matrices $[D]$ and $[\Lambda]$ are the modal damping and modal stiffness matrices respectively.

Equation (D.2) can be solved for matrix $[C]$ to express it in terms of all n eigenproperties as

$$[C] = [\Phi]^{-T} [D] [\Phi]^{-1} , \quad (D.4)$$

where there is no need to invert matrix $[\Phi]$, nor its transpose. With the help of equation (D.1), it is possible to write

$$[\Phi]^{-1} = [\Phi]^T [M] \quad , \quad [\Phi]^{-T} = [M] [\Phi] , \quad (D.5)$$

which can be substituted into equation (D.4) to get

$$[C] = [M] [\Phi] [D] [\Phi]^T [M] = [M] \sum_{j=1}^n \{\phi\}_j (2\beta_j\omega_j) \{\phi\}_j^T [M] . \quad (D.6)$$

Similarly, the stiffness and mass matrices can be written as

$$[K] = [M] [\Phi] [\Lambda] [\Phi]^T [M] = [M] \sum_{j=1}^n \{\phi\}_j (\omega_j^2) \{\phi\}_j^T [M] , \quad (D.7)$$

$$[M] = [M][\Phi][\Phi]^T[M] = [M] \sum_{j=1}^n \{\phi\}_j \{\phi\}_j^T [M] . \quad (\text{D.8})$$

Equation (D.6) is the commonly used expression to reconstruct the damping matrix from the total eigenproperties. However, in general, not all n eigenproperties are available. Only a truncated set of them, containing the properties associated to the lower r frequencies, are known. Therefore, matrix $[C]$ is here decomposed into two matrices: matrix $[C_\ell]$ associated to the retained (known) lower modes and matrix $[C_h]$ associated to the truncated (unknown) higher modes. That is,

$$[C] = [C_\ell] + [C_h] , \quad (\text{D.9})$$

where the two new damping matrices are defined as follows

$$[C_\ell] = [M] \sum_{j=1}^r \{\phi\}_j (2\beta_j \omega_j) \{\phi\}_j^T [M] = [M][\Phi_\ell][D_\ell][\Phi_\ell]^T [M] , \quad (\text{D.10})$$

$$[C_h] = [M] \sum_{j=r+1}^n \{\phi\}_j (2\beta_j \omega_j) \{\phi\}_j^T [M] = [M][\Phi_h][D_h][\Phi_h]^T [M] . \quad (\text{D.11})$$

Matrix $[\Phi_\ell]$ has dimension $(n \times r)$ and its columns contain only the first r eigenvectors. Matrix $[D_\ell]$ is diagonal with dimension $(r \times r)$ and its diagonal entries are the same as the first r diagonal entries of matrix $[D]$. Matrix $[\Phi_h]$ contain the $(n - r)$ truncated eigenvectors and has dimension $[n \times (n - r)]$. Matrix $[D_h]$ is also diagonal with dimension $[(n - r) \times (n - r)]$ and its diagonal entries are the same as the last $(n - r)$ diagonal entries of matrix $[D]$.

Since $[C_h]$ is given in terms of the unknown truncated eigenproperties, it is proposed here to express it as a linear combination of the stiffness and mass matrices associated to the truncated upper modes. That is,

$$[C_h] = \tilde{c}_1 [K_h] + \tilde{c}_2 [M_h] , \quad (\text{D.12})$$

which can be substituted into equation (D.9) to get the proposed damping matrix

$$[C] = [C_\ell] + \bar{c}_1 [K_h] + \bar{c}_2 [M_h] . \quad (D.13)$$

The matrices $[K_h]$ and $[M_h]$, though associated to the truncated modes, can still be expressed in terms of the retained modes and the total stiffness and mass matrices as follows:

$$[K_h] = [K] - [K_\ell] , \quad (D.14)$$

$$[M_h] = [M] - [M_\ell] , \quad (D.15)$$

where $[K_\ell]$ and $[M_\ell]$ can be calculated by the same procedure used for the calculation of $[C_\ell]$ and then substituted into equations (D.14) and (D.15) to get

$$[K_h] = [K] - [M] [\Phi_\ell] [\Lambda_\ell] [\Phi_\ell]^T [M] , \quad (D.16)$$

$$[M_h] = [M] - [M] [\Phi_\ell] [\Phi_\ell]^T [M] . \quad (D.17)$$

Matrix $[\Lambda_\ell]$ is diagonal with dimension $(r \times r)$ and its diagonal entries are the same as the first r diagonal entries of $[\Lambda]$.

The final expression for the proposed classical damping matrix is obtained by substituting equations (D.10), (D.16) and (D.17) into equation (D.13) to get

$$\begin{aligned} [C] &= [M] [\Phi_\ell] [D_\ell] [\Phi_\ell]^T [M] \\ &+ \bar{c}_1 \left([K] - [M] [\Phi_\ell] [\Lambda_\ell] [\Phi_\ell]^T [M] \right) \\ &+ \bar{c}_2 \left([M] - [M] [\Phi_\ell] [\Phi_\ell]^T [M] \right) . \end{aligned} \quad (D.18)$$

The damping matrix defined by equation (D.18) possesses its first r associated damping ratios equal to the damping ratios of the retained lower modes, and its

remaining $(n - r)$ associated damping ratios can be adjusted by the proper selection of the constants \bar{c}_1 and \bar{c}_2 . Thus, the damping ratios of the upper (truncated) modes are related to the constants \bar{c}_1 and \bar{c}_2 by the following expression:

$$\beta_j = \frac{1}{2} \left(\bar{c}_1 \omega_j + \frac{\bar{c}_2}{\omega_j} \right) \quad , \quad j = r + 1, r + 2, \dots, n \quad (\text{D.19})$$

In particular, for $\bar{c}_1 = 2\beta_r/\omega_r$ and $\bar{c}_2 = 0$, the damping ratios associated to the truncated modes are

$$\beta_{r+1} = \beta_r \frac{\omega_{r+1}}{\omega_r} \quad , \quad \beta_{r+2} = \beta_r \frac{\omega_{r+2}}{\omega_r} \quad , \quad \dots \quad , \quad \beta_n = \beta_r \frac{\omega_n}{\omega_r} . \quad (\text{D.20})$$

Therefore, in this case, the upper damping ratios are increasing and proportional to the frequency ratios ω_j/ω_r for $j = r + 1, \dots, n$.

Similarly, if $\bar{c}_1 = 0$ and $\bar{c}_2 = 2\beta_r\omega_r$, the upper damping ratios become

$$\beta_{r+1} = \beta_r \frac{\omega_r}{\omega_{r+1}} \quad , \quad \beta_{r+2} = \beta_r \frac{\omega_r}{\omega_{r+2}} \quad , \quad \dots \quad , \quad \beta_n = \beta_r \frac{\omega_r}{\omega_n} , \quad (\text{D.21})$$

and the upper modes possess decreasing damping ratios proportional to the inverse frequency ratios of the previous case.

Appendix E

Bouc-Wen Constitutive Model

The inelastic constitutive law proposed by Bouc [9] and Wen [56, 57] is briefly described in this appendix. The physical meaning corresponding to some of the model parameters is presented here to assist the analysis of the constitutive equations used in chapters 5 and 6. However, a more complete study of this constitutive law has been provided by Baber and Wen [5] as well as by Maldonado [30].

To model the behavior of the force-displacement relationship of inelastic materials, Wen has proposed to define the material as composed of two elements in parallel. One element possesses elastic behavior and the other behaves in an inelastic fashion. The different contributions of each element to the total force F is dictated by weighting factors. Thus,

$$F = \alpha k x + (1 - \alpha) k v(x) \quad (\text{E.1})$$

where k is an elastic stiffness, x is the principal displacement associated to the total force F , $v(x)$ is an auxiliary displacement dependent on x and associated to the inelastic behavior, and α is the weighting constant representing the relative partic-

ipations of the elastic and inelastic terms, ($0 < \alpha < 1$). Figure E.1 schematically describes the relationship between F and x as well as the relationship between $v(x)$ and x .

The hysteretic behavior is included through a nonlinear relationship between $v(x)$ and x . For this, Wen have proposed the use of Bouc's endochronic law:

$$\dot{v}(x) = \mathcal{A} \dot{x} - \mathcal{B} \dot{x} |v(x)|^\eta - \mathcal{C} v |\dot{x}| |v(x)|^{\eta-1}. \quad (\text{E.2})$$

where the different model parameters, \mathcal{A} , \mathcal{B} , \mathcal{C} , and η have been analyzed by Baber and Wen [5], and by Maldonado [30].

The tangent to the nonlinear path described in the plane v - x , is given by $dz(x)/dx$ which can be obtained by dividing equation (E.2) by \dot{x} . Thus,

$$\frac{dv(x)}{dx} = \mathcal{A} - |v(x)|^\eta \left[\mathcal{B} + \frac{\dot{x} v(x)}{|\dot{x} v(x)|} \mathcal{C} \right], \quad (\text{E.3})$$

and at the limit, as $v(x) \rightarrow x \rightarrow 0$, this tangent becomes

$$\left. \frac{dv(x)}{dx} \right|_{x=v=0} = \mathcal{A}. \quad (\text{E.4})$$

The ultimate value of $v(x)$ is denoted as v_u , and is defined as the value at which $dv/dx = 0$. Therefore, from equation (E.3), the absolute value of v_u can be written as

$$|v_u| = \left[\frac{\mathcal{A}}{\mathcal{B} + \mathcal{C}} \right]^{1/\eta}. \quad (\text{E.5})$$

The tangent stiffness of the inelastic behavior is defined by the derivative of F with respect to x :

$$\frac{dF}{dx} = \alpha k + (1 - \alpha) k \frac{dv(x)}{dx}. \quad (\text{E.6})$$

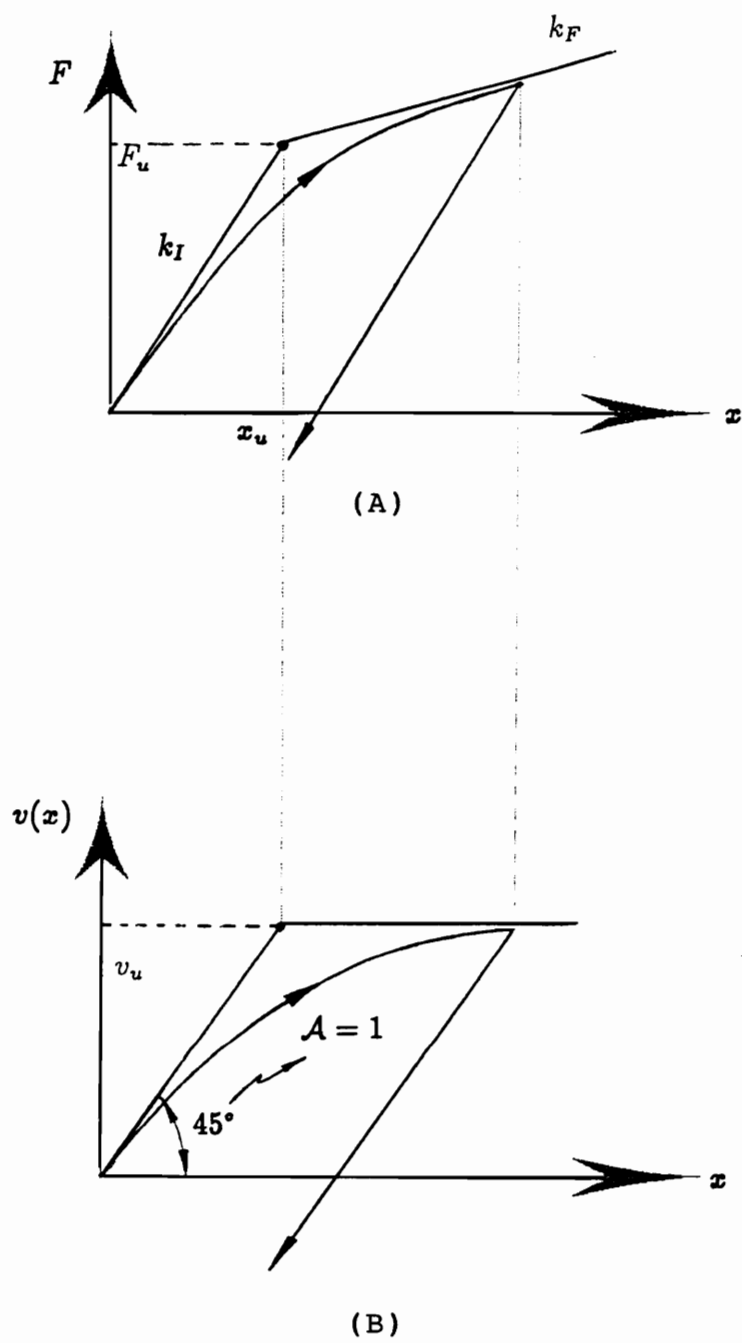


Figure E.1: Bouc-Wen hysteretic model: (A) Force vs. displacement, and (B) Auxiliary variable vs. displacement

The corresponding initial tangent stiffness at $x = v = 0$ is denoted as k_I and its expression is

$$k_I = \left. \frac{dF}{dx} \right|_{x=v=0} = \alpha k + (1 - \alpha) k \left. \frac{dv(x)}{dx} \right|_{x=v=0}, \quad (\text{E.7})$$

where equation (E.4) can be substituted to get

$$k_I = \alpha k + (1 - \alpha) k \mathcal{A}. \quad (\text{E.8})$$

For $\mathcal{A} = 1$, k_I becomes

$$k_I = k. \quad (\text{E.9})$$

The final stiffness k_F , can be defined at the asymptotic value of v when $dv/dx = 0$ as

$$k_F = \alpha k. \quad (\text{E.10})$$

Therefore, the parameter α is the ratio of the final stiffness to the initial stiffness when $\mathcal{A} = 1$,

$$\alpha = k_F/k_I \quad (\text{E.11})$$

A commonly utilized softening model uses $\mathcal{A} = 1$ and straight lines as unloading paths, which implies that $\mathcal{B} = \mathcal{C} > 0$. Therefore, k_I , k_F and α are given by equations (E.9), (E.10) and (E.11) respectively, and the values of \mathcal{B} or \mathcal{C} can be obtained from equation (E.5):

$$\mathcal{B} = \mathcal{C} = \frac{0.5}{|v_u|^\eta}. \quad (\text{E.12})$$

where the exponent η is a positive integer number that controls the proximity of the nonlinear path to the initial and final tangents. Bigger exponents correspond to closer paths to the tangents. If $\mathcal{A} = 1$, $|v_u|$ is equal to the yielding displacement x_u , and can be written in terms of the yielding force, F_u , and the initial stiffness as:

F_u ,

$$|v_u| = x_u = F_u/k , \quad (E.13)$$

equation (E.12) becomes

$$B = C = \frac{0.5}{x_u^\eta} = 0.5 (k/F_u)^\eta , \quad (E.14)$$

where B or C is written in term of the yielding displacement or in term of the yielding force. It should be noticed that the yielding force F_u is not the actual force that corresponds to the yielding displacement x_u but it is the force level associated to the intersection point of the initial and final stiffnesses.

Appendix F

Linearization Coefficients

This appendix presents the formulation leading to the expressions for the linearization coefficients of the Bouc-Wen model.

The stochastic linearization scheme adopted here, is that proposed by Atalik and Utku [3]. It is characterized by the assumption of gaussian probability density functions for the response quantities of the nonlinear system. As a consequence, it is also known as gaussian linearization. However, such assumption is probably the main cause of the error introduced by this procedure.

The Bouc-Wen nonlinear constitutive equation for a single hysteretic element can be written as

$$\dot{v} = g(\dot{x}, v) \quad (\text{F.1})$$

where the nonlinear function $g(\dot{x}, v)$ is given by

$$g(\dot{x}, v) = \mathcal{A} \dot{x} - \mathcal{B} \dot{x} |v|^\eta - \mathcal{C} v |\dot{x}| |v|^{\eta-1}, \quad (\text{F.2})$$

and the different variables have been defined in chapter C.4 and appendix E. The

equivalent linear equation for \dot{v} is

$$\dot{v} = a \dot{x} + b v + \epsilon, \quad (\text{F.3})$$

where a and b are the linearization coefficients and ϵ is the unknown error introduced by the linearization. The coefficients a and b can be obtained by minimizing the mean square value of the error ϵ with respect to them. Thus, the following two equations can be solved for a and b :

$$\frac{\partial E[\epsilon^2]}{\partial a} = 0 \quad , \quad \frac{\partial E[\epsilon^2]}{\partial b} = 0. \quad (\text{F.4})$$

However, if the conditions given by Atalik and Utku [3] are satisfied, both coefficients can also be given by

$$a = E \left[\frac{\partial g(\dot{x}, v)}{\partial \dot{x}} \right] \quad , \quad b = E \left[\frac{\partial g(\dot{x}, v)}{\partial v} \right] , \quad (\text{F.5})$$

where the expected values correspond to a joint gaussian distribution function of the variables \dot{x} and v , which have zero means. The partial derivatives of $g(\dot{x}, v)$ are

$$\frac{\partial g(\dot{x}, v)}{\partial \dot{x}} = \mathcal{A} - \mathcal{B} |v|^\eta - \mathcal{C} v |v|^{\eta-1} \dot{x} |\dot{x}|^{-1} , \quad (\text{F.6})$$

$$\frac{\partial g(\dot{x}, v)}{\partial v} = -\eta \mathcal{B} \dot{x} v |v|^{\eta-2} - \eta \mathcal{C} |\dot{x}| |v|^{\eta-1} . \quad (\text{F.7})$$

Substitution of equations (F.6) and (F.7) into (F.5), and distribution of the expected values render

$$a = \mathcal{A} - \mathcal{B} E[|v|^\eta] - \mathcal{C} E[v |v|^{\eta-1} \dot{x} |\dot{x}|^{-1}] , \quad (\text{F.8})$$

$$b = -\eta \mathcal{B} E[\dot{x} v |v|^{\eta-2}] - \eta \mathcal{C} E[|\dot{x}| |v|^{\eta-1}] . \quad (\text{F.9})$$

For odd integer values of the exponent η , it is possible to obtain simpler closed form expressions for the expected values. Thus, equations (F.8) and (F.9) become

$$a = \mathcal{A} - \mathcal{B} E[|v|^\eta] - \mathcal{C} E[v^\eta \dot{x} |\dot{x}|^{-1}] , \quad (\text{F.10})$$

$$b = -\eta B E[\dot{x} v |v|^{\eta-2}] - \eta C E[|\dot{x}| v^{\eta-1}]. \quad (\text{F.11})$$

The integrals involved in the above expected values, are not generally included in common integral tables. For this reason, they closed expressions have been developed during this study and their final forms are presented here.

The first expected value to be considered is $E[|v|^\eta]$. Since the mean value of v it is assumed to be zero, its expression is:

$$E[|v|^\eta] = \int_{-\infty}^{\infty} \frac{|v|^\eta}{\sqrt{2\pi}\sigma_v} e^{-\frac{1}{2}\left(\frac{v}{\sigma_v}\right)^2} dv = \sigma_v \sqrt{\frac{2^\eta}{\pi}} \Gamma\left(\frac{\eta+1}{2}\right), \quad (\text{F.12})$$

where σ_v is the standard deviation of v and $\Gamma(\cdot)$ is the gamma function. For positive odd integer values of η the value of the above gamma function is $\Gamma(\frac{\eta+1}{2}) = (\frac{\eta-1}{2})!$ and $E[|v|^\eta]$ becomes

$$E[|v|^\eta] = \sigma_v \sqrt{\frac{2^\eta}{\pi}} \left(\frac{\eta-1}{2}\right)!. \quad (\text{F.13})$$

The calculation of $E[v^\eta \dot{x} |\dot{x}|^{-1}]$ and $E[|\dot{x}| v^{\eta-1}]$ for odd values of η requires the use of the following expression:

$$E[x^\eta] = \sum_{k=0}^{k \leq \eta} \sigma_x^k \mu_x^{\eta-k} \sqrt{\frac{2^k}{\pi}} \binom{\eta}{k} \Gamma\left(\frac{k+1}{2}\right), \quad k = 0, 2, 4, \dots, \text{even} \quad (\text{F.14})$$

where x possesses a gaussian probability density function with mean μ_x and standard deviation σ_x . This expression has been derived from the following recursive equation provided in reference [36]:

$$E[x^\eta] = \mu_x E[x^{\eta-1}] + (\eta-1) \sigma_x^2 E[x^{\eta-2}] \quad (\text{F.15})$$

Equation (F.14) is valid for odd or even values of η . In particular, for odd values of η it becomes

$$E[x^\eta] = \sum_{j=0}^{(\eta-1)/2} \frac{\sigma_x^{2j} \mu_x^{\eta-2j}}{2^j} \left[\frac{\eta!}{j! (\eta-2j)!} \right], \quad (\text{F.16})$$

and for even values of η it is

$$E[x^\eta] = \sum_{j=0}^{\eta/2} \frac{\sigma_x^{2j} \mu_x^{\eta-2j}}{2^j} \left[\frac{\eta!}{j! (\eta-2j)!} \right]. \quad (\text{F.17})$$

By assuming a jointly gaussian distribution function with zero means for the variables v and \dot{x} , the final expressions for $E[v^\eta \dot{x} |\dot{x}|^{-1}]$ and $E[|\dot{x}| v^{\eta-1}]$ (for $\eta = \text{odd}$) are:

$$E[v^\eta \dot{x} |\dot{x}|^{-1}] = \eta! (\sigma_v \rho_{v\dot{x}})^\eta \sqrt{\frac{2\eta}{\pi}} \Sigma_a \quad (\text{F.18})$$

$$E[|\dot{x}| v^{\eta-1}] = (\eta-1)! (\sigma_v \rho_{v\dot{x}})^{\eta-1} \sigma_{\dot{x}} \sqrt{\frac{2\eta}{\pi}} \Sigma_b. \quad (\text{F.19})$$

where $\rho_{v\dot{x}} = E[v \dot{x}] / (\sigma_v \sigma_{\dot{x}})$ is the correlation coefficient, and the quantities denoted as Σ_a and Σ_b indicate the following summations:

$$\Sigma_a = \sum_{j=0}^{(\eta-1)/2} \left\{ \frac{[(\eta-2j-1)/2]!}{j! (\eta-2j)!} \left[\frac{1 - \rho_{v\dot{x}}^2}{4 \rho_{v\dot{x}}^2} \right]^j \right\}, \quad (\text{F.20})$$

$$\Sigma_b = \sum_{j=0}^{(\eta-1)/2} \left\{ \frac{[(\eta-2j-1)/2]!}{j! (\eta-2j-1)!} \left[\frac{1 - \rho_{v\dot{x}}^2}{4 \rho_{v\dot{x}}^2} \right]^j \right\}. \quad (\text{F.21})$$

By considering the same jointly gaussian distribution as before and odd values of η , the remaining quantity $E[\dot{x} v |v|^{\eta-2}]$ can be written as

$$E[\dot{x} v |v|^{\eta-2}] = \sigma_{\dot{x}} \sigma_v^{\eta-1} \rho_{v\dot{x}} \sqrt{\frac{2\eta}{\pi}} \left(\frac{\eta-1}{2} \right)! \quad (\text{F.22})$$

Substitution of equations (F.13), (F.18), (F.19) and (F.22) into equations (F.10) and (F.11), renders the final expressions for the linearization coefficients a and b :

$$a = \mathcal{A} - \sigma_v^\eta \sqrt{2\eta/\pi} \left[\mathcal{B} \left(\frac{\eta-1}{2} \right)! + \mathcal{C}(\eta)! \rho_{v\dot{x}}^\eta \Sigma_a \right] \quad (\text{F.23})$$

$$b = -\sigma_v^{\eta-1} \sigma_{\dot{x}} \sqrt{2\eta/\pi} \left[\eta \rho_{v\dot{x}} \mathcal{B} \left(\frac{\eta-1}{2} \right)! + \mathcal{C}(\eta)! \rho_{v\dot{x}}^{\eta-1} \Sigma_b \right] \quad (\text{F.24})$$

Appendix G

Frequency Integrals

This appendix presents closed form solutions to the frequency integrals involved in the stochastic response of single-degree-of-freedom oscillators. The following three integrals are analyzed:

$$J_j = \int_{-\infty}^{\infty} \Phi_g(\omega) |G_j^c(\omega)|^2 d\omega , \quad (\text{G.1})$$

$$I_j^d = \int_{-\infty}^{\infty} \Phi_g(\omega) |H_j^c(\omega)|^2 d\omega \quad , \quad I_j^v = \int_{-\infty}^{\infty} \Phi_g(\omega) \omega^2 |H_j^c(\omega)|^2 d\omega , \quad (\text{G.2})$$

where $|G_j^c(\omega)|^2$ and $|H_j^c(\omega)|^2$ are the squared modules of the frequency response functions corresponding to a massless oscillator (first order oscillator), and to a second order oscillator, respectively.

$$|G_j^c(\omega)|^2 = [(\lambda_j^r)^2 + \omega^2]^{-1} \quad , \quad |H_j^c(\omega)|^2 = [(\omega_j^2 - \omega)^2 + 4\beta_j^2 \omega_j^2 \omega^2]^{-1} . \quad (\text{G.3})$$

The existence of closed form solutions to these integrals depends mainly on the complexity of the function $\Phi_g(\omega)$, which is the power spectral density function (PSDF) of the excitation. For a unit PSDF, the integrals are denoted by \tilde{J}_j , \tilde{I}_j^d and \tilde{I}_j^v . The first is given by:

$$\tilde{J}_j = \int_{-\infty}^{\infty} |G_j^c(\omega)|^2 d\omega = \frac{1}{\lambda_j^r} \arctan \left(\frac{\omega}{\lambda_j^r} \right) \Big|_{-\infty}^{\infty} = \frac{\pi}{\lambda_j^r} . \quad (\text{G.4})$$

The expressions for \tilde{I}_j^d and \tilde{I}_j^v can be found in the random vibration literature [29], and are given by

$$\tilde{I}_j^d = \int_{-\infty}^{\infty} |H_j^c(\omega)|^2 d\omega = \frac{\pi}{2\beta_j \omega_j^3}, \quad (\text{G.5})$$

$$\tilde{I}_j^v = \int_{-\infty}^{\infty} \omega^2 |H_j^c(\omega)|^2 d\omega = \frac{\pi}{2\beta_j \omega_j}. \quad (\text{G.6})$$

The simplest PSDF to be considered is that of a white noise since its expression is a constant value:

$$\Phi_g(\omega) = S. \quad (\text{G.7})$$

However, a white noise is an idealization that it is not present in natural phenomena. A more adequate model for earthquake engineering, is the well known Kanai-Tajimi [24] PSDF. It models the seismic motion at the surface of soil layers that rest on a bedrock. The soil layers are considered as a single degree of freedom oscillator, which filters an assumed white noise motion acting at the rock level. A three term Kanai-Tajimi PSDF has the following expression:

$$\Phi_g(\omega) = \sum_{i=1}^3 S_i (\omega_i^4 + 4\beta_i^2 \omega_i^2 \omega^2) |H_i^c(\omega)|^2, \quad (\text{G.8})$$

where the parameters S_i depend on the maximum level of excitation (white noise amplitude), and the parameters ω_i and β_i depend on the characteristics of the soil.

White Noise PSDF

In this case, the PSDF is given by equation (G.7), and the integrals are straight forward:

$$J_j = S \tilde{J}_j = S \frac{\pi}{\lambda_j^r}, \quad (\text{G.9})$$

$$I_j^d = S \tilde{I}_j^d = S \frac{\pi}{2\beta_j \omega_j^3}, \quad I_j^v = S \tilde{I}_j^v = S \frac{\pi}{2\beta_j \omega_j}. \quad (\text{G.10})$$

Kanai-Tajimi PSDF

For a three-term-Kanai-Tajimi PSDF, the integral J_j become

$$J_j = \sum_{i=1}^3 S_i \int_{-\infty}^{\infty} (\omega_i^4 + 4\beta_i^2 \omega_i^2 \omega^2) |G_j^c(\omega)|^2 |H_i^c(\omega)|^2 d\omega . \quad (\text{G.11})$$

The integrand of the above expression can be expanded into partial fractions by using the procedure described in case II of appendix A. Thus,

$$J_j = \sum_{i=1}^3 S_i \int_{-\infty}^{\infty} \left[T_{ji}^{(1)} |G_j^c(\omega)|^2 + (T_{ji}^{(2)} + \omega^2 T_{ji}^{(3)}) |H_i^c(\omega)|^2 \right] d\omega , \quad (\text{G.12})$$

where the partial fraction coefficients are

$$T_{ji}^{(1)} = \left[4\beta_i^2 \omega_i^2 (\lambda_j^r)^2 - \omega_i^4 \right] (\Delta_{ji}^{II})^{-1} , \quad (\text{G.13})$$

$$T_{ji}^{(2)} = -\omega_i^4 \left[2\omega_i^2 + (\lambda_j^r)^2 \right] (\Delta_{ji}^{II})^{-1} , \quad (\text{G.14})$$

$$T_{ji}^{(3)} = -T_{ji}^{(2)} , \quad (\text{G.15})$$

with

$$\Delta_{ji}^{II} = 4\beta_i^2 \omega_i^2 (\lambda_j^r)^2 - [(\lambda_j^r)^2 + \omega_i^2]^2 . \quad (\text{G.16})$$

Equation (G.12) can be rewritten as

$$J_j = \sum_{i=1}^3 S_i \left[T_{ji}^{(1)} \tilde{J}_j + T_{ji}^{(2)} \tilde{I}_i^d + T_{ji}^{(3)} \tilde{I}_i^v \right] . \quad (\text{G.17})$$

Equations (G.4), (G.5), (G.6), (G.13), (G.14) and (G.15) can be substituted into equation (G.17) which, after some algebra, becomes

$$J_j = \frac{\pi}{2\lambda_j^r} \sum_{i=1}^3 \frac{S_i \omega_i}{\beta_i} \frac{(4\beta_i^2 \lambda_j^r + 2\beta_i \omega_i + \lambda_i^r)}{(2\beta_i \omega_i \lambda_j^r + (\lambda_j^r)^2 + \omega_i^2)} . \quad (\text{G.18})$$

The next integral to be considered is I_j^d , which for the PSDF given in equation (G.8) is

$$I_j^d = \sum_{i=1}^3 S_i \int_{-\infty}^{\infty} (\omega_i^4 + 4\beta_i^2 \omega_i^2 \omega^2) |H_i^c(\omega)|^2 |H_j^c(\omega)|^2 d\omega . \quad (G.19)$$

The integrand can be expanded into the following partial fractions:

$$I_j^d = \sum_{i=1}^3 S_i \int_{-\infty}^{\infty} \left[(T_{ij}^{(4)} + \omega^2 T_{ij}^{(5)}) |H_i^c(\omega)|^2 + (T_{ij}^{(6)} + \omega^2 T_{ij}^{(7)}) |H_j^c(\omega)|^2 \right] d\omega , \quad (G.20)$$

where the coefficients $T_{ij}^{(4)}$, $T_{ij}^{(5)}$, $T_{ij}^{(6)}$ and $T_{ij}^{(7)}$ can be obtained by the procedure described in case III of appendix A.

$$T_{ij}^{(4)} = \left\{ \Omega_{ij}^2 \left[4 - 3\Omega_{ij}^2 + 8(\beta_i^2 \Omega_{ij}^2 - \beta_j^2) \right] - 1 \right\} (\Delta_{ij}^{III})^{-1} \quad (G.21)$$

$$T_{ij}^{(5)} = \left[2 \left(\Omega_{ij}^4 - \Omega_{ij}^2 \right) + 4 \left(\beta_j^2 \Omega_{ij}^2 - \beta_i^2 \right) \right] \omega_i^{-2} (\Delta_{ij}^{III})^{-1} \quad (G.22)$$

$$T_{ij}^{(6)} = 1 - \Omega_{ij}^{-4} T_{ij}^{(4)} \quad , \quad T_{ij}^{(7)} = -T_{ij}^{(5)} , \quad (G.23)$$

with $\Omega_{ij} = \omega_i/\omega_j$, and

$$\begin{aligned} \Delta_{ij}^{III} = & 16(\beta_i^2 + \beta_j^2 - \beta_i^4 - \beta_j^4) - \Omega_{ij}^4 - \Omega_{ij}^{-4} - 6 \\ & + 4(\Omega_{ij}^2 + \Omega_{ij}^{-2}) \left[1 - 2(\beta_i^2 + \beta_j^2 - 2\beta_i^2 \beta_j^2) \right] . \end{aligned} \quad (G.24)$$

By considering equations (G.23), equation (G.20) can be rewritten as

$$I_j^d = \sum_{i=1}^3 S_i \left[T_{ij}^{(4)} \left(\bar{I}_i^d - \Omega_{ij}^{-4} \bar{I}_j^d \right) + T_{ij}^{(5)} \left(\bar{I}_i^v - \bar{I}_j^v \right) + \bar{I}_j^d \right] \quad (G.25)$$

where the integrals \bar{J}_j , \bar{I}_j^d and \bar{I}_j^v are given by equations (G.4), (G.5) and (G.6).

Substitution of these expressions into the above equation renders:

$$I_j^d = \frac{\pi}{2} \sum_{i=1}^3 S_i \left[\frac{T_{ij}^{(4)}}{\omega_i^3} \left(\frac{1}{\beta_i} - \frac{\Omega_{ij}^{-1}}{\beta_j} \right) + \frac{T_{ij}^{(5)}}{\omega_i} \left(\frac{1}{\beta_i} - \frac{\Omega_{ij}}{\beta_j} \right) + \frac{1}{\omega_j^3 \beta_j} \right] \quad (G.26)$$

Finally, the remaining integral I_j^v is

$$I_j^v = \sum_{i=1}^3 S_i \int_{-\infty}^{\infty} (\omega_i^4 \omega^2 + 4\beta_i^2 \omega_i^2 \omega^4) |H_i^c(\omega)|^2 |H_j^c(\omega)|^2 d\omega . \quad (G.27)$$

After expanding the integrand into partial fractions, it becomes

$$I_j^v = \sum_{i=1}^3 S_i \int_{-\infty}^{\infty} \left[(T_{ij}^{(8)} + \omega^2 T_{ij}^{(9)}) |H_i^c(\omega)|^2 + (T_{ij}^{(10)} + \omega^2 T_{ij}^{(11)}) |H_j^c(\omega)|^2 \right] d\omega, \quad (\text{G.28})$$

where the coefficients $T_{ij}^{(8)}$, $T_{ij}^{(9)}$, $T_{ij}^{(10)}$ and $T_{ij}^{(11)}$ can also be obtained by the procedure described in case III of appendix A.

$$T_{ij}^{(8)} = 2\omega_i^2 \Omega_{ij}^2 \left(1 - \Omega_{ij}^2 - 2\beta_j^2 + 2\beta_i^2 \Omega_{ij}^{-2} \right) (\Delta_{ij}^{III})^{-1}, \quad (\text{G.29})$$

$$T_{ij}^{(9)} = \left\{ \Omega_{ij}^4 - 1 - 8\beta_i^2 \left[1 - \Omega_{ij}^2 + 2(\beta_j^2 \Omega_{ij}^2 - \beta_i^2) \right] \right\} (\Delta_{ij}^{III})^{-1}, \quad (\text{G.30})$$

$$T_{ij}^{(10)} = -\Omega_{ij}^{-4} T_{ij}^{(8)}, \quad T_{ij}^{(11)} = -T_{ij}^{(9)}, \quad (\text{G.31})$$

where Ω_{ij} and Δ_{ij}^{III} have already been defined. Substitution of equations (G.31) into equation (G.28) produces

$$I_j^v = \sum_{i=1}^3 S_i \left[T_{ij}^{(8)} (\tilde{I}_i^d - \Omega_{ij}^{-4} \tilde{I}_j^d) + T_{ij}^{(9)} (\tilde{I}_i^v - \tilde{I}_j^v) \right], \quad (\text{G.32})$$

where the indicated integrals can be substituted by their closed expressions, given in equations (G.4), (G.5) and (G.6) to render

$$I_j^v = \frac{\pi}{2} \sum_{i=1}^3 S_i \left[\frac{T_{ij}^{(8)}}{\omega_i^3} \left(\frac{1}{\beta_i} - \frac{\Omega_{ij}^{-1}}{\beta_j} \right) + \frac{T_{ij}^{(9)}}{\omega_i} \left(\frac{1}{\beta_i} - \frac{\Omega_{ij}}{\beta_j} \right) \right]. \quad (\text{G.33})$$

REFERENCES

- [1] American National Standard Institute: "American national standard building code requirements for minimum design loads in buildings and other structures", ANSI A58.1-1982, New York, 1982.
- [2] Applied Technology Council: "Tentative provisions for the development of seismic regulations for buildings", ATC 3-06, National Bureau of Standards, Washington, D.C., 1978.
- [3] T. S. Atalik and S. Utku, "Stochastic linearization of multi-degree-of-freedom nonlinear systems", *Earthquake eng. and struct. dyn.*, 47, 150-154, (1980).
- [4] T. T. Baber, M. N. Noori, "Random vibration of degrading, pinching systems", *Engineering Mechanics Division ASCE*, 117, (10) 2407-2428, (1985).
- [5] T. T. Baber and Y. K. Wen, "Stochastic equivalent linearization for hysteretic, degrading, multistory structures", Report, Department of Civil Engineering, University of Illinois, SRS No. 471, 1979.
- [6] T. T. Baber and Y. K. Wen, "Random vibration of hysteretic degrading systems", *Engineering Mechanics Division, ASCE*, 107, (EM6), 1069-1087, (1981).
- [7] T. T. Baber and Y. K. Wen, "Stochastic response of multistory yielding frames", *Earthquake eng. and struct. dyn.*, 10, 403-416, (1982).
- [8] T. T. Baber and Y. K. Wen, "Stochastic response of multistorey yielding frames", *Earthquake eng. and struct. dyn.*, 10, 403-416, (1982).
- [9] R. Bouc, "Forced vibration of mechanical system with hysteresis", Abstract, *Proc. 4th conf. on nonlinear oscillation*, Prague, Czechoslovakia, 1967.
- [10] C. J. Camarda, R. T. Haftka and M. F. Riley, "An evaluation of higher-order modal method for calculating transient structural response", *Computers and Structures*, 27, 89-101, (1987).
- [11] F. Casciati and L. Faravelli, "Methods of non-linear stochastic dynamics for the assessment of structural fragility", *Nuclear Engineering and Design*, 90, 341-356, (1985).

- [12] F. Casciati and L. Faravelli, "Reliability assessment for non-linear random frames", *Proc. Weibull IUTAM Symp.*, Stockholm, Probabilistic Methods in the Mechanics of Solids and Structures, eds. S. Eggwertz and N. C. Ling, Springer, Berlin, 209-253, 1985.
- [13] S. D. Conte and Carl de Boor, *Elementary Numerical Analysis: an algorithmic approach*, 3rd edition, New York, McGraw-Hill, 1980.
- [14] R. D. Cook, *Concepts and Applications of Finite Element Analysis*, 2nd Edition, Wiley, New York, NY, 1981.
- [15] R. R. Craig, *Structural Dynamics: An Introduction to Computer Methods*, Wiley, New York, 1981.
- [16] A. G. Davenport, "Note on the distribution of the largest value of a random function with application to gust loading", *Proc. Inst. civ. eng.*, **28**, 187-196, (1964).
- [17] M. Ghafory-Ashtiany and M. P. Singh, "Seismic response of multicomponent earthquakes", *College of Engineering Report No. VPI-E-84-17*, Virginia Polytechnic Institute and State University, Chapter 2, 1984.
- [18] A.K. Gupta and D. C. Chen, "Combination of modal responses: a follow up", *Technical Report*, Department of Civil Engineering, North Carolina State University, Raleigh, North Carolina, 1982.
- [19] A.K. Gupta and K. Cordero, "Combination of modal responses", *Proc. 6th int. conf. struct. mech. reactor technol.*, Paper K7/15, Paris, (1981).
- [20] T. Igusa and A. Der Kiureghian, "Response spectrum method for systems with non-classical damping", *Proc. 4th eng. mech. div. specialty conf.*, **1**, 380-384, (1983).
- [21] T. Igusa, A. Der Kiureghian and J. L. Sackman, "Modal decomposition method for stationary response of non-classically damped systems", *Earthquake eng. struct. dyn.*, **12**, 121-136, (1984).
- [22] *International Mathematical and Statistical Libraries, Inc*, 6th floor, GNB Building, 7500 Bellaire Boulevard, Houston, TX, 77036.
- [23] A. E. Kanaan and G. H. Powell, "DRAIN-2D General Purpose Program for Dynamic Analysis of Inelastic Plane Structures", Earthquake Engineering Research Center, Report No. EERC 73-6 and EERC 72-22, University of California, Berkeley, April 1973.
- [24] K. Kanai, "An empirical formula for the spectrum of strong earthquake motions", *Bulletin of Earthquake Research Institute*, University of Tokyo, **39**, 85-95, (1961).
- [25] N. Krylov and N. Bogoliubov, *Introduction to nonlinear mechanics*, Kiev, 1931. English translation, Princeton, NJ: Princeton University Press, 1943.

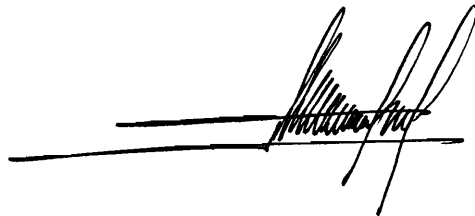
- [26] P. Leger and E. L. Wilson, "Modal summation methods for structural dynamic computations", *Earthquake eng. struct. dyn.*, **16**, 23-37, (1988).
- [27] J. W. Leonard, "An improved modal synthesis method for the transient response of piping systems", *3rd SMIRT conf.*, Paper K 7/2, 1979.
- [28] Y. T. Leung, "Fast response method for undamped structures", *Engineering Structures*, **5**, 141-149, (1983).
- [29] Y. K. Lin, *Probabilistic Theory of Structural Dynamics*, New York, McGraw-Hill, 1967.
- [30] G. O. Maldonado, "Stochastic response of single-degree-of-freedom hysteretic oscillators", Master Thesis, Department of Engineering Science and Mechanics, Virginia Polytechnic Institute and State University, 1987.
- [31] G. O. Maldonado and M. P. Singh, "An improved response spectrum method for calculating seismic design response. Part 2: Non-classically damped structures", *Earthquake eng. struct. dyn.*, **20**, 637-649, (1991).
- [32] S. R. Malushte and M. P. Singh, "Prediction of seismic design response spectra using ground characteristics", *Technical Report No. VPI-E-87-31*, College of Engineering, Virginia Polytechnic Institute and State University, Blacksburg, VA, 1987.
- [33] L. Meirovitch, "Analytical Methods in Vibrations", Macmillan, New York, 1967.
- [34] J. More, B. Garbow and K. Hillstrom, "User guide for Minpack-1", Argonne National Laboratories, Report ANL-80-74, Argonne, Illinois 1980.
- [35] National Earthquake Hazards Reduction Program, *NEHRP Recommended Provisions for the Development of Seismic Regulations for New Buildings*, Federal Emergency Management Agency, Building Seismic Safety Council, Washington, D.C., 1991.
- [36] N. C. Nigam, *Introduction to Random Vibrations*, The MIT Press, Cambridge, Massachusetts, 1983.
- [37] N. C. Nigam, P. C. Jennings, "Calculation of response spectra from strong-motion earthquake records", *Bulletin of the Seismological Society of America*, **59**, No. 2, April, 1969.
- [38] U. S. Nuclear Regulatory Commission, "Design response spectra for nuclear power plants", *Nuclear Regulatory Guide No. 1.60*, Washington, D. C., 1975.
- [39] G. M. Powell, "Missing mass correction in modal analysis of piping systems", *Trans. 5th SMIRT conf.*, K(6), (1979), Paper K10/3.
- [40] J. B. Roberts and P. D. Spanos, *Random vibration and statistical linearization*, John Wiley & Sons, 1990.
- [41] E. Rosenblueth and J. Elorduy, "Response of linear systems to certain transient disturbances", *Proc. 4th world conf. earthquake eng.*, Santiago, Chile, (1969).

- [42] R. T. Sewell, C. A. Cornell, G. R. Toro and R. K. McGuire, "A study of factors influencing floor response spectra in nonlinear multi-degree-of-freedom structures", Report No 82, Dept. of Civil Engineering, Stanford University, 1986.
- [43] M. P. Singh, "Seismic response by SRSS for nonproportional damping", *J. eng. mech. div. ASCE*, **106**, 1405-1419 (1980).
- [44] M. P. Singh, "Seismic response combination of high frequency modes", *Proc. 7th Eur. conf. earthquake eng.*, Athens, Greece, (1982).
- [45] M. P. Singh and S. L. Chu, "Stochastic considerations in seismic analysis of structures", *Earthquake eng. struct. dyn.*, **4**, 295-307, (1976).
- [46] M. P. Singh and Ghafory Ashtiany, "Modal time history analysis of non-classically damped structures for seismic motions", *Earthquake eng. struct. dyn.*, **14**, 133-146, (1986).
- [47] M. P. Singh and G. O. Maldonado, "Response spectrum method including the missing mass effect with truncated modes", *Proc. 4th U.S. nat. conf. earthquake eng.*, **2**, 167-175, Palm Springs, CA, (1991).
- [48] M. P. Singh and G. O. Maldonado, "An improved response spectrum method for calculating seismic design response. Part 1: Classically damped structures", *Earthquake eng. struct. dyn.*, **20**, 621-635, (1991).
- [49] M. P. Singh and B. E. McCown, "Mode acceleration-based response spectrum approach for non-classically damped structures", *Soil dyn. earthquake eng.*, **5**, 226-233, (1986).
- [50] M. P. Singh and K. B. Mehta, "Seismic design response by an alternative SRSS rule", *Earthquake eng. struct. dyn.*, **11**, 771-783, (1983)
- [51] L. E. Suarez and M. P. Singh, "Modal synthesis method for general dynamic systems", *Engineering Mechanics Division ASCE*, **118**, (7) 1488-1503, (1992).
- [52] E. Vanmarcke, "Seismic structural response", Chapter 8 in *Developments in Geotechnical Engineering 15, Seismic Risk and Engineering Decisions*, (Eds. C. Lomnitz and E. Rosenblueth), Elsevier, New York, 1976.
- [53] A. S. Veletsos and C. E. Ventura, "Modal analysis of non-classically damped linear systems", *Earthquake eng. struct. dyn.*, **14**, 217-243, (1986).
- [54] R. Villaverde, "Rosenblueth's modal combination rule for system with non-classical damping", *Earthquake eng. struct. dyn.*, **16**, 315-328, (1988).
- [55] R. Villaverde, "Metodos para combinar respuestas modales en el analisis sismico estructural", *VI Congreso Nacional de Ingenieria Estructural*, Paper A23-36, Puebla, Mexico, (1988).
- [56] Y. K. Wen, "Method for random vibration of hysteretic systems", *Proc. Eng. Mech. Div., ASCE*, **102**, Paper EM2, 249-263, 1976.

- [57] Y. K. Wen, "Equivalent linearization for hysteretic systems under random excitation", *Applied Mechanics*, **47**, 150-154, (1980).
- [58] Y. K. Wen, "Stochastic response and damage analysis of inelastic structures", *Probabilistic Engeneering Mechanics*, **1**, 49-57, (1986).
- [59] E. L. Wilson, A. Der Kiureghian and E. P. Bayo, "A replacement for the SRSS method in seismic analysis", *Earthquake eng. struct. dyn.*, **9**, 187-192, (1981).
- [60] D. Williams, "Displacements of a linear elastic system under a given transient load", *Aeronautical Quarterly*, **1**, 123-136, (1949).

VITA

Gustavo O. Maldonado was born in Córdoba, Argentina, in 1958. He attended a roman catholic school for his primary and secondary education, and in 1975 he received an introductory degree in business. In 1982 he received a B.S. degree in Civil Engineering (six-year curriculum) from the National University of Córdoba. After a year of compulsory military service (1982) he taught as an instructor in the College of Engineering at the National University of Córdoba and participated in numerous consulting projects for the industry as an independent engineer. He joined the Engineering Science and Mechanics department of the Virginia Polytechnic Institute and State University where he received his M.S. and Ph.D degrees in 1987 and 1992 respectively. In April of 1992 he was granted the Paul E. Torgersen Research Excellence Award by the college of engineering of VPI & SU.

A handwritten signature in black ink, appearing to read 'Gustavo O. Maldonado', is written over a horizontal line.